Principles of Inter-Areal Connections of the Macaque Cortex

Dissertation

zur

Erlangung der naturwissenschaftlichen Doktorwürde

(Dr. sc. nat.)

vorgelegt der

Mathematisch-naturwissenschaftlichen Fakultät

der

Universität Zürich

von

John Carl Anderson

aus dem

Vereinigtes Königreich

Promotionskomitee

Prof. Dr. Rodney J Douglas
Prof. Dr. Richard Hahnloser
Prof. Dr Kevan A.C. Martin (Leitung der Dissertation und Vorsitz)

Zürich, 2015

Contents …..... 1

Abstract …..... 4

Zusammenfassung …..... 6

Statement …..... 8

Chapter 1 Introduction …..... 9

1.1 The question of connectivity..... 9

1.2 Recent developments and revelations …..... 11

1.3 Proposed circuitry …..... 13

1.4 The question again …..... 13

1.5 Feedforward versus feedback …..... 14

1.6 Cell bodies and hierarchy …..... 15

1.7 Models and hierarchy …..... 16

1.8 Drivers and modulators …..... 19

1.9 Cortical areas, connections and their properties …..... 19

1.9.1 V1 and V2 …..... 19

1.9.2 V1 to V5 …..... 20

1.9.3 V2 to V5 …..... 22

1.9.4 V2 to V3A …. 23

1.9.5 V4 to V2 …. 25

1.9.5.1 Substreams of cytochrome oxidase …. 25

1.9.6 Frontal eye fields (FEF) to V4, Area 46 and Lateral intraparietal cortex (LIP) …... 26

1.9.7 Better resolution …. 31

Chapter 2 Materials and Methods …. 36

2.1 Veterinary authorities …. 36

2.2 Surgical procedures …. 36

2.3 Neuronal tracers and method of delivery …. 37

2.4 Care, recovery and perfusion …. 37

2.5 Histology …. 38

2.6 Light and electron microscopy …. 38

2.7 3D EM …. 39

2.8 Counting synapses and measuring …. 39

Chapter 3 Publications …. 40

3.1 Preamble and publication; V1 to V5 …. 40

3.2 Preamble and publication; V2 to V5 …. 41

3.3 Preamble and publication; V2 to V3A …. 43

3.4 Preamble and publication; V4 to V2 …. 45

3.5 Preamble and publication; V1 and V2 …. 47

3.6 Preamble and publication; FEF to V4, area 46 and LIP …. 49

Chapter 4 General Discussion …..... 51

4.1 The labeled hierarchy …..... 51

4.2 Interareal boutons …..... 54

4.3 Interareal synapses …..... 56

4.4 Targets: …..... 57

4.4.1 Spiny cells as targets …..... 57

4.4.2 Smooth cells as targets …..... 58

4.5 Drivers and modulators …..... 61

4.6 Influence of synapse location …..... 62

4.7 Receptive fields …..... 65

4.8 Models of attention …..... 67

4.9 Conclusion …..... 71

References …..... 73

Figures …..... 1 . Light microscopic reconstructions of strips of labeled cortex …..... 53

2 . Summary diagram of connections described in these studies …..... 54

3 . Histogram showing percent of GABAergic synaptic targets …..... 59

Curriculum vitae …..... 101

Acknowledgements …..... 106

Abstract

The circuits of the cerebral cortex are composed of neurons, which are cells most notable for forming many processes that become highly branched and connect with the processes of other neurons to form elaborate networks of cells. The cortex appears to be stereotyped in its distribution of these cells and their processes and therefore perhaps in their circuitry too. Many functionally different cortical areas form direct connections with one another via axonal projections to neighbouring areas where the axons form synapses. We chose to extend this picture of connectivity using macaque monkey because many years of research have provided us with a well documented foundation of visual pathways, in particular due to its well developed cortical areas and is similar to the human. Using injected anterograde tracers we have examined the boutons formed by these cortical interareal projections in the macaque monkey from a number of visual and vision-related pathways, using light and electron microscopy. This allows us to reconstruct from serial sections selected axon arbors, boutons, quantify their synaptic targets and synapse morphology. Light microscopic observations identify the 'type' of pathway, namely feedforward, lateral or feedback, between any two areas by noting in which lamina the labeled bouton terminals form. The boutons and their synaptic targets can be characterized in the EM and here we gather together the published body of papers that compose these investigations. The pathways examined in these publications include V1 to V5 (MT), V2 to V5, V2 to V3A, V1 to V2 and V2 to V1, FEF to LIP, FEF to V4, FEF to area 46 and V4 to V2. We chose these connections, because they represent both the earliest and some of the latest points in cortical visual processing, from striate to extrastriate areas. All labeled synapses examined proved to be asymmetric (Gray's type 1), a morphological feature which is consistent with the projection cells being pyramidal. The most frequent target of any pathway was the dendritic spine (V1 to V5, 54%; V2 to V5, 67%; V2 to V 3A,76%; V1 to V2, 75%; V2 to V1, 63%; FEF to LIP, 84%; FEF to V4, 89%; FEF to area 46, 95%, V4 to V2, 75%)

which is a feature of the dendrites of excitatory cells. The second most frequently observed target was the dendritic shaft. Features of shafts, indicate whether or not the parent cell of the dendrite is excitatory or inhibitory (V1 to V5, 26%; V2 to V5, 15%; V2 to V 3A,10%; V1 to V2, 14%; V2 to V1, 19%; FEF to LIP, 19%; FEF to V4, 5%; FEF to area 46, 5%, V4 to V2, 11%). Both types of dendrite were shown to form synapses with labeled boutons. The least frequently seen target was the cell body or soma, found in only one or two cases per projection and shown invariably to be smooth cells. Spiny or putative excitatory cells, as targets, were always numerically dominant. Cells with smooth spine-free dendrites, putative inhibitory cells occurred with a frequency similar to or significantly less than that expected by chance, given the proportion of smooth cells found in cat or monkey cortex. When the site of the synaptic specialization was reconstructed from serial sections we found both their size and shape to be highly variable. Spine synapses were the largest and most complex, somatic synapses were the smallest. The density of labeled interareal boutons was assessed using stereological techniques. The densest projection found in our studies showed labeled synapses to be only 0.16% of identified excitatory synapses in the densest zone of innervation.

The lamina preferences shown by different interareal pathways indicate that different regions of the target excitatory cells dendritic tree are innervated. The modest number of smooth cells that are targets suggest that inhibition is not being specially targeted. Sparse interareal innervation could be amplified by the recurrent local circuitry of the target area.

Zusammenfassung

Die Schaltkreise des cerebralen Cortex bestehen aus Neuronen. Diese Zellen sind miteinander verbunden und besitzen die bemerkenswerte Eigenschaft in Strukturen von feinsten Veraestelungungen zu wachsen. Deshalb besitzen sie die Faehigkeit raffinierte Netzwerke zu bilden. Die Hirnrinde weist eine stereotype Verteilung dieser Neuronen auf und vielleicht stimmt das auch fuer die Schaltkreise. Viele funktionell unterschiedliche Hirnregionen sind durch Assoziationsfasern und deren Synapsen miteinander verbunden. Durch langjaehrige Forschungen am Gehirn des Macaque Affen, besitzen wir gut dokumentierte Grundlagen der visuellen Signaluebertragung. Auch sind seine differenziert entwickelten Hirnregionen dem Menschen aehnlich. Deshalb waehlten wir das Gehirn des Macaque Affen um die interarealen Verbindungen genau zu untersuchen. Durch Injektionen eines anterograden Markierungsstoffs (Tracer) konnten wir die Axonterminale (Boutons) dieser interarealen Verbindungen zwischen visuellen und mit visuellen Signaluebertragung in Beziehung stehenden Hirnarealen, im Licht- und Elektronenmikroskop genau untersuchen. Mittels Serienschnitte konnten wir Axone, Axonterminale, Synapsen und deren Ziele rekonstruieren. So war es uns moeglich die Morphologie der Synapsen sichtbar zu machen und die postsynaptische Region zu identifizieren. Im LM beobachteten wir in welcher Lamina des Cortex sich die markierten Boutons befinden und konnten so die Art der Nervenbahnen zwischen zwei Hirnregionen bestimmen, namentlich diejenigen, welche die Hierarchie des Cortex in aufsteigender Richtung durchlaufen, die lateralen Bahnen, sowie diejenigen, die die Hierarchie in absteigender Richtung gewaehrleisten. Die Boutons und deren synaptischen Ziele konnten durch Untersuchungen im EM charakterisiert werden. Wir erwaehnen hier die publizierten wissenschftlichen Arbeiten, in denen diese Untersuchungen zusammengestellt sind. Die untersuchten Signaluebertragungen dieser Publikationen beinhalten V1 zu V5 (MT), V2 zu V5, V2 zu V3A, V1 zu V2, und V2 zu V1, FEF zu LIP, FEF zu V4, FEF zu area 46, und V4 zu V2. Wir waehlten diese

Verbindungen, weil sie repraesentativ sind sowohl fuer niedere als auch fuer einige der hoeheren Hierarchiestufen kortikaler visueller Prozesse. Alle markierten Boutons bildeten asymmetrische Synapsen (Gray's type 1), ein charakteristisches Merkmal fuer die projizierenden Pyramidalzellen. Das meist frequentierte Ziel aller Signaluebertragungen waren Dornen von Dendriten, dies ist eine Eigenschaft der Dendriten exzitatorische Zellen. Am zweithaeufigsten beobachteten wir Synapsen direkt am Schaft von Dendriten. Anhand der Erscheinung dieser Schafte, konnten wir diese den exzitatorischen oder den inhibitorischen Neuronen zuordnen (V1 zu V5, 26%; V2 zu V5, 15%; V2 zu V3A, 19%; V1 zu V2, 14%; V2 zu V1, 19%; FEF zu LIP, 19%; FEF zu V4, 5%; FEF zu area 46, 5%; V4 zu V2, 11%). Beide Typen von Dendriten besassen Synapsen von markierten Boutons. Am seltensten beobachteten wir Synapsen an Zellkoerpern, dies nur ein bis zweimal pro Projektion, diese gehoerten immer zu inhibitorischen Zellen. Zellen, die Dendriten mit Dornen besitzen sind mutmasslich exzitatorische Zellen, diese waren als Ziel in jedem Fall zahlenmaessig ueberwiegend. Zellen mit glatten, ohne Dornen besetzten Dendriten, also mutmasslich inhibitorische Neuronen erschienen als Ziel der markierten Axone seltener als die erwartete Wahrscheinlichkeit, beruecksichtigt man die Proportion von hemmenden Neuronen im Katzen- oder Affencortex. Die Rekonstruktion der Synapsen durch die Serenschnitte zeigt, dass deren Form und Groesse stark variiert. Synapsen an Dornen waren groesser und sehr komplex, die an Zellkoerpern waren kleiner.Die Dichte der markierten interarealen Axonterminale wurde mittels stereologischen Messungen bestimmt. Die dichteste Projektion in unserer Studie zeigte nur 0.16% von identifizierten exzitatorischen Synapsen mit markierten Boutons dies in Zonen wo die Innervation am dichtesten war.

Die Praeferenz der Laminae durch die verschiedenen interarealen Signaluebertragungen zeigt, dass die Dendriten an unterschiedlichen Orten ihrer Veraestellung innerviert werden. Die geringe Anzahl von inhibitorischen Dendriten als Ziel der Axone weist darauf hin, dass die Inhibition kein ausgesuchtest Ziel ist. Die spaerliche interareale Innervation koennte durch lokale Schaltkreise verstaerkt werden.

Statement

The surgery and injections of tracer when carried out in Zurich were done by Professor Kevan AC Martin and myself, including help from his team. The surgery, injections and histology carried out in Iowa, USA was completed by Professor Kathy Rockland and her team. The surgery in Lyon, France was carried out by Pascal Barone and Professor Henry Kennedy and the injections by myself, Prof Martin and Prof Kennedy. The appropriate veterinary guide lines were always adhered to.

The preparation of material for light and electron microscopy was carried out by myself with (first class) assistance from Rita Bopp and German Koestinger, who willingly shared many tasks with me.

The preparation of material for publication was carried out by Prof Martin and myself.

Chapter 1 Introduction

1.1 The question of connectivity.

Since the advent of Cell Theory of Schwann in 1839 the emphasis on understanding any system by knowing the cells at work in the system has been dominant in many areas of biology. In the case of the brain however it is perhaps more relevant to understand the connections made between cells in order to obtain greater insight into the functioning of the system. The simple fact that nerve cells or neurons as they became known (Waldeyer-Hartz, 1891) form very extensive and elaborate processes which have been shown to be the means by which connections are formed, tells us something of the investment, and hence importance, of connectivity for these cells. These connected groups of cells go on to form long distance connections with other groups of cells and it is this connectivity that we intend examine.

From the early days of the 19th century the description of the fine processes of neurons has been a magnet to scientific inquiry. It was not until the work of Camillo Golgi in 1875 did things take a significant turn when after using his new technique he generated results that surpassed the visualization of neurons unlike anything before. Using the 'Golgi' technique, a method of silver staining which produced a 'reazione nera' (black reaction), the astonishing detail of highly branched dendrites could be seen, along with their spine-like protuberances and the extensive branching of the axis cylinder or axon as it became known (Kölliker, 1896). We are still in the process of describing and understanding these patterns of connectivity between neurones after more than 100 years of study.

In the latter part of the 19th century Ramon y Cajal improved and exploited the technique of Golgi

and after close microscopic examination of olfactory bulb, cerebellum and vertebrate retina, Cajal, in a moment of great insight, began to put direction of conduction of the nerve impulse onto his neuronal wiring diagrams (1888/9, see Shepherd 1991, pp 197-198). This was the moment of instantiation of the law of dynamic polarization which could be applied to any part of the nervous system including the neocortex. With this idea embedded in the understanding that information passed from cell to cell via the axon of one cell to the dendrite of another and then to soma and to axon and so on it became increasingly important to know who talks to whom. The Golgi technique has certain limitations in what it can reveal, such as only labeling about 1% of cells and being effective only on tissue from young animals. The myelin sheath that coated many axons, particularly in adult animals, is impenetrable to Golgi's reagents and meant that following axons over long distances was not possible and consequently at best the technique only provided a detailed network based upon local wiring patterns (Ramon y Cajal, 1888; Szentágothai, 1978). Other techniques were available to reveal further properties of cortical structure over distance but lacked the detailed resolution of Golgi. Degeneration techniques (Nauta and Gygax, 1951; Kuypers et al, 1965) and transneuronal autoradiographic techniques (Grafstein, 1971; Lasek et al, 1968) demonstrated long range connectivity and Nissl staining revealed a remarkably consistent six layered distribution of the cells of cortex (O'Leary, 1941; Lund et al, 1979). Electrophysiological techniques had demonstrated that the brain showed specific localization of function (Hitzig and Fritsch, 1870; Ferrier, 1874) and this in conjunction with the subdivision of cortex using cytoarchitecture (Brodmann, 1905, 1909; Campbell, 1905; Economo and Koskinos, 1925) indicated that the functioning of the brain was a process that happened both near and far, in more than one place at any moment, as it functioned in the service of different requirements. Nevertheless the idea of cytoarchitectonics was contested even into the 1940's (Lashley and Clarke, 1946), as were many of the ideas we take for granted today, such as spatial representation of the visual field and binocularity, in V1 of rabbit, cat, and monkey (Talbot and Marshal, 1941; Thompson et al, 1950; Daniel and

Whitteridge, 1959) .

1.2 Recent developments and revelations.

More recent techniques for labeling cells with retrograde tracers such as horseradish peroxidase (HRP), demonstrated extensive projection of processes that could be traced back to the cells of origin and hence identify their lamina of origin (Gilbert and Kelly, 1975; Lund et al. 1975). Single cell injections made intracellularly (Stretton and Kravitz, 1969) showed that the local axon of a cell was far more extensive than had been considered and constitutes about 80% of the axon of most cortical cells (Gilbert and Wiesel, 1979; Martin and Whitteridge, 1984; Binzegger et al, 2004; 2007). This labeling method can fill and reveal the neuron in its entirety, axon and all. The striking features of the intracellularly labeled cells were the dense axon arbors within the local vicinity of the soma and dendrites and the long laterally projecting axons spanning millimeters. At this point the building of reliable libraries of cell morphologies began, made possible by replacement of the capricious Golgi method for the axoplasmically transported HRP (McEwen and Grafstein, 1968; Meller, 1992). The cells that appeared were of a type or several types, at least in the extensively studied cat and monkey. It was found that the same kind of cells populate the same layers and project their processes similarly, an approach that had proven useful since Cajal exploited the Golgi technique. Layer 1 shows very few cells and so appears almost empty. Layers 2 and 3 show a preponderance of cells with a triangular looking soma, referred to as pyramidal, which becomes larger with increasing depth, and with the largest dendrite, the apical dendrite, projecting radially from the top of the soma to terminate in the superficial layers. The dendrites of pyramidal cells are spiny. The axon of these cells projects down through the thickness of cortex producing many collaterals in layer 2/3 and 5 before it leaves the cortex and enters white matter. Layer 4 in some areas of cortex contains another type of spiny neuron, the

spiny stellate. Cell bodies in layer 4 tend to be more rounded as they do not have a distinct apical dendrite as do layer 2/3 pyramidal cells. Layer 4 is perhaps the most variable lamina in appearance depending upon species and cortical area. In the primate primary visual cortex there are up to four subdivisions of this lamina and either two (O'Leary, 1941) or three (Otsuka and Hassler, 1962) in primary visual cortex of the cat. Layer 4 is often the termination site for the incoming axons of thalamus and other, more distant areas, and the spiny stellate cells (found in only a few sensory areas) have axons that project locally, though still spanning several millimeters laterally, sometimes ascending to layer 3. Layer 5 is a slightly rarefied lamina populated by large pyramidal cells with axons that tend to rise superficially if the soma is located in upper layer 5 or remain deep if the soma is located in deep layer 5. The main axon projects down to leave the cortex. Stacks or palisades of smaller pyramidal cells fill layer 6 and in the primate an occasional solitary giant pyramidal cell of Meynert (layer 5 in the cat) sits at the border between layers 5 and 6. Most layer 6 pyramidal cells have an axon that projects superficially to innervate layer 4 with an efferent axon projecting to white matter in more than half of cases (Martin and Whitteridge, 1984). And this is the same pattern, more or less, seen everywhere in the cortex of mammals (with rodents a possible exception) that have been examined. One point not used in this summary being that this picture is based primarily on the excitatory cells which provide the main lamina structure of the cortex. The intrinsic, non-projecting, putative inhibitory cells which form about 20% of the population (Gabbott and Somogyi, 1986; Hendry et al, 1987) arborize locally, are roughly uniformly distributed between layers and so do not contribute to this broad brush-stroke picture of pyramidal cells.

1.3 Proposed circuitry.

There have been a number of attempts to embrace the structure of cortex and come up with something

universal, a simplification that would explain some of the complexity of cortex (Lorento de No, 1949; Hubel and Wiesel, 1974; Creutzfeld, 1977; Edelman and Mountcastle, 1978; Szentágothai, 1978; Rockel et al, 1980; Gilbert, 1983). All attempts at models used microscopic observations of neurons that together had a “basic uniformity of structure” (Rockel et al, 1980) and could be grouped in some manner to form repeatable chains or ensembles. What these models lacked was physiology.

The local recurrent axon was seized as a means to explain some of the physiological observations made by Douglas and colleagues (1989a, b; Douglas and Martin, 1991) in cat primary visual cortex. They noted that stimulating a cell in cat cortex via the optic radiations above the LGN resulted in a short duration excitatory postsynaptic potential (EPSP) followed by a long duration inhibitory postsynaptic potential (IPSP) first seen in cat motor cortex (Phillips, 1959). In addition, and most importantly, they noted that the cells of the deeper layers appeared to show more inhibition than those of superficial layers. The model they developed to account for the observed behaviour had a small excitatory thalamic input to a pool of recurrently connected excitatory neurons representing layers 2/3 and 4 and a balanced pool of similarly connected inhibitory neurons. Excitatory cells of the deep layers were represented too but with a much smaller contribution from thalamus to cortex and a larger weight of inhibition. This circuit which they referred to as the 'canonical microcircuit' and was felt could be applied to any cortical area as it was based upon a structural organization that could be found anywhere in cortex, hence 'canonical'.

1.4 The question again.

If the above intrinsic organization of an area contains the germ of a ubiquitous and repeatable circuit then how might an area obtain its functional specialization? If the intrinsic structure is the same everywhere that only leaves the long range or interareal connections to provide the difference. After

all, no cortical area remains unconnected from another areas or from subcortical nuclei.

The majority of cortical excitatory neurons are pyramidal cells, most of which possess an efferent axon (Martin and Whitteridge, 1984). This is an axon that projects through the cortex to the white matter, from there to another hemisphere, a sub cortical nuclei, or to re-innervate the cortex nearby in the same area, in an adjacent area, or even many millimeters away, centimeters even, depending on species. How and where these projections terminate, what pattern they form, has been yet another enormous endeavour to discover. The early work in this field used degeneration techniques to provide answers (Nauta and Gygax 1951). Using reduced silver techniques degenerating axon terminals could be identified with precision enough to reveal that the thalamic innervation of cortex terminated in cortical layer 4 (Kuypers et al, 1965) for example, a general observation that was to become the forerunner to describing many interareal connections. Though often this technique was a problem when distinguishing between retrograde and anterograde degeneration (Powell and Cowan 1964) as both were believed to occur at different rates when in fact the signal was ambiguous.

1.5 Feedforward versus feedback.

Using neuronal tracers such as HRP and Phaseolus vulgaris leucoagglutinin (PHA-L) Rockland and Pandya (1979) made a significant observation when using anterograde tracing to locate terminal arbors and their bouton-like swellings of interareal projections in monkey visual cortex. They found that axons in the occipital lobe of macaque that projected rostrally terminated in layer 4 and those that projected caudally terminated in layer 1. Something of this lamina specificity for termination sites had been seen earlier, as hinted at above (Kuypers, et al., 1965), and can be considered as an important feature of cortical organization. The authors went on to qualify their observations by referring to the layer 4 termination site as part of a 'feedforward' pathway and the layer 1 termination site as part of a

'feedback' pathway. The principle model for this being the projection from the dorsal lateral geniculate nucleus (dLGN) of the thalamus, which is close to sensory input, ascending to the primary visual cortex and terminating in layer 4. Progressing through occipital cortex in a rostral direction we ascend to higher visual cortical areas, hence the feedforward tag. In the caudal direction we descend through higher visual areas to lower visual areas, hence feedback.

There is a third pattern of connectivity between areas that is referred to as 'lateral' or 'columnar' (Maunsell and Van Essen, 1983). In this pattern we find all laminae innervated by axon with no apparent lamina preference. This kind of projection usually occurs between neighbouring, higher order areas. Originally referred to, tentatively, as an 'intermediate' projection it proved highly variable from experiment to experiment in that it was not always identified (Maunsell and Van Essen, 1983). It seems likely that the different patterns depend on what subgroups of projection cells have been labeled.

1.6 Cell Bodies and Hierarchy

The retrograde labeling of somata has provided another key structural feature. The feed forward pathway tends to be provided by the pyramidal cells of the superficial or supragranular layers plus a small contribution from infragranular layers and feedback to be provided by cells of the deep or infragranular layers with a small contribution of supragranular cells (Rockland and Pandya, 1979; Barone et al, 2000). Exploiting this fact, and using the relatively easy and reliable technique of retrograde labeling of cell bodies with fluorescence it became clear that physically or functionally close areas were extensively interconnected, as denoted by the number of labeled cells bodies. This degree of connectivity lessened with distance from the injection site (Kennedy and Bullier, 1985; Salin and Bullier, 1995, Rockland, 1997) and became known as the “distance rule”. This rule was refined and it became possible to establish a graded parameter with which to position cortical areas in relation to one

another (Barone et al, 2000). This provides a much more graded response to the question of relations with connected areas. The criteria of hierarchy for Barone et al, (2000) were based upon counting cell bodies in superficial laminae after having made large injections of fluorescent retrograde label in areas V1 and V4 thus providing them with a value, an SLN (percentage of labeled supergranular layer neurons). The SLN values provide directionality to the Felleman and Van Essen (1991) model in almost all tested cases.

This division of roles for pyramidal cells is not always so clear cut however and in some pathways there are contributions of axon made by cells from other laminae not normally associated with a particular pathway. An example as such is the feed forward V1 to V2 projection in macaque that also involves cells in layer 5 as well as layer 3 (Kennedy and Bullier, 1985). But these are dis-tractors to the great mass of data used to generate this model.

1.7 Models and hierarchy.

By describing feed forward and feed back pathways doors were opened for yet more structural organization and potential circuitry. Maunsell and Van Essen (1983) seized the opportunity to extend the back and forth relationship established by projections between cortical areas as described by Rockland and Pandya (1979) to create the idea of a hierarchy of cortical processing. This proposal has been consistently exploited ever since (Friedman 1983; Maunsel and Van Essen, 1983; Felleman and Van Essen, 1991; Young, 1992; Jouvé et al, 1998; Sporns et al, 2000; Barone et al, 2000; Ts'o et al, 2001). The description of the inter areal connections meant that the relationship between any two areas was known and could be fitted into a bigger picture. Felleman and Van Essen (1991) extended this by examining the reports of all available publications with a description of an interareal connection. They selected some 32 visual areas and 7 visual association areas amounting to 305 pathways. From this

pool of reported data they gleaned the appropriate information to build a hierarchical model of visual and visual association cortex accounting for some 55% of the cortex and produced a figure that became one of the most iconic wiring diagrams of its time. A figure that showed the relationships between cortical areas over 10 levels of 'processing'. It has all the inherent complexity and at the same time a known organization that we see in an engineering wiring diagram.

The Felleman and Van Essen diagram is not complete. The information they won came from published papers but also abstracts and even reports in direct conflict with one another. The majority of connections showed bi-directionality, an observation noted earlier in the squirrel monkey (Tigges et al., 1973: Rockland and Pandya, 1979). But often those reports failing to identify a reciprocal innervation simply did not look for it (Felleman and Van Essen, 1991). Again, it is possible that the location of the injection becomes critical, such as in terms of eccentricity of field (Zeki, 1978). But it seems more likely that connections are reciprocal as a rule, rather than not. Another generalization appears to be that feed forward arbors can be limited in their spread, but may consist of more than one terminal cluster in the target area. Feedback connections on the other hand show much more divergence in the spread of their terminal branches, as was inferred earlier, before single axons could be reconstructed (Krubitzer and Kaas, 1989; Shipp and Zeki, 1989). From this it was reasoned that the terminal arbor must cross functionally defined domains such as ocular dominance or cytochrome oxidase (CO) columns (Rockland, 1997). However this must occur with a great many axons in cortex, even extending over several millimeters, both intrinsic or local and interareal.

Some projections terminate in more than one lamina, the V1 to MT projection for example which terminates primarily in layer 4 but also layer 6 (Rockland, 1989). Feed forward projections like this also are predictable in that the secondary lamina of innervation is consistently smaller than that of the primary site. Similarly the feedback pathway from V4 to V2 shows a primary termination zone in layers 1 and 2 and a secondary termination in layer 6, again, always smaller with fewer collaterals than

the primary termination zone. This is the case also for the thalamocortical projection (Blasdel and Lund, 1983; Freund et al., 1989); the X and Y (cat) (Freund et al. 1985) or magno and parvicellular (monkey) components of which has been shown to terminate principally in layer 4 with a small contribution to layer 6. Much of the detailed light microscopy of single interareal axons of cortex has been studied by Rockland and colleagues using neuronal tracers (Rockland and Pandya,1979; Rockland 1989, 1992; 1994, 1995; Rockland and Virga, 1989, 1990; Rockland et al., 1994). Their extensive body of work amplifies what we know about the location of interareal axon terminals by providing the necessary detail. Feedforward axons terminate in layer 4, but sometimes focus on upper layer 4 and lower layer 3. One arbor of a single axon can selectively innervate layer 3 and another, from the same axon, to innervate layer 4. Collaterals may mostly innervate layer 4 but can also appear in layer 5 (V1 to V2, Rockland and Virga, 1990). Others can be seen to target layers 1 and 2 (V2 to V4, Rockland 1992; Rockland, 1997). But aside from these exceptions (which it is difficult to ascertain the significance of) it is the termination in layer 4 that characterizes the connection. The bi-stratified connection made by individual V1 axons in V5 (or MT) (Rockland, 1989, 1995; Anderson et al, 1998) appears to be thus far unique amongst feed forward corticocortical projections. V1 projections to neighbouring V2 have not been reported as bi stratified (Rockland and Virga, 1990) nor has V2 to V5 (Rockland,1995). The feedback path way as mentioned above terminates principally in layer 1 but also in layer 2 and layer 5 or 6. The detail reveals that layer 3 may also be targeted (V4 to V1 and V2, Rockland, 1994).

However neither the hierarchy nor the feed forward/feedback principle along with detail of anatomical connection tell us how all this connectivity functions to compute what it can. So again we come back to models which require a little more 'gradient' in their contribution.

1.8 Drivers and modulators.

Another theory proposed to account for cortical behaviour and derived from some of the above observations is the view that amongst neural pathways there are drivers and there are modulators (Crick and Koch, 1998; Sherman and Guillery, 1998; Guillery and Sherman, 2001; 2002). This view is essentially derived from the corticothalamic circuit in which the thalamus is considered to be closer to the periphery (the retina – the source of input), and the cortex, which is further from the retina and higher in the processing hierarchy. The feed forward input pathway from thalamus to cortex can be characterized as a driver targeting and driving cells in layer 4 and the feedback from cortex to thalamus as a modulator. The idea is that the driver transmits properties and activates the cortical cell under suitable stimulus conditions whereas the 'modulator' changes certain aspects of those properties through its influence on the classical receptive field for amplification and the non-classical receptive field for suppression of unsuited stimuli (Hupé et al. 1998). Given this ascending and descending pattern the same could be applied to corticocortical connections as they ascend and descend the cortical hierarchy. In the original proposition Crick and Koch (1998) used the selfsame organization as seen by Rockland and Pandya in their LM studies, with layer 4 receiving the driver input and layer 1 receiving the modulatory input. They proposed that there should be no 'strong' loops between areas. Two areas would never drive each other.

1.9 Cortical areas, connections and their properties.

1.9.1 V1 and V2

The connection between macaque cortical areas V1 and V2 shows features such as an ascending connection from V1 terminating in layer 4 of V2 and a descending projection from V2 terminating in superficial layers. Together these two areas are estimated to cover 24% of the macaque cortex

(Felleman and Van Essen, 1991) and to be massively reciprocally connected (Kennedy and Bullier, 1985). Kennedy, Barone and colleagues (2000) have shown that 81% of the corticocortical cells in V1 project to V2 and 88% of the corticocortical cells in V2 project to V1. Yet despite this apparent equity of numbers V1 remains responsive even after removing the huge feedback input from V2 (Hupé et al, 2001), but the same is not true in the reverse direction and V2 is reduced to silence when V1 is inactivated (Schiller and Malpeli, 1977; Girard and Bullier, 1989). This could be argued to fit nicely into the 'driver-modulator' hypothesis. But these interpretations in themselves do not explain the behaviour we see as the ideas of 'driving' and 'modulating' contribute no physiology other than a hypothesized net synaptic effect. In view of the above, a point worth raising here is the fact that although the dLGN may show driver properties the projection in monkey V1 may form as few as 10% of the excitatory synapses in layer 4 (Latawiec et al, 2000) and only 6% in the cat (Da Costa and Martin, 2009). Using biologically realistic models of thalamorecipient layer 4 spiny stellate cells, Banitt et al (2007) showed that not unless all dLGN afferent synapses fire in synchrony will the spiny stellate respond and once in steady state it requires the noise of background activity to respond (Banitt et al, 2007).We need something more functional to drive these arguments such as identifying synapses and their targets. There is another level of complexity to the V1-V2 dialogue involving the connectivity that underlies the patchy system of blobs of CO in V1 and their relation to thicker stripes of the same in V2 (Livingstone and Hubel, 1983; Sincich and Horton, 2002 a,b, 2005 a, b). This has some relevance for the V2 projection to V4 and V5, as will be described below.

1.9.2 V1 to V5

Another well trodden and extensively investigated pathway in visual cortex is that which takes us to area V5 or MT. This area receives a direct connection from V1 and was amongst the first extrastriate visual areas anterior to V2 to be identified, first by anatomical means in macaque (Zeki 1969) then by

both physiological and anatomical means in the New World owl monkey equivalent, or homologue, area MT (Allman and Kaas 1971). Accessibility to MT in the owl monkey made it the model of choice for Allman and Kaas (1974, 1975, 1976) who, using microelectrodes to record from individual and small clusters of cells, first described a complete map of the contralateral half of the visual field in this anatomically distinct area. The properties of cells in V5 have made it attractive though the input is intriguing too (Movshon and Newsome, 1984). The cells projecting from V1 to V5, determined by antidromic activation of cells in V1 (Movshon and Newsome, 1996) were fast conducting (suggesting heavy myelination and/or large diameter axons), binocular, complex, sensitive to high contrast, had contrast independent direction preferences, high spontaneous discharge (Gilbert, 1977) and large receptive fields (Zeki 1974). These properties are remarkably consistent between cells. The striking thing about cells in V5 is that they are sensitive to direction and velocity of motion (Dubner and Zeki, 1971; Malonek et al, 1994) which affects the perception of motion (Salzman et al, 1992). The emerging properties of the V5 cell appear to have gone through a phenomenal shift to a new capacity for motion processing computation. Visual areas less elevated within the hierarchical system have smaller receptive fields and do not show such sensitivities to motion. This is not to say that the receptive fields of these cells are not changing through successive stages of V1, V2, V3 and V4. In fact they get larger at each subsequent stage. However they all have visual receptive fields that respond to oriented gratings but not to the apparent motion created by two cross oriented sets of drifting gratings forming a plaid. They respond to movement of the component parts and not the composite. V5 does however have pattern selective neurons which the authors used to demonstrate that adaptation to a pattern or grating may reduce its sensitivity more than to other patterns. V5 receives direct input from excitatory cells of layer 4B and the large pyramidal cells of upper layer 6 in V1 in the form of large boutons distributed in patches (Lund et al, 1975; Shipp and Zeki, 1989; Rockland, 1989, 1995). There are indirect routes from V1 to V5 also, via superior colliculus (Fries et al, 1985) and pulvinar (Benevento and Rezak, 1976;

Ungerleider et al, 1983; Shipp, 2001). There is some ambiguity to the dependence of V5 upon V1 as V5 activity can be reduced by cooling or blocking V1 unlike V2 but activity in V5 will persist (Rodman et al, 1989). In the case of cooling it may be that the blocking effect may not reach the deep layer of V1 where the less frequent but very large Meynert cells are found (Lund et al, 1975; Shipp and Zeki, 1989). However another lesion in superior colliculus renders V5 largely unresponsive (Rodman et al, 1990) whereas a superior colliculus lesion alone has little effect.

1.9.3 V2 to V5

The extrastriate cortex closest to primary, striate, visual cortex is of course V2. As has already been pointed out there is a close relationship between V1 and V2. But what of the influence of V2 on V5? The projection is formed principally by pyramidal cells of layers 3B. A light scattering of contributing cells in layers 2, 3A and 5 complete the picture. This picture was derived from retrograde labeling with tracers (Lund et al, 1975; Maunsel and Van Essen, 1983; Ungerleider and Desimone, 1986) and the anterograde picture shows axons focusing terminals into layer 4 but spreading into superficial layers, even to layer 1 (Rockland, 1995), unlike the V1 projection to V5 which bifurcates to innervate layer 6 also, as stated above. Also unlike the V1 projection to V5, which was described as made up of large boutons borne on large caliber axons, the V2 projection is described as much more fine and bearing small boutons, though still with a patchy distribution, as in the case of the V1 projection (Rockland, 1995). How these morphological features might have an effect is unclear. Raiguel et al, (1989) showed that response latencies to a moving stimulus in V5 neurons, like those of V2, responded some 10 msec after V1 neurons. Yet the distance to V5 is considerably greater than from V1 to adjacent V2 and the authors note that the latencies are predictable from the known anatomy.

The V2 to V5 projecting cells are found in the thick stripes that stain for mitochondrial marker CO (Shipp and Zeki, 1985, 1989; DeYoe and Van Essen, 1985) . There is also evidence that projecting cells

in thick and pale CO stripes of V2 respond 20 msec earlier than those found in thin CO stripes (Munk et al, 1995). Regions of V2 that project toV5, have been shown to have a high proportion of binocular disparity selective cells and a low incidence of direction selective cells (DeYoe and Van Essen, 1985; Peterhans and von der Heydt, 1993). Reversible inactivation by cooling of V2 (and V3) led to V5 showing an extensive loss of tuning for binocular disparity relative to directional tuning (Ponce et al, 2008). Encoding for size and speed however still persists in V5 during inactivation (Ponce et al, 2011). Using data from human functional magnetic resonance imaging (fMRI) that measures the Blood Oxygen Level Derived (BOLD) signal, the effective connectivity between the 'driver' V2 and the target V5 has been shown to be modulated by attentional feedback, during visual motion (Friston and Buchel, 2000), from posterior parietal cortex (PPC), which provides an attentional input. In their model PPC provides a significant part of the input to V5/MT during attention.

1.9.4 V2 to V3A

After their description of area V3, Van Essen and Zeki (1978) went on to describe another two areas that lay rostral and medial to V3 and became known as PO (parieto occipital or V6) and V3accessory. After discovering that the area V3Accessory possessed a complete representation of both upper and lower hemifields (Zeki, 1978) the 'Accessory' was dropped in favour of V3A. Many of the visual areas in early extrastriate cortex showed similar properties to one another (Zeki, 1978). Cells of V2, V3 and V4 were largely orientation and motion selective with high numbers of colour-sensitive cells showing only in V4 and because of this it was felt that V3A must be part of the dorsal stream to parietal cortex. However it was shown also that there was temporal frequency tuning making it low pass filtered and with spatial frequency tuning similar to V1. This led to the idea that it was part of the ventral stream to V4 and the inferotemporal cortex (Gaska et al, 1988). Studies of stereoscopic depth perception in V3A (and V3) suggest there is encoding for absolute and not relative disparities, and neurons with similar

disparity selectivity are clustered (Anzai et al, 2011). In examining stereoscopy in both monkey and man the strongest activation to near/far disparity using fMRI was found to be in V3A (and V3). V3A appears also to be more motion sensitive in humans than in monkey when tested by fMRI (Tootell et al., 1997; Orban, et al, 2003). There are a number of higher order influences identified relating to eye position were first mentioned in the 'V2 to V5' section above. These influences have been seen in awake behaving monkey experiments, which found activity to be modulated by attention, anticipation, memory and saccadic eye movements (Nakamura and Colby, 2000). These authors and others found also remapping or updating of the stimulus representation in V3A (Thiele et al, 1999; Nakamura and Colby, 2002) as it appears also in lateral intraparietal cortex (LIP) (Duhamel et al, 1992). Remapping may be the means we have of keeping a stable visible world despite constant eye movement.

The influence of modulation clearly anticipates the involvement of hierarchically placed 'higher' areas such as frontal eye fields (FEF), which we know to be reciprocally connected to V3A (Schall et al, 1995; Stanton et al, 1995). Placed the fourth level within the Felleman and Van Essen (1991) model of cortex, V3A receives input from V1 (Zeki, 1978; Van Essen et al, 1986), V2 (Gattass et al, 1997), and V3 (Felleman et al, 1997). When V1 is cooled (reversibly blocked) about 30% of V3A cells continue to respond to moving stimuli while V3 is silenced (Girard et al, 1991). Both LIP and FEF have been shown to be reciprocally connected with V3A (Morel and Bullier, 1990; Blatt et al, 1990; Baizer et al, 1991; Nakamura et al, 2001;Stanton et al, 1993). Other areas connected to V3A include the ventral as well as the dorsal (e.g. V5/MT) streams. Dorsal targets include medial superior temporal area (MST; Boussaoud et al, 1990), superior temporal visual area (FST; Boussaoud et al, 1990), PO (Colby et al, 1988; Shipp et al, 1998) and ventral targets including ventral posterior area (VP; Felleman et al, 1997), TEO (Morel and Bullier 1990; Webster et al, 1994). The detailed axonal morphology of V3A projections has not been described.

1.9.5 V4 to V2

The V4 to V2 projection in macaque must be the archetypal feed back projection if only because it is amongst the first pathways to be encountered by Rockland and Pandya (1979) in their discovery of the rostro-caudal feed forward/feedback rule in visual cortex. Also, it is readily accessed both for injecting tracers and recovering axon terminals. Felleman and Van Essen (1991) placed V4 at about the fifth level in their model of cortical hierarchy. The characteristic of feedback projections is that they terminate in layer 1. Layer 1 is a layer almost devoid of cell bodies except for a few cells with smooth dendrites that stain immunopositive for glutamicacid decarboxylase (GAD) (Ribak, 1978) or γ aminobutyricacid (GABA) (Gabbott and Somogyi, 1986; Fitzpatrick et al, 1987), though there have been accounts of stray spiny pyramidal cells being filled in layer 1 in the case of cat cortex (Anderson et al, 1992). Rockland describes the termination as mostly in layer 1 and sometimes other layers but *avoiding* (my italics) layer 4 (Rockland, 1997). Axon collaterals can encroach on layer 2 also and layers 5 (when terminating in V1) or 6 (Rockland, 1992; Rockland et al, 1994). We expect to see clustered feed forward axon terminals. In contrast, feedback terminals have been found to spread, up to 1 or 2mm (Krubitzer and Kaas, 1989; Ship and Zeki, 1989; Suzuki et al, 2000; Stettler et al, 2002; Rockland, 1997).

1.9.5.1 Substreams of Cytochrome Oxidase.

Many of the 'early' stages in the cortex no doubt received a lot of attention because of their proximity to the sensory periphery. But whatever it is that draws interest to early visual processing it was here that an apparent divergence into dorsal and ventral streams was discovered and first described by Ungerleider and Mishkin (1982). The dorsal stream was considered an extension of the magnocellular

pathway and the ventral to be parvicellular. Chasing these streams has been another neuroscientific industry. One of the means for doing this is in the use of CO staining. As described above the staining of different (thick, thin and pale) stripes in V2 is also congruent with cell properties devoted to particular stripes so that the cells of the thicker stripes respond some 20 msec sooner than those of thin stripes (Livingstone and Hubel, 1982; Munk et al, 1995). The mapping of CO rich patches or blobs, part of the parvicellular pathway, from V1 to V2 (Sincich et al, 2010) and V4 indicates that V2 receives input from the patchy, or blob, system of V1 (Sincich and Horton, 2005b) and thicker pale and dark staining stripes in V2 project to V3 and V5 leaving the thin stripes to project to V4 in the ventral stream (Yoshioka and Dow, 1996; Shipp and Zeki, 1985, 1989, 1995; De Yoe and Van Essen, 1985; Sincich and Horton, 2003).

1.9.6 Frontal eye fields (FEF) to V4, Area 46 and Lateral intraparietal cortex (LIP)

FEF has been variously described, sometimes known as area 8A (Saleem and Logothetis, 2007), 8Ad and 8Av (Petrides et al, 1999, 2005) and 8A inclusive of some of area 45 (Walker, 1940). FEF has been shown to lie in the anterior region of the cortex between the principal and arcuate sulci of prefrontal cortex (PFC). The area is well known if not understood since the presentation of a landmark paper on the brain of the anaesthetized monkey by Ferrier in 1874, to the Royal Society. One of several things he reported was that with electrical stimulation of this anterior region of the brain there was a shifting of the eyes and head that redirected the gaze. This behaviour has since been defined as being composed of saccadic and smooth pursuit eye movement (Fuchs, 1967). Even today this region is most accurately defined by relatively low electrical currents being applied to the region to induce eye movement behaviour (Robinson and Fuchs, 1969; Schiller et al, 1979; Goldberg and Bushnell, 1981). There are histological features which distinguish the area, such as large pyramidal cells in layer 5 (Stanton et al, 1989), which is also a feature of motor cortices (Campbell, 1905). Large layer 3 pyramidal cells have

also be identified (Stanton et al, 1989) as well as a granular layer 4. This latter feature being normally associated with sensory or cognitive but not motor cortices.

Despite its location remote from sensory cortices there is a clear connection with the most posterior occipital lobe and specifically V4 (Huerta et al, 1987; Stanton et al, 1995). FEF is placed in a high position in the hierarchical model relative to V4 (Maunsell and Van Essen, 1983; Felleman and Van Essen, 1991). Given this configuration we would expect and in fact find a modulatory effect on the bottom up or feedforward pathway (Ekstrom et al, 2008). Using microstimulation of FEF in macaque whilst using fMRI to detect cortical activity Ekstrom et al, (2008) found higher order areas were modulated, independent of a visual stimulus. They found also that early visual areas could be strongly enhanced or suppressed, but only with a relevant stimulus plus distractors. The source of this FEF projection has been shown by use of retrograde tracers to be supragranular pyramidal cells (Pouget et al, 2009)

The hierarchical distance between FEF and V4 within the Felleman and Van Essen (1991) model was not confirmed when using the criteria of Baronne et al, (2000). Felleman and Van Essen assembled their hierarchy by comparing pairs of areas starting with the earliest area, V1. This meant that there were a huge number of possible configurations (Hilgetag et al, 1996) due to the lack of information about what distance went between hierarchical levels. Barone et al (2000), using their SLN approach provided a much more finely grained parameter for determining hierarchy which largely confirmed the picture of Felleman and Van Essen (1991) with one exception of FEF to V4. Felleman and Van Essen had FEF placed two levels higher than V4 which predicts a feedforward pattern to FEF (Barbas and Mesulam, 1981) and therefore a feedback connection to V4. Barone et al, (2000) using their SLN method had FEF in a feedforward relationship to V4. The authors go on to indicate a number of discrepancies in the relation of FEF with other areas of the hierarchy based upon anatomy such as TEO and TE forming latereal connections with FEF (Distler et al, 1993, Webster et al, 1994; Schall et al,

1995). This led Markov and Kennedy (2013) to propose a hierarchical model, still using their SLN values, but based on the short path length and high clustering of the so-called Small-World-Graph (Watts and Strogatz, 1998) in which they also included the dorsal and ventral streams of visual processing (Ungerleider and Mishkin, 1982). In their model FEF has a feedforward projection to V4. FEF has been a magnet to researchers which has led to extensive functional investigation. There have been roles for FEF demonstrated in spatial working memory (Balan and Ferrera, 2003), in decision making by rapid shifting of category boundaries, suggesting flexible links underlying cognitive processes, (Ferrera et al, 2009) and perhaps most topically, mechanisms of attention (Moore and Fallah, 2001; 2004). Attention could be described as something that regulates the flood of sensory information into a manageable stream (Buschman and Miller, 2009). That 'something' has been hotly sought, and often 'found' in the form of an enhanced or oscillatory relationship between FEF and extrastriate visual cortex. Reynolds et al. (1999, 2000) reported that there are competing populations of neurons and that attention biases the competition. The apparent increase in sensitivity to a stimulus falling within an attended receptive field was an increase of 1.5 in effective contrast. Spontaneous activity was up to 30-40% higher when attention is directed to a receptive field even with no stimulus in the receptive field (Luck et al, 1997). Performance in an awake behaving monkey can be improved when an attended object falls within the site of microstimulation (that is, less than sufficient to evoke movement) (Moore and Fallah, 2001). Serial covert shifts in attention during search strategies have been shown to be related to neuron population oscillations (Buschman and Miller, 2009). Enhanced oscillatory coupling between FEF and V4 can be seen when a stimulus falls within the receptive fields of both areas (Gregoriou et al, 2009). V4 neuron responses to selectivity were enhanced by 26% when attended and in V1 by 8%. Selectivity however was not systematically changed by attention nor was there systematic change of a neurons undriven activity (McAdams and Maunsell, 1999). Individual neurons in V4 have also been shown to code for both spatial and feature directed attention (McAdams and Maunsell, 2000).

Passively attending monkeys have been stimulated, sub threshold, in FEF to influence V4 and producing changes similar to voluntary effects (Armstrong et al, 2006;Armstrong and Moore, 2007). The most anatomical attempt at building the circuitry of attention is perhaps that of Mitchel et al, (2007). Awake behaving monkeys performed a task of attention as action potentials in V4 were recorded. The action potential width was classifiable as either narrow or broad and those with a narrow spike were more attention dependent, producing increases in firing rate. The significance of spike width led the authors to believe that they were recording from parvalbumin positive interneurons and were either basket cells or chandelier cells, both known to be inhibitory, (Connors and Gutnick, 1990; Kawaguchi, 1993; Nowak et al, 2003) and showed higher and larger attention dependent increases in firing rates (Mitchell et al, 2007). Neurons with broad action potentials were inferred to be pyramidal or excitatory cells (Connors and Gutnick, 1990). This bimodal distinction has been made in a number of cortical areas including PFC (Wilson et al, 1994: Rao et al, 1999; Constantinidis and Goldman-Rakic, 2002). If this scenario were the case we would expect a monosynaptic connection from FEF (Huerta et al, 1987; Stanton et al, 1995) to arrive on inhibitory cells in V4. This pattern would occur to a lesser extent in V2 (Markov et al, 2011) and V1 (Clavagnier et al, 2004) if only because the attention related effects are diminished in V2 and V1 (Luck et al, 1997; Buffalo et al, 2010) perhaps due to more inhibition.

Strongly bound to and physically adjacent to FEF is area 46 of prefrontal cortex (PFC), which forms a reciprocal monosynaptic connection with FEF (Barbas and Mesulam, 1981; Barbas and Pandya, 1989; Huerta et al, 1987; Schall et al, 1995; Stanton et al, 2005; Petrides and Pandya, 2007). Placed in the Felleman and Van Essen (1991) hierarchy at two levels higher than FEF, this area has been shown to be involved in movement preparation (Goldman-Rakic, 1987) and reward expectation (Leon and Shadlen, 1999). Visual motion is represented in area 46 with precision equal to that of neurons in cortices

involved in early visual processing (Hussar and Pasternack, 2009). Linking visual information to appropriate motor output is strongly implicated in area 46 (Miller and Cohen, 2001) and awake behaving monkey studies have demonstrated that direction selectivity decreases in narrow-spiking cells when judging motion speed and ignoring direction (Hussar and Pasternack, 2009). When direction of the stimulus remains relevant both narrow-spiking and broad-spiking cells remain sensitive. To explain these results the fast or narrow-spiking neurons were again assumed to be GABAergic inhibitory cells (Connors and Gutnick, 1990), which showed a more pronounced decrease in activity than the broad spiking neurons that were assumed to be pyramidal neurons. A further experiment by Hussar and Pasternak (2012) attempted to demonstrate the top down influence of area 46 providing maintenance and comparison. When two stimuli are separated by a delay the broad spiking cells exhibit anticipatory modulation and during the second stimulus presentation both narrow and broad spiking cells show modulation. For the authors this meant that two types of modulation are supported by two types of neurons, indicating the circuitry underlying decisions. In this case, again following Connors and Gutnick (1990), the narrow and broad spiking types were inferred to be inhibitory interneurons and excitatory pyramidal cells respectively. This interpretation was also defended by the argument that pyramidal cells provide the top down modulations and the inhibitory cells the local processing (Rockland, 1997; Markram et al, 2004). This is at odds with the view that local processing is clearly dominated by the locally arborizing axons of pyramidal cells of which 80% is local (Douglas and Martin, 1989a; Binzegger et al, 2007). The GABAergic inhibitory cells form only 20% of cortical neurons in V1 (25% in areas 4, 3b, 1, 2, 5, 7, 18 and 21, Hendry et al, 1987; 25% in mPFC, Gabbott and Bacon, 1996) and symmetric synapses only 16% of all synapses (Beaulieu and Colonnier, 1985; Beaulieu et al, 1992).

In posterior parietal cortex of macaque lies the lateral intraparietal area (LIP) at one level below FEF

within the Felleman and Van Essen (1991) hierarchy. Using single cell recording and neuronal tracers the region as a whole has been shown to be clearly segregated into somatosensory (area 7) and visual or visuo-motor areas (LIP) (Andersen et al, 1990) with reciprocated connections to extrastriate cortex. Cells of LIP have shown saccade related and pre saccadic planning responses (Barash et al, 1991). In reaction time motion discrimination tasks with a saccadic response, sub threshold microstimulation drives the saccade to the response field of the cell clusters being stimulated (Hanks et al, 2006) which indicates decision formation in the discharge of these neurons. Receptive fields in LIP are larger than those of neighbouring areas, and form an orderly progression and a rough topographic representation (Blatt et al, 1990) though the degree of organization is debated (Patel et al, 2010). The majority (60%) of neurons in LIP of alert monkeys are direction selective (Fanini and Assad, 2009). Neurons in LIP are known to have their response activity modulated by the reward expected from an eye movement (Platt and Glimcher, 1999; Bendiksby and Platt, 2006). In fact most LIP neurons (96%) respond when a saccade brings the location of a previously flashed stimulus into the receptive field (Nakamura and Colby, 2001). LIP has also been described as the shape area because of the sub group of cells found to encode stimulus shape (Janssen et al, 2008). This could be important in relation to the nearby area of anterior intraparietal cortex and its significance in hand shaping for grasping (Sereno and Maunsell, 1998; Sereno and Amador, 2006). There are indications also that LIP is also involved in proactive or non-reactive movement preparation achieved by increases in spike activity during periods of pro-activity that do not result in movement (Maimon and Assad, 2006).

1.9.7 Better resolution

The above is a description of some of the behaviour we can find from amongst different cortical areas. What is missing from most of the above is the synapse. Without some knowledge of the synapse we are

at a disadvantage when having put the parts together, how to weight their function. We have already introduced the term synapse in the earlier section on the canonical microcircuit of Douglas et al (1989a) without going into detail. The first appearance of the term was in a contribution by Charles Sherrington in 1897 to a text book of physiology (Foster 1897). The word meaning 'clasp', derived from the Greek, and was introduced to account for the connections predicted to exist between neurons. It was not accepted too readily by anatomists as they still had an investment in the idea of a network or reticulum connected by anastomosing fine-process-to-fine-process rather like the venus and arterial blood vessels, and born of a syncitium or common pool of undifferentiated cell protoplasm and nuclei. Physiologists on the other hand accepted it more readily to help account for some of their findings in the reflex arc for instance. Their problems revolved around differences in the sensory nerve terminal from the peripheral nerve such as delay in transmission, resistance requiring summation, persistence and one-way transmission. The synapse it was felt could solve these issues, but it was not until the 1950's that the cortical synapse was identified in the electron microscope as a specialized surface of separation between pre and post synaptic structures in cerebellum (Palade, 1954), neuromuscular junction (Palade and Palay, 1954) and cerebrum (Palay, 1956). Schultz et al (1957) described a number of features now accepted as 'key' to synapse identification, yet they went on to dismiss them as being unlikely to be specific criteria for synapse identification. The membrane specialization, using the criteria now in common use, was the means of identifying the two types of synapse (Gray, 1959a; Gray, 1959b) which Gray called Type 1 and Type 2. The former also known as asymmetric because of the extensive postsynaptic density, were usually found forming with spines and the latter, known as symmetric because of the much smaller postsynaptic density, with soma and dendritic shafts. The morphology of the vesicles in the presynaptic bouton was also characteristic, Type 1 had round vesicles and Type 2 had pleomorphic vesicles (Colonnier, 1968). The attribution of different functions of the two types of synapse came from Eccles et al, (1964) who had been working on inhibition and excitation the

cerebellum and was led to conclude the function from form we use today (Uchizono, 1965) which is that Type 2 are inhibitory and therefore Type 1 are excitatory. In the 1970's Szentagothai (1978) began to use the EM in conjunction with light microscopy to look for synapses in the EM where he had seen close appositions in the LM. This process of correlating light and electron microscopy (Blackstad, 1965; Stell, 1965) using degeneration or Golgi in conjunction with other labels, was used to identify chains of connectivity (Peters et al, 1977; Somogyi, 1978; Somogyi et al, 1979; Freund and Somogyi, 1983).

All of the above techniques provide the possibility of making great insight into connectivity and function at fairly high resolution and today is a vital component many network models. What is still almost entirely without the support of data is a quantitative, synaptic level description of the interareal connections in the Old World monkey. The only existing EM documentation of connections between areas in monkey neocortex, prior to the studies described here, were carried out by Rockland and Douglas (1993) in layer 1 of area V1 after injecting into V2 a bolus of biocytin. From a number of short series of ultrathin sections they could identify target spines and dendritic shafts forming asymmetric synapses with the anterogradely labeled 'feedback' axon. The majority of targets were spines (82%) which the authors point out is in agreement with 'the general principles of pyramidal cell connectivity' from many earlier EM studies of local circuitry of injected cells in cat and monkey (McGuire et al, 1984; Saint Marie and Peters, 1985; Kisvarday et al,1986; Gabbott et al, 1987; White, 1989; McGuire et al, 1991; Anderson et al, 1994a). The one exception to this is the finding of Melchitzky et al (2001) in the local connections of macaque area 9 of PFC. They showed that targets were equally divided between spines and GABAergic dendrites. Projection cells are pyramidal cells bearing spines (Lund et al, 1975), and their synapses are type 1 or asymmetric and most are formed with spines (Beaulieu and Colonnier, 1985) which are a morphological feature of the two types of excitatory cells: pyramidal and spiny stellate cells. The picture for excitation is well-supported but what this picture does not provide is

the GABAergic smooth cell targets. Since the GABAergic target of certain pathways features strongly in a number of models used to explain the observed physiology this information is clearly important.

It has been demonstrated that measured areas of postsynaptic densities showed a range of sizes in cat primary visual cortex (Ahmed et al, 1994; 1997; Anderson et al, 2009; Da Costa et al, 2011, Da Costa, 2012;), rat hippocampus (Harris and Stevens, 1989) and mouse barrel cortex (Knott et al, 2006). What the relationship between synapse size, functionality and location might be is receiving some attention, but brings forth little that is conclusive as yet. There is evidence of a relationship between spine head size and synapse size though the strength of this relationship varies between studies. In hippocampus (Harris and Stevens, 1989) and mouse (Knott et al, 2006) the relationship is much stronger than for intracellularly injected spiny stellate cells in cat (da Costa and Martin, 2011). Although when the sample is analyzed closely it appears that there maybe more than one population present in the former two studies and removing the large outliers renders the relationship much weaker. Issues relating to the inhibitory synapses have not received the same attention as yet.

From all of the above it is clear more information is needed to confirm or modify models and their assumptions for which the EM is perfectly suited. Clearly however there is more to be gained from detailed microscopy than simply confirming or otherwise the fine points of the models of others. The identification of synapses formed between areas and the targets with which they synapse becomes important if we are to move from untethered neurophysiology and assumptions about function. It seems that at its center the cortex is devoted to the local network where computations are synthesized using most of the cells resources (~80% of its synapses). The distribution of these computations to other areas appear similar in obvious ways, namely excitatory synapses forming with excitatory cells with a modicum of inhibition amongst their targets. The difference in the processing being that the

information is passed between areas using such small numbers of synapses, hence the need for amplification. The high resolution detail of microscopy and neurophysiology can change both the appearance and performance of our models and provide circuits to explain cortical properties but as yet this expectation has been slow to follow. It seems unlikely that any circuit composed of overly simplistic or overly extended connection patterns will explain the biology. Having said this however just over 100 years ago we had the first models of circuits as chains of connected cells behaving much as we want our models to do now and in their time such early models were enough to help generate the concept of the reflex arc for instance which still stands today. Much more highly developed networks are now possible and these can be used to create elaborate behaviours such as a model for reading based upon the canonical microcircuit and what is known of FEF saccadic eye movements (Heinzle et al, 2007) which has been established by using anatomy (both known and predicted) and physiology. The flow of information through the network not only makes the local computation possible but it can be also distributed in such a way as to enhance or suppress, creating relevance for the organism which our models try to capture, using limited knowledge.

Instead, like the canonical microcircuit, which appears superficially simple, like a rope, but is in fact the sum of many better understood threads.

Chapter 2 Materials and Methods

Numbers and species of Old World monkeys used in these studies are described in each Materials and Methods section of the published papers.

2.1 Veterinary Authorities

Experiments were carried out in the Stem Cell and Brain Research Institute, Lyon, France; University of Iowa, Hospitals and Clinics, USA; Institute for Neuroinformatics, Zurich, CH.

Animal treatment and surgical protocols were carried out in accordance with the guidelines of the Direction départementale de services vétérinaires du Rhône, the Kanonal Veterinaeramt of Zurich or the institutional and federal guidelines as specified in the Animal Care and Use Research Forms of the USA.

2.2 Surgical procedures

Animals were prepared for surgery after intramuscular premedication with Largactil (0.5 ml), atropine (1.25 mg) and dexamethasone (4 mg) followed by ketamine hydrochloride (20 mg/kg) or ketamine hydrochloride (10 mg/kg) and xylazine (0.5 mg/kg) followed by alphaxalone/alphadalone (Saffan). Anaesthesia was continued with Halothane in N_2O and O_2 (70:30).

Alternatively surgery followed a premedication of ketamine (11 mg/kg) and deep anaesthesia following intravenous Nembutal (25 mg/kg) supplemented as required.

In the final alternative procedure animals were prepared for surgery after the administration of an intramuscular premedication of xylazine (Rompun, Beyelar, 0.5 mg/kg)/ketamine (Ketalar, Parke Davis, 10 mg/kg). This was followed by cannulation of a femural vein for the delivery of

alphaxalone/alphadalone (Saffan, Glaxo) to establish complete anaesthesia.

Lidocaine gel (Streudi & Co.) was applied to pressure points.

Anaesthesia was continued with Halothane in N_2O and O_2 (70:30).

2.3 Neuronal tracers used and method of delivery:

pressure injections of the neuronal tracers biotinylated dextran amine (BDA) (Molecular Probes, Leiden, Netherlands) and *Phaseolus vulgaris* leucoagglutinen (PHA-L) (Vector Laboratories, Burlingame, CA). Injections of 10% BDA in 0.01 M phosphate buffered saline (PBS) and 2.5% PHA-L in 10nM phosphate buffer (PB). The pressure injections were made with a Hamilton syringe. Ionophoretic injection of biocytin (Sigma) as a 4% solution in Tris buffered KCl (0.2M). The ionophoretic injections were made with a glass micropipette using a pulsed ionophoretic current ranging from 1mA -4 mA over a 7-10 minute period.

2.4 Care, Recovery, Perfusion

Post experimentally antibiotics were applied topically to the head wound (Soframycin, Aventis) and intramuscularly (Clamoxyl, GaxoSmithKline, 10 mg/kg. Analgesia was managed with buprenorphinum (0.01 mg/kg, Temgesic, Essex Chemie AG). Survival periods ranged from 1 to 14 days.

Prior to perfusion each animal was induced with alphaxalone/alphadalone and deeply anaesthetized with intravenous pentobarbital (20 mg/kg) and then perfused transcardially with a normal saline solution, followed by a solution of 3.5 - 4% paraformaldehyde, 0.3 – 0.8 % gluteraldehyde and 15% picric acid in 0.1 M PB pH7.4. In some cases the fixative perfusion was followed by perfusion with sucrose (10-20 %) in 0.1M PB

2.5 Histology

The brain was removed from the skull and a block of cortex containing the injection site and other areas were separated from the brain. The block was allowed to sink in sucrose solutions of 10, 20 and 30% in 0.1 M PB, then freeze-thawed in liquid nitrogen and washed in 0.1 M PB. Sections were cut from the block at 80 μm in the parasagittal or coronal plane and collected in 0.1 M PB.

washes in PBS were followed by 10% normal swine serum (NSS) in PBS (1 hour). Further washes in NSS preceded overnight exposure (5°C) to an avidin-biotin complex (Vector ABC kit - Elite). The peroxidase activity was identified using 3, 3-diaminobenzidene tetrahydrochloride (DAB). After assessment by light microscopy selected regions of tissue were treated with 1% osmium tetroxide in 0.1M PB. Dehydration through alcohols (1% uranyl acetate in the 70% alcohol) and propylene oxide allowed flat mounting in Durcupan (Fluka) on glass slides.

2.6 Light and Electron Microscopy

Light microscopic (LM) observations and digitization of labeled axons, using Traka, an in-house 3D LM reconstruction system, were carried out to locate and select regions of interest for electron microscopy (EM). We reconstructed individual collaterals in the less densely innervated areas for correlated light and electron microscopy. Serial ultrathin sections were collected at 60 or 70nm thickness on Pioloform coated single slot copper grids. Labeled boutons were photographed at a magnification of 21,000. Synapses and associated structures were classified using conventional criteria (Peters et al, 1991). We used a Philips CM100 electron microscope with a Morada camera and ITM software.

2.7 3D EM

Collections of serial sections were digitized and reconstructed using Trakem, an in-house EM-digitization package. Trakem generates a series of wire frame profiles which gives a 3D impression. This effect was enhanced by fitting a skin to the digitized structure and then rendering the surface. The skin fitting used Nuages (B. Geiger, 1996) and the rendering used Geomview and Blue Moon Rendering Tools (L. Gritz). We also used Reconstruct (Fiala, 2005) for reconstructing and measuring profiles.

Synapse reconstruction was necessary for the measurement of post synaptic densities. A semi-automated process first grouped the serially sectioned components of synapses. The postsynaptic surface was represented as a 3D grid that was created by interpolating points between components and measurements were made by summing the areas of the triangles formed between the interpolated points. To show the ranked areas we presented an optimal plane of view for each reconstruction, they are not 'flattened' in these figures.

2.8 Counting Synapses and Measuring

To estimate the density of labeled synapses we used unbiased stereological methods (Sterio, 1984) and the adaptation by da Costa et al, (2009). This procedure requires the random sampling of many (~1000) small sites from the tissue area to be tested. This proved to be more unbiased than our previous measures of density in which we used collections of analogue prints taped together.

To measure ultrathin section thickness we used the Small fold method (Small, 1968).

Chapter 3 Publications

The following publications are presented chronologically.

3.1 The first in the series of studies on interareal connectivity was a collaboration between the Rockland lab and Zurich looking at striate V1 to extrastriate MT (V5). Rockland had made a number of LM observations about this projection that could prove interesting at EM. The appearance of the terminals was very 'thalamic -looking' in that the boutons appeared large, the axon to be well myelinated and the collaterals to be in two characteristic laminae, 4 and 6. These facts and the extensive body of physiological work looking at the coding of cells in MT for motion in this classic feedforward pathway made this a very interesting place to begin.

The Journal of Neuroscience, December 15, 1998, *18*(24):10525–10540

The Connection from Cortical Area V1 to V5: A Light and Electron Microscopic Study

John C. Anderson,[1] Tom Binzegger,[1] Kevan A. C. Martin,[1] and K. S. Rockland[2]

[1]*Institute for Neuroinformatics, 8057 Zürich, Switzerland, and* [2]*University of Iowa Hospitals and Clinics, Iowa City, Iowa 52242*

Area V5 (middle temporal) in the superior temporal sulcus of macaque receives a direct projection from the primary visual cortex (V1). By injecting anterograde tracers (biotinylated dextran and *Phaseolus vulgaris* lectin) into V1, we have examined the synaptic boutons that they form in V5 in the electron microscope. Nearly 80% of the target cells in V5 were spiny (excitatory). The boutons formed asymmetric (Gray's type 1) synapses with spines (54%), dendrites (33%), and somata (13%). All somatic targets and some (26%) of the target dendritic shafts showed features characteristic of smooth (inhibitory) cells. Each bouton formed, on average, 1.7 synapses. The larger boutons formed multiple synapses with the same neuron and completely enveloped the entire spine head. On most dendritic shafts and all somata the postsynaptic density *en face* was disk-shaped but in about half the cases the reconstructed postsynaptic densities of synapses on spines appeared as complete or partial annuli. Even in the zones of densest innervation only 3% of the asymmetric synapses were formed by the labeled boutons. Although the V1 projection forms only a small minority of synapses in V5, its affect could be considerably amplified by local circuits in V5, in a way analogous to the amplification of the small thalamic input to area V1.

Key words: visual cortex; area MT; corticocortical; synapse morphology; postsynaptic target; 3-D reconstruction

The best-studied extrastriate area is that first discovered by Zeki (1969), who used anatomical methods to define an area in the posterior bank of the superior temporal sulcus in macaque monkey that received an input from area 17. The homologous area in the new-world monkey is the middle temporal area (MT) (Allman and Kaas, 1971). From the earliest recordings, it was evident that the neurons of this area, now called MT or V5, were particularly sensitive to the direction and velocity of motion of the stimulus (Dubner and Zeki, 1971).

There are both direct and indirect projections from V1 to area V5 (Zeki, 1969; Ungerleider and Mishkin, 1979; Maunsell and Van Essen, 1983; Fries et al., 1985). The neurons that project directly from V1 have been identified as spiny stellates and pyramidal cells in layer 4B and large pyramidal cells in upper layer 6 (Lund et al., 1975; Shipp and Zeki, 1989). Their afferent axons form large boutons in a patchy distribution in layers 3, 4, and 6 of V5 (Rockland, 1989, 1995). The receptive fields of the V1 neurons that project to V5 have also been studied. The projecting neurons were identified by antidromically activating them from V5 (Movshon and Newsome, 1996). They had fast-conducting axons and all were binocular, complex cells, with high-contrast sensitivity and contrast-independent direction preferences. They responded at least as well to short stimuli as to long stimuli. Such complex cells are referred to as special (Palmer and Rosenquist, 1974) and have the largest receptive fields, the highest velocity preference, and the highest spontaneity of striate cortical cells (Gilbert, 1977). This degree of uniformity in physiological properties seems to indicate that MT uses this output from V1 for further stages of specific processing. Movshon and Newsome (1996) suggested that these V1 neurons form the first stage of motion processing, in which the motion of the individual components of a pattern is extracted (Adelson and Movshon, 1982; Movshon and Newsome, 1984). The second stage occurs outside V1, in areas such as V2 and V5, where the motion of the entire pattern is computed.

If the V1 output to V5 is blocked, by making lesions or cooling V1 or blocking the magnocellular pathway, some activity persists in V5, but it is greatly diminished from normal. Although these experiments do not distinguish between the direct and indirect projection from V1 to V5, it is likely that the output from V1 is significant for V5. Anatomically, however, the picture is unclear. As yet there are not even qualitative estimates of the numbers of synapses involved in the V1 to V5 projections. In the present study we assessed the synaptic connections formed in V5 by the V1 projection neurons. Although the manner of connection of the V1 afferents to neurons in V5 was morphologically distinct, quantitatively they formed only a few percent of the synapses within their major termination zones in V5.

MATERIALS AND METHODS

The materials examined in this study were obtained from two adult *Macaca mulatta* monkeys in the laboratory of K.S.R. (University of Iowa Hospitals and Clinics). The monkeys were prepared for surgery with a premedication of ketamine (11 mg/kg). Surgery was performed under deep anesthesia induced by intravenous delivery of Nembutal (25 mg/kg) and supplemented as required. All procedures were performed under sterile conditions in accordance with institutional and federal guidelines as specified in approved Animal Care and Use Research Forms.

One animal received a single microinjection of 10% biotinylated dextran amine (BDA) (Molecular Probes, Eugene, OR) in 0.0125 M PBS into cortical area V1. The second animal received a similar microinjection of BDA and a second injection of 2.5% *Phaseolus vulgaris* leucoag-

Received June 23, 1998; revised Aug. 27, 1998; accepted Sept. 14, 1998.

This work was supported by a Schweizer Schwerpunkt Programme Swiss National Science Foundation grant to Professor R. J. Douglas and K.A.C.M. and by National Institute of Mental Health/National Science Foundation Grants MH 53598 and IBN 9421970 to K.S.R. We are grateful to Professors W. T. Newsome and M. N. Shadlen for their critical reading of an earlier draft of this manuscript.

Correspondence should be addressed to John C. Anderson and Kevan A. C. Martin, University/ETH Zürich, Winterthurerstrasse 150, 8057 Zürich, Switzerland.

 0270-6474/98/1810525-16$05.00/0

glutinen (PHA-L) (Vector Laboratories, Burlingame, CA) in 10 nM phosphate buffer (PB) (see Fig. 1). Each injection was ~0.5 μl. After an 18 d survival period the animals were anesthetized and perfused transcardially with a solution of paraformaldehyde (4%) and gluteraldehyde (0.25%) in saline, followed by sucrose solutions of 5, 10, and 15% in 0.1 M PB. After the brain was removed from the skull, a block of tissue (~15 mm in dorsoventral extent) was trimmed through the superior temporal sulcus (STS) intended to include cortical area V5 or MT. The selected block of cortex was bisected and vibratome-sectioned in the horizontal plane at 50 μm. Sections were collected in 20% sucrose in PB and kept overnight in the refrigerator. Sections were then immersed in liquid nitrogen for rapid freezing as a way of promoting penetration. After thawing, the sections were processed according to a Vector ABC kit (Elite) protocol to visualize labeled axons. We used 3, 3-diaminobenzidene tetrahydrochloride (DAB) to reveal peroxidase activity. For tissue injected with BDA, this followed 24 hr in ABC solution. For PHA-L-injected tissue, this followed 2 d in anti-PHA-L (1:2000) and repeated 70 min steps through secondary antibody and ABC solutions. Selected sections were treated with a 0.5–1% osmium tetroxide solution in 0.1 M PB. Dehydration through an ascending series of alcohols (including 1% uranyl acetate in the 70% alcohol) and propylene oxide preceded flat mounting in Durcupan (Fluka ACM, Buchs, Switzerland) onto glass slides.

The labeled axons were reconstructed by light microscopy. Regions of special interest were photographed and re-embedded for correlated electron microscopy (EM). Serial ultrathin sections were cut at 70 nm thickness and collected on Pioloform-coated single-slot copper grids. Labeled profiles were photographed at 21,000× magnification. The classification of synapses as symmetric or asymmetric was made on the basis of conventional criteria (Gray, 1959; Colonnier, 1968). The presence of reaction product in the presynaptic bouton obviously compromises the visibility of the presynaptic membrane. However, the unlabeled boutons in the adjacent neuropil indicated marked differences in the thickness of the postsynaptic density of symmetric and asymmetric synapses (see Fig. 4). This allowed us to make definitive classifications of the synapses formed by labeled boutons. Serial electron micrographs of labeled synaptic boutons were digitized and reconstructed using an in-house computer system (Trakem). From the digitized and reconstructed data, we measured structures such as postsynaptic specializations and bouton area. Trakem generates a series of wire frame profiles, which gives a three-dimension (3-D) impression. The "object" can be rotated to offer different views of synapses. We enhanced this effect by fitting a skin to the digitized structure and then rendering the surface. The skin fitting used Nuages (B. Geiger, 1996), and the rendering used Geomview and Blue Moon Rendering Tools (L. Gritz).

To reconstruct and measure the area of postsynaptic densities of labeled boutons in 3-D, we developed our own computer software. A semiautomated process first grouped the serially sectioned components of synapses. The postsynaptic surface was represented as a 3-D grid that was created by interpolating points between the components. The area was measured by summing the areas of the triangles that appeared between the interpolated points. To represent the reconstructed synapses in two dimensions, we selected an appropriate plane on which to project each synapse.

We used the physical disector method of Sterio (1984) to obtain a stereological estimate of the percentage of labeled synapses in area MT. Serial ultrathin (70 nm) sections were cut and collected as above. Reference and look-up sections were separated by one intervening section. Each section was photographed in the EM at 11,500×. Only those synapses that appeared in the reference section but not in the look-up section were counted here.

RESULTS

Light microscope observations

Pressure injections of biotinylated dextran amine (one animal) or BDA and PHA-L (one animal) were made into the parafoveal representation in area 17 (V1) (Fig. 1). After processing, the injections were found to be 1–2 mm in diameter and confined to the gray matter. At one site the white matter was damaged by the injection needle itself. In area V5, labeled axons arborized in layers 3, 4, and 6. The lack of labeled cell bodies in extrastriate cortex was taken as evidence that the transport was anterograde only. The largest diameter (3 μm) axons showed the label only at the cut ends and not in the middle of the section. Presumably this is because the avidin complex could not penetrate the thick myelin sheath surrounding the labeled axons, despite the freeze–thaw procedure. These heavily myelinated fibers, originating from V1, arose from the white matter and branched to produce collaterals of decreasing diameter as they ascended through the cortical layers. The smaller-diameter collaterals retained a myelin sheath, which was not so thick as to prevent penetration of the reagents. The axons appeared unmyelinated in the light microscope (LM) at the point where boutons formed. This was confirmed in the electron microscope. Long, uninterrupted lengths of very fine collaterals also criss-crossed the termination zones. The boutons formed by these fine collaterals were very small and infrequent (<1/100 μm). The fine collaterals were not from a separate population of afferents, but branched from axons that bore large boutons. All boutons selected for this study were located in layers 4 and 6 of area V5.

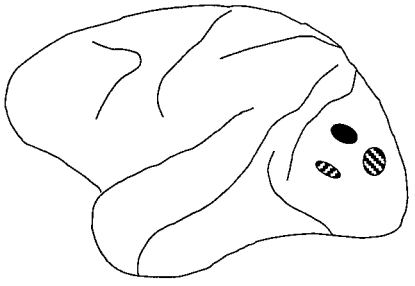

Figure 1. Summary schematic of macaque brain showing position of three injections of neuronal tracers (2 of BDA and 1 of PHA-L) into primary visual cortex, area V1, of two animals.

Short strings of large boutons (up to 3 μm diameter) of both *en passant* and *terminaux* morphology were gathered in local clusters. Some of these boutons formed close appositions with somata. From the LM views (Fig. 2*A*; see also Fig. 5*A*) we chose collaterals that formed clusters of boutons that were more or less parallel to the face of the section. This selection somewhat reduces the number of serial ultrathin sections from unmanageable to very large. Long lengths of collaterals, including the interbouton segments, were also traced through the serial ultrathin sections. We examined 86 boutons (32 from layer 6 and 54 from layer 4) in the electron microscope. Each bouton formed at least one asymmetric (Gray's type 1) synapse.

Electron microscopy

Synapses formed with dendritic spines

Figure 2 illustrates a correlated LM and EM sample from labeled collaterals in layer 4. The reaction end-product was very intense in many of the boutons. Where this reaction end-product was most intense it produced "chatter" over the labeled regions in the ultrathin section. The heavy labeling made the details of the presynaptic structures difficult to see, but the synaptic cleft and the postsynaptic specialization were unaffected by the labeling. The synaptic vesicles and mitochondria within the bouton did not contain any significant deposit of reaction end-product. The labeled boutons were usually packed with mitochondria and round vesicles (Fig. 2*B–E*). Some of the boutons and parts of the axon contained vacuoles (e.g., Fig. 2*C–E*). These were clearly artifacts of the labeling process, because unlabeled structures in the adjacent neuropil were intact. Similar vacuoles have been reported with the use of wheat-germ agglutinin as a tracer (LeVay, 1986). Vacuoles might contribute to the distinctive size of boutons when

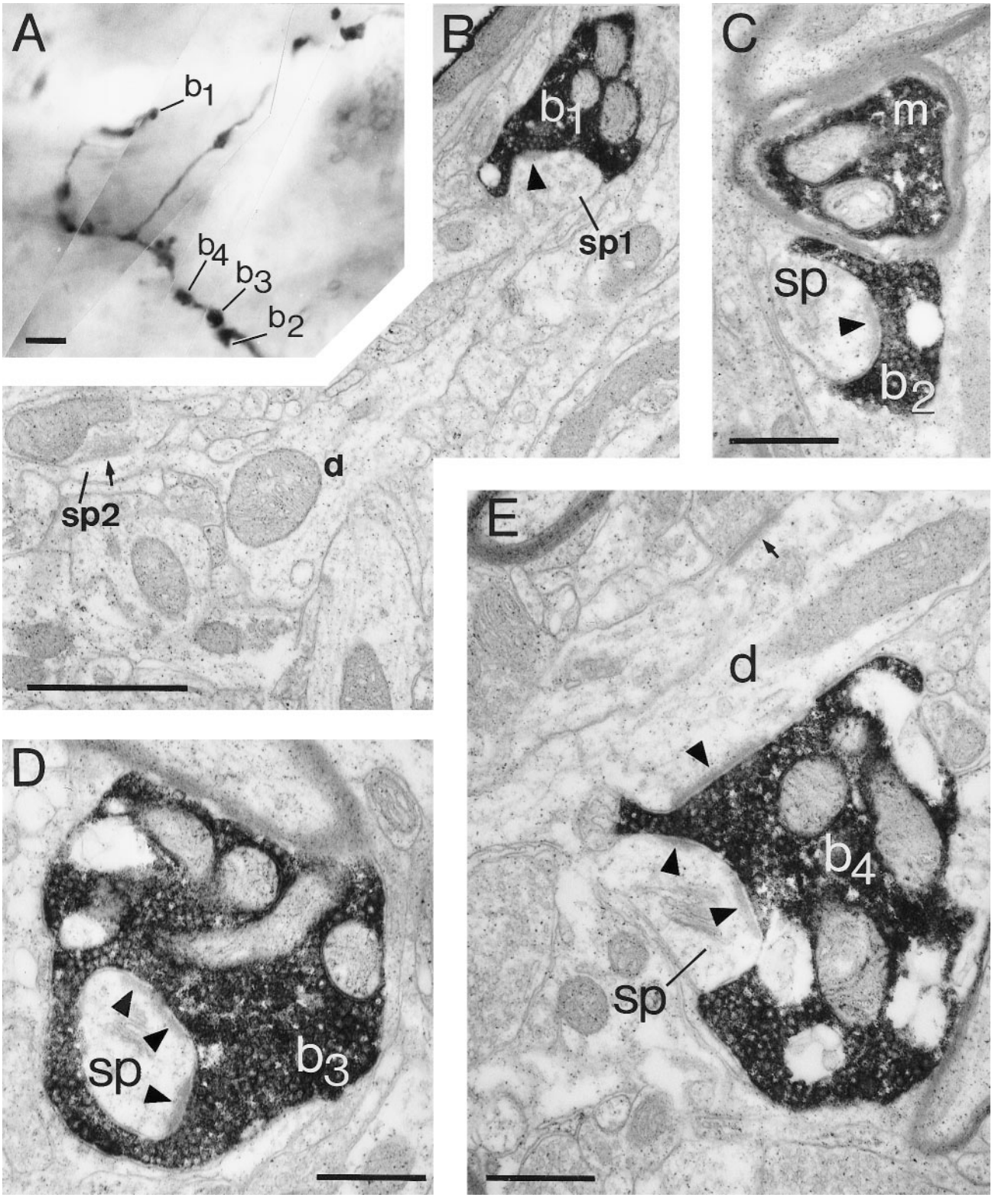

Figure 2. Correlated light and electron micrographs of BDA/PHA-L-labeled electron dense axon and boutons. *A*, Photomontage of an axon collateral located in lower layer 4 of area V5; b1, b2, b3, and b4 are selected boutons. The associated synapses of these boutons are shown in the following electron micrographs. *B*, Bouton b1 forms an asymmetric synapse (*solid arrowhead*) with a spine head (*sp1*) that can be traced back to the parent dendrite (*d*) in a single section. The dendrite produces a second spine (*sp2*), which receives an asymmetric synapse (*small arrow*) from an unidentified bouton. *C*, A myelinated axon collateral (*m*) gives rise to a bouton (*b2*) forming an asymmetric synapse (*solid arrowhead*) with a spine (*sp*). *D*, A large bouton (*b3*) packed with vesicles and mitochondria forms an asymmetric synapse (*solid arrowheads*) with a spine (*sp*). The spine profile has been completely embraced by the filled bouton. The postsynaptic density does not appear as a continuous structure but instead is perforated or complex. *E*, Another large bouton (*b4*) forms asymmetric synapses (*solid arrowheads*) with a spine (*sp*) and the shaft of a dendrite (*d*). The spine apparatus is clearly visible. The dendrite also forms an asymmetric synapse (*small arrow*) with an unidentified bouton. Scale bars: *A*, 10 μm; *B*, 1 μm; *C–E*, 0.5 μm.

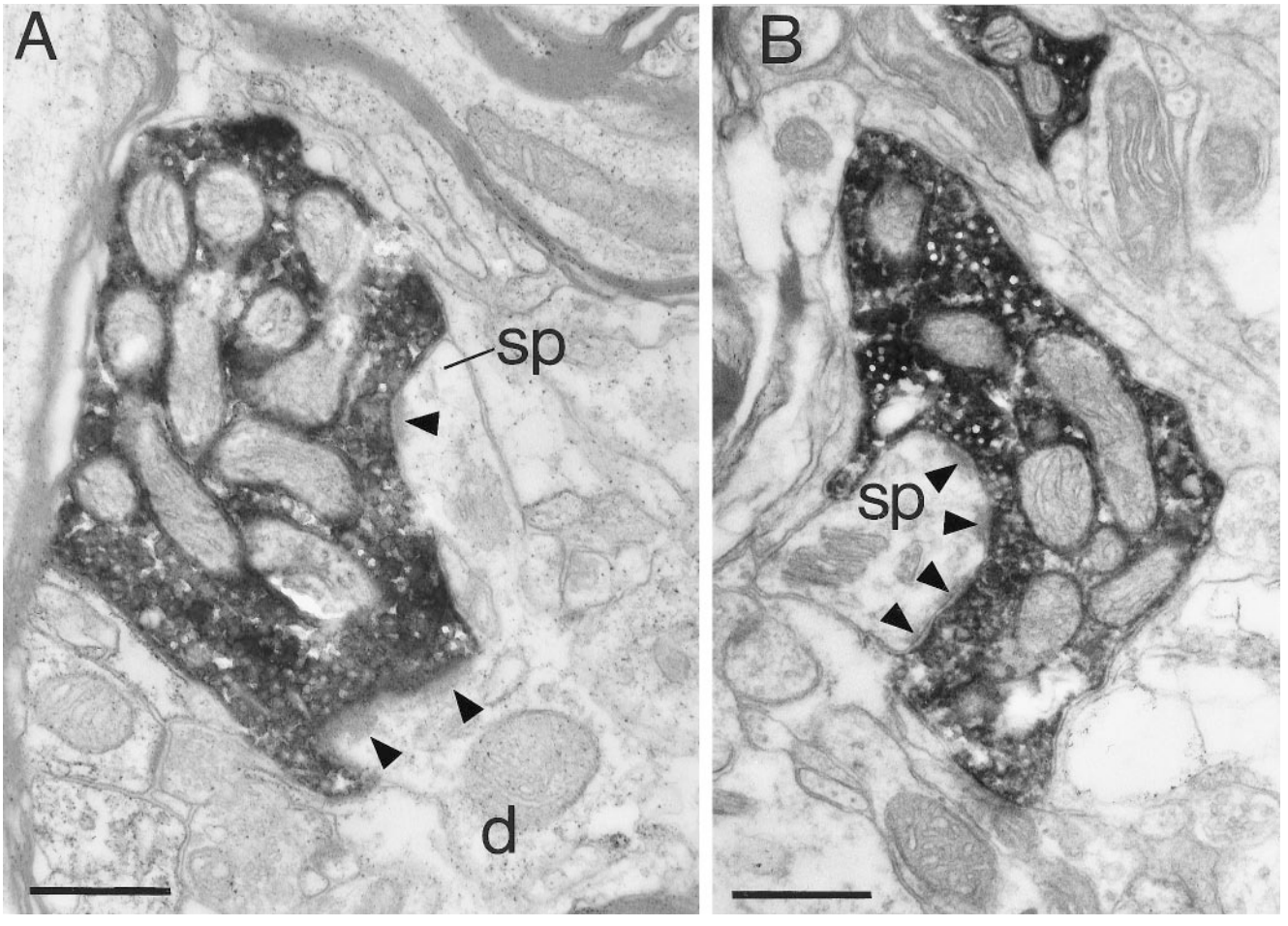

Figure 3. Electron micrographs of BDA/PHA-L-labeled boutons found in layer 6 of area V5. *A*, Bouton filled with mitochondria forming two asymmetric synapses (*solid arrowheads*) with the same target neuron. One of the targets is clearly a spine (*sp*; note the spine apparatus) that can be traced back to the parent dendrite (*d*). The second synapse forms on a region of the dendritic shaft that projects slightly into the neuropil. Serial section reconstruction showed this projection to be a sessile or "neckless" spine. *B*, A spine (*sp*) containing spine apparatus forms an asymmetric synapse with the labeled bouton, which shows a complex postsynaptic density (*solid arrowheads*) within the spine. Scale bars, 0.5 μm.

viewed in an LM, although the largest boutons in our sample contained no vacuoles.

The collaterals that gave rise to strings of boutons were frequently myelinated, but not so strongly that the avidin complex could not penetrate (Fig. 2*A,C*). The boutons along the collaterals formed asymmetric (Gray's type 1) synapses (Figs. 2, 3). The standard ultrastructural criteria, particularly spine apparatus (Peters et al., 1991) in conjunction with serial section reconstruction of the bouton and its target, helped to identify the target. Sometimes the spine neck could be traced back to the parent dendrite, either over several sections or occasionally in a single section (Figs. 2*B,E*, 3*A*). This was made possible because in some cases the spines had a relatively thick spine neck that was only a little smaller in cross section than the spine head. The majority of spines, unfortunately, could not be traced to their parent dendrites despite care being taken in collecting serial sections.

Some spine heads were actually embedded deep in the bouton itself (Fig. 2*D*) and in many cases the bouton wrapped around the spine head (Figs. 2*B,C,E*, 3*A,B*). Further detailed reconstructions are given below. The postsynaptic densities were not single entities but were frequently divided into a number of separate zones, as indicated in Figures 2*D* and 3*B*, *arrowheads*. The labeled bouton was the only source of asymmetric synapse to the spine. In three cases the spine formed a second, symmetric (Gray's type 2) synapse with an unlabeled bouton. When reconstructed, eight of the boutons that formed a synapse with a spine also formed synapses with the parent dendrite or a sessile spine from the parent dendrite. One bouton formed synapses with two spines and a dendritic shaft; all three targets belonged to the same neuron (b1 in Fig. 2*A,B*).

Synapses formed with the shafts of dendrites

Dendritic shafts were identified by their numerous mitochondria and microtubules, and in some cases by their projecting spines. Figure 4 illustrates the synapses formed with dendritic shafts. Figure 4*A* illustrates a bouton sampled from layer 4 that forms a synapse (*large, filled arrowhead*) with a large caliber dendrite (*d*) and a spine (*sp, large, filled arrowhead*). The dendrite forms numerous synapses from unlabeled boutons (*small and unfilled arrowheads*). The dendrite contained many large mitochondria, particularly in the dendritic varicosities or "beads." The beads (one is evident in the Fig. 4*A*) were more evident in serial reconstruction. No spines emerged from the shaft. These features are all characteristic of the dendrites of smooth neurons (Somogyi et al., 1983; Peters and Saint Marie, 1984; Kisvárday et al., 1985; Ahmed et al., 1997). Some of the adjacent unidentified

synapses on the same target dendrites were symmetric (Fig. 4*A*, *open arrowheads*), although the majority were asymmetric (Fig. 4*A*, *small, filled arrowheads*). Smaller-diameter dendrites with no symmetric synapses but otherwise similar features were also the targets of labeled boutons. One dendrite of small diameter formed a synapse with a labeled segment of axon. This contact was not anticipated, because at the LM level there was no suggestion of a bouton. Despite lengthy serial sections of axons, this was the only synapse discovered, indicating that such axonal synapses must be exceedingly rare.

The bouton illustrated in Figure 4*B* (sampled from layer 6) formed a synapse with a smooth beaded dendritic shaft similar to that described above (Fig. 4*A*). In the higher-power view of the synapse (Fig. 4*C*), the additional unlabeled boutons that form synapses with the dendrite were packed together. One formed symmetric synapses (*open arrowheads*), one formed asymmetric synapses (*small, filled arrowhead*). Approximately 26% of the dendritic shafts in V5 that formed synapses with the V1 afferents were of this smooth neuron type.

Synapses formed with somata

Neuronal somata in both layers 4 and 6 also formed synapses with V1 afferent boutons. Figure 5 illustrates a soma in layer 4 that forms synapses with four separate boutons (Fig. 5*B, b1–b4*) that arose from one myelinated axon collateral. Contacts between somata and the darkly labeled boutons of the V1 axons were easily visible at the LM level (Fig. 5*A,B*). The postsynaptic somata contained large, deeply invaginated nuclei, and the cytoplasm was packed with mitochondria (examples indicated by *arrows* in low-power electron micrograph in Fig. 5*C*) and rough endoplasmic reticulum. Crystalline inclusion bodies were sometimes found within the mitochondria of contacted somata (Fig. 5*H*). These have previously been seen within the mitochondria of Meynert cells in area V1 of monkey cortex (Chan-Palay et al., 1974). The Meynert cells project to V5 (Lund et al., 1975; Maunsell and Van Essen, 1983; Fries et al., 1985). All of the synapses formed with the soma by unlabeled boutons were asymmetric. However, the postsynaptic density of somatic synapses was far less prominent than those formed with spines and shafts. The ultrastructural features of the somata are characteristic of GABAergic smooth neurons (Peters and Saint Marie, 1984).

Three-dimensional reconstructions of synapses

One intriguing aspect of the large labeled boutons became evident when we reconstructed them and their synaptic targets more fully. Because the geometry might be of significance for the diffusion of transmitter to receptors from the presynaptic release sites (Uteshev and Pennefather, 1997; Rusakov and Kullmann, 1998a,b) we have made complete reconstructions of some boutons to illustrate the feature (Figs. 6, 7). The asymmetric synapses formed with spines were made by boutons that enveloped the spine head, which formed a virtual pocket within the volume of the bouton (Fig. 6*A,B*). Sometimes the bouton completely engulfed the spine head (Fig. 6*C,D*). Almost half (46%) of the spine heads in our sample were enveloped by the bouton. When synapses were formed, as these examples show, the synapse itself could be located at the tip of the spine or close to the point of penetration of the spine into the bouton, or both. The large bouton illustrated in Figure 7 formed synapses with four spines and a dendritic shaft. This exceptional bouton formed eight distinct synapses. The entire heads of two bulbous spines were almost completely enveloped by the bouton. The other two spines were also less completely enveloped. The entire circumference of a dendritic shaft was enveloped by the bouton. It formed three synapses with the labeled bouton. The target dendrite was varicose, packed with mitochondria, and formed one other synapse with an unidentified bouton. It had no spines in the reconstructed section and most likely was a dendrite of a smooth neuron.

The detail of the postsynaptic membrane was sufficiently well preserved that we could reconstruct the complete postsynaptic surface of synapses. It became clear that different types of target formed synapses of different size and shape. The shape of the postsynaptic disk could vary because of perforations in the postsynaptic density (Peters et al., 1991). This results in a "complex" synapse. Figure 8 depicts the two-dimensional projection of the postsynaptic densities from the sample of complete 3-D reconstructions of the synapses. Postsynaptic densities in the form of annuli and horseshoe shapes were more frequent on spines. Dendritic shafts and somata in particular had the least perforated or complex postsynaptic densities. It was a matter of opinion whether the numerous, small synapses formed with somata were in fact one synapse, but because each synaptic site could be separated by up to seven sections they were considered to be individual sites. However, the arrangement of vesicles above these multi-synaptic sites was of a continuous dense cloud of vesicles. Sessile spines could form synapses with regular or complex postsynaptic densities.

The histogram of synaptic areas (Fig. 9) indicates that synapses made by the boutons contacting somata were the smallest: mean area 0.031 μm^2 (SEM = 0.008). Spine synapses were the largest on average (0.127 μm^2; SEM = 0.011), and those with dendritic shafts were intermediate (0.071 μm^2; SEM = 0.07). The synapse areas of the three groups are significantly different from each other ($p = 0.01$; Wilcoxson paired rank test). Most synapses extended over only two or three sections; however, one bouton could provide up to five small synapses.

Mitochondria in boutons

Evidence is accumulating that because of their role in calcium metabolism, the mitochondria in axonal boutons may have a significant influence on the dynamics of synaptic transmission (Nicholls and Åkerman, 1982; Herrington et al., 1996; Tang and Zucker, 1997; Xu et al., 1997; Peng, 1998). We have thus fully reconstructed several boutons to examine the details of their mitochondrial contents more completely. These 3-D reconstructions indicated that the region adjacent to the synapse had the greatest accumulation of vesicles. Mitochondria of variable diameter filled out the remainder of the volume of the bouton. Up to 12 mitochondrial profiles, sometimes branched, could appear in any single ultrathin section. Three-dimensional reconstructions of mitochondria have rarely been made in such boutons, so the actual number of individual mitochondria is unknown. After reconstructing some of these structures (Fig. 10) we discovered that there was considerable variation in the organization of mitochondria. In some boutons the densely packed mitochondria were relatively short (0.5 μm) and straight, and in others they formed continuous loops within the volume of the bouton (Fig. 10). Hence the same mitochondrion was sectioned many times in each ultrathin section. As the bouton volume increased, so the number of mitochondrial profiles increased, but not necessarily the total number of mitochondria. We could follow individual mitochondria as they streamed from the bouton into the axon [e.g., the mitochondria represented in *dark orange* and *pale green* (Fig. 10*C,D*)]. The reconstructions also showed that the mito-

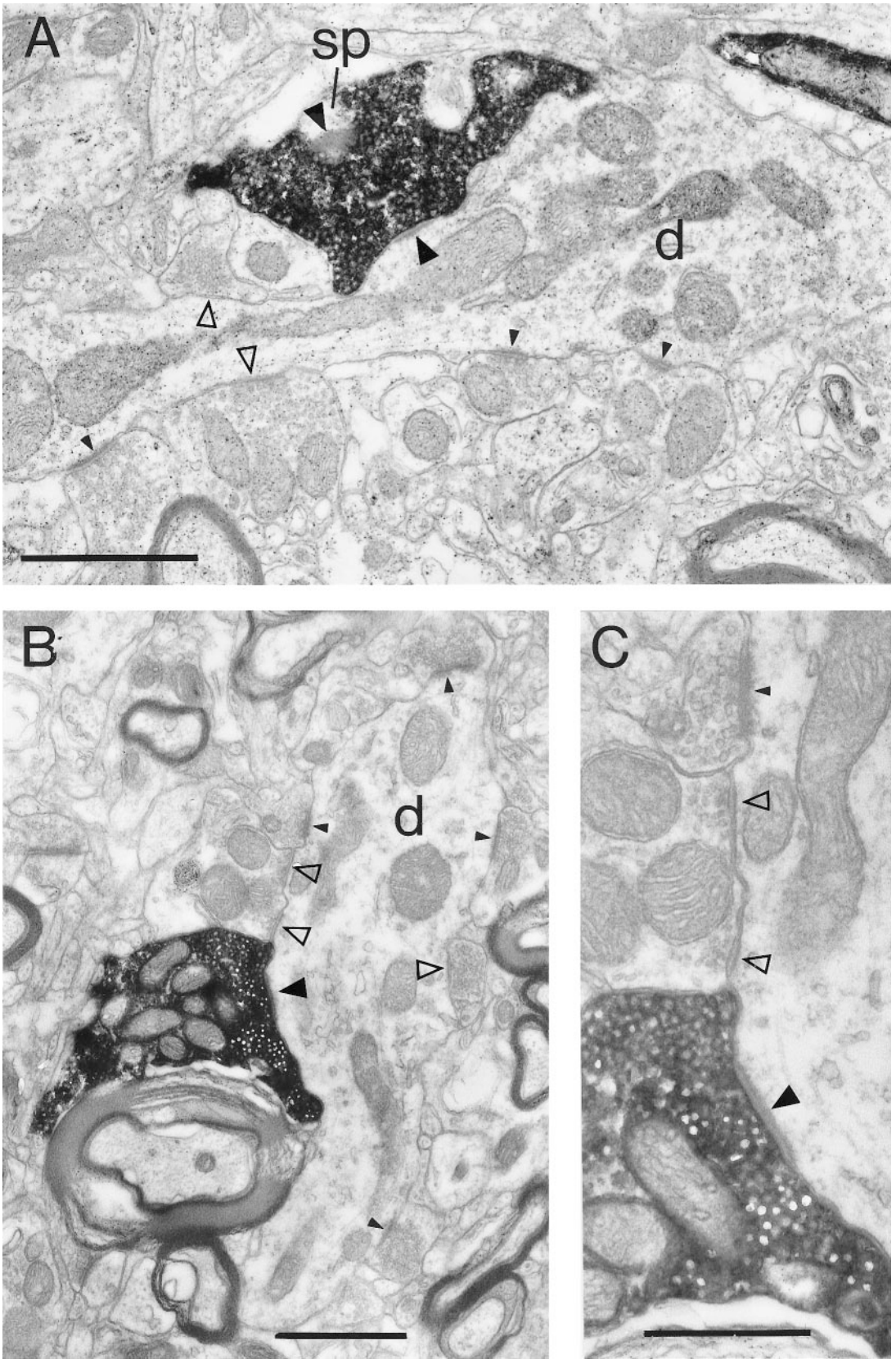

Figure 4. Electron micrographs of labeled synaptic boutons in contact with dendrites of smooth cells. *A*, Characteristically large bouton, filled with vesicles, located in lower layer 4 forms two asymmetric synapses (*large, solid arrowheads*), one with a dendrite (*d*) and the other with a spine (*sp*). The dendrite contains numerous mitochondria and forms many synapses of the symmetric (*open arrowheads*) and asymmetric (*small, solid arrowheads*) types with unidentified boutons. When the target dendrite was reconstructed over several serial sections, it became clear that the variations in diameter, which can be visible in the micrograph, were caused by a varicose or beaded morphology. These features are consistent with (*Figure legend continues*)

chondria accumulated at one side of the bouton, away from the synapses themselves. This space immediately around the synapses was filled with vesicles. Measurements in three fully reconstructed boutons revealed that the mitochondria occupied an average volume of 0.57 μm^3, which was fully 22% of the entire average volume of the boutons. The total surface area of the mitochondria within a bouton was approximately equal to the surface area of the bouton.

Targets of synapses

Data from layers 4 and 6 were pooled because no significant differences between the two samples were observed. The principal synaptic targets of the V1 afferents were spines, which formed 54% of targets. Dendritic shafts formed a large proportion of targets (33%), about a quarter of which originated from smooth neurons. Somata, probably also of smooth neurons, formed the remaining 13% of targets (Fig. 11). Thus, ~78% of the V1 afferent synapses were formed with spiny excitatory neurons in V5. Most boutons formed only one asymmetric synapse (Fig. 12). However, some formed two or more synapses, so that on average each V1 afferent bouton formed 1.7 synapses.

Proportion of asymmetric synapses formed by V1 afferents in layer 4 of V5

When sections were viewed in the LM it was clear that the labeled processes were not distributed evenly (Rockland, 1989) but formed zones of higher and lower density. From one monkey we selected two patches of particularly dense labeling within layer 4 for a stereological assessment by the unbiased "disector" method (Sterio, 1984) of the proportion of labeled synapses. This method entails the use of serial sections. Synapses appearing in the "reference" section but not in the "look-up" section are counted. We found that 2.7% (5 of 185) and 3.5% (3 of 85) of boutons with disappearing synapses (Sterio, 1984) were labeled. The area (micrometers squared) of all labeled and nonlabeled boutons with disappearing synapses ($n = 270$) was measured. The size distribution of the unlabeled and labeled profiles was broad (Fig. 13). Labeled profiles did not occupy the lowest end of the distribution but were evident among the largest measured. In the same tissue we could assess labeled versus nonlabeled myelinated axon profiles. Labeled myelinated axons occurred with about the same frequency (2.8%) as labeled synapses. The largest diameter axons (~2 μm) in layer 4 were both labeled and nonlabeled. All of the large-diameter axons were covered with a myelin sheath. The wall of the myelin sheath associated with these large fibers ranged from 0.12 to 0.4 μm thick.

DISCUSSION

In the present experimental work we have studied the direct projection from the parafoveal regions of V1 to V5 with the view of establishing a structural basis for the transmission of the component motion signal from V1 to V5. The source of the V1 afferents is known to be the spiny stellates and pyramidal cells of layer 4B and large pyramidal cells (Meynert cells) of layer 6 (Lund et al., 1975; Fries et al., 1985; Shipp and Zeki, 1989; Elston and Rosa, 1997). These neurons formed asymmetric (Gray's type 1) synapses with their targets. Nearly 80% of the synaptic targets of V1 afferents in V5 were the spines and dendritic shafts of excitatory cells. The remaining synapses were with the dendrites and somata of smooth (GABAergic inhibitory) neurons.

The similarity between the thalamic and feedforward intracortical pathways has been noted by Johnson and Burkhalter (1996) in their comprehensive study of feedforward and feedback connections in the rat visual cortex. Both the thalamic afferent projection in the primate and the V1 to V5 projection have similar terminal laminae and have spiny neurons as their major target. Compared with the projection from V1 to V5, the projections from V1 to lateral extrastriate cortex in the rat show some minor variations in the cells of origin and in the laminar distribution of the terminals. However, the types and proportions of synaptic targets are quite comparable to those found here, with pyramidal cells forming 90% of the targets and GABAergic interneurons the remainder (Johnson and Burkhalter, 1996). Comparable distributions were also found for the projection from the area 17–18 border to the posterior lateral suprasylvian visual area in the cat (Lowenstein and Somogyi, 1991). This suggests a conservation of function of the interareal feedforward projections in mammalian visual cortex. The commissural and "feedback" connections differ in that a much smaller proportion (~2–4%) of synapses is formed with smooth neurons (Jones and Powell, 1970; Czeiger and White, 1993; Johnson and Burkhalter, 1996).

The injection sites in V1 included all layers, so it is very likely that the sample of boutons included those originating from both the large pyramidal cells (solitary cells of Meynert) on the border between layers 5 and 6 in monkey V1 and the layer 4B neurons. The layer 5/6 Meynert cells are outnumbered by the layer 4B neurons that project to V5 by ~10:1 (Maunsell and Van Essen, 1983; Shipp and Zeki, 1989). Although the terminal arborizations of these two neuronal types have yet to be distinguished, the marked differences in the numbers of these two types that project to V5 suggest that most of the terminals we sampled would have originated from the 4B neurons. Qualitatively, however, we did not get any hint that we might be sampling from two quite distinct populations, at least in terms of their morphology and synaptic targets, and we have therefore treated the V5 population as one homogenous sample. The appearance of anatomical homogeneity may reflect the physiological homogeneity seen by Movshon and Newsome (1996). Six of the neurons they recorded were from layer 4B, and six were from the layer 5/6 border, i.e., probably Meynert cells. All 12 had similar receptive field properties, including strong contrast-independent direction selectivity, and all had fast-conducting axons. This relation of projection pattern to physiology led Movshon and Newsome (1996) to follow Zeki (1974) and characterize V1 as a vast "clearing house" that selectively distributes different specific information to different visual areas.

←

those of neurons with smooth dendrites, which contain GABA. In subsequent sections of the series, the same labeled bouton formed another two synapses with the dendrite. The spine target is almost completely enveloped by the bouton. The extensive postsynaptic density within the spine indicates that the synapse has been sectioned at an oblique plane. *B*, Large bouton located in layer 6 with a dendritic target similar to the one described above (Fig. 3*A*). The labeled bouton forms an asymmetric synapse (*large, solid arrowhead*) with the dendrite, which also forms symmetric synapses (*open arrowheads*), and other asymmetric synapses (*small, solid arrowheads*) from unidentified boutons. *C*, A higher-power micrograph of the adjacent section in the series of the bouton shown in Figure 3*B*. Detail of the unlabeled symmetric synapse (*open arrowhead*) and the labeled and unlabeled asymmetric synapses (*large, solid* and *small, solid arrowheads*, respectively) can be compared. Scale bars: *A, B*, 1 μm: *C*, 0.5 μm.

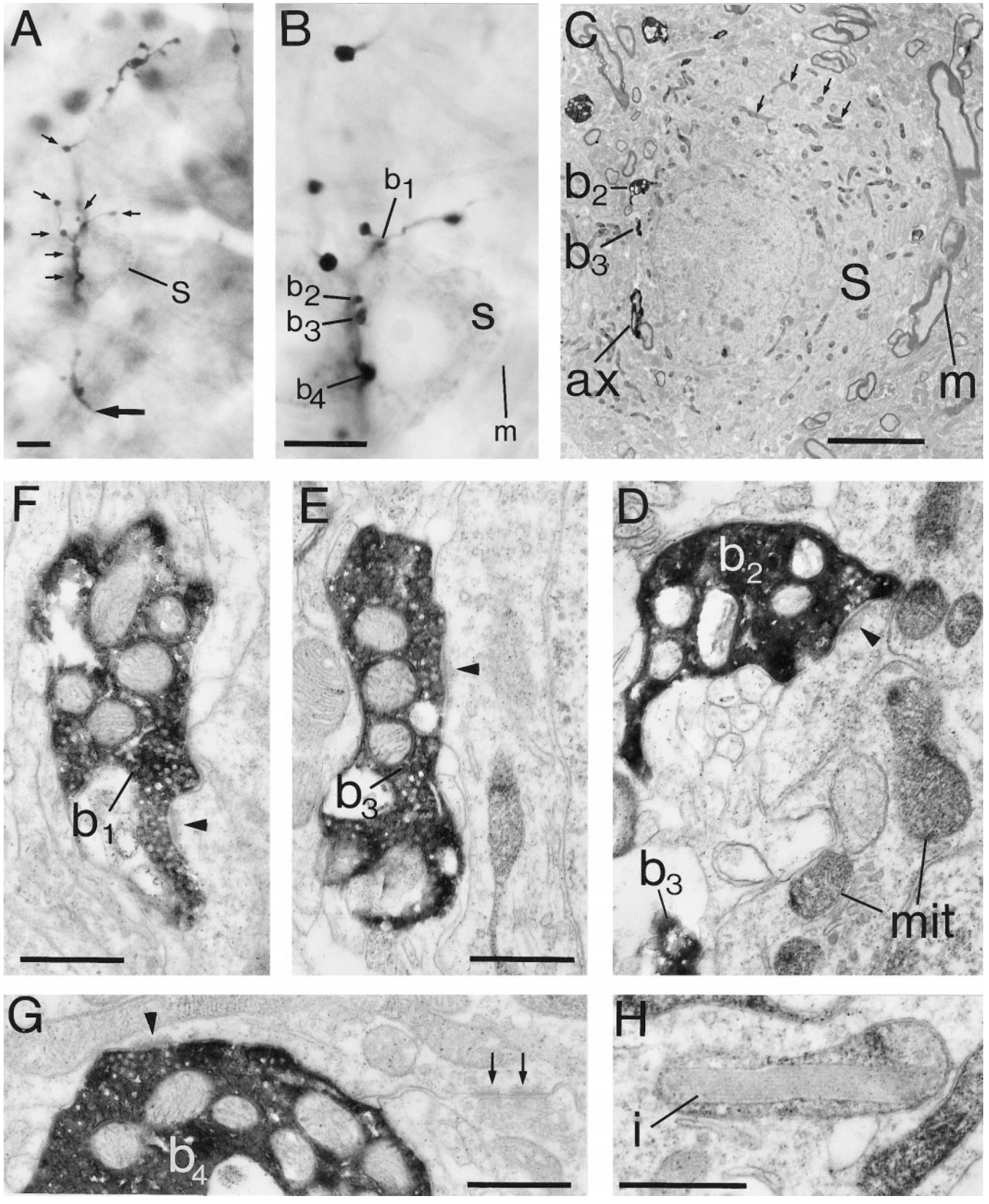

Figure 5. Correlated light and electron micrographs of BDA/PHA-L-filled boutons in synaptic contact with a soma (*S*) located in layer 4 of area V5. *A*, Low-power light micrograph of an identified axon collateral (*large, solid arrow*) rising through lower layer 4. The soma (*S*) and some of the boutons (*small arrows*) appear at higher magnification in *B*. *B*, Numbered boutons (*b1, b2, b3, b4*) all form contacts with the soma (*S*). A large-diameter myelinated axon (*m*) is indicated for reference. *C*, Low-power electron micrograph of the soma (*S*) seen in *B*. The myelinated axon (*m*) referred to in *B* can be seen in close contact with the soma. Some of the mitochondria appear to be lightly stained (*small arrows*) (*Figure legend continues*),

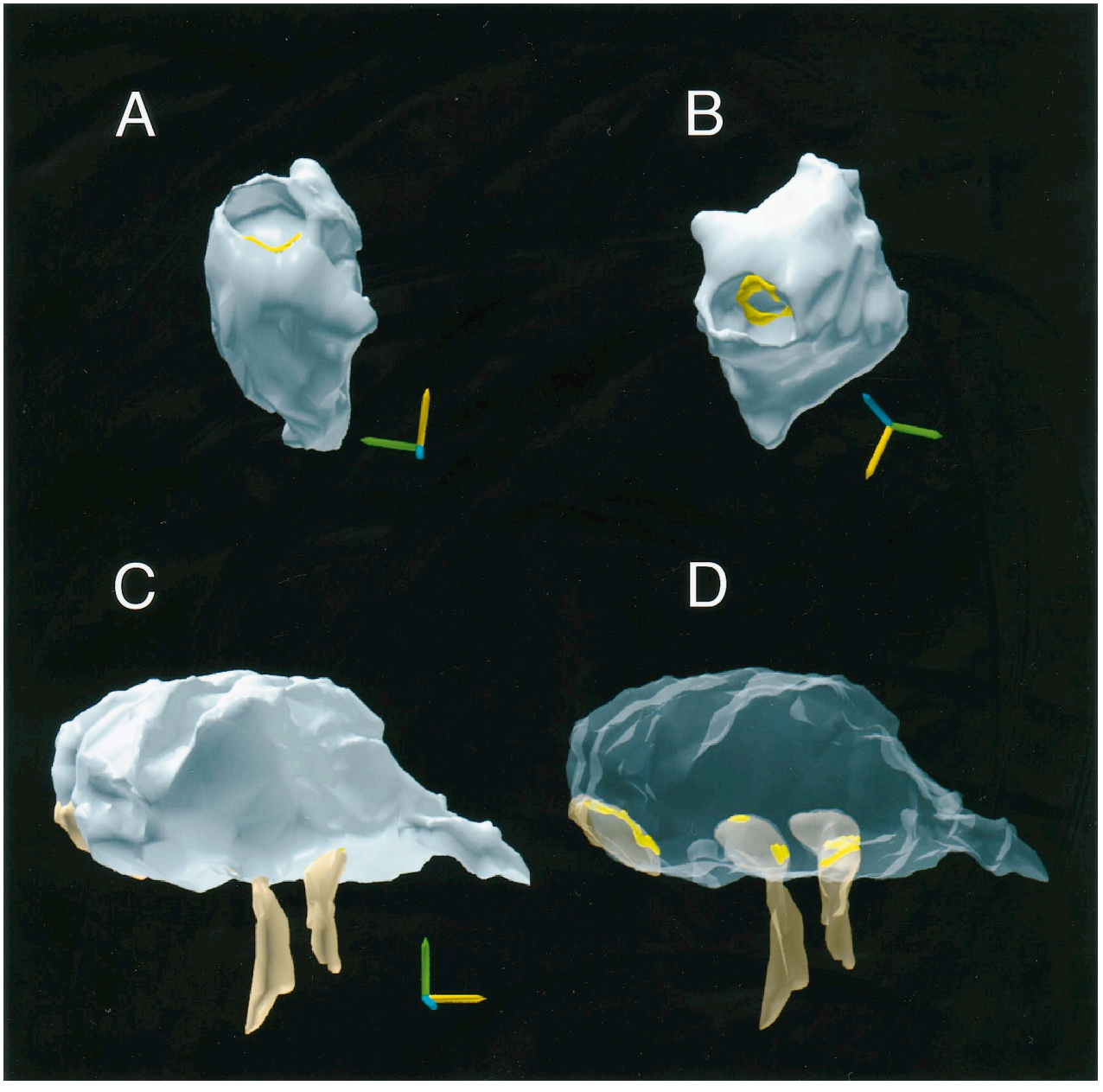

Figure 6. Three-dimensional reconstructions from serial ultrathin sections of filled boutons in area V5 showing how targets are enveloped by the bouton. *A, B*, Two views of a bouton (*blue*) found in layer 6. In *A* a clear depression or pocket can be seen at the *top* (uppermost pole) of the bouton. The edge of the postsynaptic density (*yellow*) can be seen at the lip of the depression. In *B* the bouton was rotated around a vertical axis (~180°) to provide a better view of the postsynaptic density. *C, D*, A large layer 6 bouton (*blue*) that forms synapses with three spines (*brown*). In *C* the bouton and spines have an opaque skin, and in *D* the skin is transparent. The two spines on the *right* are deeply embedded within the bouton. The postsynaptic surface (*yellow*) is shown in apposition with the spines. Axes, 0.5 μm.

Identification of target neurons and likely synaptic efficacy

The pyramidal cells in V5 are more highly branched and more spiny than those of V1 pyramidal cells (Elston and Rosa, 1997). This is perhaps a consequence of the higher density of neurons in V1 that may prevent elaboration of the dendritic tree. The number of excitatory synapses formed on these V5 pyramidal cells is probably in the range of 5000 to 10,000, as in other cortical areas.

←

thus enabling the soma to be seen at the light microscopic level. The large filled axon (*ax*) gives rise to the boutons (*b2, b3*) after losing its myelin sheath (not illustrated). *D*, High-power electron micrograph of boutons b2 and b3. The bouton b2 forms an asymmetric synapse (*solid arrowhead*) with the soma. Electron dense mitochondria (*mit*) can be seen within the cytoplasm of the soma. *E, F*, In sections after that shown in *D*, boutons b3 and b1 can be seen to form asymmetric synapses (*solid arrowheads*) with the soma. *G*, The asymmetric synapse (*solid arrowhead*) of the fourth bouton (*b4*) in contact with the soma can be compared with the asymmetric synapses (*small arrows*) formed by an unlabeled bouton also in contact with the soma. *H*, High-power micrograph of a crystalline inclusion (*i*) within the body of a mitochondria found in the soma contacted by the above boutons. Scale bars: *A, B*, 10 μm; *C*, 5 μm; *D–H*, 0.5 μm.

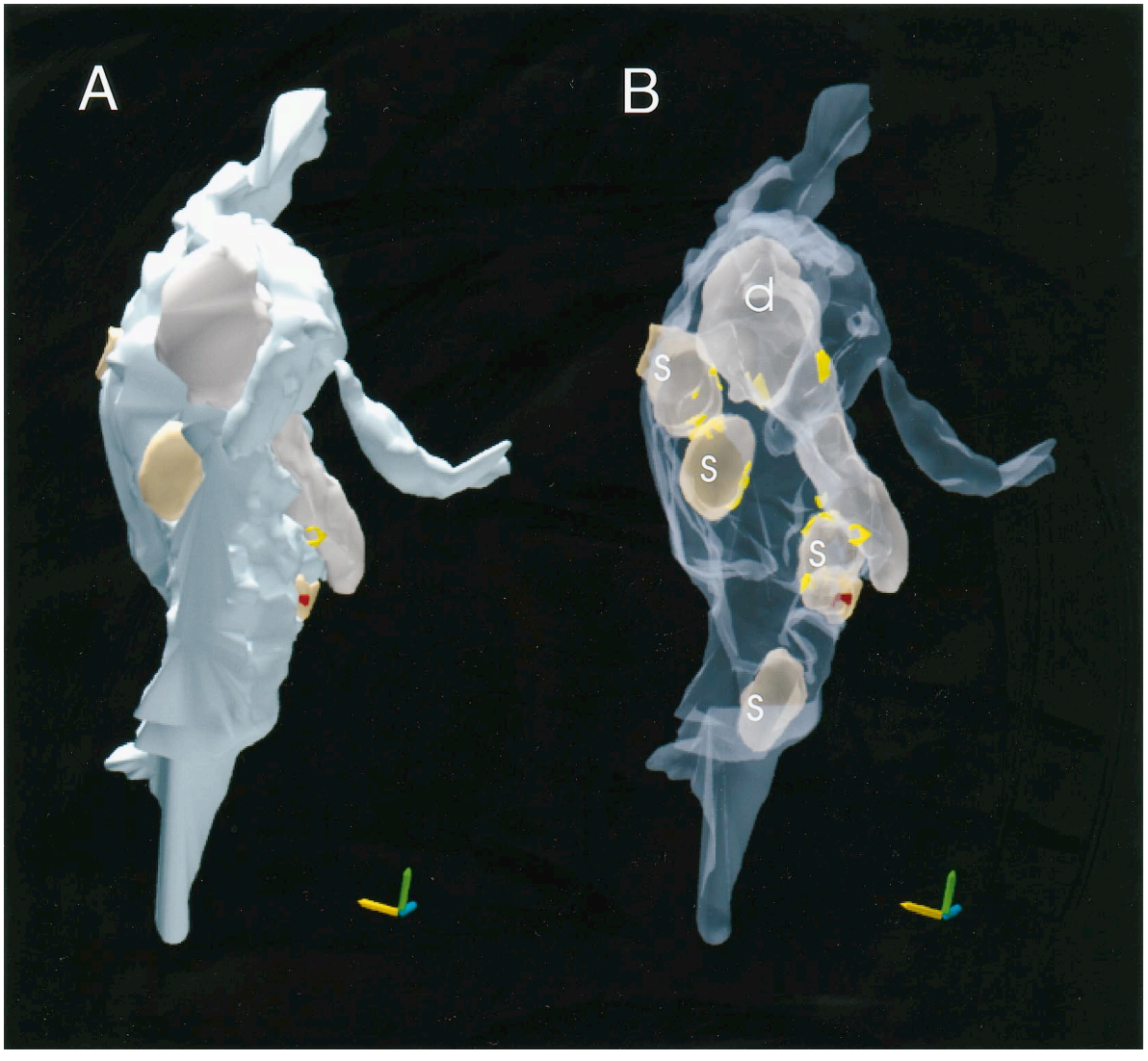

Figure 7. Reconstruction of a large bouton (*blue*) in layer 4 of area V5 that forms synapses with four spines and a dendrite. *A*, When the bouton is rendered with an opaque skin it can be seen to wrap around the dendrite (*d* in *B*). This dendrite forms three synapses with the identified bouton. The spines (*s* in *B*) are all deeply embedded in the bouton. *B*, Both bouton and targets are rendered transparent, showing the postsynaptic density. The asymmetric synapses are *yellow*. One of the spines also forms a symmetric synapse (*red*) with an unidentified bouton. Axes, 0.5 μm.

For the basket cells the number is probably similar (Ahmed et al., 1997). Our estimates clearly suggest that the afferents of V1 can only provide a few percent of these excitatory synapses. The unbiased method of counting (Sterio, 1984) makes it likely that we have correctly assessed the percentage of labeled synapses in layer 4 of V5. However, there are possible technical issues that would lead to an underestimate of the actual number. One obvious issue is that not all of the projecting neurons at the site of injection might have taken up and transported the label, or that the transport is incomplete. A more significant issue concerns the divergence and convergence of the V1 to V5 projection. If a single region of V5 receives its input from a very large region of V1, our injections in V1 would have failed to label all of the neurons projecting to the sampled terminal region in V5. However, if not all of the boutons were labeled, this estimate cannot be greatly in error, given that the V5 projection neurons in V1 are sparse andhave to map retinotopically in V5. It is likely that each target neuron in V5 must form at most only a few hundred synapses with V1 afferents. This raises the interesting functional problem for the computation of pattern motion. If V1 does form the first stage of the motion computation and V5 the second, then the signal is being conveyed from V1 to V5 by a small fraction of the synapses. How then does the V1 signal avoid being swamped or corrupted by the activity of all of the other excitatory synapses simultaneously active on the dendritic tree of the recipient V5 neuron?

One possible answer to this question is that the V1 afferent synapses are particularly powerful relative to the other excitatory synapses formed with the V5 neurons. The size of the synaptic potentials in V5 neurons has yet to be measured. However, the size of the postsynaptic densities of the V1 afferent synapses may provide an approximate indication of the number of receptors that could be located in the postsynaptic membrane of the V5 recipient neurons. For example, 1000 AMPA receptors of 10 nm diameter could be packed side by side into 0.1 μm^2. Our measurements of the area of the postsynaptic densities of the synapses formed by the labeled boutons indicate that the largest (those on spines) are slightly smaller (0.13 μm^2) than those of the thalamo-

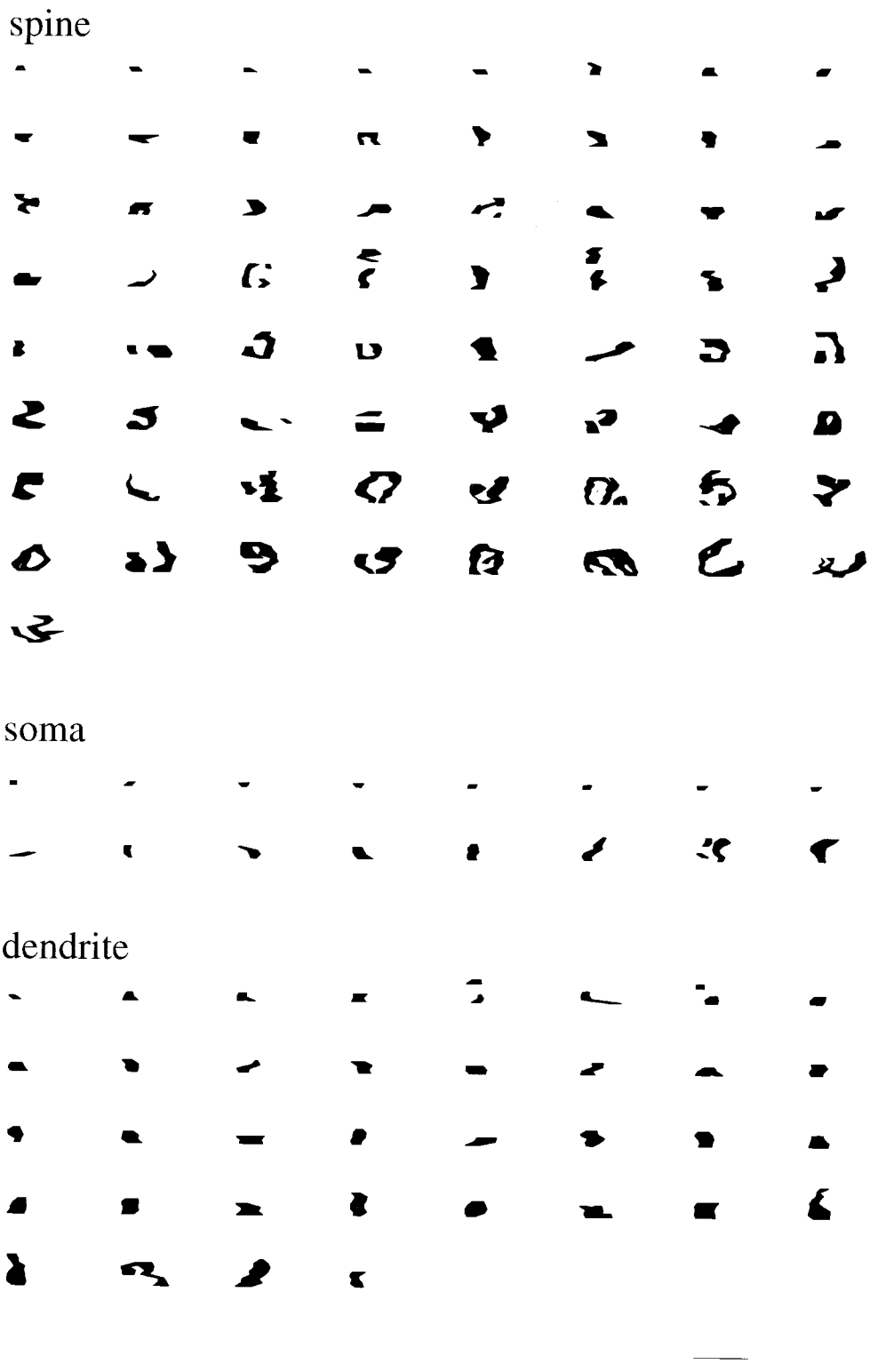

Figure 8. Two-dimensional projection of the reconstructed postsynaptic densities found on spines, soma, and dendrites postsynaptic to labeled boutons in area V5. The densities are from individual synapses and are ordered by increasing surface area calculated from the 3-D reconstructions. Scale bar, 1 μm.

cortical synapses in the cat, which are ~0.18 μm^2 (Dehay et al., 1991; Friedlander et al., 1991). These postsynaptic densities in V5 are at least threefold larger in area than those observed at comparable excitatory synapses formed with spines of CA1 pyramidal cells in the mouse and rat hippocampus (Harris and Stevens, 1989; Schikorski and Stevens, 1997). They are slightly smaller than the individual synapses formed by single mossy fiber boutons with the branched dendritic spines of the CA3 pyramids (Chicurel and Harris, 1992).

Individual geniculocortical fibers in the cat visual cortex pro-

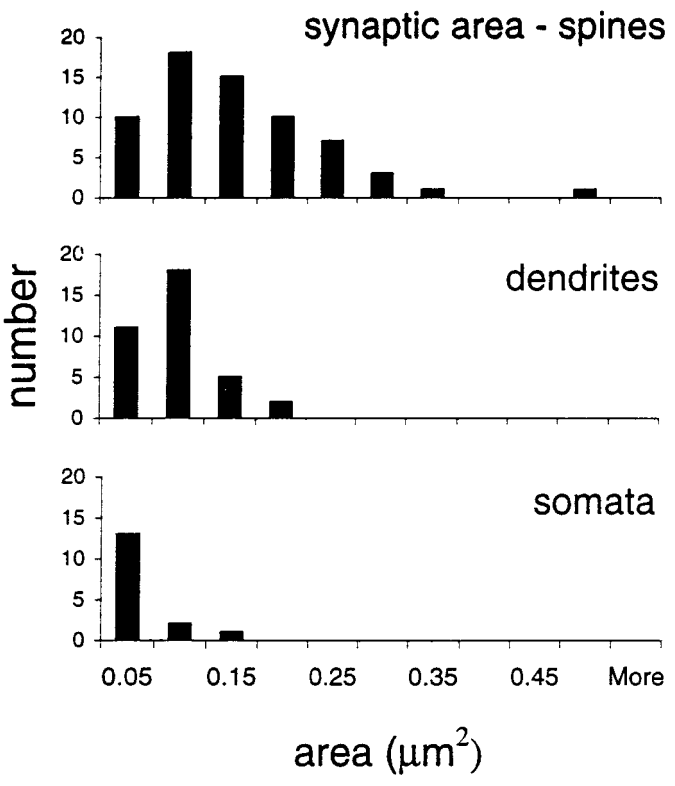

Figure 9. Histogram of the distribution of postsynaptic areas (μm^2) formed by labeled boutons in area V5.

vide average EPSP amplitudes of nearly 2 mV, which would require >400 postsynaptic ion channel openings (Stratford et al., 1996). The extraordinarily low coefficient of variation of 8% suggests that they could arise from multiple release sites with an extremely high release probability or single large synapses (Stratford et al., 1996). By analogy with these cat data, the size of the V5 synapses studied here suggest that the mean amplitudes of the unitary AMPA receptor EPSPs will be ~1–2 mV. This remains to be tested. We also found evidence of multisynaptic connections from single afferents to single neurons in V5. Unfortunately, our method cannot provide an estimate of the frequency of such multisynaptic connections, but such multiple synapses would lead to larger EPSPs and so provide V5 with a functionally powerful input from V1 despite the small number of synapses that the V1 projection provides in V5.

Influence of synapse morphology on transmitter diffusion

The 3-D reconstruction of the postsynaptic elements revealed that the postsynaptic densities formed with dendritic shafts were single disks. By contrast the synapses formed with spines had perforated postsynaptic densities that formed complex horseshoe or circular arrangements when viewed *en face*. In addition, the larger presynaptic boutons enveloped the entire head of the postsynaptic spines and occasionally dendritic shafts. We do not yet understand why the spine synapses in the V1 to V5 projection form such elaborate morphology, but presumably one reason is to secure more efficient and reliable transmission with the fewest possible synapses. Previously we have observed such embedding of the postsynaptic target in the presynaptic bouton in the magnocellular boutons of the thalamic afferents in V1 of the macaque monkey (Freund et al., 1989) and in boutons of the nondeprived Y-axons in area 18 of long-term monocularly deprived cats (Friedlander et al., 1991). Elsewhere, the giant mossy fiber boutons in CA3 of the hippocampus also appear to embed their targets (Chicurel and Harris, 1992). An additional feature of such large boutons is that they form multiple synapses. Such arrangements could have some significance for the spillover of neurotransmitter between receptor domains within a single postsynaptic or perisynaptic complex and for spread of transmitter between synapses.

The diffusion of glutamate neurotransmitter from the synapse has been modeled in some detail (Uteshev and Pennefather, 1997; Rusakov and Kullmann, 1998a,b). Kullman and Asztely (1998) have reviewed the relevant experimental literature. The modeling shows that both the viscosity (determined by the diffusing molecules interactions with cell walls and macromolecules in the extracellular space) and geometry of the tissue have a significant effect on diffusion. Rusakov and Kullman (1998a) show that NMDA receptors, but not AMPA receptors, located at a distance of ~500 nm from the center of the synaptic cleft will be activated by the release of one vesicle. The synapses formed by the multisynaptic boutons in V5 tended to have intersynaptic distances in excess of 500 nm. This, together with the envelopment of the synapses by the bouton, would restrict the cross-talk between these synapses. However, this same morphology might increase the concentration of neurotransmitter in the region surrounding the synapse and so increase the probability of the activation of receptors on both the postsynaptic and the presynaptic membrane. The "gap" between the synaptic densities in the perforated synapses averaged ~300 nm (range, 168 to 476 nm) (Fig. 8), which is within the effective diffusion range of the contents of a single vesicle (Rusakov and Kullman, 1998a). The same constraints of diffusion studied by Rusakov and Kullman (1998a,b) of course applies to the movement of extracellular ions, such as Ca^{2+}, into the boutons. If the diffusion of Ca^{2+} is slow, then it may become locally depleted and so modify synaptic activity (Montague, 1996).

Little attention has been paid to the correlation between synaptic morphology and physiology in the visual cortex. Nevertheless, there are some quite distinct differences in the synaptic physiology of the inputs to layer 4 of cat visual cortex, as noted above. In particular the thalamocortical synapses in the cat produce EPSPs of large amplitude and exceedingly low variance (Stratford et al., 1996). This is most easily explained if only a single release site were active. However, the contents of a single vesicle [~5000 molecules of neurotransmitter (Riveros et al., 1986)] may not contain enough transmitter to produce 100% double occupancy (saturation) of the receptors that such low variance implies (Larkman et al., 1991). Thus, multiple release sites, each having a high probability of release, may invariably be involved in such synapses if the diffusion distance between any single release site and target receptors is to be reduced.

Synapses with multiple release sites that have large-amplitude low-variance synaptic currents have been observed in the multisite glutamatergic synapses that mossy fibers form with granule cells in the rat's cerebellum (Silver et al., 1996). At these sites the synaptic current appears to be limited by the number of postsynaptic channels rather than by the amount of neurotransmitter released. This is probably because the transmitter released from neighboring sites overlaps and so changes both the concentration and length of occupancy of the transmitter in the cleft (Faber and Korn, 1988). Importantly too, the perisynaptic concentration of

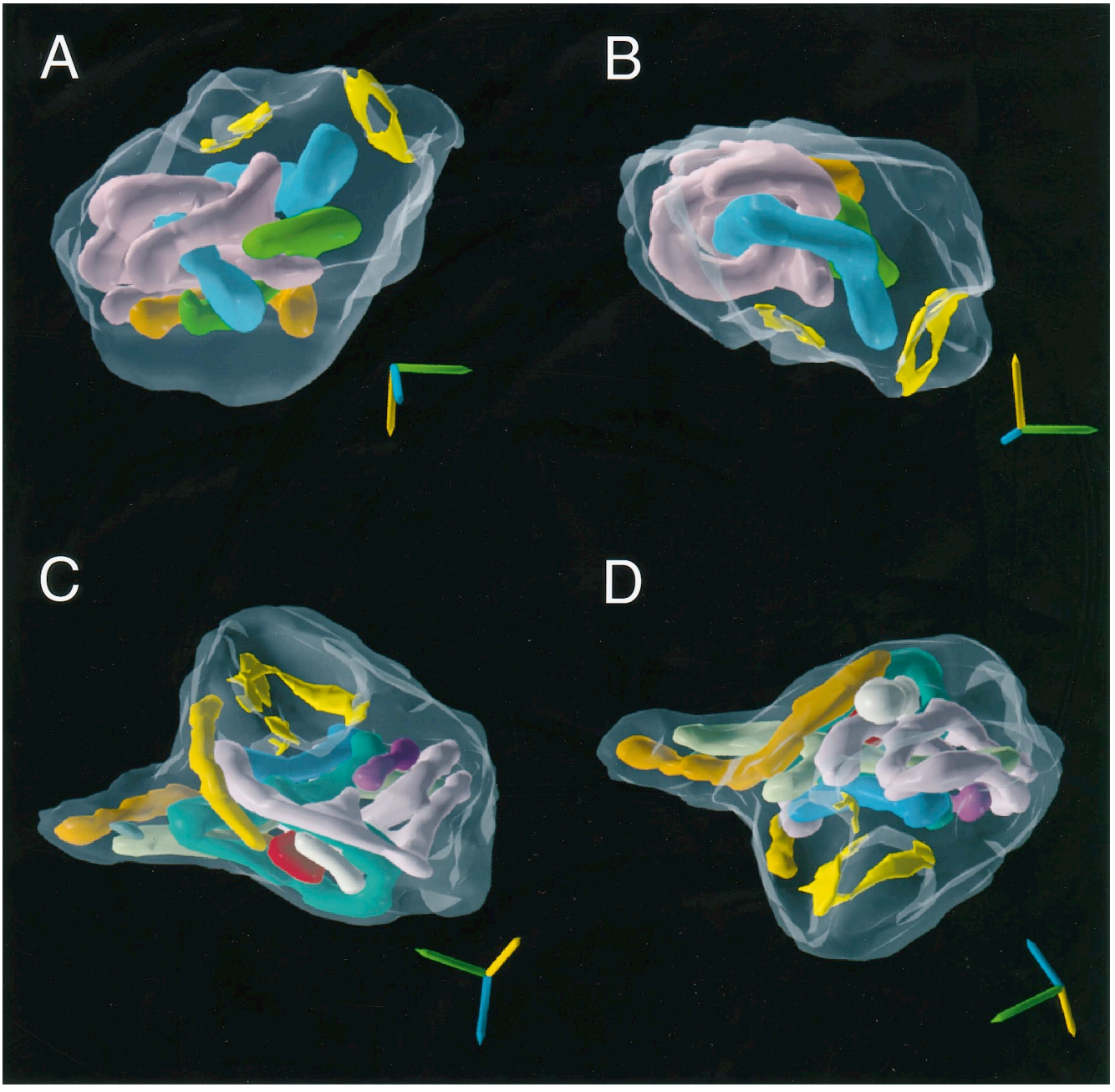

Figure 10. Two different views of two boutons reconstructed and rendered with transparent skins to show solid mitochondria and postsynaptic specializations (*yellow*). The mitochondria are color-coded for identification of individual structures. For both boutons the right-hand image (*B, D*) is rotated (~180°) about the horizontal axis of the left-hand image. *A, B*, Bouton found in layer 6 that formed synapses with two spines and contained four mitochondria (*pink, blue, orange*, and *green*). The longest mitochondrion (*pink*) was branched and formed three loops. Both synaptic surfaces (*yellow*) are presented at oblique, nonoptimal elevations but appear as incomplete annuli. *C, D*, Layer 4 bouton formed synapses with two spines and contained nine mitochondria. One mitochondrion (*pink*) is branched and forms loops. The synaptic specializations (*yellow*) become superimposed on each other in these views. One synapse is horseshoe-shaped and the second is composed of two small patches. Axes, 0.5 μm.

transmitters would also be raised. One possibility is that there are receptors located in the perforation of the postsynaptic density—for example, the metabotropic glutamate receptors (Nusser et al., 1994; Baude et al., 1995). Extrasynaptic receptors located at the center of the horseshoe would be at a relative advantage because they would receive a higher concentration of spillover neurotransmitter from multiple release sites than receptors located outside the ring. Unfortunately the neurochemistry and distribution of V5 receptors is unknown.

The smallest postsynaptic densities seen in the present study were formed mainly with dendritic shafts. In the cat, the smallest postsynaptic densities are also on the dendritic shafts, but their source is local layer 6 pyramidal cells. (Ahmed et al., 1994, 1997). These layer 6 pyramidal cell synapses show strong paired-pulse facilitation and not the paired-pulse depression seen with the layer 4 spiny stellate synapses or the thalamic afferent synapses (Stratford et al., 1996; Tarczy-Hornoch et al., 1998). The mechanisms that determine this dynamic behavior of synapses are

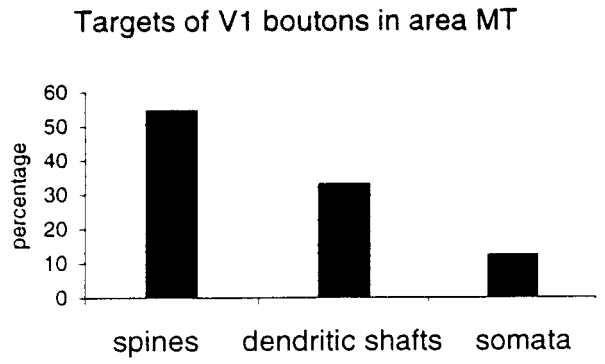

Figure 11. Histogram of synaptic targets of boutons in area V5 originating from neurons labeled in area V1.

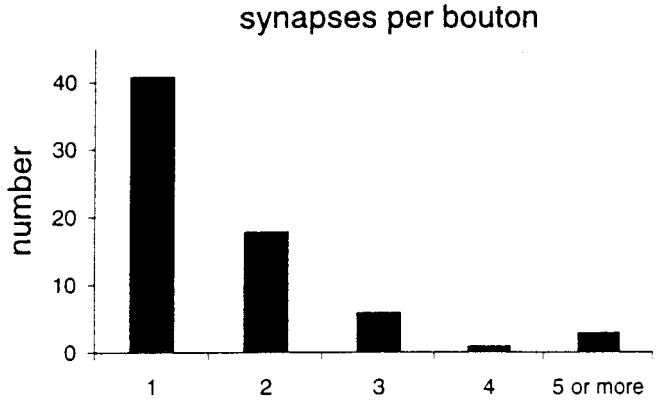

Figure 12. Histogram of the number of synapses (*1, 2, 3, 4, 5 or more* per bouton) formed by individual labeled boutons in layers 4 and 6 of area V5.

largely unknown. However, it has recently been discovered that the mitochondria may have an important role in the dynamics of synaptic function.

Mitochondria in the synaptic boutons

A striking morphological feature was the considerable volume occupied by mitochondria within the terminal boutons of the V1 afferent neurons. In a previous study in the cat it was noted that the number of mitochondrial profiles seen in a single cross section of a thalamic afferent bouton scaled linearly with the size of the bouton (Friedlander et al., 1991). By making the 3-D reconstructions, it became clear that the many mitochondrial profiles seen in a single cross section actually arose from the tortuous folding and branching of individual mitochondria within the bouton. The functional role of the mitochondria in the presynaptic terminals is beginning to be understood from work in invertebrates and lower vertebrates. In the crayfish, the axon terminals of phasic motoneurons contain fewer mitochondria and show marked synaptic depression, whereas the terminals of tonic motoneurons have more mitochondria, more oxidative activity, and a greater resistance to synaptic depression. The synapses of the tonic motoneurons also show strong frequency-dependent facilitation (Nguyen et al., 1997). These data suggest the possibility that the V1 neurons projecting to MT have a tonic activity and that one role of the mitochondria in the boutons is to prevent or reduce depression in this synapse.

Mitochondria play an important role in calcium metabolism in cells (Nicholls and Åkerman, 1982; Herrington et al., 1996; Xu et al., 1997), but despite the importance of calcium in synaptic

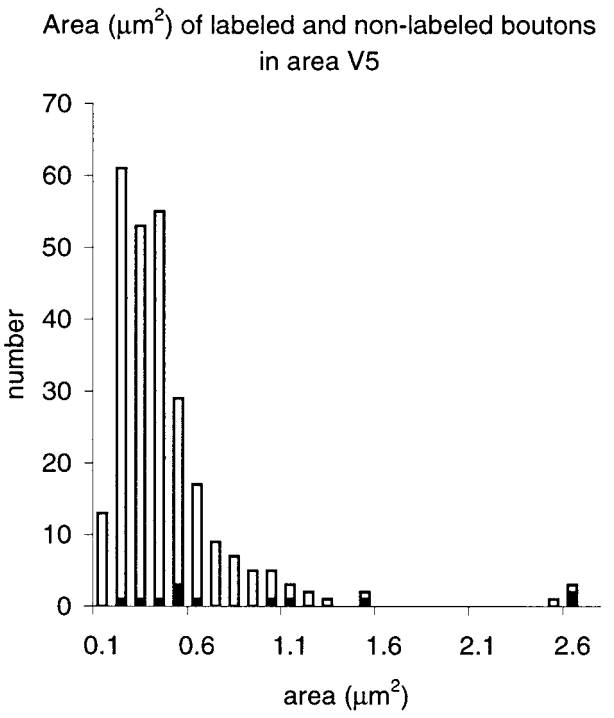

Figure 13. Histogram showing the distribution of area (μm^2) of labeled (*black bars*) and nonlabeled (*white bars*) synaptic boutons in area V5. Only those boutons with disappearing synapses were measured.

transmission, the significance of mitochondria for synaptic transmission has only recently been recognized. Calcium enters the synaptic bouton through voltage-gated channels, and it is the key ion in producing the release of neurotransmitter. Increasing the calcium concentration within the bouton increases the probability of transmitter release. In the bullfrog sympathetic ganglia (Peng, 1998), calcium entering the bouton is taken up by the mitochondria, but in a frequency-dependent manner. If the terminal is activated at low rates, then the calcium transporters in the mitochondria can provide adequate buffering. If the rates of activation are high, the mitochondria cannot buffer adequately, and calcium accumulates within the bouton. This uptake during repetitive stimulation also explains the development of post-tetanic potentiation at synapses. Tang and Zucker (1997) have found that mitochondria in the neuromuscular junction of the crayfish also slowly release the calcium they accumulated during tetanic stimulation. It is this maintained higher concentration of calcium within the bouton that is responsible for post-tetanic potentiation.

Although the role of mitochondria at central synapses in mammals has still to be studied, it is most likely that their role in the boutons studied here includes the mechanisms referred to in the above studies of invertebrate and lower vertebrate synapses. Thus, the quantification of the contribution of mitochondria within the synaptic boutons of identified neurons may provide another important link between morphology and function of these synapses.

Common basic circuits in V1 and V5

On anatomical grounds, therefore, it seems that both the light and electron microscopic pattern of innervation of the V1 afferents in V5 does not differ markedly from that of the dLGN input to V1. Johnson and Burkhalter (1996) have suggested schemes of how the thalamic and interareal feedforward and feedback circuits

might connect into the local recurrent microcircuits of the visual cortex (Douglas et al., 1989a,b). Models of component direction selectivity have been simulated on such recurrent microcircuits (Douglas and Martin, 1991; Suarez et al., 1995). In principal, the extraction of global motion should be possible using the same machinery as is used for the component motion analysis. Simoncelli and Heeger (1998) have developed an abstract linear model to explain how global motion in V5 can be derived from a component motion input from V1 by means of essentially the same algorithm. Although their model does not map directly onto the known circuitry and biophysics of the cortex, they pointed out that the commonality of their computation for V1 and V5 is conceptually related to the structural commonality of circuits in different cortical areas. It is this same principle of multifunctionality of a basic circuit that is captured in the concept of the recurrent microcircuit (Douglas et al., 1989a,b; Douglas and Martin, 1991).

Future prospects

The present study has raised some important questions about the possible role of the V1 input to V5. Obviously, V5 receives other inputs from areas such as V2, V3, VP, MST, and the thalamus. Blocking all of the activity transmitted from V1 either by cooling appropriate retinotopic regions (Girard et al., 1992) or by ablation (Rodman et al., 1990) leaves V5 quite impaired but still partly functional. The remaining active neurons are directional. Combined lesions of the colliculus and V1 eliminate activity in V5 (Rodman et al., 1990). These alternative routes are not evidence against the hypothesis of Movshon and Newsome (1996) that the computation of pattern motion takes place in V5. However, considerable work still needs to be done to settle the matter. Clearly, in view of the results obtained in this study, it will be important to establish whether V5 is built of recurrent circuits comparable in structure and function to those of V1.

REFERENCES

Adelson EH, Movshon JA (1982) Phenomenal coherence of moving visual patterns. Nature 300:523–525.

Ahmed B, Anderson JC, Martin KAC, Nelson JC (1994) Polyneuronal innervation of spiny stellate neurons in cat visual cortex. J Comp Neurol 341:39–49.

Ahmed B, Anderson JC, Martin KAC, Nelson JC (1997) Map of the synapses onto layer 4 basket cells of the primary visual cortex of the cat. J Comp Neurol 380:230–242.

Allman JM, Kaas JH (1971) A representation of the visual field in the caudal third of the middle temporal gyrus of the owl monkey (*Aotus trivirgatus*). Brain Res 31:85–105.

Baude A, Nusser Z, Molnár E, McIlhenny RAJ, Somogyi P (1995) High-resolution immunogold localization of AMPA type glutamate receptor subunits at synaptic and non-synaptic sites in rat hippocampus. Neuroscience 69:1031–1055.

Chan-Palay V, Palay SL, Billings-Gagliardi SM (1974) Meynert cells in the primate visual cortex. J Neurocytol 3:631–658.

Chicurel ME, Harris KM (1992) Three-dimensional analysis of the structure and composition of CA3 branched dendritic spines and their synaptic relationships with mossy fiber boutons in the rat hippocampus. J Comp Neurol 325:169–182.

Colonnier M (1968) Synaptic patterns of different cell types in the different laminae of the cat visual cortex: an electron microscopic study. Brain Res 9:268–287.

Czeiger D, White EL (1993) Synapses of extrinsic and intrinsic origin made by callosal projection neurons in mouse visual cortex. J Comp Neurol 330:502–513.

Dehay C, Douglas RJ, Martin KAC, Nelson JC (1991) Excitation by geniculocortical synapses is not "vetoed" at the level of dendritic spines in cat visual cortex. J Physiol (Lond) 440:723–734.

Douglas RJ, Martin KAC (1991) A functional microcircuit for cat visual cortex. J Physiol (Lond) 440:735–769.

Douglas RJ, Martin KAC Whitteridge D (1989a) A canonical microcircuit for neocortex. Neural Comput 1:480–488.

Douglas RJ, Martin KAC, Whitteridge D (1989b) A functional microcircuit for cat visual cortex. J Physiol (Lond) 440:735–769.

Dubner R, Zeki S (1971) Response properties and receptive fields in an anatomically defined region of the superior temporal sulcus in the monkey. Brain Res 35:528–532.

Elston GN, Rosa GP (1997) The occipitoparietal pathway of the macaque monkey: comparison of pyramidal cell morphology in layer 3 of functionally related cortical visual areas. Cereb Cortex 7:432–452.

Faber DS, Korn H (1988) Synergism at central synapses due to lateral diffusion of transmitter. Proc Natl Acad Sci USA 85:8708–8712.

Freund TF, Martin KAC, Soltesz I, Somogyi P, Whitteridge D (1989) Arborisation pattern and postsynaptic targets of physiologically identified thalamocortical afferents in striate cortex of the macaque monkey. J Comp Neurol 289:315–336.

Friedlander MJ, Martin KAC, Wassenhove-McCarthy D (1991) Effects of monocular visual deprivation on the innervation of cortical area 18 in the cat by individual thalamocortical axons. J Neurosci 11:3268–3288.

Fries W, Keizer K, Kuypers HG (1985) Large layer VI cells in macaque striate cortex (Meynert cells) project to both superior colliculus and prestriate visual area V5. Exp Brain Res 58:613–616.

Gilbert CD (1977) Laminar differences in receptive field properties of cells in cat primary visual cortex. J Physiol (Lond) 268:391–421.

Girard P, Salin PA, Bullier J (1992) Response selectivity of neurons in area MT of the macaque monkey during reversible inactivation of area V1. J Neurophysiol 67:1437–1446.

Gray EG (1959) Axosomatic and axodendritic synapses in the cerebral cortex: an electron microscopic study. J Anat 93:420–433.

Harris KM, Stevens JK (1989) Dendritic spines of CA1 pyramidal cells in the rat hippocampus: serial electron microscopy with reference to their biophysical characteristics. J Neurosci 9:2982–2997.

Herrington J, Park YB, Babcock DF, Hille B (1996) Dominant role of mitochondria in clearance of large Ca^{2+} loads from rat adrenal chromaffin cells. Neuron 16:219–228.

Johnson RR, Burkhalter A (1996) Microcircuitry of forward and feedback connections within rat visual cortex. J Comp Neurol 368:383–398.

Jones EG, Powell TPS (1970) An electron microscope study of the laminar pattern and mode of termination of afferent fibre pathways in the somatic sensory cortex of the cat. Philos Trans R Soc Lond B Biol Sci 257:45–62.

Kisvárday ZF, Martin KAC, Whitteridge D, Somogyi P (1985) Synaptic connections of intracellularly filled clutch neurons, a type of small basket neuron in the visual cortex of the cat. J Comp Neurol 241:111–137.

Kullmann DM, Asztely F (1998) Extrasynaptic glutamate spillover in the hippocampus: evidence and implications. Trends Neurosci 21:8–14.

Larkman A, Stratford KJ, Jack JJB (1991) Quantal analysis of excitatory synaptic action and depression in hippocampal slices. Nature 350:344–347.

LeVay S (1986) Synaptic organization of claustral and geniculate afferents to the visual cortex of the cat. J Neurosci 6:3564–3575.

Lowenstein PR, Somogyi P (1991) Synaptic organization of corticocortical connections from the primary visual cortex to the posteromedial lateral suprasylvian visual area in the cat. J Comp Neurol 310:253–266.

Lund JS, Lund RD, Hendrickson AE, Bunt AH, Fuchs AF (1975) The origin of efferent pathways from the primary visual cortex, area 17, of the macaque monkey as shown by retrograde transport of horseradish peroxidase. J Comp Neurol 164:287–303.

Maunsell JH, Van Essen DC (1983) The connections of the middle temporal visual area (MT) and their relationship to a hierarchy in the macaque. J Neurosci 3:2563–2586.

Montague PR (1996) The resource consumption principle: attention and memory in volumes of neural tissue. Proc Natl Acad Sci USA 93: 3619–3623.

Movshon JA, Newsome WT (1984) Functional characteristics of functional cortical neurons projecting to MT in the macaque. Soc Neurosci Abstr 10:933.

Movshon JA, Newsome WT (1996) Visual response properties of striate cortical neurons projecting to area MT in macaque monkeys. J Neurosci 16:7733–7741.

Nguyen PV, Marin L, Atwood HL (1997) Synaptic physiology and mi-

tochondrial function in crayfish tonic and phasic motor neurons. J Neurophysiol 78:281–294.
Nicholls DG, Åkerman KEO (1982) Mitochondrial calcium transport. Biochim Biophys Acta 683:57–88.
Nusser Z, Mulvihill E, Streit P, Somogyi P (1994) Subsynaptic segregation of metabotropic and ionotropic glutamate receptors as revealed by immunogold localization. Neuroscience 61:421–427.
Palmer LA, Rosenquist AC (1974) Visual receptive fields of single striate cortical units projecting to the superior colliculus in the cat. Brain Res 67:27–42.
Peng Y-Y (1998) Effects of mitochondrion on calcium transients at intact presynaptic terminals depend on frequency of nerve firing. J Neurophysiol 80:186–195.
Peters A, Saint Marie RL (1984) Smooth and sparsely spinous nonpyramidal cells forming local axonal plexuses. In: Cerebral cortex, Vol 1. Cellular components of the cerebral cortex (Jones EG, Peters A, eds), pp 419–445. New York: Plenum.
Peters A, Palay SL, Webster HDeF (1991) The fine structure of the nervous system: neurons and their supporting cells, Ed 3. Oxford, UK: OUP.
Riveros N, Fieldler J, Lagos N, Munoz C, Orrego G (1986) Glutamate in rat brain cortex synaptic vesicles: influence of the vesicle isolation procedure. Brain Res 386:405–408.
Rockland KS (1989) Bistratified distribution of terminal arbors of individual axons projecting from area V1 to middle temporal area (MT) in the macaque monkey. Vis Neurosci 3:155–170.
Rockland KS (1995) Morphology of individual axons projecting from area V2 to MT in the macaque. J Comp Neurol 355:15–26.
Rodman HR, Gross CG, Albright TD (1990) Afferent basis of visual response properties in area MT of the macaque. II. Effects of superior colliculus removal. J Neurosci 10:1154–1164.
Rusakov DA, Kullman DM (1998a) Extrasynaptic glutamate diffusion in the hippocampus: ultrastructural constraints, uptake, and receptor activation. J Neurosci 18:3158–3170.
Rusakov DA, Kullman DM (1998b) Geometric and viscous components of the tortuosity of the extracellular space in the brain. Proc Natl Acad Sci USA 95:8975–8980.
Schikorski T, Stevens CF (1997) Quantitative ultrastructural analysis of hippocampal excitatory synapses. J Neurosci 17:5858–5867.
Shipp S, Zeki S (1989) The organisation of connections between area V5 and V1 in macaque monkey visual cortex. Eur J Neurosci 1:309–332.
Silver RA, Cull-Candy SG, Takahashi T (1996) Non-NMDA glutamate receptor occupancy and open probability at a rat cerebellar synapse with single and multiple release sites. J Physiol (Lond) 494:231–250.
Simoncelli EP, Heeger DJ (1998) A model of neuronal responses in visual area MT. Vision Res 38:743–761.
Somogyi P, Kisvárday ZF, Martin KAC, Whitteridge D (1983) Synaptic connections of morphologically identified and physiologically characterised large basket cells in the striate cortex of cat. Neuroscience 10:261–294.
Sterio DC (1984) The unbiased estimation of number and sizes of arbitrary particles using the disector. J Microsc 134:127–136.
Stratford KJ, Tarczy-Hornoch K, Martin KAC, Bannister NJ, Jack JJB (1996) Excitatory synaptic inputs to spiny stellate cells in cat visual cortex. Nature 382:258–261.
Suarez HH, Koch C, Douglas RJ (1995) Modeling direction selectivity of simple cells in striate visual cortex within the framework of the canonical microcircuit. J Neurosci 15:6700–6719.
Tang Y-G, Zucker RS (1997) Mitochondrial involvement in post-tetanic potentiation of synaptic transmission. Neuron 18:483–491.
Tarczy-Hornoch K, Martin KAC, Jack JJB, Stratford KJ (1998) Synaptic interaction between smooth and spiny neurons in layer 4 of cat visual cortex. J Physiol (Lond) 508:351–363.
Ungerleider LG, Mishkin M (1979) The striate projection zone in the superior temporal sulcus of Macaca mulatta: location and topographic organisation. J Comp Neurol 188:347–366.
Uteshev VV, Pennefather PS (1997) Analytical description of the activation of multi-state receptors by continuous neurotransmitter signals at brain synapses. Biophys J 72:1127–1134.
Xu T, Naraghi M, Kang H, Neher E (1997) Kinetic studies of Ca^{2+} binding and Ca^{2+} clearance in the cytosol of adrenal chromaffin cells. Biophys J 73:532–545.
Zeki S (1969) Representation of central fields in prestriate cortex of monkey. Brain Res 19:63–75.
Zeki S (1974) Functional organisation of a visual area in the posterior bank of the superior temporal sulcus of the rhesus monkey. J Physiol (Lond) 236:549–573.

3.2 The second in the series was the V2 to MT projection, a pathway for which there was good LM background. Another feedforward projection to MT, spanning extrastriate cortices and not showing the LM features noted in the case of the V1 to MT projection. In this case the axons and their boutons appear smaller with only one principle layer of innervation, layer 4, with other laminae receiving fewer boutons but with more widespread distribution even up to layer 1.

THE JOURNAL OF COMPARATIVE NEUROLOGY 443:56–70 (2002)

Connection From Cortical Area V2 to MT in Macaque Monkey

JOHN C. ANDERSON* **AND KEVAN A.C. MARTIN***
Institute for Neuroinformatics, University of Zürich and ETH Zürich,
Winterthurerstr. 190 8057 Zürich, Switzerland

ABSTRACT

The extrastriate visual area of the macaque monkey called MT or V5, receives its input from multiple sources. We have previously examined the synaptic connections made by V1 cells that project to MT (Anderson et al., 1998). Here, we provide a similar analysis of the projection from V2 to MT. The major target of the V2 projection in MT is layer 4, where it forms clusters of asymmetric (excitatory) synapses. Unlike the V1 projection, it also forms synapses in layers 1 and 2 and does not form synapses in layer 6. The most frequently encountered targets of boutons labeled from V2 were spines (67% in layer 4; 82% in layer 2/3). Unusually, only 5/12 boutons examined in layer 1 actually formed synapses. Unlike the V1 projection, multisynaptic boutons were rare (mean, 1.1 synapses per bouton vs. 1.7 for the V1 projection). Like the V1 projection, the input to MT from any point in V2 is sparse (contributing approximately 4–6% of the asymmetric synapses in the densest clusters in layer 4). The synapses of the V2 projection were similar in size to those of the V1 projection (0.1 μm^2 vs. 0.09 μm^2) and both formed more complex postsynaptic densities on spines than on dendritic shafts. The clear differences between the V1 and V2 projection to MT indicate that their functions are complementary rather than completely overlapping. J. Comp. Neurol. 443: 56–70, 2002.

Indexing terms: visual cortex; area MT; corticocortical; light and electron microscopy; synapse morphology; postsynaptic target

The interconnections between cortical areas have been intensively explored in the primate since anatomists began their concerted effort to trace these pathways at the end of the 1960s. The extensive database that has since emerged has been used to develop models of the basic circuits of primate visual cortex, the most prominent of which are hierarchical models (Rockland and Pandya, 1979; Friedman, 1983; Maunsell and Van Essen, 1983; Felleman and Van Essen, 1991; Young, 1992; Jouve et al., 1998; Sporns et al., 2000; Barone et al., 2000) that use differences in the laminar patterns of interconnections to define projections as feedforward, lateral, or feedback. The anatomic studies have also formed the critical mass of data that has been crucial for the functional exploration of extrastriate visual cortex and for interpreting the results from human functional imaging studies. In their extreme simplification, the convenient divisions into feedforward, feedback, and lateral may obscure subtle but important differences between projections in a particular division. To explore this possibility, we compare here the connections made by two feedforward projections with the same target area MT.

We have previously examined, at light and electron microscopic level, the projection from V1 to MT, so for comparative purposes, we made a similar analysis of the projection from V2 to MT. The neurons that are the source of this V2 projection have been identified by retrograde transport of tracers (Lund et al., 1981; Maunsell and van Essen, 1983; Ungerleider and Desimone, 1986). They are pyramidal cells located mostly in layer 3B, with some scattered in layers 2, 3A, and 5. With anterograde tracers and light microscopy, Rockland (1995) found that both V1 and V2 axons terminate in the middle layers of MT, but unlike the V1 axons, the V2 axons do not form collateral

Grant sponsor: The EU; Grant number: QULG3-1999-01064; Grant sponsor: HFSP; Grant number: RG0123/2000-B; Grant sponsor: Swiss National Science Foundation.

*Correspondence to: John G. Anderson and Kevan A.C. Martin, Institute for Neuroinformatics, University of Zürich and ETH Zürich, Winterthurerstr.190, 8057 Zürich, Switzerland. E-mail: kevan@ini.phys.ethz.ch

Received 30 July 2001; Revised 10 October 2001; Accepted 23 October 2001

DOI 10.1002/cne.10100

projections in layer 6. A subsequent electron microscopic analysis (Anderson et al., 1998) indicated that the synapses formed in MT by the V1 axons are mainly with spiny dendrites (80%), with the remainder being with somata and dendrites of smooth neurons The large terminal boutons of the V1 afferents in MT were multisynaptic and formed morphologically heterogeneous synaptic specializations. The results of the present study indicate that, although there are basic similarities between the two projections, in that both have a dominant input to excitatory neurons in layer 4 of MT, there are sufficient points of difference to suggest that the feedforward pathways may be interestingly heterogenous in the fine structure and function of their connections.

MATERIALS AND METHODS

The material presented here was taken from two adult female macaque monkeys (*Macaca mulatta*). Animals were prepared for surgery after the administration of an intramuscular premedication of xylazine (Rompun, Beyelar, 0.5 mg/kg)/ketamine (Ketalar, Parke Davis, 10 mg/kg). This was followed by cannulation of a femoral vein for the delivery of alphaxalone/alphadalone (Saffan, Glaxo) to establish complete anaesthesia. Sterile surgery was carried out in accordance with the guidelines of the Cantonal Veterinary Authority of Zürich.

Each animal received pressure injections (~0.5 μl each) of the neuronal tracers biotinylated dextran amine (BDA; Molecular Probes, Leiden, The Netherlands) and *Phaseolus vulgaris* leucoagglutinin (PHA-L; Vector Laboratories, Burlingame, CA). One animal received four injections of 10% BDA in 0.01 M phosphate buffered saline pH 7.4 (PBS) and two of PHA-L in 10 nM phosphate buffer pH 7.4 (PB). The second animal received five and three injections of the above, respectively. After a 14-day survival period, the animals were very deeply anesthetized with i.v. pentobarbital (20 mg/kg) and then perfused transcardially with a normal saline solution, followed by a solution of 4% paraformaldehyde, 0.3% glutaraldehyde, and 15% picric acid in 0.1 M PB pH 7.4. The brain was removed from the skull, and a block of cortex containing the injection site and area MT was removed. The block was allowed to sink in sucrose solutions of 10, 20, and 30% in 0.1 M PB. Sections were cut from the block at 80 μm in the parasagittal plane and collected in 30% sucrose in 0.1 M PB. The sections were then freeze-thawed in liquid nitrogen and washed in 0.1 M PB. We used standard procedures to reveal the neuronal tracers. In brief outline; washes in PBS were followed by 10% normal swine serum (NSS) in PBS (1 hour). The antibody to PHA-L was diluted in the above at 1:200 and exposed for 48 hours at 5°C. Further washes in NSS preceded overnight exposure (5°C) to an avidin-biotin complex (Vector ABC kit-Elite). The peroxidase activity was identified by using 3,3-diaminobenzidene tetrahydrochloride (DAB). After assessment by light microscopy, selected regions of tissue were treated with 1% osmium tetroxide in 0.1 M PB. Dehydration through alcohols (1% uranyl acetate in the 70% alcohol) and propylene oxide allowed flat mounting in Durcupan (Fluka) on glass slides.

Light microscopic observations of labeled axons were carried out to locate and select regions of interest for electron microscopy. We reconstructed individual collaterals in the less densely innervated areas for correlated light and electron microscopy. Serial ultrathin sections were collected at 70-nm thickness on Pioloform-coated single-slot copper grids. Labeled boutons were photographed at a magnification of 21,000. Synapses and associated structures were classified by using conventional criteria. Collections of serial sections were digitized and reconstructed by using Trakem, an in-house EM-digitization package. To measure and display the postsynaptic densities of labeled boutons, we used software developed by ourselves which has been described in outline elsewhere (see Materials and Methods section; Anderson et al., 1998).

The estimates of labeled bouton density were derived by using the physical disector method (Sterio, 1984). We selected regions of particularly dense innervation by labeled axons for re-embedding. Serial 70-nm-thick sections were collected from these regions and a "reference" and "look-up" section was selected. The reference and look-up sections were separated by one section. Photomicrographs were taken with the electron microscope to form strips of tissue, 12 to 16 images abutted together, or patches of tissue, e.g., 2 × 8 images. All electron photomicrographs were taken at 11,500× magnification. Synapses that were in the reference section, but that disappeared in the look-up section were counted. Synapses that were present in both look-up and reference sections were not counted (Sterio, 1984). However, all photographed labeled synapses were used in some part of the following analysis.

RESULTS

Light microscopy

Each of two monkeys received pressure injections of BDA and PHA-L into area V2 (area 18) along the crest of the lunate gyrus (Fig. 1A). With one exception, needle tracks were all confined to the gray matter of V2 and could be followed through all laminae (Fig. 1B). In one animal, the injections were made into the dorsal surface of V2, the needle track being almost parallel to the cortical laminae. Penetrations made in the second animal traversed the tip of the gyrus and extended into the lunate sulcus (e.g., Fig. 1B). One track in this animal went through the white matter. The resulting label spread over 5–7 mm mediolaterally. BDA labeling was poor at the injection site, but PHA-L labeling was excellent. Labeling was densest along the path of the penetrations. Most of the uptake was by pyramidal cells of layer 2/3, covering most of the tip of the gyrus, but labeled cell bodies were also found in layers 4, 5, and 6. Strong anterograde labeling was seen in striate and extrastriate visual areas, including MT, along with some pale-stained cell bodies (Fig. 2). The strongest transport was to V1, where the retrograde labeling was similar to that previously reported by Kennedy and Bullier (1985), i.e., predominantly in layers 2/3 and 4B, with some sparse cell bodies scattered along the layer 5/6 border. No cell or terminal labeling was evident in layer 4. Patches of labeled axons and palely stained cell bodies were also seen in the fundus and anterior bank of the lunate sulcus and in the posterior bank of the superior temporal sulcus. The distinctive myelination of MT was evident in the osmicated sections, and the labeled axons terminated at a point where MT forms a small bulge in the sulcus.

In area MT, the labeled axons entered from the white matter and sometimes branched as they passed through layers 5 and 6. On reaching layer 4, the axons branched

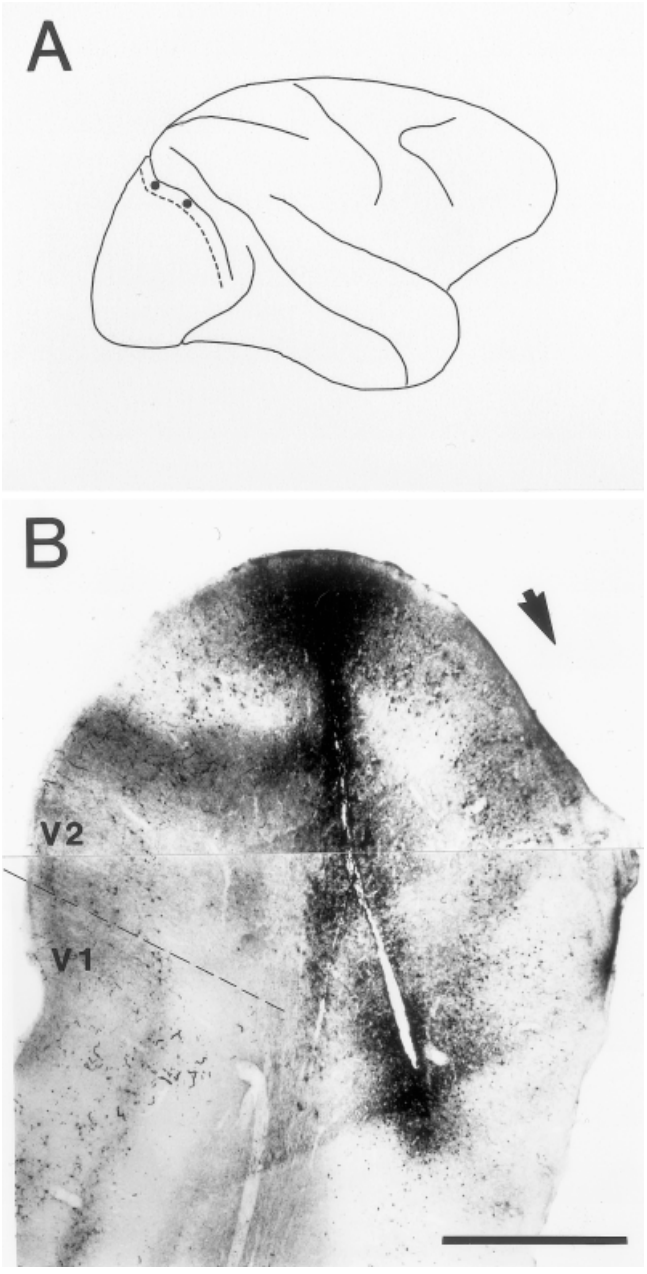

Fig. 1. Location of injection sites. **A:** Schematic drawing of macaque brain showing region in which injections were made (in zone between filled circles) along the edge of the lunate sulcus. The V1/V2 border is indicated by the dotted line. **B:** Photomontage of light photomicrographs of parasagittal section of the lunate gyrus showing an example of an injection site and label. The lunate sulcus is indicated by an arrow and the V1/V2 border by a dotted line. Scale bar = 1 mm in B.

extensively and formed synaptic boutons. This profusion of axons and both *en passant* and *terminaux* boutons gave an overall patchy appearance to the innervation site when viewed at low power in the light microscope (Fig. 2). The largest boutons were formed by axons with the thickest diameter, but bouton size and axon diameter was highly variable within layer 4.

Axons that projected into the more superficial layers were more slender than the main trunks seen in layer 4. They gave rise to *en passant* boutons of a fairly uniform size (Figs. 2, 4A,B) spaced at fairly regular intervals. Most of these axons terminated in or before upper layer 2/3. Occasionally thicker axons, passing through layer 3, branched before reaching layer 2 and produced a fanlike arborization. The axon diameter in these superficial layer axons reduced rapidly as they branched. A few axons could be followed up to the top of layer 2 and into layer 1 (Fig. 7). Axons that branched in layer 2 and sent a projection to layer 1 were fine and produced small, mostly *en passant* boutons. Axons that passed straight up to layer 1 without forming collaterals in layer 2 had larger boutons. Layer 1 had the poorest tissue quality for light and electron microscopy.

Weak retrograde labeling (Fig. 2) was evident by palely stained neuronal somata and proximal portions of the dendrites, in some instances. These cells were sparse and were clearly of a pyramidal morphology. The majority of retrogradely labeled somata occurred in layer 6 and 2/3. Less frequently somata could be seen within the elaborate tangle of anterograde labeled axon collaterals in layer 4. It was difficult to determine the nature of their morphology, pyramidal or stellate, due to the light staining of the somata and the intense staining of the labeled axon arbors arising from the anterogradely labeled V2 projection. The density of the labeling in layer 4 made it impossible to reconstruct at a light microscope level extensive portions of single axons. This density also made tight LM/EM correlation impossible. Thus, we selected for EM analysis areas of layer 4 with the densest labeling as determined in the light microscope. This sample included the greatest range of variation of bouton sizes for our EM study. The projections to the superficial layers were sparser and this enabled us to correlate light and electron microscopy.

Electron microscopy

We examined a total of 189 boutons from layers 1, 2/3, and 4 (12 from layer 1, 64 from layer 2/3, and 113 from layer 4). Of this sample, 133 boutons were serially sectioned and completely reconstructed and the remaining 56 were used for estimates of synaptic density, where we required only three sequential sections. A total of 199 labeled synapses were examined, all of which were asymmetric (Gray's type 1). We reproduced the electron photomicrographs of boutons from this study at approximately the same magnification as the images used in a previous study of V1 afferent boutons in MT (Anderson et al., 1998). This choice was made to facilitate a comparison of the two projections to MT.

The reaction end product was dark, although of variable intensity in different boutons. Vesicles and mitochondria were clearly visible inside the boutons and the synaptic clefts were not obscured by label. Myelinated axons were also labeled, confirming that the antibody had penetrated well, despite the insulating sheath. Small vacuoles formed in labeled structures (e.g., Figs. 3A,B, 5A). Most boutons were small (~0.5 μm diameter), compact structures containing one or two mitochondria and a cluster of vesicles over the region of the synaptic specialization (e.g., Figs. 3, 4, 6, 7). The synapse was indicated by the presence of presynaptic vesicles, a synaptic cleft and a postsynaptic density in the target structure. Occasionally, we saw a density within the labeled bouton that was mirrored by a

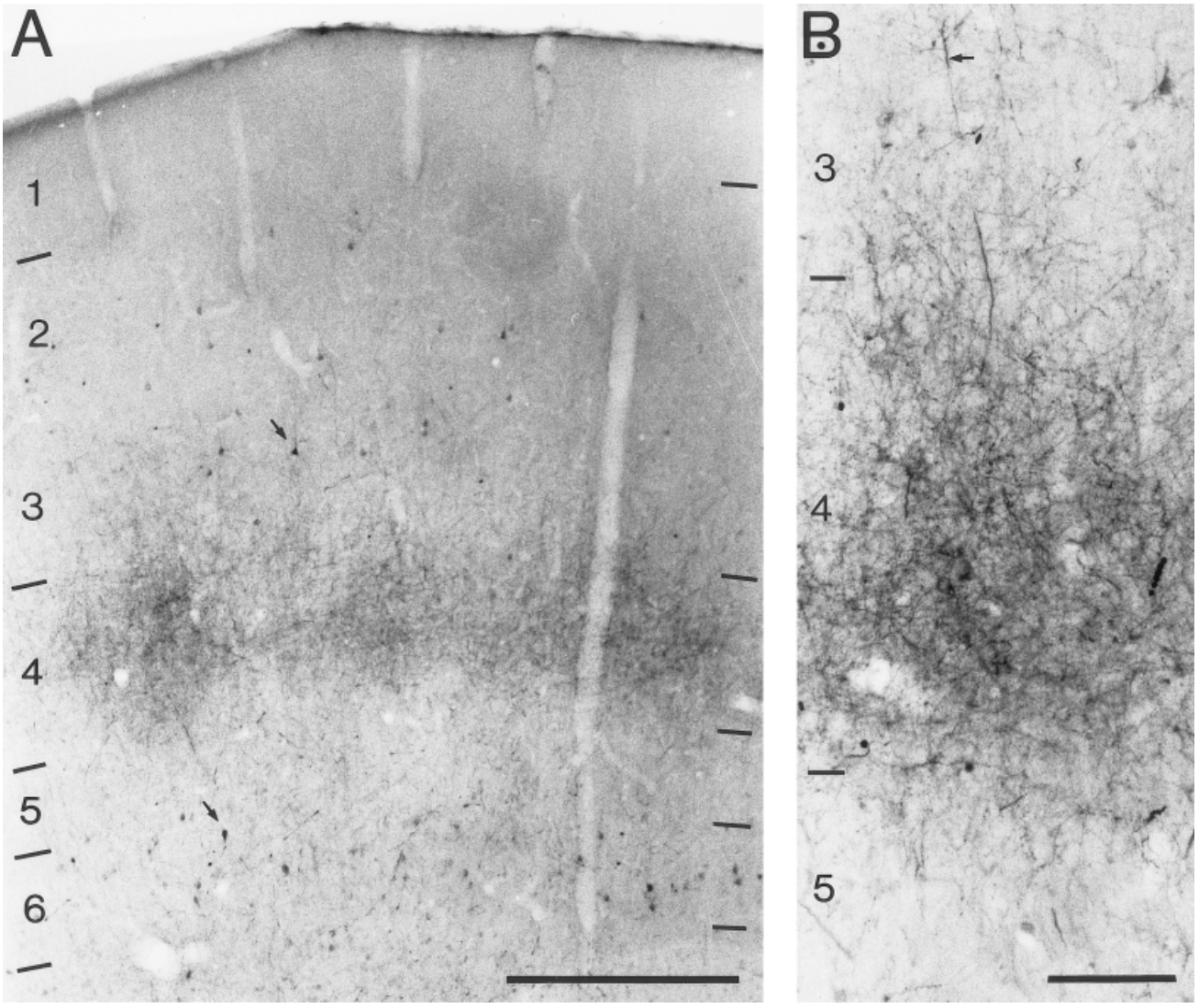

Fig. 2. Light photomicrographs of cortical area V5 showing *Phaseolus vulgaris* leucoagglutinin (PHA-L) -labeled axon termination zone. **A:** Labeled terminals form dense patches in layer 4 and lesser projections into layer 3. Laminae and their boundaries are indicated to the left and right. Lightly stained, retrogradely labeled cell bodies are located in layers 3 and 6 (small arrows). **B:** Adjacent section to A taken at higher-power magnification. The labeled fibres branch profusely in layer 4 to form a dense network of axon collaterals and terminals. Numerous small and large (small arrow) caliber axons can be seen projecting through superficial layer 3. Laminae and their boundaries are indicated to the left. Scale bars = 0.5 mm in A, 100 μm in B.

similar density within the target (Fig. 5A,B,C). In the immediate vicinity of the presynaptic density, there were no vesicles. This mirror-like configuration was always seen close or adjacent to a conventional asymmetric synapse and was classified as a *puncta adherens* (Peters et al., 1991). We did not include these *puncta* in our reconstructions or estimates and measurements of synapses.

Spines. Serially sectioning the bouton, synapse, and target structures greatly assisted in determining the type of target that formed synapses with the labeled boutons. We also used standard ultrastructural criteria to classify targets (Peters et al., 1991). The most frequent targets were small spines (Figs. 3, 4, 7). Occasionally, we were able to trace spines back to a parent dendrite (Fig. 3B). A second synapse from an unlabeled bouton was seen on six of the spines and, in all cases, was of a symmetric morphology (Gray's type 2) (Fig. 3C). Only one spine was of the short and neckless "sessile" variety. Spines were the sole targets of the five synapses found in layer 1. Spine synapses formed 58 of the 71 synapses examined in layer 2/3, and 81 of the 121 synapses identified in layer 4.

Dendrites. Dendrites were also the targets of labeled boutons. These were usually identified by reconstruction from serial sections or by the presence of mitochondria and microtubules. The majority of dendrites were of fairly small caliber (~0.5–1 μm diameter) (Fig. 3E,D). The larger diameter dendrites were more easily characterized, although more infrequent (Fig. 3F). By using serial sections, dendrites could be grouped into two classes. One class had little variation in diameter when reconstructed

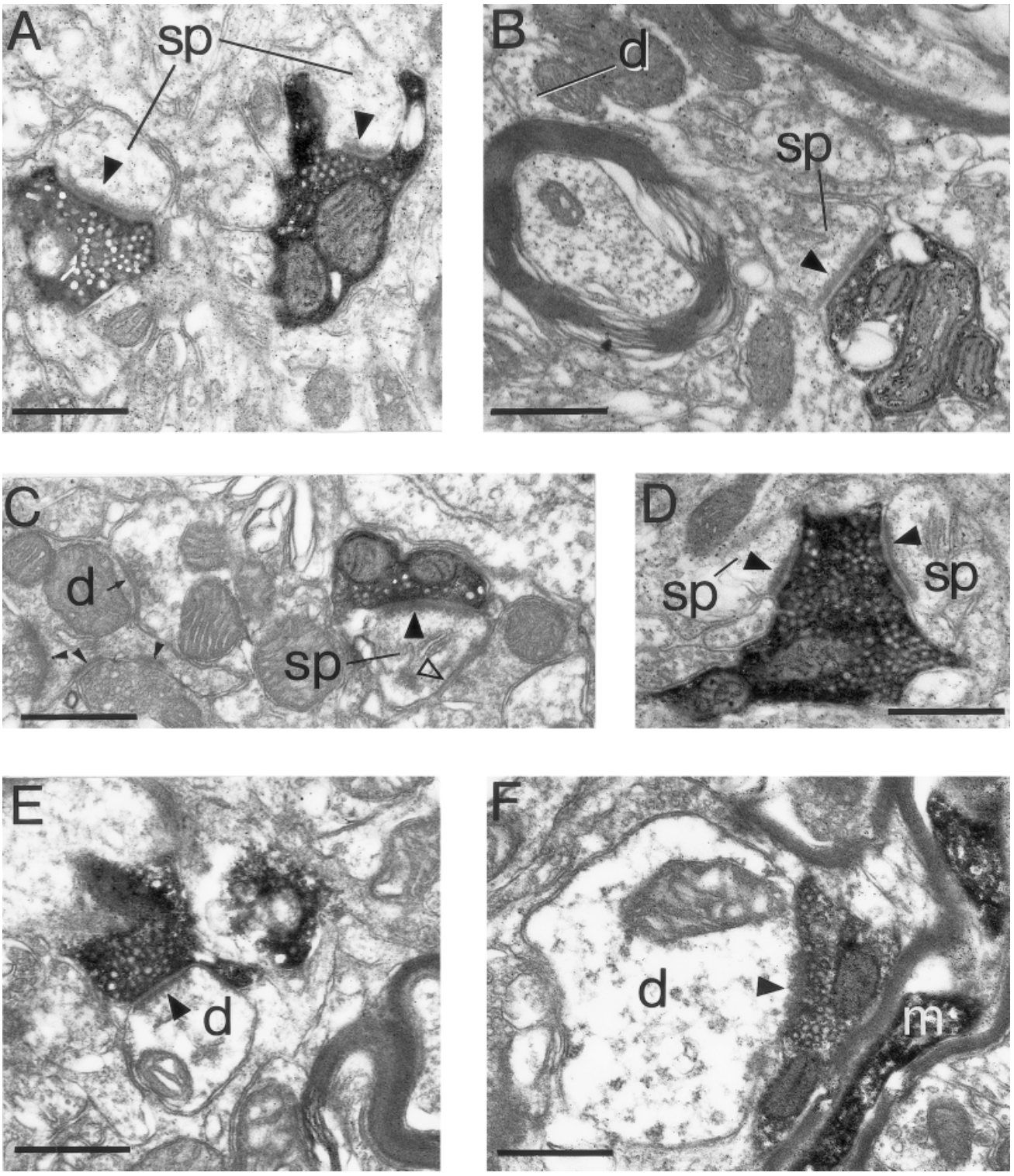

Fig. 3. Electron photomicrographs of *Phaseolus vulgaris* leucoagglutinin (PHA-L) -labeled electron dense axon and boutons located in layer 4 of area V5. A–D: Examples of synapses formed with spines. **A:** Two small boutons form asymmetric synapses (solid arrowheads) with spines (sp). This bouton/target configuration was characteristic of the majority of synaptic contacts seen in this study. Both boutons and their target spines have a small profile, the bouton contains at least one mitochondria and the remaining small space (usually above the synapse) is vesicle filled. **B:** A labeled bouton forms an asymmetric synapse (arrowhead) with a spine (sp), which can be traced back to the parent dendrite (d) within the same section. **C:** A spine forms an asymmetric synapse (large solid arrowhead) with a labeled bouton and a symmetric synapse (open arrowhead) with an unidentified bouton. A spine apparatus can be seen within the spine. For comparison of synapses within the same picture an unidentified dendrite (d) forms asymmetric (small solid arrowheads) and symmetric (small arrow) synapses with unidentified boutons. **D:** Two spines (sp) form asymmetric synapses (arrowheads) with a labeled bouton. The spine to the right contains a clearly identifiable spine apparatus. **E,F:** Examples of synapses formed with dendrites containing few mitochondria, forming synapses infrequently and showing little variation in diameter. These features are characteristic of neurons with spiny dendrites. **E:** A small caliber dendrite (d) forms an asymmetric synapse with a labeled bouton (arrowhead). **F:** A large caliber dendrite (d) forms an asymmetric synapse (arrowhead) with a labeled bouton. Adjacent to the bouton is a labeled myelinated axon (m). Scale bars = 0.5 μm in A–F.

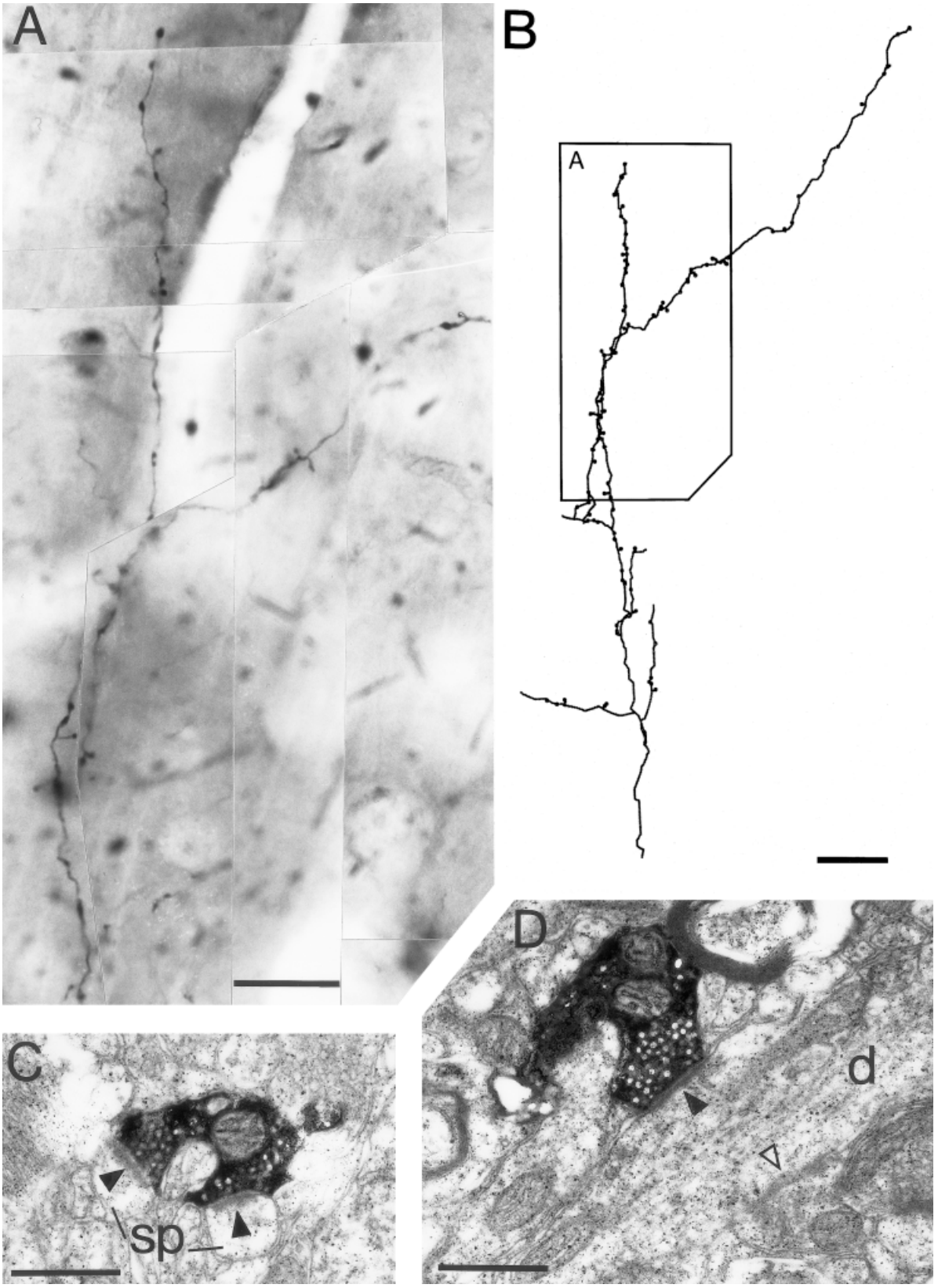

Fig. 4. Light and electron photomicrographs of *Phaseolus vulgaris* leucoagglutinin (PHA-L) -labeled axon and boutons located in layer 2/3. **A:** Photomontage of a single ascending collateral taken from the middle of layers 2 and 3. Numerous varicose swellings of the *en passant* and *terminaux* types can be clearly seen along the axon length. **B:** Light microscopic reconstruction of the collateral shown in A. The border between layers 1 and 2 is approximately 200 μm from the uppermost bouton, and the border between layers 3 and 4 is approximately 400 μm from the lowest point of the reconstructed axon. The box-shaped boundary represents the area shown in the photomontage (A). C,D: Electron photomicrographs of labeled boutons taken from the collateral shown in A. **C:** A small labeled bouton forms asymmetric synapses (arrowheads) with two spines (sp). **D:** A labeled bouton forms an asymmetric synapse (solid arrowhead) with a dendrite (d), and an unidentified bouton forms an obliquely sectioned symmetric synapse (open arrowhead) with the same dendrite. The dendrite shows little variation in diameter, forms synapses infrequently, and contains few mitochondria. Neurons with spiny dendrites show these features. Scale bars = 20 μm in A, 40 μm in B, 0.5 μm in C,D.

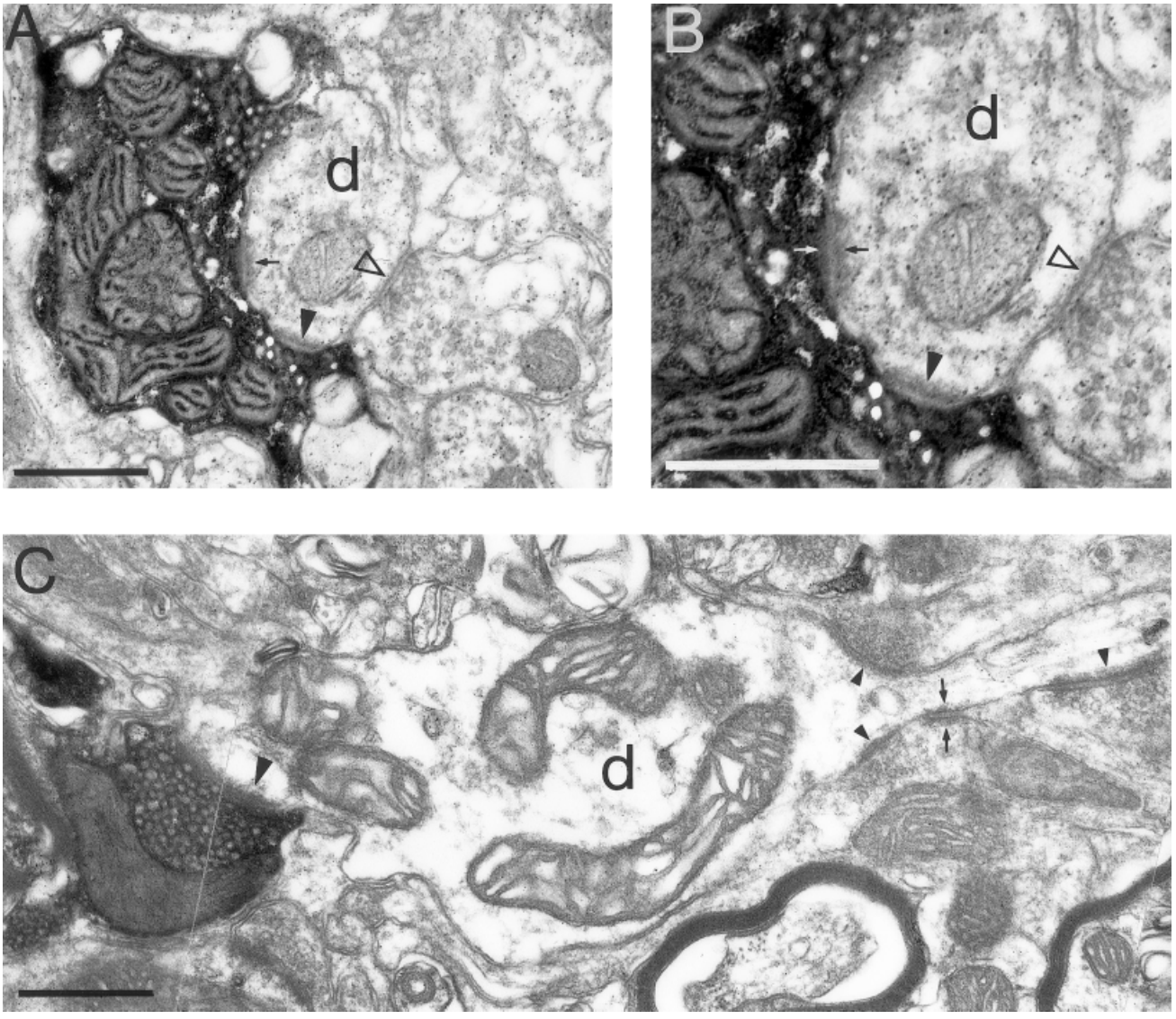

Fig. 5. Electron photomicrographs of *Phaseolus vulgaris* leucoagglutinin (PHA-L) -labeled boutons of layer 4 forming synapses with dendrites that contained numerous mitochondria, form many synapses, and have a smooth and beaded morphology. These are features associated with GABA-ergic neurons with smooth dendrites. The morphology of the dendrite was determined by serial section reconstruction. **A:** A large labeled bouton forms an asymmetric synapse (solid arrowhead) and a puncta adherens (small arrow) with a dendrite (d). The puncta appears as a density seen within the dendrite. It was situated adjacent to the asymmetric synapse and opposite the symmetric synapse. The dendrite also forms a symmetric synapse (open arrowhead) with an unidentified bouton. **B:** A higher-power photomicrograph of the dendrite (d) showing detail of the puncta and synapses indicated in B. The two synapses are indicated as in A. The puncta can be characterized by the density seen within the dendrite (black arrow) and a similar density within the labeled bouton (white arrow; the density appears gray against the black reaction product). Synaptic vesicles are clearly absent in the vicinity of the density within the bouton and present in the region presynaptic to the asymmetric synapse. **C:** A labeled bouton forms a synapse (large arrowhead) with a dendrite (d) that is of variable diameter. The dendrite contains several mitochondria within the segment of greatest diameter, and three asymmetric synapses (small solid arrowheads) form with unidentified boutons as the dendrite narrows rapidly. One of the boutons also forms a puncta (arrows) with the dendrite. Scale bars = 0.5 μm in A–C.

and formed few synapses, which is characteristic of the spiny dendrites of excitatory neurons. Six of the 12 dendritic synapses in layer 2/3 were of this variety and 9 of 19 of the completely reconstructed synapses in layer 4 were with spiny dendrites.

Another morphology of dendrite had a widely variable diameter (Fig. 5). A fortuitous plane of section along the length of such a dendrite make the changes in diameter obvious (Fig. 5C). In others, the varicose form of the dendrite was obvious after serial reconstruction. Such dendrites usually contained numerous mitochondria and even in single sections would form multiple synapses with other unidentified boutons. These dendrites are quite characteristic of neurons with smooth, varicose, or beaded dendrites that contain the inhibitory neurotransmitter GABA (Somogyi et al., 1983; Peters and Saint Marie, 1984; Kisvár-

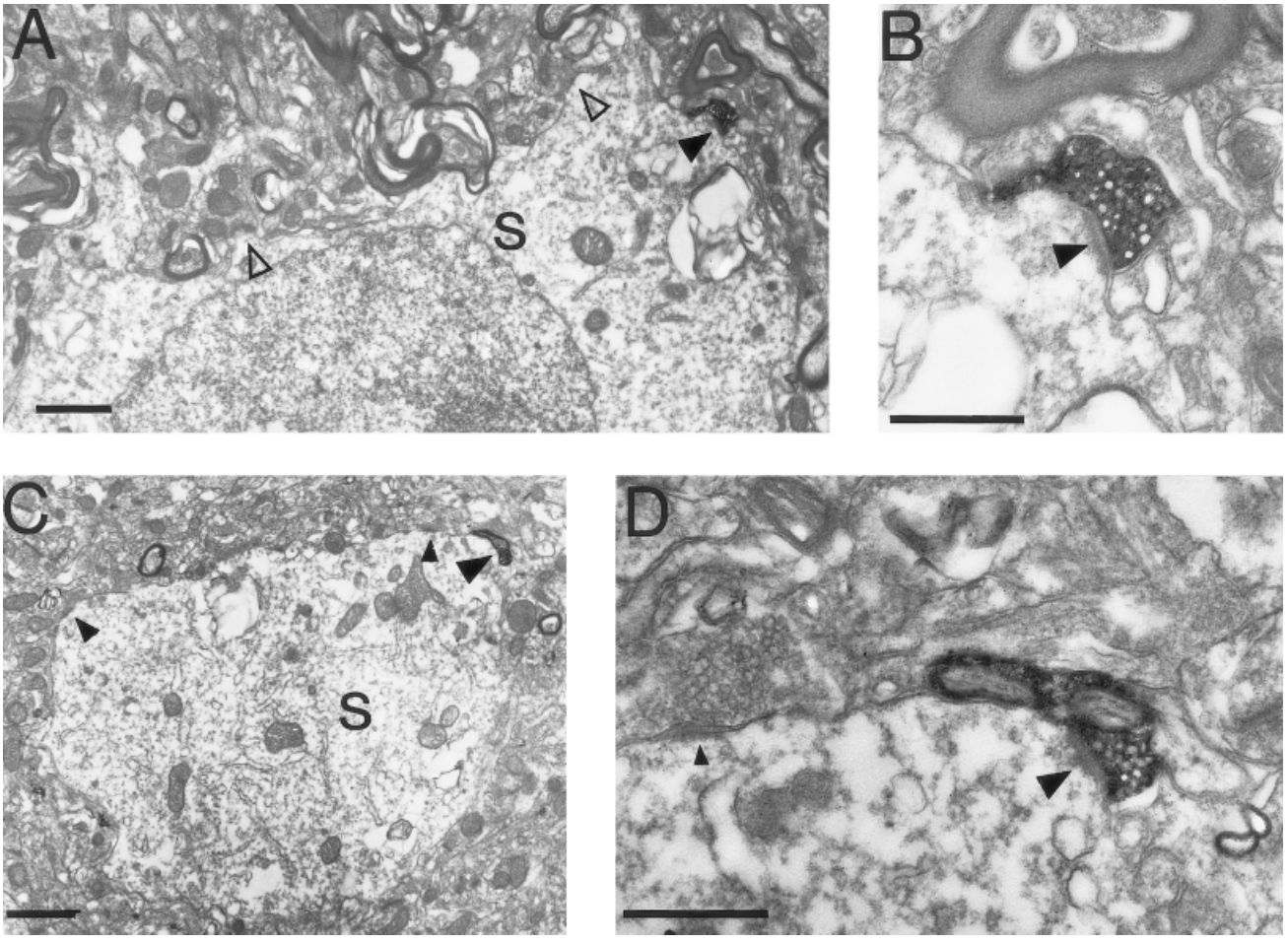

Fig. 6. Electron photomicrographs of labeled boutons in synaptic contact with soma. A,B: Bouton and soma from layer 4. **A:** Low-power electron photomicrograph of soma (s) forming an asymmetric synapse (solid arrowhead) with a small labeled bouton. The soma contains few mitochondria or organelles of the perikaryon and formed few synapses other than symmetric synapses (open arrowheads). These features are observed in excitatory neurons with spiny dendrites. **B:** High-power image of detail of the asymmetric synapse (solid arrowhead) indicated in A. **C:** Low-power electron photomicrograph of soma (s) from layer 3 in contact with labeled bouton (large arrowhead). The soma contained numerous mitochondria and perikaryal organelles as well as forming asymmetric synapses (small arrowheads) with unidentified boutons. These features are associated with γ-aminobutyric acid–containing neurons with smooth dendrites. **D:** High-power view of the adjacent section to that shown in C of the labeled bouton forming an asymmetric synapse (large arrowhead). For comparison of synapses, an adjacent asymmetric synapse (small arrowhead) formed by an unidentified bouton is included. Scale bars = 1 μm in A,C, 0.5 μm in B,D.

day et al., 1985; Ahmed et al., 1997). A surprisingly high proportion of serially reconstructed target dendrites had the features of smooth (GABAergic) neurons. In layer 2/3, 6 of 12 labeled synapses formed on these dendrites, and 10 of 19 synapses (52%) in layer 4 formed on smooth dendrites. By comparison, only 26% of the dendritic targets of the V1 projection to MT were smooth dendrites (Anderson et al., 1998). The only target that could be demonstrated to receive multiple synapses (3) from a labeled bouton was a smooth dendrite located in layer 2/3.

Somata. Only two neuronal somata were found to form synapses with labeled boutons (Fig. 6). Both of these synapses were from tiny boutons forming equally tiny synapses. One of these target soma was located in layer 4 and contained few mitochondria and organelles of the perikaryon and formed few synapses other than symmetric synapses. These features are generally attributed to neurons with spiny dendrites or excitatory neurons. The second soma was in layer 2/3. It contained numerous mitochondria, showed a lot of rough endoplasmic reticulum and formed asymmetric synapses with nonlabeled boutons. This finding is characteristic of a GABAergic cell soma, where asymmetric synapses on the soma are common.

Layer 1. We examined two axons projecting to layer 1 (Fig. 7). One axon showed labeling of a quality as we had seen in other laminae (left in Fig. 7A). The postsynaptic densities and synaptic clefts were clearly identified (Fig. 7B). The labeling of the second axon was very intense (right in Fig. 7A) and affected the structures surrounding the bouton. Only one bouton and its synapse could be used from this collateral (Fig. 7C). Only 5 of 12 of the optimally preserved boutons examined from layer 1 showed any synaptic specialization. However, the boutons all contained mitochondria and were filled with vesicles. The same collateral that provided most of the layer 1 data was

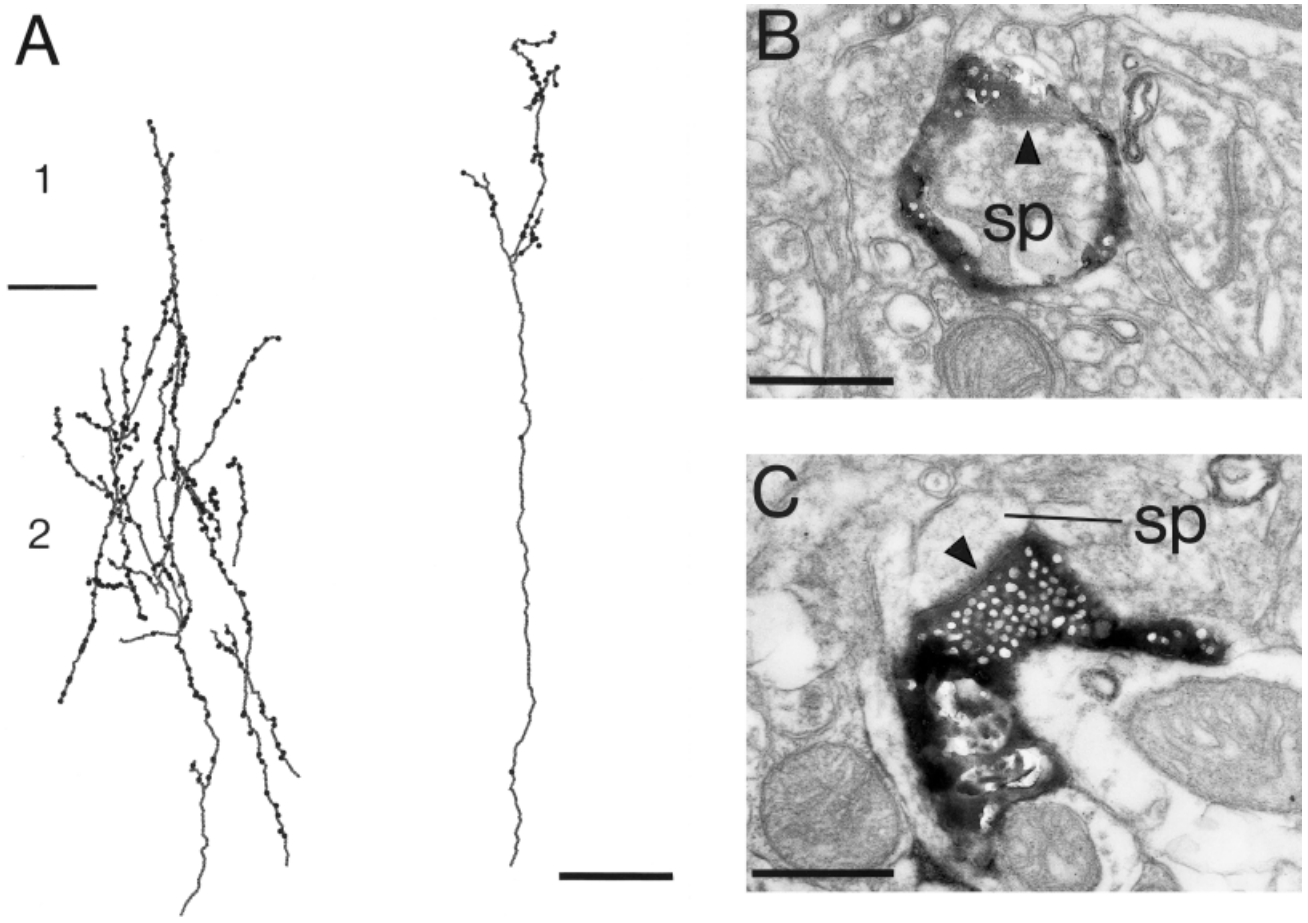

Fig. 7. Reconstructions and electron photomicrographs of the most superficially projecting *Phaseolus vulgaris* leucoagglutinin (PHA-L) -labeled axons. **A:** Two light microscopic reconstructions of axons projecting to layers 1 and 2. The axon on the left produces many collaterals and varicose swellings in layer 2 and continues with a smaller projection into layer 1. The axon on the right projects directly to layer 1 before producing collaterals or swellings. The laminae are indicated to the left. **B:** A labeled layer 1 bouton taken from the left-hand axon shown in A. The bouton forms an asymmetric synapse (arrowhead) with a spine (sp) and wraps around the circumference of the spine. **C:** A labeled layer 1 bouton taken from the right-hand axon shown in A forming an asymmetric synapse (solid arrowhead) with a spine (sp). Only half of the bouton swellings of layer 1 examined in the electron microscope formed synapses, although all were filled with vesicles. Scale bars = 10 μm in A, 0.5 μm in B,C.

also examined in layer 2. Six labeled boutons located slightly deeper (~10 μm) in the cortex at the border of layers 1 and 2 were examined and all formed synapses. Boutons in layer 1, synaptic or nonsynaptic, were also invaded by one or sometimes two nonlabeled structures, usually identifiable as boutons. All of the identified synaptic targets in layer 1 were spines.

Postsynaptic density. Reconstructing the bouton and its target gave us the opportunity to view the complete postsynaptic density as a two-dimensional (2-D) or 3-D structure. We have used this technique previously to obtain values of the surface area of synapses (Anderson et el., 1998). By focusing on the postsynaptic specialization rather than the presynaptic membrane, we avoided detail being obscured by reaction end-product in the bouton. We show a 2-D projection of the postsynaptic densities in Figure 8. There was no difference seen in the distributions of the areas of synapses made with the two main target types, spines and dendrites. Both had a mean of approximately 0.09 μm^2. When comparing synapses from different laminae, the distributions overlapped considerably (Fig. 9). Nevertheless, the layer 2/3 synapses were significantly smaller (mean, 0.076 μm^2; SEM, 0.004) than those of layer 4 (mean, 0.107 μm^2; SEM, 0.008) ($P = 0.0008$, two tailed t test). This significant difference was caused mainly by the higher frequency of very small synaptic areas seen in layers 2/3.

The postsynaptic density can be perforated giving it a doughnut or horseshoe morphology, as opposed to a simple disc. Figure 8 shows that the synapses with the more complex morphology are often formed with spines. A similar observation was made in the study of synapses made by V1 afferent boutons in area MT. However, the synapses formed by the V2 afferent boutons did not reach the degree of variety seen for the synapses of V1 boutons (Anderson et al., 1998). The mean size of the synapses of V2 in layer 4 (mean, 0.107 μm^2; SEM, 0.008) was slightly larger than that of the V1 boutons in layer 4 (mean, 0.093 μm^2; SEM, 0.007) (Fig. 10), but the difference was not significant ($P = 0.2$, two tailed t test). The synapses of V1

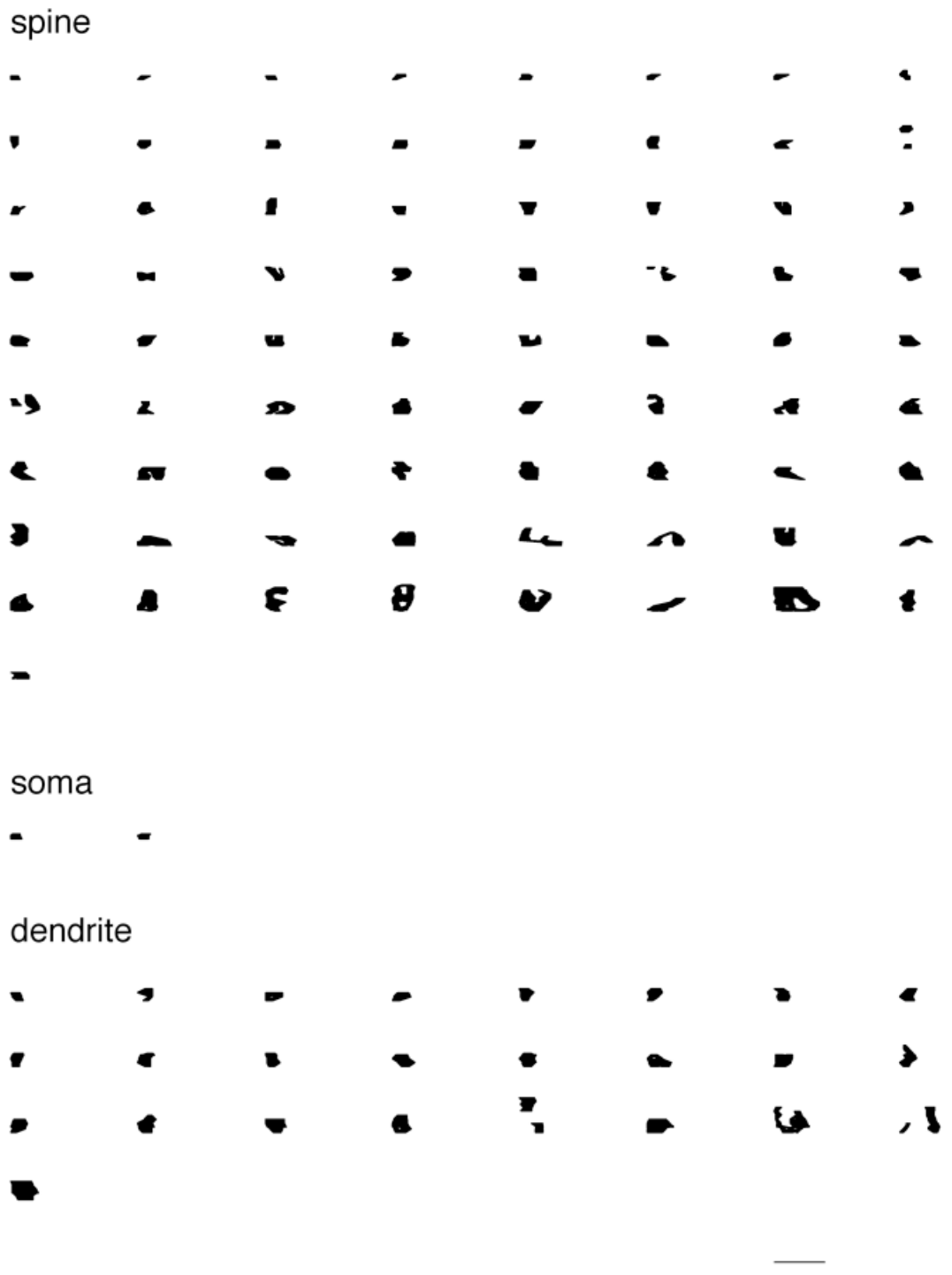

Fig. 8. Two-dimensional projection of the reconstructed postsynaptic densities found on spines, soma, and dendrites postsynaptic to V2-labeled boutons in area V5. The densities are ordered by increasing surface area. Scale bar = 1 μm.

boutons in MT tended to show more perforations. This condition gave the V1 synapses a more fragmented appearance. Some spines would form two synapses with V1 boutons, on opposite sides of the same spine head. The V1 synapses formed with somata were small, but beneath one bouton, there could be up to five separate active zones.

Target types. The most frequently encountered target of V2 labeled boutons were spines. The difference between boutons from the different principal laminae of innervation was the proportion of spines to dendrites as targets (Fig. 11). For this reason, we have not pooled the data from different laminae. In layer 4, 67% of the labeled

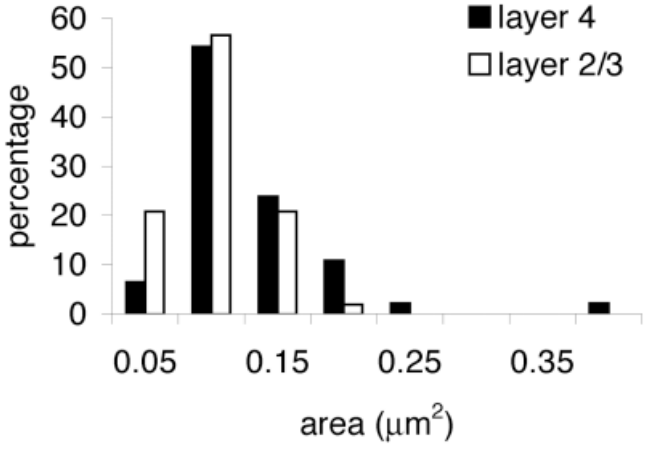

Fig. 9. Histogram of the distribution of postsynaptic areas (μm^2) formed by labeled V2 boutons in layers 2/3 (n = 53) and 4 (n = 46) of areaV5.

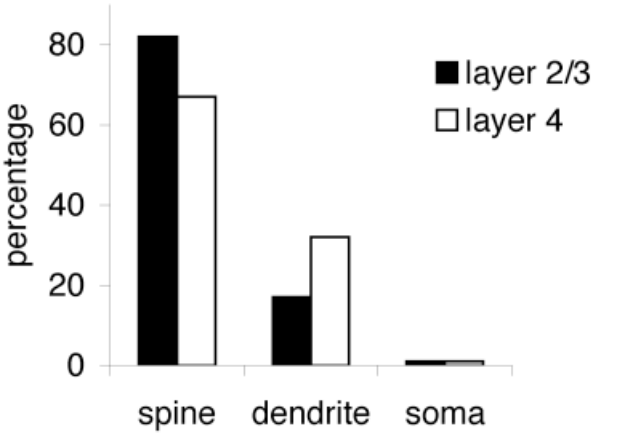

Fig. 11. Histogram of the synaptic targets of labeled V2 boutons in area V5. For layer 2/3, n = 53; for layer 4, n = 46.

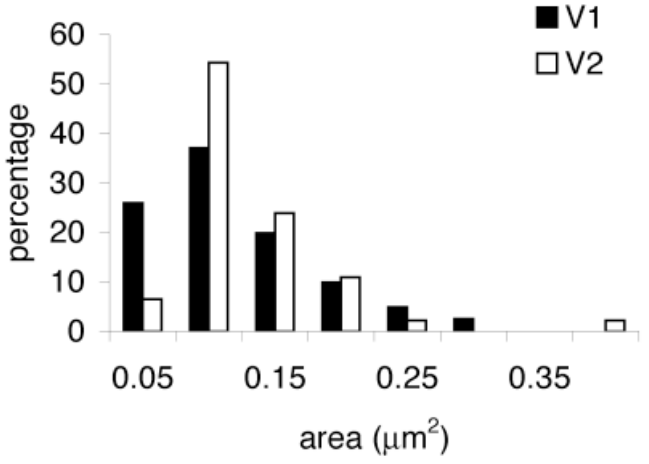

Fig. 10. Histogram of the distributions of postsynaptic areas (μm^2) formed by labeled V1 (n = 81) and V2 (n = 46) boutons in layer 4 of area V5.

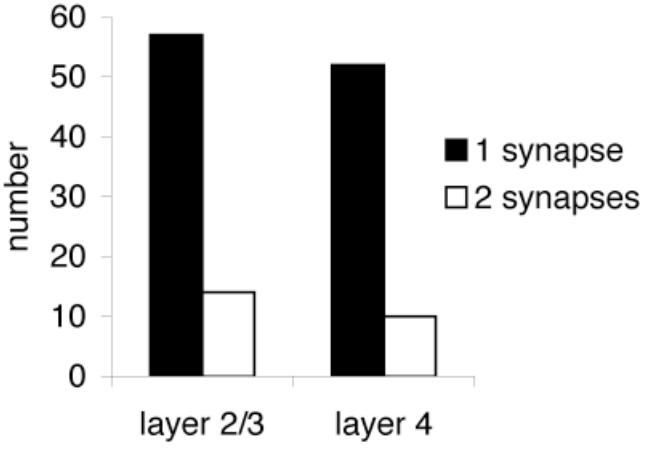

Fig. 12. Histogram of the number of synapses formed per labeled bouton in layers 2/3 and 4 of area V5.

synapses were formed with spines and 31% formed with dendritic shafts. This compares well with the quantitative disector analysis of layer 4, where we discovered that 65% of the targets that form asymmetric synapses were spines, with dendritic shafts forming the remaining 35% (n = 419). In layer 2/3, 82% of the synapses were formed with spines and 17% with dendritic shafts. A disector analysis was not made for layers 2/3. Neuronal somata accounted for approximately 1% of synaptic targets in both laminae. As indicated above (see *Dendrites*), smooth neurons provided approximately half of the dendritic shaft targets in layers 4 and 2/3. The two sections used for the disector analysis of layer 4 were too few to permit an accurate subdivision of the dendritic shafts into smooth and spiny types. Serial reconstructions indicated that most boutons made only one synapse and only rarely more than two synapses (Figs. 3D, 4C, 12). On average, there were 1.1 synapses per labeled bouton.

Synaptic density measurements. To estimate the relative proportion of synapses being contributed by V2 to area MT, we made an unbiased stereologic analysis of layer 4. We selected two sections from one animal in which the labeling was particularly dense. In Figure 2, we see that the terminal labeling in layer 4 has a patchy appearance. We selected regions from within the densest patches for our analysis by using the unbiased disector method (Sterio, 1984). We counted only those labeled synapses that disappeared in the "look-up" section when compared with a near adjacent "reference" section. Although the blocks of tissue used for re-embedding were selected from the densest zones of innervation, the distribution of labeled synapses in any ultrathin section could vary greatly. If the disector region was selected by using nonbiased features such as the edge of the tissue or a scratch on the block face, we counted no labeled synapses. If we selected the location of the disector by finding a labeled bouton and then sampling in the vicinity, we counted 5% (11 of 218) and 4.9% (10 of 205) of disappearing labeled synapses. The form of the disector altered the number of observations.

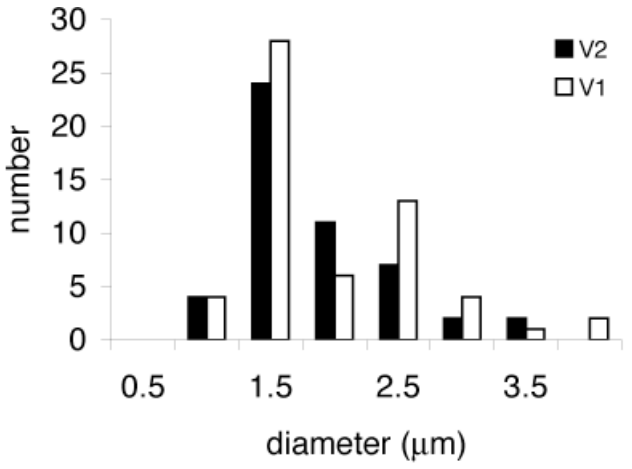

Fig. 13. Histogram of the distributions of diameters of labeled V1 and V2 axons near the border between the white matter and layer 6. All measurements were made with the light microscope by using a 100× oil immersion objective.

Strips of tissue tended to give lower values (3.8%; 8 of 211) than patches of tissue (6.2%; 13 of 211). This may indicate that even the most prolifically innervated regions of layer 4 have another, local level of "ultrastructural" organization.

Axons and myelin. The conduction times from V1 to MT are known (1.0–1.7 msec, Movshon and Newsome, 1996), but those for the V2 projection are not. As the axon diameter gives some indication of the relative conduction velocities of the axons, we compared the diameters of axons originating in V1 with those originating in V2. We measured in the light microscope the axon diameters of axons labeled from V1 and V2 as they entered MT but before they branched in the gray matter (Fig. 13). Axons originating in V1 and V2 have similar diameters. The terminal arbors also show a reduction in diameter, and this could also contribute significantly to the conduction times. We used electron microscopy to examine the diameters of the myelinated segments of the terminal arbors in layer 4 (Fig. 14) and found that again the V1 and V2 axons were comparable. These findings suggest that the axon conduction velocities of the two projections may be quite similar.

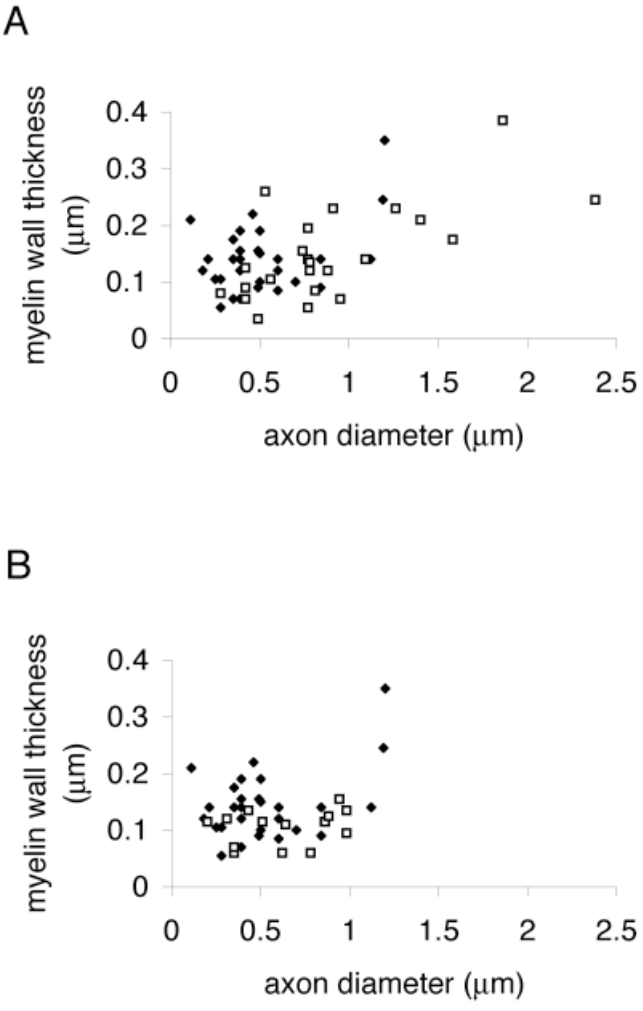

Fig. 14. Relationship between axon diameter and the thickness (μm) of the associated myelin sheath. All measurements were made in layer 4. **A:** Nonlabeled (open squares) and V2 labeled (filled diamonds) axons in area V5. **B:** Labeled axons in V5 originating from neurons located in areas V1 (open squares) and V2 (filled diamonds).

DISCUSSION

Both the V1 and the V2 projection to MT are classified as "feedforward" projections in that their dominant target is layer 4 of MT. However, they also differ in several important respects, including the fact that the layers of origin in the two areas are different. The V1 projection originates from large pyramids in 5–6 and the spiny stellate and pyramidal cells of layer 4B (Elston and Rosa, 1997), whereas the V2 projection originates mainly from pyramidal cells in layer 3B (Lund et al., 1981; Maunsell and Van Essen, 1983; Ungerleider and Desimone, 1986; Shipp and Zeki, 1989). Unlike the V1 axons, the V2 axons did not innervate the deep layers, and unlike the V1 projection, V2 did innervate the superficial layers, including layer 1. This finding confirms the pattern of the V2 to MT described previously by Rockland (1995). At the ultrastructural level, we discovered that the V2 axons did not form the elaborated and large multisynaptic boutons of the V1 projection to layer 4 (Anderson et al., 1998). The smaller boutons of the V2 projection could reflect a comparatively diminished activity of the V2 vs. the V1 pathway.

In some important respects, the differences between the V1 and V2 projection to MT mirror those of the thalamic projections to V1, where the relay cells in the parvicellular and magnocellular layers of the dorsal lateral geniculate nucleus provide the input to layers 4 and 6 through large multisynaptic boutons (Winfield et al., 1982, Freund et al. 1989), whereas the koniocellular layers project to layers 1–3. As yet, however, we only know a fragment of physiology of the V1 neurons that project to MT and nothing of the neurons that project from V2. In a "rather trying" study, Movshon and Newsome (1996) used antidromic activation to identify 12 V1 neurons projecting to MT. Most

of these neurons were strongly directional, had special complex receptive fields, and were unusually sensitive to low contrast characteristic of the magnocellular pathway. The equivalent study in V2 has yet to be done, but it seems plausible that as with the different thalamocortical streams, each path conveys different aspects of a given stimulus to the target area. The difference in termination pattern would then reflect the differences in local processing required for the given signal, differences in the further destinations of the signal, or both.

If the retrogradely filled cells in V1 included those that project to MT, they might have contributed to the labeling in V2. However, PHA-L or BDA did not give Golgi-like filling of the local axon collaterals of the retrogradely labeled neurons. Together with the above observations of the key differences between the V1 and V2 projections to MT, it was highly unlikely that retrogradely filled cells contributed to the axonal labeling in MT. The proportion of synapses contributed by the injected area in V2 was tiny, only approximately 4–6% of all excitatory synapses in the densest portions of the terminal arbors. However, it is clear that this underestimates the contribution of V2 to MT, because there is extensive convergence of V2 neurons upon MT (Shipp and Zeki, 1985) and our localized injections would label only a subset of these.

The ultrastructural features of the synapses and their targets indicate that the V2 axons in layer 4 form putative excitatory synapses with spiny (putative excitatory) neurons. The electron microscopic analysis showed that, in layer 2/3, there was a decrease in the number of dendritic shafts that were targets. This may simply reflect a different selectivity of the presynaptic axons in the different layers. Alternatively, there may simply be fewer spines in layer 4 with which they can form synapses. Some support for this idea comes from the studies of Elston and Rosa (1997), which indicate that pyramidal cells in layer 3 of MT have larger basal dendrites and slightly higher peak spine densities (7.95 spines/10 μm) than the equivalent layer 3 (4B) pyramids in area 17 (5.79 spines/10 μm). This increased density may provide for more spine targets for the V2 projection to the superficial layers of MT.

The more complicated geometry of the postsynaptic density on spine synapses, which we first noted for the V1 projection to MT, was repeated in the V2 projection, albeit in a less florid form. The reason for the frequent appearance of a doughnut or horseshoe-shaped postsynaptic density on spines, in particular, remains unclear, but one possibility is that it constitutes some optimal geometry for the diffusion of neurotransmitter to both synaptic and possibly extrasynaptically located receptors (see Discussion section in Anderson et al., 1998). Thus, an analysis of the spatial distribution of the various receptor subtypes in these synapses might be fruitful.

The clustering of terminals in layer 4 of the V2 projection is typical of many cortical projections. The projection from V1 to MT also clusters in layer 4 (Rockland, 1989) and so might interdigitate with the V2 projection, but, as yet, there is no evidence for this. Earlier studies on the cells of origin of the V1 projection in layers 4B and 6 indicated that the cells were not clearly organized in slabs or blobs (Lund et al., 1975; Shipp and Zeki, 1989), but recent work of Boyd and Casagrande (1999) does show the projection cells co-aligned with cytochrome blobs in three species, including macaque. The V2 projection to MT arises from clusters of neurons that lie within regions of intense cytochrome oxidase staining, known as the "thick stripes" (Livingstone and Hubel, 1983). MT itself shows indications of clustered physiology in the macaque, e.g., neurons with common direction preference are clustered together (Albright et al., 1984). In MT of the owl monkey, distinct functional and anatomic columns exist for processing local vs. wide field motion (Berezovskii and Born, 2000). This parallelism is a familiar picture in V1 and V2 and evidently is found even in apparently more specialized visual areas like MT.

Although the properties of neurons in different cortical areas have been extensively studied, the role of the multiple interareal connections remains obscure. Rostral visual areas receive convergent projections from the posterior areas, which themselves are extensively interconnected. Thus, for example, area MT receives direct projections from all the caudal visual areas, including V1, V2, V3, V3A, VP, PO, and V4 (see Felleman and Van Essen, 1991). These same areas also receive feedforward connections from their more caudal relations. Neurons in MT, in common with other rostral areas, receive feedforward inputs that are temporally staggered in onset and can be tens to hundreds of msec in duration. The earliest activation is found in V1; subsequently, neurons in V3 and MT become active; and then, even later, neurons in V2 and V4 become active (Raiguel et al., 1989, 1999; Munk et al., 1995; Nowak et al., 1995; Schmolesky et al., 1998).

In all of these areas, the latency and duration of the response also varies according to laminar location of the neurons. Part of the differences of latency of response may be due to conduction times. As yet, the transmission times of the intra-areal axons have only been measured, with difficulty, for the feedforward projection from V1 to MT (Movshon and Newsome, 1996). An additional clue to the conduction times comes from measurements of the diameter and myelination of the axons.

Rockland (1995) commented on the much smaller caliber of the myelinated axons originating in V2 compared with those originating in V1 (~1 μm vs. ~3 μm). The largest pyramidal cells in V1, the Meynert cells, project to MT (Fries et al., 1985) and are likely to have very large axons. Our light microscopic measurements of the diameter of the axons in the white matter beneath MT indicated that, although there are indeed some very large axons, they can arise from both V1 and V2. Sampling from this population indicates that, on entering MT, the V2 axons have similar diameters to the V1 axons (mean diameter: V2 = 1.6 μm, V1 = 1.7 μm). Because a significant length of an axon is also contained in its terminal arbor, where the axons branch extensively and become thinner, the terminal arbor might contribute significantly to the total conduction time. A comparison at electron microscope level of the myelinated portions of the terminal arbors in layer 4 indicated that the diameter of V1 and V2 collaterals were also comparable. Taken altogether, its seems that whatever differences of axon diameter might exist at their source, these differences are virtually washed out by the time the axons reach MT. This finding means that the spread of visual latencies in MT is probably more due to the times of processing within the antecedent visual areas and not in the transmission times.

The role of the multiple projections to single extrastriate cortical areas remains speculative. Of course, it is

supposed that the different streams bring different components to the computation being carried out by local circuits. Functionally, however, it has been difficult to separate out the different sources of input to MT. When the input to MT from V1 is removed, by ablation (Rodman et al., 1990) or cooling (Girard et al., 1992), some function remains. However, this residual function cannot be carried by the V2 projection, because V2 itself is silenced by inactivation of V1 (Schiller and Malpeli, 1977; Girard and Bullier, 1989), thus, it is possible that the V2 projection to MT provides some overlapping functions with the projection from V1.

Interesting evidence for the V2 pathway to MT has emerged from human studies. For example, Vaina et al. (2000) have studied a patient with a selective lesion in V2. He was found to be impaired in several motion tasks, including those involving first order, but not second-order motion. One possible interpretation is that the loss of the V2 input to MT produces this effect. One human model that uses the V2 connection as the major drive to MT is that of Friston and Buchel (2000). Their evidence from human functional magnetic resonance imaging was that the hemodynamic responses recorded in the human MT and in posterior parietal cortex are enhanced by attention during visual motion, but the responses in pulvinar and V2 are not. They proposed a model in which the connection between V2 and MT was modulated by afferents of the parietal cortex. In their model, V2 and pulvinar provided "driving" inputs to MT, whereas the posterior parietal cortex provided an attentional signal that augmented the V2 input in a nonlinear way. Their model indicates that the activity in the posterior parietal cortex could account for a significant component of the V5 responses under conditions of attention. In this model, the V2 afferents have no different role from "driving" inputs from any other cortical area, e.g., V1. Nevertheless, such models offer a means of exploring this interesting question in other primate species.

LITERATURE CITED

Ahmed B, Anderson JC, Martin KAC, Nelson JC. 1997. Map of the synapses onto layer 4 basket cells of the primary visual cortex of the cat. J Comp Neurol 380:230–242.

Albright TD, Desimone R, Gross CG. 1984. Columnar organization of directionally-selective cells in visual area MT of macaques. J Neurophysiol 51:16–31.

Anderson JC, Binzegger T, Martin KAC, Rockland KS. 1998. The connection from cortical area V1 to V5: a light and electron microscopic study. J Neurosci 18:10525–10540.

Barone P, Batardiere A, Knoblauch K, Kennedy H. 2000. Laminar distribution of neurons in extrastriate areas projecting to visual area V1 and V4 correlates with the hierarchical rank and indicates the operation of a distance rule. J Neurosci 20:3263–3281.

Berezovskii VK, Born RT. 2000. Specificity of projections from wide-field and local motion-processing regions within the middle temporal visual area of the owl monkey. J Neurosci 20:1157–1169.

Boyd JD, Casagrande VA. 1999. Relationship between cytochrome oxidase (CO) blobs in primate primary visual cortex (V1) and the distribution of neurons projecting to the middle temporal area (MT). J Comp Neurol 409:573–591.

Elston GN, Rosa GP. 1997. The occipitoparietal pathway of the macaque monkey: comparison of pyramidal cell morphology in layer 3 of functionally related cortical visual areas. Cereb Cortex 7:432–452.

Felleman DJ, Van Essen DC. 1991. Distributed hierarchical processing in the primate cerebral cortex. Cereb Cortex 1:1–47.

Freund TF, Martin KAC, Soltesz P, Somogyi P, Whitteridge D. 1989. Arborization patterns and postsynaptic targets of physiologically identified thalamocortical afferents in striate cortex of the macaque monkey. J Comp Neurol 289:315–336.

Friedman DP. 1983. Laminar patterns of termination of corticocortical afferents in the somatosensory system. Brain Res 273:147–151.

Fries W, Keizer K, Kuypers HG. 1985. Large layer VI cells in macaque striate cortex (Meynert cells) project to both superior colliculus and prestriate visual area V5. Exp Brain Res 58:613–616.

Friston KJ, Buchel C. 2000. Attentional modulation of effective connectivity from V2 to V5/MT in humans. Proc Natl Acad Sci U S A 97:7591–7596.

Girard P, Bullier J. 1989. Visual activity in area V2 during reversible inactivation of area 17 in the macaque monkey. J Neurophysiol 62: 1287–1302.

Girard P, Salin PA, Bullier J. 1992. Response selectivity of neurons in area MT of the macaque monkey during reversible inactivation of area V1. J Neurophysiol 67:1437–1446.

Jouve B, Rosenstiehl P, Imbert M. 1998. A mathematical approach to the connectivity between the cortical visual areas of the macaque monkey. Cereb Cortex 8:28–39.

Kennedy H, Bullier J. 1985. Double-labeling investigation of the afferent connectivity to cortical areas V1 and V2 of the macaque monkey. J Neurosci 10:2815–2830.

Kisvárday ZF, Martin KAC, Whitteridge D, Somogyi P. 1985. Synaptic connections of intracellularly filled clutch neurons, a type of small basket neuron in the visual cortex of the cat. J Comp Neurol 241:111–137.

Livingstone MS, Hubel DH. 1983. Specificity of cortico-cortical connections in monkey visual system. Nature 304:531–534.

Lund JS, Lund RD, Hendrickson AE, Bunt AH, Fuchs AF. 1975. The origin of efferent pathways from the primary visual cortex, area 17, of the macaque monkey as shown by retrograde transport of horseradish peroxidase. J Comp Neurol 164:287–303.

Lund JS, Hendrickson AE, Ogren MP, Tobin EA. 1981. Anatomical organization of primate visual cortical area VII. J Comp Neurol 202:19–45.

Maunsel JH, Van Essen DC. 1983. The connections of the middle temporal visual area (MT) and their relationship to a hierarchy in the macaque. J Neurosci 3:2563–2586.

Movshon JA, Newsome WT. 1996. Visual response properties of striate cortical neurons projecting to area MT in macaque monkeys. J Neurosci 16:7733–7741.

Munk M, Nowak L, Girard P, Chounlamountri N, Bullier J. 1995. Visual latencies in cytochrome oxidase bands of macaque area V2. Proc Natl Acad Sci U S A 92:988–992.

Nowak LG, Munk MH, Girard P, Bullier J. 1995. Visual latencies in areas V1 and V2 of the macaque monkey. Vis Neurosci 12:371–384.

Peters A, Saint Marie RL. 1984. Smooth and sparsely spinous nonpyramidal cells forming local axonal plexuses. In: Jones EG, Peters A, editors. Cerebral cortex. Vol. 1. Cellular components of the cerebral cortex. New York: Plenum Press. p 419–445.

Peters A, Palay SL, Webster HD. 1991. The fine structure of the nervous system: neurons and their supporting cells. 3rd ed. Oxford: Oxford University Press.

Raiguel SE, Lagae L, Gulyas B, Orban GA. 1989. Response latencies of visual cells in macaque areas V1, V2 and V5. Brain Res 493:155–159.

Raiguel SE, Xiao DK, Marcar VL, Orban GA. 1999. Response latency of macaque area MT/V5 neurons and its relationship to stimulus parameters. J Neurophysiol 82:1944–1956.

Rockland KS. 1989. Bistratified distribution of terminal arbors of individual axons projecting from area V1 to middle temporal area (MT) in the macaque monkey. Vis Neurosci 3:155–170.

Rockland KS. 1995. Morphology of individual axons projecting from area V2 to MT in the macaque. J Comp Neurol 355:15–26.

Rockland KS, Pandya DN. 1979. Laminar origins and terminations of cortical connections of the occipital lobe in the rhesus monkey. Brain Res 179:3–20.

Rodman HR, Gross CG, Albright TD. 1990. Afferent basis of visual response properties in area MT of the macaque. II. Effects of superior colliculus removal. J Neurosci 10:1154–1164.

Schmolesky MT, Wang Y, Hanes DP, Thompson KG, Leutgeb S, Schall JD, Leventhal AG. 1998. Signal timing across the macaque visual system. J Neurophysiol 79:3272–3278.

Schiller PH, Malpeli JG. 1977. The effect of striate cortex cooling on area 18 cells in the monkey. Brain Res 126:366–369.

Shipp S, Zeki S. 1985. Segregation of pathways leading from area V2 to areas V4 and V5 of macaque monkey visual cortex. Nature 315:322–325.

Shipp S, Zeki S. 1989. The organization of connections between area V5 and V1 in macaque monkey visual cortex. Eur J Neurosci 1:309–332.

Somogyi P, Kisvárday ZF, Martin KAC, Whitteridge D. 1983. Synaptic connections of morphologically identified and physiologically characterized large basket cells in the striate cortex of cat. Neuroscience 10:261–294.

Sporns O, Tononi G, Edelman GM. 2000. Theoretical neuroanatomy: relating anatomical and functional connectivity in graphs and cortical connection matrices. Cereb Cortex 10:127–141.

Sterio DC. 1984. The unbiased estimation of number and sizes of arbitrary particles using the disector. J Microsc 134:127–136.

Ungerleider LG, Desimone R. 1986. Cortical connections of visual area MT in the macaque. J Comp Neurol 248:190–222.

Vaina LM, Soloviev S, Bienfang DC, Cowey A. 2000. A lesion of cortical area V2 selectively impairs the perception of the direction of first-order visual motion. Neuroreport 7:1039–1044.

Winfield DA, Rivera-Dominguez M, Powell TPS. 1982. The termination of geniculocortical fibres in area 17 of the visual cortex in the macaque monkey. Brain Res 231:19–32.

Young MP. 1992. Objective analysis of the topological organization of the primate cortical visual system. Nature 358:152–155.

3.3 The third study in the series is another feedforward projection, V2 to V3A, through extrastriate cortex. Very little detailed anatomic information for this projection exists. However V3A has become increasingly interesting in human fMRI studies revealing, as for macaque but more so in humans, that this area is something of a hub or crossroad. The two streams of dorsal and ventral begin to emerge here, sometimes referred to as the 'where' and 'what' streams respectively.

THE JOURNAL OF COMPARATIVE NEUROLOGY 488:320–330 (2005)

Connection from Cortical Area V2 to V3A in Macaque Monkey

JOHN C. ANDERSON[1,2]* AND KEVAN A.C. MARTIN[1,2]
[1]Institute for Neuroinformatics, University of Zürich, 8057 Zürich, Switzerland
[2]Eidgenossiche Technische Hochschule Zürich, 8057 Zürich, Switzerland

ABSTRACT

The V2 projection to V3A was labeled by pressure microinjecting biotinylated dextran amine (BDA) and *Phaseolus vulgaris* lectin (PHA-L) into V2 just posterior to the lunate sulcus. Dense terminal labeling in clusters was found in layer 4, with a weaker terminal projection in layer 3. About 3.5–4.1% of the synapses in the densest bouton clusters in layer 4 were made by labeled boutons. All were asymmetric (Gray's type 1) synapses, made by spiny, excitatory neurons. The most frequently encountered synaptic targets were spines (76% in layer 4, 98% in layer 2/3). The remainder of the synaptic targets were dendritic shafts, of which just less than half (44%) had the characteristic ultrastructure of smooth (inhibitory) cells. Multisynaptic boutons were rare (mean synapses per bouton for layer 4 1.2, for layer 2/3 1.1). The mean size of the postsynaptic densities found on spines (0.11 μm^2) was not significantly different from that for dendrites (0.09 μm^2). In terms of their type, laminar location, number, and targets, the synapses that formed the V2 projection to V3A are typical of a major, excitatory, feedforward projection of macaque visual cortex. J. Comp. Neurol. 488: 320–330, 2005.

Indexing terms: visual cortex; area V3A; corticocortical; light and electron microscopy; synapse morphology; postsynaptic target

In studies of visual processing in extrastriate cortex in the monkey, the areas V2, V4, and MT (V5) have received the most intense scrutiny. An early study by Zeki (1978a) in macaque showed that, in the proportions of orientation and motion selective cells, V3A was indistinguishable from V2, V3, and V4. Area V4 stood out by having large numbers of color-sensitive cells, whereas MT was prominent because of its large numbers of direction-selective cells. With the development of functional imaging, one of the areas that emerges with some prominence in imaging studies in both humans and monkeys is V3A, which shows strong activation with motion and depth stimuli and has high contrast sensitivity (Tootell et al., 1997; Backus et al., 2001; Tsao et al., 2003). In humans, the functional magnetic resonance imaging (fMRI) data indicate that V3A appears to be more sensitive to motion than in monkeys (Tootell et al., 1997; Orban et al., 2003).

There are relatively few single-unit studies of V3A in the macaque. With anesthetized monkeys, Gaska et al. (1988) found that the spatial frequency tuning was similar to that of V1 neurons for the same eccentricity and that the temporal frequency tuning was low-pass. These properties led them to suppose that V3A forms part of the ventral pathway to V4 and inferotemporal cortex. Against this, Zeki (1978a) noted that V3A neurons have no color sensitivity, suggesting rather a role in the dorsal stream to parietal cortex. Indeed, Galletti and Battaglini (1989) found neurons in V3A of behaving monkeys whose responses were modulated by eye position. Nakamura and Colby (2000, 2002) also emphasized the role of V3A neurons in coordinate transformations for retinal and eye position. In addition, some neurons carried memory- and saccade-related signals. Attention and expectation of reward modulate the responses of V3A neurons (Thiele et al., 1999; Nakamura and Colby, 2000).

Area V3A is richly connected to surrounding cortical areas and also makes reciprocal connections with frontal eye fields (Schall et al., 1995; Stanton et al., 1995). It receives feedforward connections from caudal cortical areas, including a sparse connection from V1 (Zeki, 1978b; Van Essen et al., 1986), and a strong input from V2 (Gat-

Grant sponsor: European Union; Grant number: QULG3-1999-01064 (to K.A.C.M.); Grant sponsor: Human Frontier Science Program; Grant number: RG0123/2000-B (to K.A.C.M.); Grant sponsor: Swiss National Science Foundation (to K.A.C.M.).

*Correspondence to: John C. Anderson, Institute for Neuroinformatics, University of Zürich and ETH Zürich, Winterthurerstr. 190, 8057 Zürich, Switzerland. E-mail: jca@ini.phys.ethz.ch

Received 13 July 2004; Revised 24 January 2005; Accepted 16 February 2005

DOI 10.1002/cne.20580

Published online in Wiley InterScience (www.interscience.wiley.com).

tass et al., 1997) and V3 (Felleman et al., 1997). If V1 is cooled, V3 stops responding to visual stimulation, but many neurons in V3A continue responding (Girard et al., 1991). After V1 inactivation, residual activity is found in MT, to which V3A is reciprocally connected (Girard et al., 1991). In addition to MT in the dorsal stream, V3A is also connected to lateral intraparietal area (LIP; Cavada and Goldman-Rakic, 1989; Andersen et al., 1990; Blatt et al., 1990, Morel and Bullier, 1990, Baizer et al., 1991; Nakamura et al., 2001), dorsal prelunate area (Andersen et al., 1990), medial superior temporal area (MST; Boussaoud et al., 1990), and fundus of the superior temporal visual area (FST; Boussaoud et al., 1990) and the parietooccipital area (PO; Colby et al., 1988; Shipp et al., 1998). V3A also has reciprocal connections to areas of the ventral stream, including ventral posterior area (VP, Felleman et al., 1997), V4 (Felleman and Van Essen 1983), and TEO (Morel and Bullier, 1990; Webster et al., 1994).

From both physiological and anatomical evidence, it is clear that V3A lies at a key crossroads in the extrastriate circuit. Surprisingly, however, nothing is known of the synaptic profile of any input to V3A. In the present study, we examined quantitatively the synapses formed in V3A by one of its major feedforward inputs, that arising in V2, and provide comparisons, where possible, with other quantitative electron microscopic studies of projections in extrastriate cortex.

MATERIALS AND METHODS

The material presented here was taken from two adult female macaque monkeys (*Macaca mulatta*). Animal treatment and surgical protocols were carried out in accordance with the guidelines of the Kantonales Veterinaeramt of Zürich. The projection from V2 to MT in these same two animals has been described (Anderson and Martin, 2002), and the following procedures are identical. Animals were prepared for surgery after the administration of an intramuscular premedication of xylazine (Rompun; Beyelar; 0.5 mg/kg)/ketamine (Ketalar; Parke Davis; 10 mg/kg). This was followed by cannulation of a femoral vein for the delivery of alphaxalone/alphadalone (Saffan; Glaxo) to establish complete anesthesia.

Each animal received pressure injections (~0.5 μl each) of the neuronal tracers biotinylated dextran amine (BDA; Molecular Probes, Leiden, The Netherlands) and *Phaseolus vulgaris* leucoagglutinen (PHA-L; Vector Laboratories, Burlingame, CA). One animal received four injections of 10% BDA in 0.01 M phosphate-buffered saline (PBS), pH 7.4, and two of PHA-L in 10 nM phosphate buffer (PB), pH 7.4. The second animal received five injections of BDA and three injections of PHA-L. Both tracers were used in order to assess their relative merits in a study of this type. The tracers were injected into area V2 (area 18) along the crest of the lunate gyrus (see, e.g., Anderson and Martin, 2002; see Fig. 1). With one exception, needle tracks were all confined to the gray matter of V2, and the label could be followed through all laminae. In one animal, the injections were made into the dorsal surface of V2, the needle track being almost parallel to the cortical laminae. Penetrations made in the second animal traversed the tip of the gyrus and extended into the lunate sulcus (see, e.g., Anderson and Martin, 2002; see Fig. 1B). One track in this animal went through the white matter.

After a 14-day survival period, anesthesia was again induced with ketamin/xylazine, and the monkeys were deeply anesthetized with i.v. pentobarbital (20 mg/kg) and immediately perfused transcardially with a normal saline solution, followed by a solution of 4% paraformaldehyde, 0.3% gluteraldehyde, and 15% picric acid in 0.1 M PB, pH 7.4. The brain was removed from the skull, and a block of cortex containing the injection site and area V3A was removed. The block was allowed to sink in sucrose solutions of 10%, 20%, and 30% in 0.1 M PB. Sections were cut from the block at 80 μm in the parasagittal plane and collected in 30% sucrose in 0.1 M PB. The sections were then freeze-thawed in liquid nitrogen and washed in 0.1 M PB. We used standard procedures to reveal the neuronal tracers. In brief outline; washes in PBS were followed by 10% normal swine serum (NSS) in PBS (1 hour). The biotinylated antibody to PHA-L was diluted in the above at 1:200 and exposed for 48 hours at 5°C. Further washes in NSS preceded overnight exposure (5°C) to an avidin-biotin complex (Vector ABC Elite Kit), which precludes the need for a secondary antibody. The peroxidase activity was identified by using 3,3-diaminobenzidene tetrahydrochloride (DAB). After assessment by light microscopy (LM) selected regions of tissue were treated with 1% osmium tetroxide in 0.1 M PB. Dehydration through alcohols (1% uranyl acetate in the 70% alcohol) and propylene oxide allowed flat mounting in Durcupan (Fluka) on glass slides.

LM observations of labeled axons were carried out to locate and select regions of interest for electron microscopy (EM). We reconstructed individual collaterals in the less densely innervated areas for correlated LM and EM. Serial ultrathin sections were collected at 70 nm thickness on Pioloform-coated single-slot copper grids. Labeled boutons were photographed at a magnification of ×21,000. Synapses and associated structures were classified by using conventional criteria. Collections of serial sections were digitized and reconstructed using Trakem, an in-house EM digitization package. To measure and display the postsynaptic densities of labeled boutons, we used software developed by ourselves, which has been described in outline elsewhere (see Materials and Methods in Anderson et al., 1998).

The estimates of labeled bouton density were derived using the physical disector method (Sterio, 1984). We selected regions that were densely innervated by labeled axon for reembedding. Serial 70-nm-thick sections were collected from these regions, and a reference section and a look-up section were selected. The reference and look-up sections were separated by one section. Photographs were taken with the electron microscope to form patches of tissue, e.g., 2 × 8 images. All electron micrographs were taken at ×11,500. Synapses that were in the reference section but that disappeared in the look-up section were counted. Synapses that were present in both look-up and reference sections were not counted (Sterio, 1984). Adobe Photoshop CS and Adobe Illustrator CS were used to prepare digital photomicrographs and enhance image contrast.

RESULTS

LM

The pressure injections into V2 immediately posterior to the lunate sulcus resulted in label spread over 5–7 mm

mediolaterally. BDA labeling was poor at the injection site, but PHA-L labeling was excellent. From this we assume that the axons seen in V3A were labeled with PHA-L. Labeling was densest along the path of the penetrations. Most of the uptake was by pyramidal cells of layer 2/3, covering most of the tip of the gyrus, but labeled cell bodies were also found in all other layers. Strong anterograde labeling was seen in striate and extrastriate visual areas, including V1, V3A, and V5, along with some pale retrogradely stained cell bodies. The strongest transport was to V1, where the retrograde labeling was similar to that previously reported by Kennedy and Bullier (1985), i.e., predominantly in layers 2/3 and 4B, with some sparse cell bodies scattered along the layer 5–6 border. No cell or terminal labeling was evident in layer 4 of V1. The border between areas V3 and V3A was identified as the axon clustering found in the lunate sulcus (Felleman et al., 1997; Fig. 6B), in one case in the fundus and in the other case in the anterior bank of the lunate sulcus (Fig. 1).

Beck and Kaas (1999) consider V3 and V3A to be part of a single dorsomedial visual area, identified anatomically by its dense myelin staining. Despite the fact that the osmium gave excellent staining of myelin, we were unable to distinguish V3A from surrounding areas on the basis of differences in myelin staining. The border between these two visual areas, V3 and V3A, represents the vertical meridian (Adams and Zeki, 2001). Because of the retinotopic correspondence in connections, we expected to see labeled axons close to the representation of the vertical meridian at the V3–V3A border, where the labeled axons were indeed found. No labeling was seen at the V2–V3 border, where the horizontal meridian is represented.

In area V3A, the labeled axons entered from the white matter. On reaching layer 4, most of the axons branched extensively and formed synaptic boutons (Fig. 2). Layer 4 was identified by dark staining in the osmicated material and by a dense granular appearance in the Nissl-stained material. These features also coincided with the highest density of labeled terminations. Labeled axons (>0.5 μm) traversed extensively within layer 4. Seen in EM, many axons possessed a thick coating of myelin. This profusion of myelinated axons, fine bouton-bearing axons, and both en passant and terminaux boutons gave an overall patchy appearance to the innervation site of one animal when viewed at low power in the light microscope. However, this patchiness was less distinct that that seen in area V5 or MT in the same material (see Anderson and Martin, 2002; Fig. 2). In the second animal, the axon labeling in layer 4 was confined to the fundus of the sulcus, adjacent to labeling in area V3 (Fig. 1).

Axons that projected into the more superficial layers were more slender than the main trunks seen in layer 4. They gave rise to mostly en passant boutons of a fairly uniform size spaced at fairly regular intervals. Most of these axons terminated in or before upper layer 2/3. Occasionally, thicker axons, passing through layer 3, branched before reaching layer 2 and produced a radially aligned, fanlike arborization. The axon diameter in these superficial layer axons was reduced rapidly as they branched.

Weak retrograde labeling was evident as palely stained neuronal somata and proximal dendrites, in some instances. These cells were sparse and were clearly of a pyramidal morphology. The majority of retrogradely labeled somata occurred in layer 2/3, occasionally in layer 6.

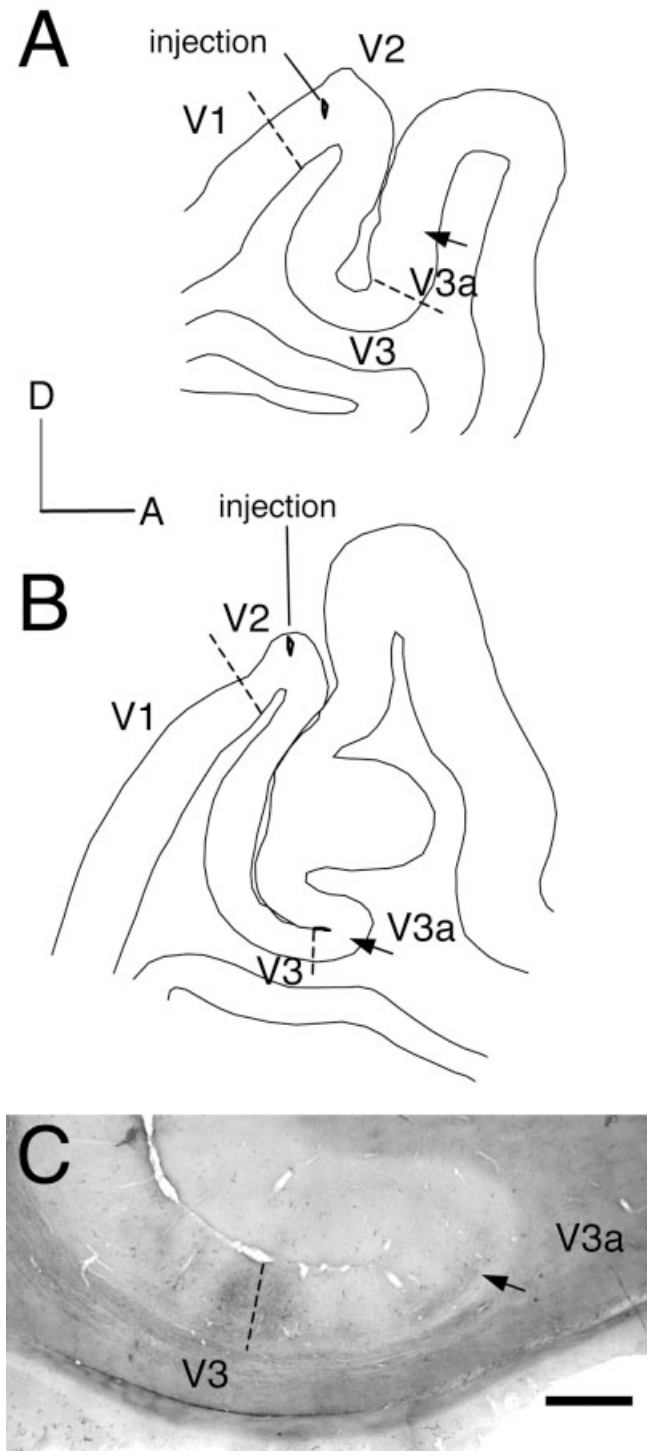

Fig. 1. Drawings of two parasagittal sections (**A,B**) from macaque brain and a photomicrograph (**C**) from one of these sections. Indicated are region in which injections were made along the edge of the lunate sulcus and the region from which labeled axons were sampled for electron microscopic analysis (arrows). The borders between visual areas are indicated by a dashed line. D, dorsal; A, anterior. Scale bar = 1 mm.

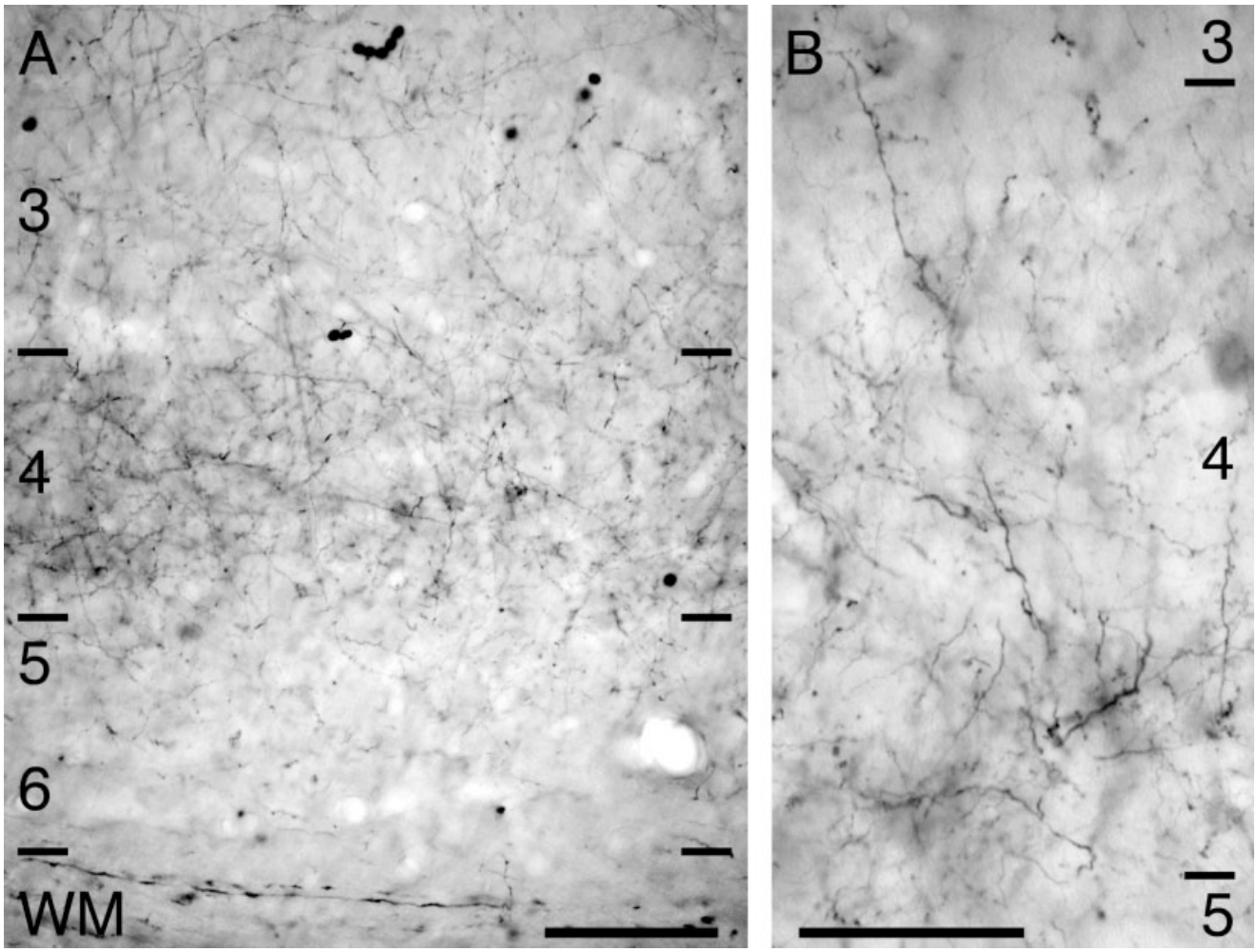

Fig. 2. Light micrographs of cortical area V3A showing PHA-L-labeled axon termination zone. **A:** Labeled terminals form dense band in layer 4 and lesser projections into layer 3. Laminae and their boundaries are indicated to the left and right. **B:** Section from a second monkey at higher magnification. The labeled fibers branch profusely in layer 4 to form a dense network of axon collaterals and terminals. Laminae and their boundaries are indicated at right. Scale bars = 0.1 mm in A; 50 μm in B.

One spiny stellate cell and one star pyramidal cell were found within the cloud of axons near the layer 3–4 border. The density of the labeling in layer 4 made it impossible to reconstruct at LM level extensive portions of single axons. This density also made tight LM/EM correlation impossible. Thus, we selected for EM analysis areas of layer 4 with the densest labeling as determined in the light microscope. The projections to the superficial layers were sparser, and this enabled us to correlate LM and EM.

EM

We sampled a total of 106 boutons from layers 2/3 and 4 (48 from layer 2/3 and 58 from layer 4). All were serially sectioned and completely reconstructed. In total, 120 labeled synapses were examined, all of which were asymmetric (Gray's type 1). We reproduce the electron micrographs of boutons in this study at approximately the same magnification as the images used in previous studies of V1 and V2 afferent boutons in MT (Anderson et al., 1998; Anderson and Martin, 2002), to facilitate a comparison with other corticocortical projections we have studied in the macaque.

The reaction end product was dark, though of variable intensity, in different boutons. Vesicles and mitochondria were clearly visible inside the boutons, and the synaptic clefts were not obscured by label. Myelinated axons were also labeled, confirming that the antibody had penetrated well, despite the insulating sheath. Some axons were myelinated right up to the synaptic bouton. Most boutons were small (~0.5 μm diameter), compact structures containing one or two mitochondria and a cluster of vesicles over the region of the synaptic specialization (see, e.g., Figs. 3, 4). The synapse was indicated by the presence of presynaptic vesicles, a synaptic cleft, and a postsynaptic density in the target structure. Occasionally, we saw a density within the labeled bouton that was mirrored by a similar density within the target. In the immediate vicinity of the presynaptic density, there were no vesicles. This mirror-like configuration was always seen close or adjacent to a conventional asymmetric synapse and was clas-

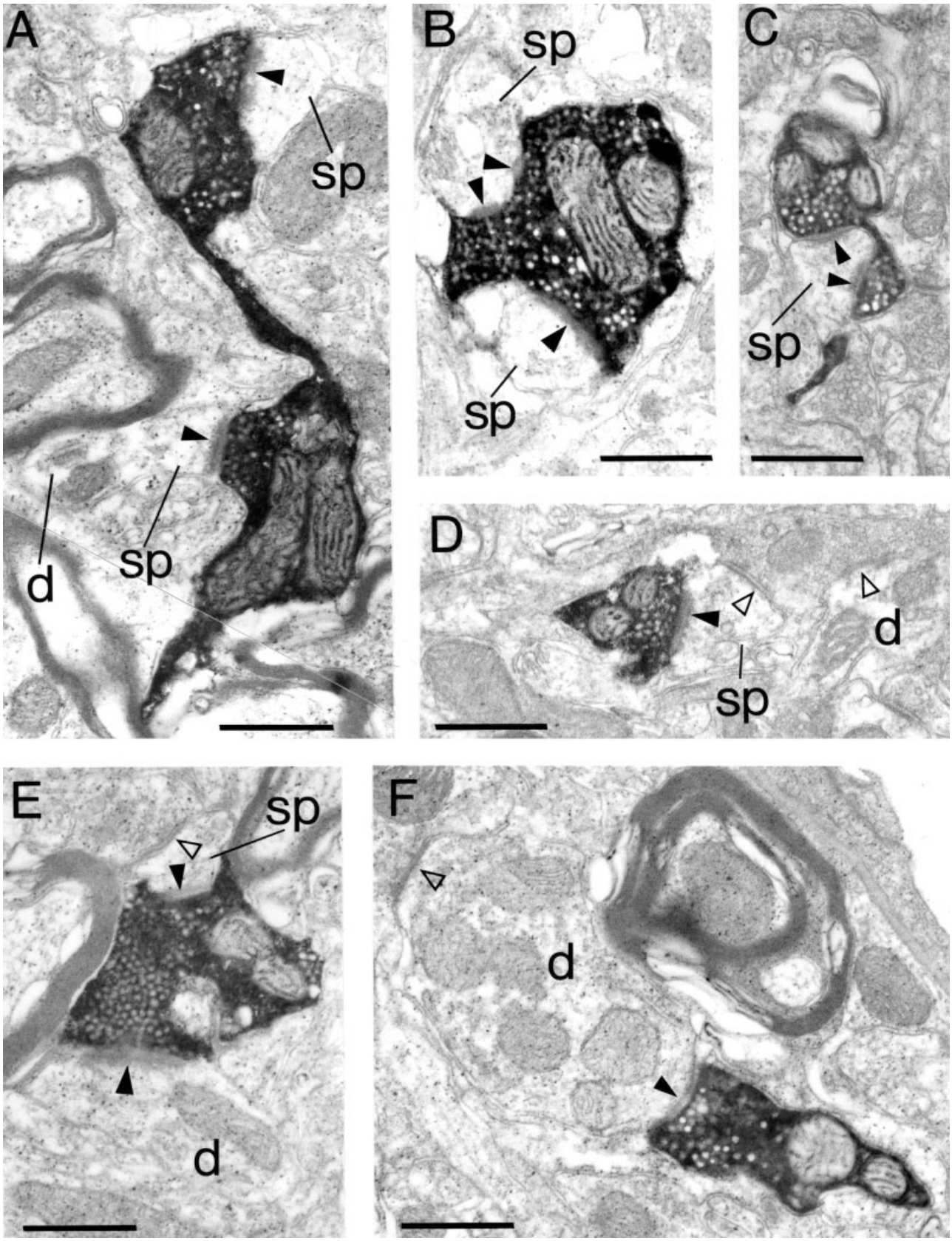

Figure 3

sified as a puncta adherens (Peters et al., 1991). We did not include these puncta in our reconstructions or estimates and measurements of synapses.

Spines. Serially sectioning the bouton, synapse, and target structures greatly assisted in determining the type of target that formed synapses with the labeled boutons. We also used standard ultrastructural criteria to classify targets (Peters et al., 1991). The most frequent targets were small spines (Figs. 3, 4). Occasionally, we were able to trace spines back to a parent dendrite (Figs. 3A, 4E). A second synapse from an unlabeled bouton was seen on five spines and in all cases was of a symmetric morphology (Gray's type 2). All five dual-input spines were located in layer 4 (Fig. 3D,E). Spine synapses formed 52 of the 53 synapses examined in layer 2/3 and 51 of the 67 synapses identified in layer 4.

Boutons sometimes had the target spine or part of the spine embedded within the bouton (Figs. 3C, 4B,C,E). We have previously reported similar observations in the case of the V1 afferent boutons in MT. The synapses in MT were complex, highly perforated, and extensive (see Fig. 8 in Anderson et al., 1998). The synapses in V3A were not as complex as those found on V1 boutons in MT but were quite extensive and often covered a large part of the spine that was embedded or "pinched" into the bouton (Figs. 3C, 4B,C,E).

Dendrites. Dendrites were also the targets of labeled boutons. These were usually identified by reconstruction from serial sections or in individual sections by the presence of mitochondria and microtubules. Most dendrites were about 0.5 μm diameter (Fig. 3E), the largest measuring ~0.9 μm diameter. Reconstructions of serial sections indicated that there were two basic classes of target dendrites. One class possessed spines and had dendritic shafts that showed little variation in diameter when reconstructed. The shaft formed few synapses, which is characteristic of the spiny dendrites of excitatory neurons (Fig. 3E). The sole dendritic synapse in layer 2/3 and 9 of 16 of the completely reconstructed synapses in layer 4 were formed with such spiny dendrites.

The other class of dendritic target had a morphology that differed markedly from that of the putative spiny dendrites. Such dendrites varied greatly in diameter in the serial reconstructions; they usually contained numerous mitochondria and, in single sections, could form multiple synapses with other unidentified boutons (Fig. 3F). These dendrites are quite characteristic of neurons with smooth, varicose dendrites that contain the inhibitory neurotransmitter γ-aminobutyric acid (GABA; Somogyi et al., 1983; Peters and Saint Marie, 1984; Kisvárday et al., 1985; Ahmed et al., 1997). A high proportion of serially reconstructed target dendrites in layer 4 had the features of smooth (putative GABAergic) neurons; 7 of 16 synapses (44%) formed on smooth dendrites. By comparison, smooth dendrites formed 26% of the dendritic targets of the V1 projection to MT and 52% of the dendritic targets of the V2 projection to MT (Anderson et al., 1998; Anderson and Martin, 2002).

Postsynaptic density. Reconstructing the bouton and its target gave us the opportunity to view the complete postsynaptic density as a 2-D or 3-D structure. We have used this technique previously to obtain values of the surface area of synapses (Anderson et el., 1998; Anderson and Martin, 2002). By focusing on the postsynaptic specialization rather than the presynaptic membrane, we avoided detail being obscured by the reaction end product in the bouton. The postsynaptic density can be perforated, giving it a doughnut or horseshoe morphology rather than that of a simple disc. Figures 5 and 6 show that the synapses with the more complex morphology are usually formed with spines.

The 2-D projection of all the postsynaptic densities is shown in Figures 5 and 6. There was little difference in the distributions of the areas of synapses made with the two main target types in layer 4, spines and dendrites ($P = 0.08$, two-tailed t-test). Spine synapses had a mean area of 0.11 μm^2 compared with 0.09 μm^2 for synapses with dendritic shafts. In comparisons of synapses from different laminae, the distributions overlapped considerably (Fig. 7). The layer 2/3 synapses (mean 0.110 μm^2, SEM 0.008) were not significantly different from those of layer 4 (mean 0.101 μm^2, SEM 0.006; $P = 0.4$, two-tailed t-test). The V2 boutons forming synapses with spines in layer 4 of areas V3a (mean 0.108 μm^2, SEM 0.007) and MT (mean 0.107 mm^2, SEM 0.01) were not significantly different ($P = 0.9$, two-tailed t-test). However, the spine synapses in layer 2/3 of V3a (mean 0.11 μm^2, SEM 0.008) were significantly larger than those in layer 2/3 of MT (mean 0.08 μm^2, SEM 0.005; $P = 0.005$, two-tailed t-test).

The mean size of the pooled synapses from V2 in layer 4 of V3A (mean 0.101 μm^2, SEM 0.006) was slightly less than that of the synapses of boutons from V2 in layer 4 of MT (mean 0.107 μm^2, SEM 0.008), but the differences were not significant ($P = 0.89$, two-tailed t-test). In single sections, some spines appeared to form two synapses with labeled boutons on opposite sides of the same spine head (Figs. 3C, 4B,E), but on reconstruction this proved to be a single synapse formed by a single bouton.

Target types. The most frequently encountered targets of V2 labeled boutons were spines. There was a dif-

Fig. 3. Electron micrographs of PHA-L-labeled electron-dense axon and boutons located in layer 4 of area V3A. A–D: Examples of synapses formed with spines. **A:** Two boutons en passant form asymmetric synapses (solid arrowheads) with spines (sp). One of the spines can be traced back to the small parent dendrite (d). Spines were the most frequent synaptic target seen in this study: small to medium-sized boutons targeted small spines, the labeled bouton containing at least one mitochondria, and the remaining space (usually above the synapse) is vesicle filled. **B:** Two spines (sp) form asymmetric synapses (solid arrowheads) with a labeled bouton. The postsynaptic density of the uppermost spine does not appear as a continuous structure but instead appears to be perforated or complex. This spine also contains a spine apparatus. **C:** A spine is partially embraced by a small labeled bouton that forms a perforated asymmetric synapse (solid arrowheads) with a spine (sp). **D:** A spine forms an asymmetric synapse (solid arrowhead) with a labeled bouton and a symmetric synapse (open arrowheads) with an unidentified bouton. The unidentified bouton also forms a symmetric synapse with a small dendrite (d). E,F: Examples of synapses formed with dendrites. **E:** A small-caliber dendrite (d) and a spine (sp) form asymmetric synapses (solid arrowheads) with a labeled bouton. Dendrites such as this containing few mitochondria, forming synapses infrequently, and showing little variation in diameter are characteristic of neurons with spiny dendrites. The spine also forms a symmetric synapse (open arrowhead) with an unidentified bouton. **F:** A large caliber dendrite (d) forms an asymmetric synapse (solid arrowhead) with a labeled bouton and a symmetric synapse (open arrowhead) with an unidentified bouton. The dendrite contains many mitocondria, forms many synapses, and has a beaded morphology. These features are characteristic of putative GABAergic neurons with smooth dendrites. Scale bars = 0.5 μm.

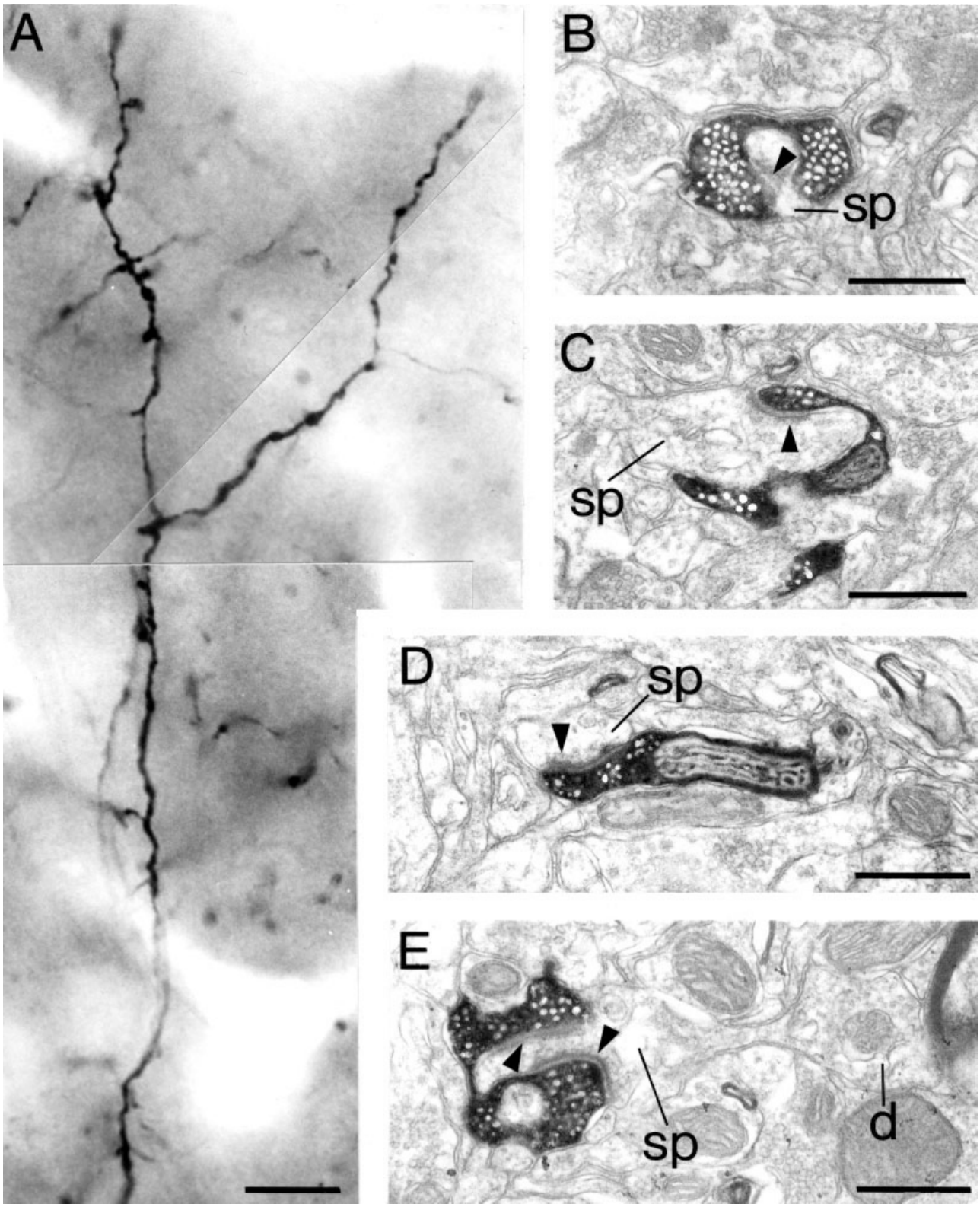

Fig. 4. Light and electron micrographs of PHA-L-labeled axon and boutons located in layer 2/3 of area V3A. **A:** Photomontage of an intensely labeled ascending collateral taken from layers 2 and 3. Numerous varicose swellings of the en passant and aux terminaux types can be clearly seen along the axon length. **B–E:** Electron micrographs of labeled boutons taken from the area between and inclusive of the branched collateral shown in A. Each bouton forms an asymmetric synapse (arrowheads) with a spine (sp). E: A labeled bouton forms an asymmetric synapse (arrowhead) with a spine. The spine can be traced back to the parent dendritic shaft (d). Scale bars = 10 μm in A; 0.5 μm in B–E.

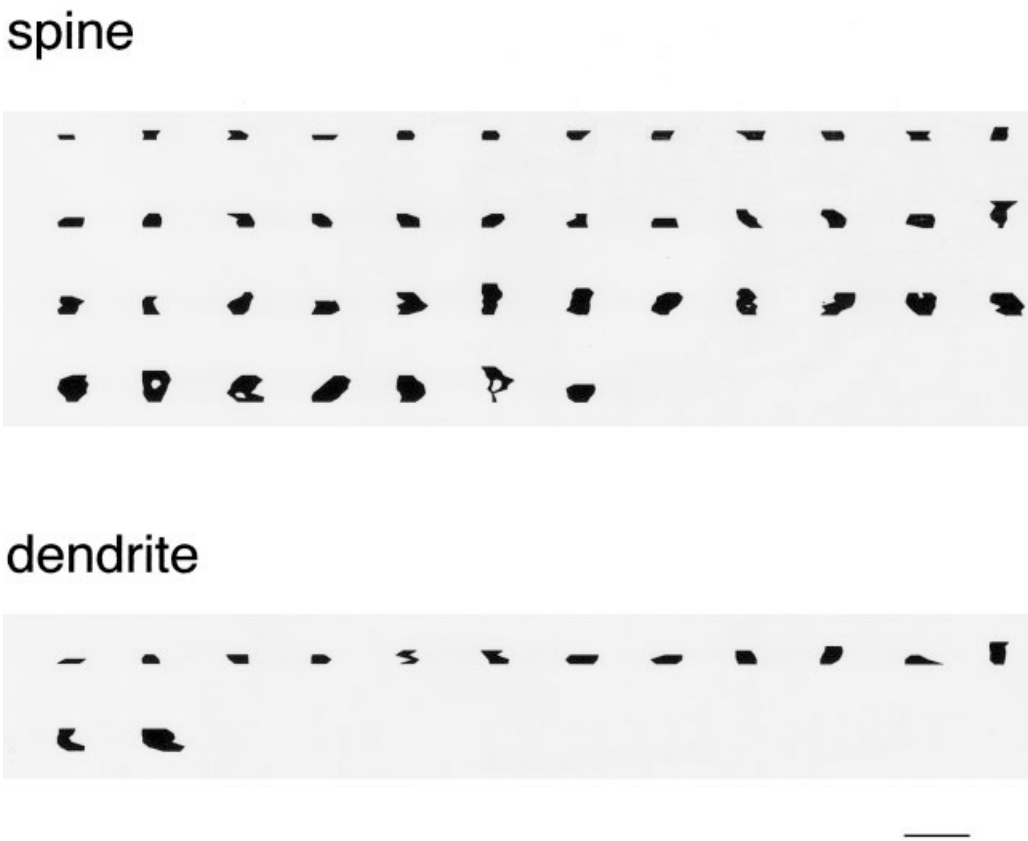

Fig. 5. Two-dimensional projection of the reconstructed postsynaptic densities found in layer 4 on spines and dendrites postsynaptic to labeled V2 boutons in area V3A. The densities are ordered by increasing surface area. Scale bar = 1 μm.

ference in the proportion of spines to dendrites as targets for the different laminae of innervation (Fig. 7). For this reason, we have not pooled the data from the two laminae. In layer 4, 76% of the labeled synapses were formed with spines and 24% with dendritic shafts, whereas, in layer 2/3, 98% of the synapses were formed with spines and 2% with dendritic shafts (Fig. 8).

As indicated above (see above under Dendrites), smooth neurons provided just under half of the dendritic shaft targets in layer 4. Serial reconstructions indicated that most boutons made only one synapse and only rarely more than two synapses (Fig. 9). On average, there were 1.1 and 1.2 synapses per labeled bouton in layers 2/3 and 4, respectively.

The same electron micrographs of labeled synaptic boutons and their targets were used to estimate the proportion of synapses formed with spines and dendrites in the neuropil of V3A. We found that, in layer 4 (n = 282) and layer 3 (n = 242), 63% and 86% of synapses, respectively, were formed with spines and the remainder with dendritic shafts. The dendritic profiles could be classed as either putative GABAergic smooth neurons or spiny neurons. We based our classification of the dendrites on serial reconstructions. For layers 4 and 3, we found 21% and 9%, respectively, of all targets to be putative GABAergic neurons (56% of dendrites in layer 4 and 60% in layer 3). We compared the labeled and nonlabeled synapses and the synapses of layer 3 and layer 4 by using a contingency table analysis. The proportions of targets of pooled layer 3 synapses were significantly different from those of pooled layer 4 targets ($P < 0.001$). Labeled and nonlabeled synapses from layer 4 showed no significant difference in the distribution of their target types ($P < 0.05$). The corresponding analysis for the targets of layer 3 synapses could not be performed because of low counts ($n < 5$) for labeled dendritic targets. The pooled data from labeled layers 3 and 4 was not significantly different from the pooled nonlabeled data from layers 3 and 4 ($P < 0.05$).

To estimate the relative proportion of synapses being contributed by V2 to area V3a, we made an unbiased stereological analysis of layer 4. We selected one section from each animal in which the labeling was particularly dense. In Figure 2 we show the terminal labeling in layer 4. We selected regions from within the densest patches of terminal innervation for our analysis with the unbiased disector method (Sterio, 1984). Although the blocks of tissue used for reembedding were selected from the densest zones of innervation, the distribution of labeled synapses in any ultrathin section could vary greatly. If the disector region was selected by using nonbiased features, such as the edge of the tissue or a scratch on the block face, we counted no labeled synapses. If we selected the location of the disector by finding a labeled bouton and then sam-

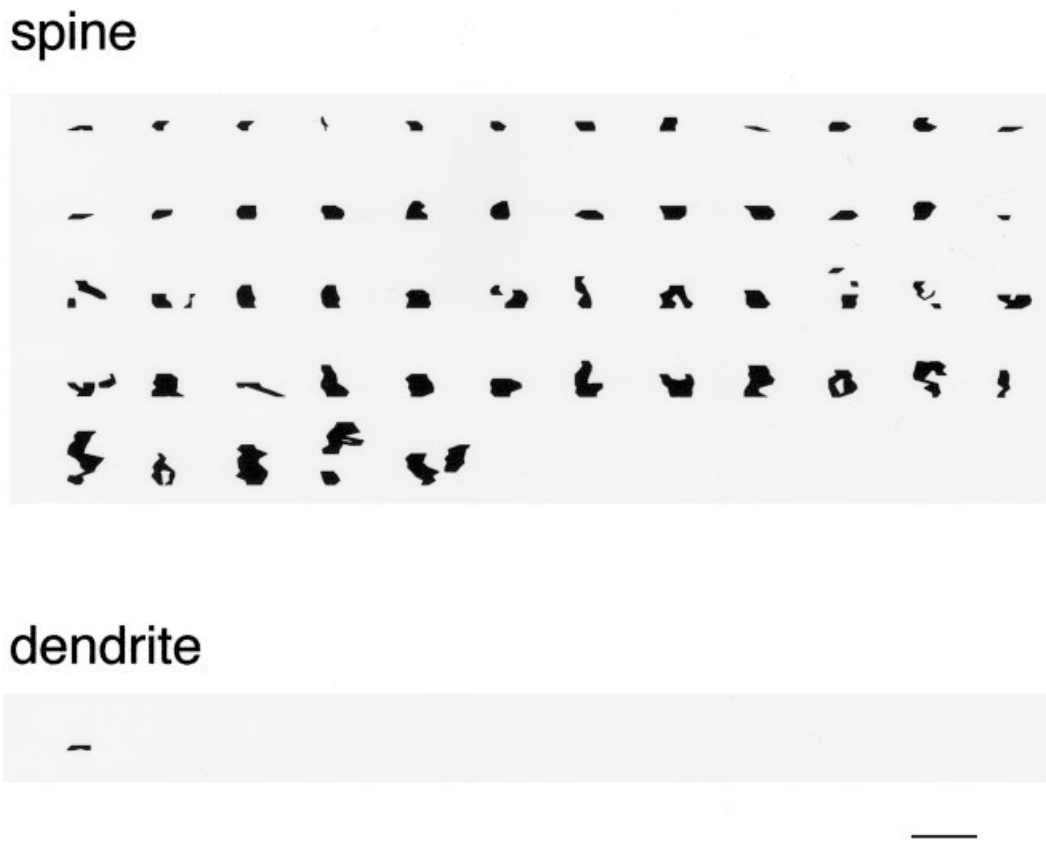

Fig. 6. Two-dimensional projection of the reconstructed postsynaptic densities found in layer 2/3 on spines and dendrites postsynaptic to labeled V2 boutons in area V3A. The densities are ordered by increasing surface area. Scale bar = 1 μm.

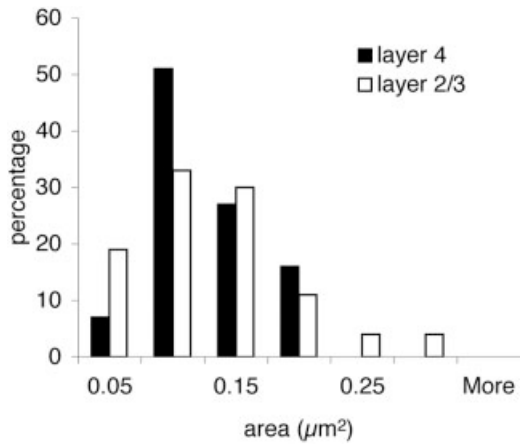

Fig. 7. Histogram of the distribution of postsynaptic areas (μm^2) formed by labeled V2 boutons in layers 2/3 (n = 54) and 4 (n = 46) of area V3A.

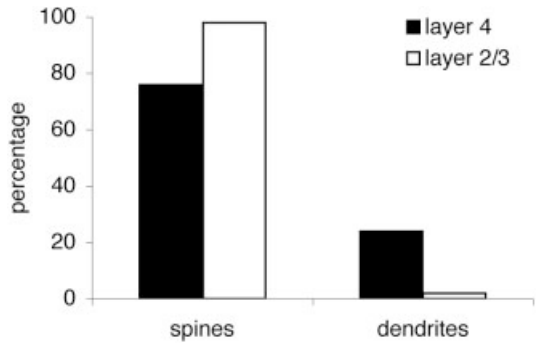

Fig. 8. Histogram of the synaptic targets of labeled V2 boutons in area V3A [for layer 2/3 (n = 53) and for layer 4 (n = 46)].

pling in the vicinity, we counted 3.5% (2 of 57) and 4.1% (7 of 169) of disappearing labeled synapses. This provides between two and six labeled V2 synapses per 10 × 10 × 10 μm cube of layer 4 in V3A.

DISCUSSION

We have shown that the projection from V2 to V3A, which is classified as "feedforward," forms asymmetric (excitatory) synapses principally with spiny (excitatory) neurons in layer 4, with a smaller projection almost exclusively to spiny neurons in layer 3. At the LM level, the terminal labeling in V3A was as strong as we have seen for any extrastriate projection we have studied (Anderson et al., 1998; Anderson and Martin, 2002). Counts of the

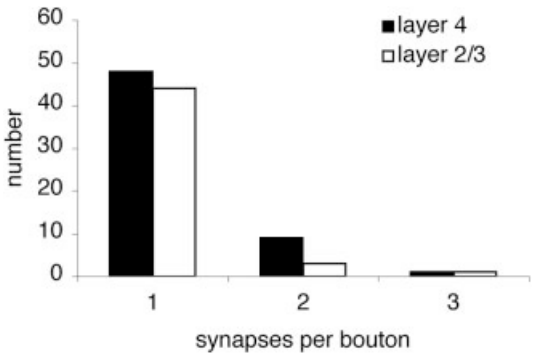

Fig. 9. Histogram of the number of synapses formed per labeled V2 bouton in layers 2/3 and 4 of area V3A.

identified synapses in the zones of densest labeling in layer 4 revealed that about 4% of the synapses originated from V2. This is similar to the proportion of labeled synapses found in layer 4 of MT after these same injections in V2 (Anderson and Martin, 2002). Both of these are comparable to the proportion of thalamic synapses in layer 4C of V1 (Latawiec et al., 2000) and slightly more than the 3% found for the projection from V1 to MT (Anderson et al., 1998). Thus the contribution of synapses from V2 to V3A is as numerous as any feedforword projection in primate visual cortex.

Rockland et al. (1999) estimated the contribution of pulvinocortical synapses in the lunate sulcus to be 0.18% of all excitatory synapses. Their estimate, based on LM observations in combination with ultrastructural data on V1 from other sources, may seem small compared with the 3–5% for the V2-V3A projection, but, as we have pointed out, the numbers are very location dependent. Our estimates are derived from the regions of high bouton density, whereas, if we select a region of layer 4 at random, the chances of finding even one labeled synapse are remote.

A feature of feedforward projections to layer 4, such as the thalamic projection to V1 or the V1 projection to V2 or the V2 projection to V3A and MT, is that they form segregated, stripe-like patches. For example, the ocular dominance stripes in the case of the thalamus, and the V1 projection segregates into thick, thin, and pale stripes seen in V2 after cytochrome oxidase staining. This tendency of the afferents to segregate themselves into mutually exclusive territories suggests that, in layer 4 at least, each stripe is an indication that only one afferent dominates the territory. Thus, in the case of the V2 projection to V3A, it is likely that no other area would form patches that overlap with the same stripes formed by the V2 projection. Instead, it is likely that a second projection would interdigitate in much the same way that thalamic afferents representing the left and right eyes do in V1. The second source of afferents is not known, but it must be another feedforward projection if it ends in layer 4. Because V3A appears early in the hierarchy of visual areas, the only possible candidates are V1 and V3. The projection from V1 is sparse (Zeki, 1978b; Van Essen et al., 1986), but, like the projection from V2 (Gattass et al., 1997), the projection from V3 is substantial (Felleman et al., 1997), and it is likely that it forms a feedforward projection to layer 4 that interdgitates with that from V2.

The mean surface area of synapses formed in layer 4 with spines was as large (0.101 μm^2) as the spine synapses formed by V2 axons in layer 4 of MT (0.107 μm^2; Anderson and Martin, 2002) but was smaller than those formed by V1 axons in layer 4 of MT (0.127 μm^2; Anderson et al., 1998). However, there was a large range in the size of the postsynaptic density for all projection synapses examined, both in MT and in V3A (see, e.g., Fig. 8 in Anderson et al., 1998; Fig. 8 in Anderson and Martin, 2002). In general, the largest synapses had a more elaborate shape than the simpler disk shape found for smaller synapses. The largest synapses are formed with spines, and this means that spine synapses may appear more elaborate than those commonly found on the dendritic shaft. Although the significance of these differences in shapes and sizes has yet to be elucidated, experiments in hippocampal slice cultures indicate that larger excitatory postsynaptic current (EPSCs) are correlated with larger postsynaptic densities (Schikorsky and Stevens, 1997), so the measurements of synaptic densities in neocortex may provide insights into the comparative efficacy of synapses originating in different pathways.

The difference in the target neurons between layer 4 and layer 3 was unusual. From our evidence, only the V2 projection to layer 4 forms synapses with smooth (putative GABAergic) neurons, which were about 10% of the targets. The V2 projection to the superficial layers formed synapses exclusively with spiny neurons. We noted a similar trend, albeit not quite so marked in the projection of V2 to MT, in which 15% of the targets in layer 4 were smooth neurons, whereas, in layer 3, only 8% of the targets were smooth neurons. This raises the question of whether the same set of fibers provides this differential input to the two layers. From our data, it seems that single fibers do span the layer 3–4 border, but, in general, too many fibers were labeled to be able to trace any single fiber over several sections. Thus, we cannot be sure that there is not a population that arborizes exclusively in layer 3, as seems to be the case in the projection from V1 to V2 (Rockland and Virga, 1990). One additional difference between layer 3 and layer 4 was that, in layer 4, five of the target spines formed a second synapse with an unlabeled bouton. The second synapse was always symmetric. We had observed this same configuration in the context of the thalamic input to cortex (Dehay et al., 1991). Despite the fact that spines were the exclusive target in layer 3, we found no dual-input spines.

Physiological studies of macaqueV3A indicate that the neurons are not color sensitive (Zeki, 1978a) and that, compared with the case in MT, the proportion of direction-selective neurons is low (Zeki, 1978a; Galletti et al., 1990). Nevertheless, behavioral studies show that there are neurons in V3A sensitive to eye position (Galletti and Battaglini, 1989; Nakamura and Colby, 2000, 2002). Attention and expectation of reward in a task involving motion judgments modulate the responses of V3A neurons (Thiele et al., 1999; Nakamura and Colby, 2000). Thus, one view of V3A is that it forms a component of a visuosomatomotor pathway to the premotor cortex (Shipp et al., 1998). However, given the anatomical evidence of V3A's connections to the inferotemporal cortex and the physiological evidence from Gaska et al. (1988) that the temporal frequency tuning was low-pass, both the input and the output from V3A might be more heterogeneous than the traditional divisions into dorsal and ventral processing streams would imply. Given the anatomical and functional segregation of V2 (DeYoe and Van Essen, 1985; Shipp and Zeki, 1985; Hubel and Livingstone, 1987; Ts'o et al., 2001), it would be interesting to know which subdivisions of V2 provide the input to V3A.

ACKNOWLEDGMENTS

We thank German Koestinger and Nuno da Costa for their expert assistance.

LITERATURE CITED

Adams DL, Zeki S. 2001. Functional organization of macaque V3 for stereoscopic depth. J Neurophysiol 46:2195–2203.

Ahmed B, Anderson JC, Martin KAC, Nelson JC. 1997. Map of the synapses onto layer 4 basket cells of the primary visual cortex of the cat. J Comp Neurol 380:230–242.

Andersen RA, Asanuma C, Essick G, Siegel RM. 1990. Corticocortical connections of anatomically and physiologically defined subdivisions within the inferior parietal lobule. J Comp Neurol 296:65–113.

Anderson JC, Martin KAC. 2002. Connection from cortical area V2 to MT in macaque monkey. J Comp Neurol 443:56–70.

Anderson JC, Binzegger T, Martin KAC, Rockland KS. 1998. The connection from cortical area V1 to V5: a light and electron microscopic study. J Neurosci 18:10525–10540.

Backus BT, Fleet DJ, Parker AJ, Heeger DJ. 2001. Human cortical activity correlates with stereoscopic depth perception. J Neurophysiol 86:2054–2068.

Baizer JS, Ungerleider LG, Desimone R. 1991. Organization of visual inputs to the inferior temporal and posterior parietal cortex in macaques. J Neurosci 11:168–190.

Beck PD, Kaas JH. 1999. Cortical connections of the dorsomedial visual areas in the Old World macaque monkey. J Comp Neurol 406:487–502.

Blatt GJ, Andersen RA, Stoner GR. 1990. Visual receptive field organization and cortico-cortical connection of the lateral intraparietal area (area LIP) in the macaque. J Comp Neurol 299:421–445.

Boussaoud D, Ungerleider LG, Desimone R. 1990. Pathways for motion analysis: cortical connections of the medial superior temporal and fundus of the superior temporal visual areas in the macaque. J Comp Neurol 296:462–495.

Cavada C, Goldman-Rakic PS. 1989. Posterior parietal cortex in rhesus monkey. I. Parcellation of areas based on distinctive limbic and sensory corticocortical connections. J Comp Neurol 287:393–421.

Colby CL, Gattass R, Olson CR, Gross CG. 1988. Topographical organization of cortical afferents to extrastriate visual area PO in the macaque: a dual tracer study. J Comp Neurol 269:392–413.

Dehay C, Douglas RJ, Martin KAC, Nelson JC. 1991. Excitation by geniculocortical synapses is not "vetoed" at the level of dendritic spines in cat visual cortex. J Physiol 440:723–734.

DeYoe EA, Van Essen DC. 1985. Segregation of efferent connections and receptive field properties in visual area V2 of the macaque. Nature 317:58–61.

Felleman DJ, Van Essen DC. 1983. The connection of area V4 of macaque monkey extrastriate cortex. Soc Neurosci Abstr 9:153.

Felleman DJ, Burkhalter A, Van Essen DC. 1997. Cortical connections of areas V3 and VP of macaque extrastriate visual cortex. J Comp Neurol 379:21–47.

Galletti C, Battaglini PP. 1989. Gaze-dependent visual neurons in area V3a of monkey prestriate cortex. J Neurosci 9:1112–1125.

Galletti C, Battaglini PP, Fattori P. 1990. "Real-motion" cells in area V3A of macaque visual cortex. Exp Brain Res 82:67–76.

Gaska JP, Jacobson LD, Pollen DA. 1988. Spatial and temporal frequency selectivity of neurons in visual cortical area V3a of the macaque monkey. Vis Res 28:1179–1191.

Gattass R, Sousa APB, Mishkin M, Ungerleider LG. 1997. Cortical projections of area V2 in the macaque. Cereb Cortex 7:1047–3211.

Girard P, Salin PA, Bullier J. 1991. Visual activity in areas V3a and V3 during reversible inactivation of area V1 in the monkey. J Neurophysiol 66:1493–1503.

Hubel DH, Livingstone MS. 1987. Segregation of form, colour, and stereopsis in primate area 18. J Neurosci 7:3378–3415.

Kennedy H, Bullier J. 1985. Double-labeling investigation of the afferent connectivity to cortical areas V1 and V2 of the macaque monkey. J Neurosci 10:2815–2830.

Kisvárday ZF, Martin KAC, Whitteridge D, Somogyi P. 1985. Synaptic connections of intracellularly filled clutch neurons, a type of small basket neuron in the visual cortex of the cat. J Comp Neurol 241:111–137.

Latawiec D, Martin KAC, Meskenaite V. 2000. Termination of the geniculocortical projection in the striate cortex of macaque monkey: a quantitative immunoelectron microscopic study. J Comp Neurol 419:306–319.

Morel A, Bullier J. 1990. Anatomical segregation of two cortical visual pathways in the macaque monkey. Vis Neurosci 4:555–578.

Nakamura H, Kuroda T, Wakita M, Kato A, Mikami A, Sakata H, Itoh K. 2001. From three-dimensional space vision to prehensile hand movements: The lateral intraparietal area links the area V3a and the anterior intraparietal area in macaques. J Neurosci 21:8174–8187.

Nakamura K, Colby CL. 2000. Visual, saccade-related, and cognitive activation of single neurons in monkey extrastriate area V3a. J Neurophysiol 84:677–692.

Nakamura K, Colby CL. 2002. Updating of the visual representation in monkey striate and extrastriate cortex during saccades. Proc Natl Acad Sci U S A 99:4026–4031.

Orban GA, Fize D, Hendrik P, Denys K, Nelissen K, Sunaert S, Todd J, Vanduffel W. 2003. Similarities and differences in motion processing between the human and macaque brain: evidence from fMRI. Neuropsychologia 41:1757–1768.

Peters A, Saint Marie RL. 1984. Smooth and sparsely spinous nonpyramidal cells forming local axonal plexuses. In: Jones EG, Peters A, editors. Cerebral cortex, vol 1. Cellular components of the cerebral cortex. New York: Plenum Press. p 419–445.

Peters A, Palay SL, Webster HDeF. 1991. The fine structure of the nervous system: neurons and their supporting cells, 3rd ed. Oxford: Oxford University Press.

Rockland KS, Virga A. 1990. Organization of individual cortical axons projecting from area V1 (area 17) to V2 (area 18) in the macaque monkey. Vis Neurosci 4:11–28.

Rockland KS, Andresen J, Cowie RJ, Robinson DL. 1999. Single axon analysis of pulvinocortical connections to several visual areas in the macaque. J Comp Neurol 406:221–250.

Schall JD, Morel A, King DJ, Bullier J. 1995. Topography of visual cortex connections with frontal eye field in macaque: convergence and segregation of processing streams. J Neurosci 15:4464–4487.

Schikorski T, Stevens CF. 1997. Quantitative ultrastructural analysis of hippocampal excitatory synapses. J Neurosci 17:5858–5867.

Shipp S, Zeki S. 1985. Segregation of pathways leading from area V2 to areas V4 and V5 of macaque monkey visual cortex. Nature 315:322–325.

Shipp S, Blanton M, Zeki S. 1998. A visuo-somatomotor pathway through superior parietal cortex in the macaque monkey: cortical connections of areas V6 and V6a. Eur J Neurosci 10:3171–3193.

Somogyi P, Kisvárday ZF, Martin KAC, Whitteridge D. 1983 Synaptic connections of morphologically identified and physiologically characterised large basket cells in the striate cortex of cat. Neuroscience 10:261–294.

Stanton GB, Bruce CJ, Goldberg ME. 1995. Topography of projections to posterior cortical areas from the macaque frontal eye fields. J Comp Neurol 353:291–305.

Sterio DC. 1984. The unbiased estimation of number and sizes of arbitrary particles using the disector. J Microsc 134:127–136.

Thiele A, Distler C, Hoffmann KP. 1999. Decision-related activity in the macaque dorsal visual pathway. Eur J Neurosci 11:2044–2058.

Tootell RBH, Mendola JD, Hadjikhani NK, Leddon PJ, Liu AK, Reppas JB, Sereno MI, Dale AM. 1997. Functional analysis of V3a and related areas in human visual cortex. J Neurosci 17:7060–7078.

Tsao DY, Vanduffel W, Sasaki Y, Fize D, Knutson TA, Mandeville JB, Wald LL, Dale AM, Rosen BR, Van Essen DC, Livingstone MS, Orban GA, Tootell RBH. 2003. Stereopsis activates V3a and caudal intraparietal areas in macaques and humans. Neuron 39:555–568.

Ts'o DY, Wang Roe A, Gilbert CD. 2001. A hierarchy of the functional organization for color, form and disparity in primate visual area V2. Vis Res 41:1333–1349.

Van Essen DC, Newsome WT, Maunsell JH, Bixby JL. 1986. The projections from striate cortex (V1) to areas V2 and V3 in the macaque monkey: asymmetries, areal boundaries, and patchy connections. J Comp Neurol 244:451–480.

Webster MJ, Bachevalier J, Ungerleider LG. 1994. Connections of inferior temporal areas TEO and TE with parietal and frontal cortex in macaque monkeys. Cereb Cortex 4:470–483.

Zeki SM. 1978a. Uniformity and diversity of structure and function in the rhesus monkey prestriate visual cortex. J Physiol 277:273–290.

Zeki SM. 1978b. The cortical projections of foveal striate cortex in the rhesus monkey. J Physiol 277:227–244.

3.4 V4 toV2 was the first feedback projection that we studied. In this case we were able to identify three individual axon terminals and extract them from the mass of labeled axon. In the classic feedback pattern the axons mostly innervated layer 1and a small projection to layer 6 plus what looks like a spillover of exuberant axon in from layer 1 to layer 2. It was important to sample from a feedback projection as so much of the cortical hierarchy story depends on that concept.

THE JOURNAL OF COMPARATIVE NEUROLOGY 495:709–721 (2006)

Synaptic Connection from Cortical Area V4 to V2 in Macaque Monkey

JOHN C. ANDERSON* AND KEVAN A.C. MARTIN*
Institute for Neuroinformatics, University of Zürich, and ETH Zürich, 8057 Zürich, Switzerland

ABSTRACT

The major target of the V4 projection in V2 is layer 1, where it forms a tangential spread of asymmetric (excitatory) synapses. This is characteristic of a "feedback" projection. Some axons formed discrete clusters of bouton terminaux between lengths of myelinated axon, while others were unbranched and formed a continuous distribution of en passant boutons with no intercalated myelin. Minor projections were found in layers 2/3 and 6. Dendritic spines were the most frequently encountered targets of the V4 projection (80% in layer 1 and layer 2/3, 94% in layer 6). The remaining targets were dendritic shafts. In layer 1, 69% of target dendrites (12% of all targets) had characteristics identifying them as smooth (GABAergic) cells. In layer 2/3 and layer 6 virtually all the shaft synapses were on smooth dendrites (86% and 100%, respectively). Multisynaptic boutons were rare (mean 1.1 synapses per bouton). Synapses formed in layer 6 were smaller than those of layer 1 (mean area 0.073 μm^2 vs. 0.117 μm^2). Synapses formed with spines had a more complex postsynaptic density than those formed with dendritic shafts. With respect to targets and synaptic type and size and morphology of synapses, the feedback projection from V4 to V2 resembles those of feedforward projections. The principal difference between the feedforward and feedback projection is in the lamina location of their terminal boutons. The concentration of the V4 projection on layer 1, where it forms asymmetric synapses mainly with spines, suggests that it excites the distal apical dendrites of pyramidal cells. J. Comp. Neurol. 495:709–721, 2006.

Indexing terms: visual cortex; area V2; corticocortical; light and electron microscopy; synapse morphology; postsynaptic target

The existence of "feedback" cortical projections that are thought to perform "top-down" operations has long been known. Although these projections are a crucial part of the interpretation of behavioral and physiological studies, surprisingly little is known of the details of these projections. In the primate cortex such projections have been defined mainly on the basis of their pattern of termination in the different laminae of the target cortical area. Unlike "feedforward" projections, whose canonical pattern is to terminate principally in layer 4, the feedback projections terminate outside layer 4, with layer 1 being a prominent target. These projections have been studied mainly at the light microscope level and much of what we know about the details of individual axonal arborizations comes from the extensive reconstructions of feedback and feedforward projections made by Rockland and colleagues (reviewed in Rockland, 1994, 1997). Their reconstructions of the feedback axons from V4 to V2 indicate that layers 1, 2, and 6 are the preferred layers of innervation and this laminar organization seems to be a cardinal feature of the feedback projections seen at the single fiber level. An additional feature of the feedback projection noted in a number of studies is that they are more divergent, spreading over a wider territory than the feedforward projections (Krubitzer and Kaas, 1989; Shipp and Zeki, 1989a,b; Suzuki et al., 2000; Stettler at al., 2002). The studies of Rockland at the single fiber level also indicate such divergence in the feedback connections, including those from V4 to V2

Grant sponsor: European Union; Grant number: QULG3-1999-01064 (to K.A.C.M.); Grant sponsor: Human Frontier Science Program; Grant number RG0123/2000-B (to K.A.C.M.).

*Correspondence to: John C. Anderson or Kevan A.C. Martin, Institute for Neuroinformatics, University of Zürich and ETH Zürich, Winterthurerstr.190, 8057 Zürich, Switzerland.
E-mail: jca@ini.phys.ethz.ch or kevan@ini.phys.ethz.ch

Received 2 August 2005; Revised 5 October 2005; Accepted 11 November 2005

DOI 10.1002/cne.20914

Published online in Wiley InterScience (www.interscience.wiley.com).

(Rockland et al., 1994). Presumably these features reflect basic differences in the functional role of the two types of intracortical projection.

The projection from V2 to V4 has been extensively studied because it is part of the fan-out from early visual areas to the dorsal and ventral processing streams. Staining V2 with the mitochondrial enzyme cytochrome oxidase provided evidence for stripe-shaped compartments within V2 (Livingstone and Hubel, 1982), which reflect differences in the input from V1 (Sincich and Horton, 2005) and the output projections from V2 to anterior visual areas. Thick and thin stripes alternate and are separated by paler staining interstripes. The thick stripes project mainly to area V3 and V5, while the thin stripes and interstripes project to V4 (Shipp and Zeki, 1985, 1989a,b; De Yoe and Van Essen, 1985). Interestingly, the visual latencies of neurons in V2 are closely correlated with their position with the stripes (Munk et al., 1995). Neurons in thick and pale stripes respond on average 20 ms before those in the thin stripes.

The projection from V4 to V2 is far less well studied and there are no studies at the ultrastructural level. Here we studied the projection of individual axons and groups of axons at the light (LM) and electron (EM) microscope level. Our motivation was to gather at the ultrastructural level clues as to the differences between the feedforward projections we have studied previously and the feedback projections. By taking a classic feedback pathway, we could describe quantitatively the synaptic organization and so provide a direct comparison of feedforward projections. This study shows that with respect to their target neurons, and the size and density of synapses, the V4 to V2 projection is similar to the feedforward projections from V1 to MT, V2 to V3A, and V2 to MT. Unlike the feedforward projections, the feedback projection seldom forms patches in its terminal layers. Its concentration in layer 1 suggests that it connects principally to the distal apical dendrites of pyramidal cells.

MATERIALS AND METHODS

The material presented here was taken from two adult male macaque monkeys (*Macaca mulatta*). Animal treatment and surgical protocols were carried out in accordance with the guidelines of the Kantonal Veterinaeramt of Zurich. The following procedures are similar to those used in Anderson and Martin (2002). Animals were prepared for surgery after the administration of an intramuscular premedication of xylazine (Rompun, Beyelar, 0.5 mg/kg)/ketamine (Ketalar, Parke Davis, 10 mg/kg). This was followed by cannulation of a femoral vein for the delivery of alphaxalone/alphadalone (Saffan, Glaxo) to establish complete anesthesia.

Each animal received ionophoresed injections of the neuronal tracer biotinylated dextran amine (BDA) (Molecular Probes, Eugene, OR). One animal received four injections of 10% BDA in 0.01 M phosphate-buffered saline, pH 7.4 (PBS). The second animal received seven injections. The BDA was delivered from a glass micropipette using a pulsed ionophoretic current of 2–4 mA over a 7–10-minute period. After a 14-day survival period the animals were very deeply anesthetized with intravenous (i.v.) pentobarbital (20 mg/kg) and then perfused transcardially with a normal saline solution, followed by a solution of 3.5% paraformaldehyde, 0.8% glutaraldehyde, and 15% picric acid in 0.1 M PB, pH 7.4. The brain was removed from the skull and a block of cortex containing the injection site and areas V1/V2 was removed. The block was allowed to sink in sucrose solutions of 10, 20, and 30% in 0.1 M PB, then freeze-thawed in liquid nitrogen and washed in 0.1 M PB. Sections were cut from the block at 80 μm in the parasagittal plane and collected in 0.1 M PB. We used standard procedures to reveal the neuronal tracers. In brief outline, washes in PBS were followed by 10% normal swine serum (NSS) in PBS (1 hour). Further washes in NSS preceded overnight exposure (5°C) to an avidin-biotin complex (Vector Laboratories, Burlingame, CA; ABC kit, Elite). The peroxidase activity was identified using 3,3-diaminobenzidene tetrahydrochloride (DAB). After assessment by light microscopy, selected regions of tissue were treated with 1% osmium tetroxide in 0.1 M PB. Dehydration through alcohols (1% uranyl acetate in 70% alcohol) and propylene oxide allowed flat mounting in Durcupan (Fluka, Buchs, Switzerland) on glass slides.

Light microscopic observations of labeled axons were carried out to locate and select regions of interest for electron microscopy. We reconstructed individual collaterals in the less densely innervated areas for correlated light and electron microscopy. Serial ultrathin sections were collected at 60 or 70 nm thickness on Pioloform-coated single slot copper grids. Labeled boutons were photographed at a magnification of 21,000. Synapses and associated structures were classified using conventional criteria (Peters et al., 1991). Collections of serial sections were digitized and reconstructed using Trakem, an in-house EM-digitization package. To measure and display the postsynaptic densities of labeled boutons we used software developed by ourselves, described in outline elsewhere (see Materials and Methods; Anderson et al., 1998).

The estimates of labeled bouton density were derived using the physical disector method (Sterio, 1984). We selected regions of particularly dense innervation by labeled axon for reembedding. Serial 70-nm-thick sections were collected from these regions and a "reference" and "look-up" section was selected. The reference and look-up sections were separated by one section. Photographs were taken with the electron microscope to form patches of tissue, e.g., 5×5 images. Five different patches of cortex were photographed in this way, ranging in area from 500–1,070 μm^2. All electron micrographs were taken at 11,500×. Synapses that were in the reference section, but that disappeared in the look-up section, were counted. Synapses that were present in both look-up and reference sections were not counted (Sterio, 1984). Adobe Photoshop CS (San Jose, CA) and Adobe Illustrator CS were used to prepare digital photomicrographs and enhance image contrast.

RESULTS

Light microscopy

Each of two monkeys received ionophoretic injections of BDA into area V4 along the edge of the prelunate gyrus and close to the lunate sulcus (Fig. 1A). Ionophoretic injections were all confined to the gray matter of V4 and BDA label could be seen in all laminae (Fig. 1B) except layers 1 and 2, which made it impossible to identify the precise laminar location of the cells of origin of the projection to V2. In both animals the injections were made into

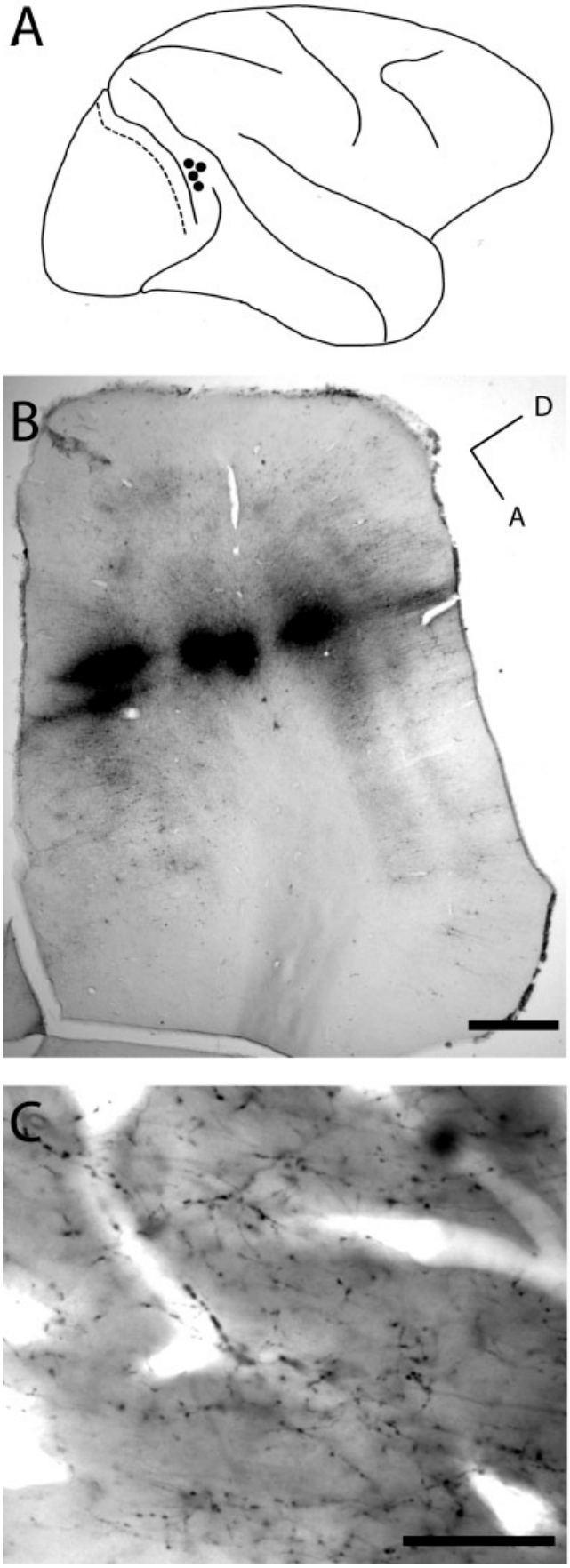

the dorsal surface of V4; approaching from directly above the gyrus and passing through cortex to run parallel with the laminae in the anterior bank of the sulcus, or from a more lateral position and passing through the thickness of cortex. In the latter case one ionophoretic site was very close to the white matter (Fig. 1B), although the label was taken up by layer 6 neurons and a few cells in the white matter. BDA labeling was excellent at the injection site. In one animal the labeling was densest at the site of ionophoresis (Fig. 1B). In the second animal the labeling was densest in a halo of processes around the site of ionophoresis. Most of the uptake was by pyramidal cells of layers 2/3, 5, and 6.

Myelin on axons provides a barrier to the penetration of the reagents and thus were not stained other than at their cut ends, nodes, or where the beaded collaterals emerged. However, because the osmium staining enhanced the contrast of the myelinated fibers, they could be followed through the neuropil.

Anterograde labeling was seen in extrastriate visual areas along with some pale-stained somata deep in layer 6 and occasionally layer 3 of the superior temporal sulcus. In one animal the strongest anterograde transport was to V2 where the fibers entered from the white matter and, with minor branchlets in layer 6, passed directly through all cortical laminae until layer 1, where they divided to produce long rays of aligned fibers that coursed through layer 1 for several millimeters. Most of the fibers appeared to traverse layer 1 toward the tip of the gyrus in the direction of the V1/V2 border, although many had clearly been sectioned, contributing to the puncta-like appearance of the innervation site. The axons showed numerous distinct varicose swellings that proved to be synaptic boutons. Occasionally, collaterals descended from the areas of dense innervation in layer 1 to form additional boutons in layer 2/3. There was also a rather sparse innervation of layer 6 by very fine collaterals, which had tiny varicose swellings. No cell or terminal labeling was evident in other layers. In the second animal, two collaterals passed through layer 1 in V2, where they traversed several millimeters of layer 1, climbing to the tip of the gyrus to almost the V1/V2 border.

The profusion of axons and en passant and terminaux boutons in layer 1 did not present the typically patchy appearance to the innervation characteristic of feedforward projections. Although occasional individual axons did form clusters (Fig. 3B,C), most axons radiated through layer 1 to form an extensive homogenous tangle of processes (e.g., Figs. 1C, 2A, 4A,B). The density of the innervation of layers 2 and 3 fell away rapidly with lateral distance from the main projection zone in layer 1.

Fig. 1. Location of injection sites. **A:** Schematic drawing of a macaque brain showing region in which injections were made (filled circles) in the prelunate gyrus. The border between visual areas V1 and V2 is indicated by a dotted line. **B:** Photomontage of parasagittal section through prelunate gyrus of macaque brain showing five injection sites in area V4. Axes indicate: dorsal (D), anterior (A). **C:** Light micrograph showing labeled axon termination site in layer 1 of V2. Scale bars = 1 mm in B; 25 μm in C.

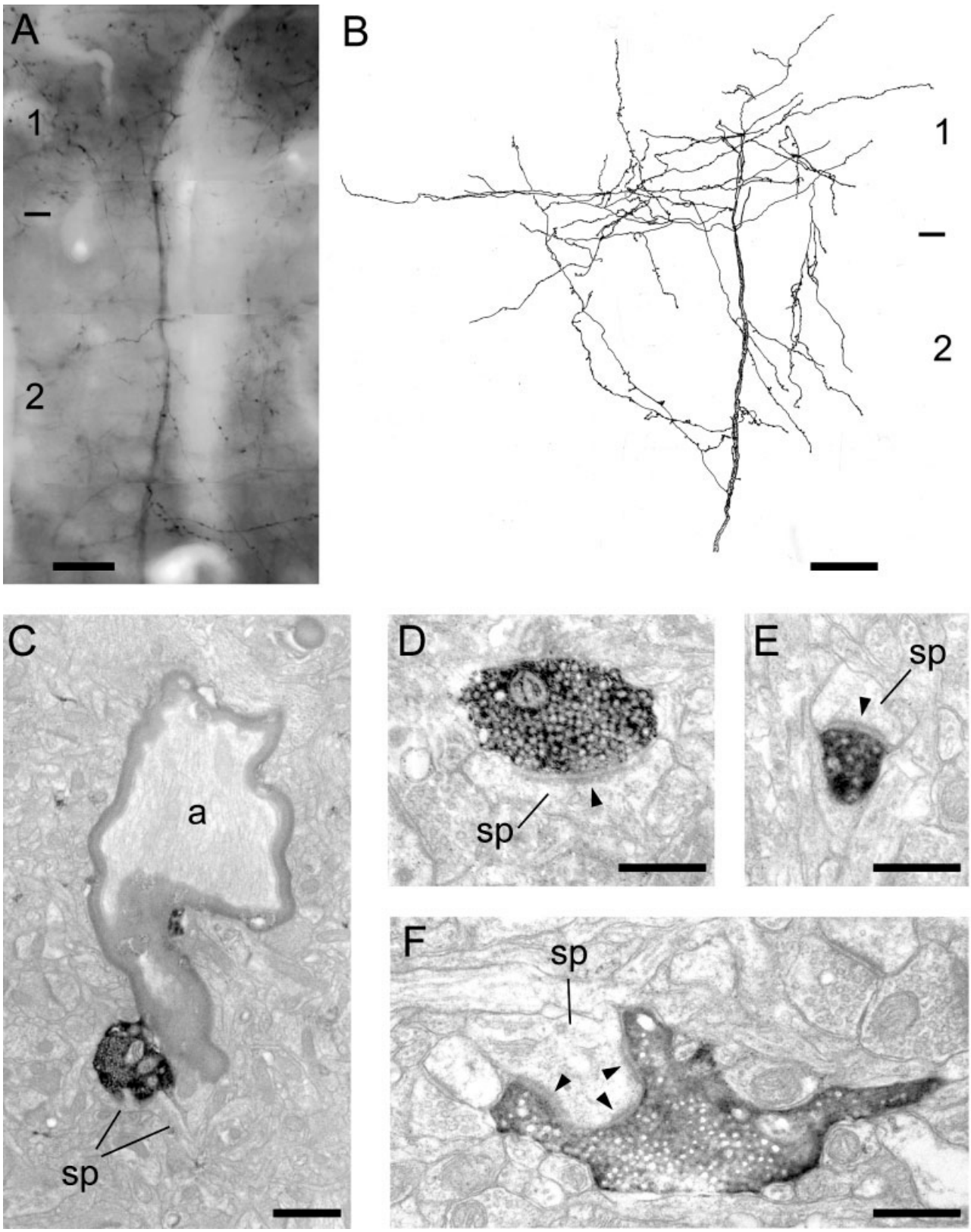

Fig. 2. Light and electron micrographs taken from cortical area V2 showing BDA labeled axons and their terminals. **A:** Labeled terminals form dense band in layer 1 and lesser projections into layer 2/3. A large-caliber labeled axon can be seen rising through the cortex to arborize from an intensely labeled node in layer 1. Laminae and their boundaries are indicated to the left. **B:** Light microscopic reconstruction of large-caliber axon seen in A. The reconstruction is made from a single 80-μm-thick section. Laminae and their boundaries are indicated to the right. **C–F:** Electron photomicrographs of labeled boutons taken from layers 1 and 2 shown in A. C: Low-power picture of large labeled bouton in layer 2 adjacent to the thick parent axon (a) seen in A and B. The bouton forms a synapse with a spine (sp). The axon appears not labeled due to the axon being covered with a myelin sheath. The axon is visible in the LM because the myelin is stained by the osmium. D: A medium-sized labeled bouton in layer 2 forms an asymmetric synapse (solid arrowhead) with a spine (sp). E: A small labeled bouton in layer 2 forms an asymmetric synapse (solid arrowhead) with a small spine (sp). F: A large labeled bouton forms a perforated asymmetric synapse (solid arrowheads) with a spine (sp). Scale bars = 25 μm in A; 50 μm in B; 1 μm in C; 0.5 μm in D–F.

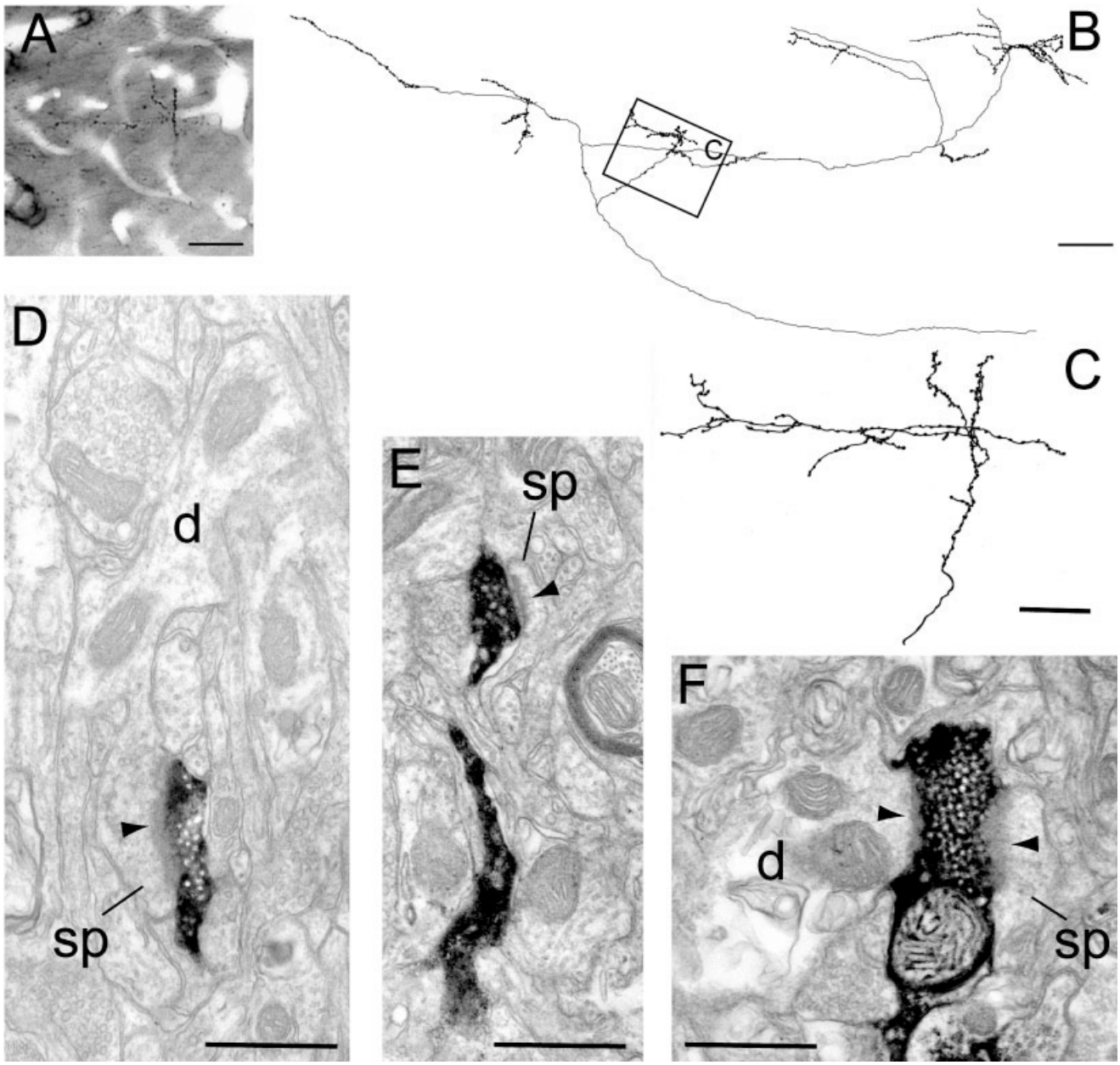

Fig. 3. Light and electron micrographs of BDA-labeled axon and boutons located in layer 1 of area V2. **A:** Photomicrograph showing collateral and varicose swellings of axon in layer 1. **B:** Light microscopic reconstruction of axon (seen in A) forming arbors restricted to layer 1. The box-shaped boundary (C) represents the area shown in the photomicrograph in A and the reconstructed detail shown in C. **C:** A light microscopic reconstruction of a single clustered arbor shown in A and highlighted in the reconstruction in B. The varicose swellings or boutons were restricted to the arbors. **D–F:** Examples of synapses formed with spines and dendrites. D: A labeled bouton forms an asymmetric synapse (solid arrowhead) with a spine (sp) that can be traced back to the parent dendrite (d). E: A small labeled bouton forms an asymmetric synapse (solid arrowhead) with a small spine (sp). F: A labeled bouton forms asymmetric synapses with a spine (sp) and a dendritic shaft (d). Following the dendrite through serial sections showed that it contained numerous mitochondria and formed synapses with unidentified boutons. Such dendrites belong to GABA containing neurons with smooth dendrites. Scale bars = 25 μm in A; 0.1 mm in B; 25 μm in C; 0.5 μm in D–F.

Electron microscopy

We examined a total of 145 boutons, including 90 boutons from layer 1, 27 from layer 2/3, and 28 from layer 6. Of this sample, 136 single boutons were serially sectioned and completely reconstructed so that the area of the synaptic density could be measured. The remaining nine boutons were not sufficiently complete for quantification of their synapses, but were used in the assessment of synaptic targets. All synapses

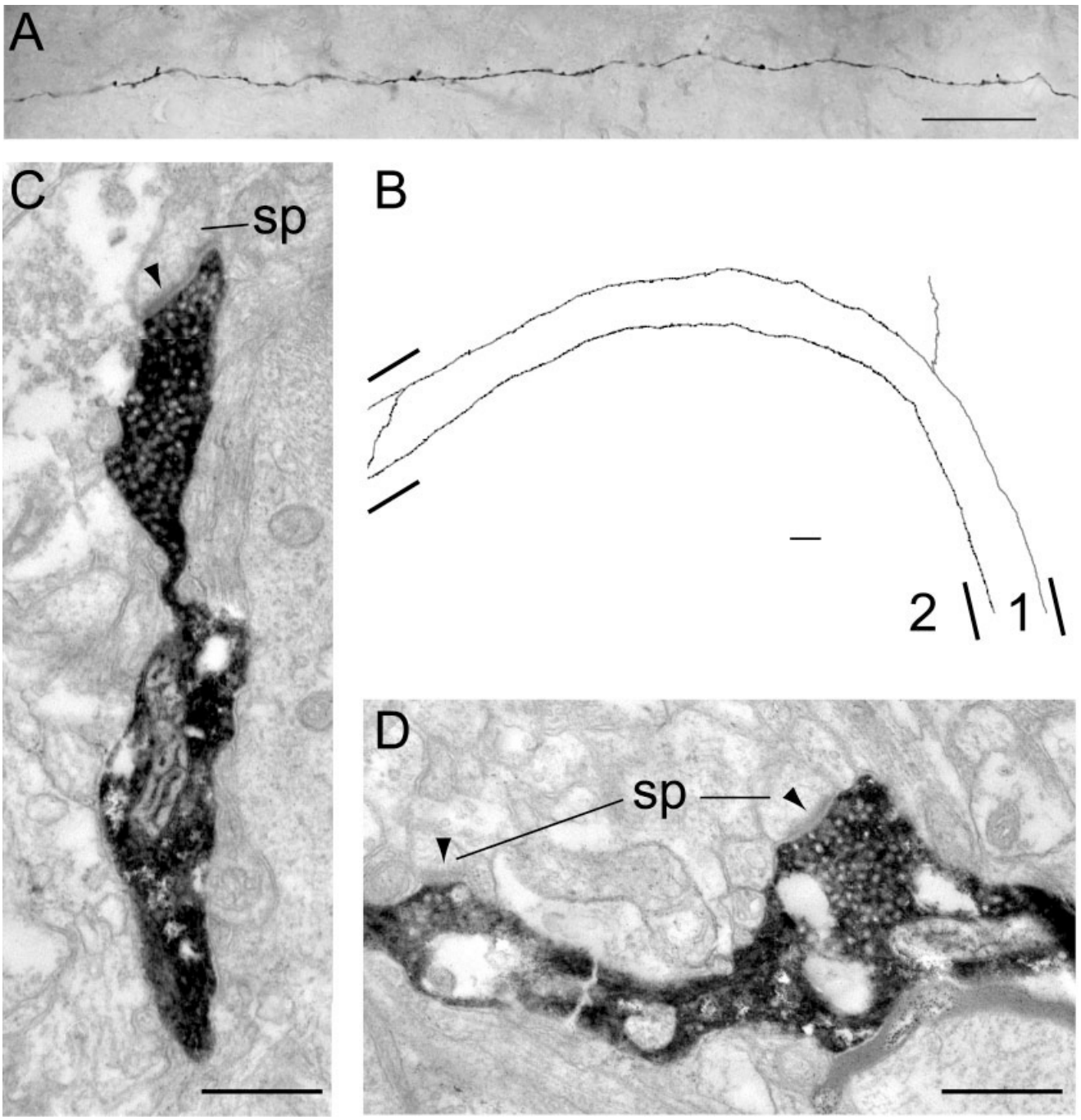

Fig. 4. Light and electron micrographs of BDA-labeled axons and boutons located in layer 1 of area V2. **A:** Photomontage of a labeled collateral taken from layer 1. Numerous varicose swellings of the en passant and aux terminaux types can be seen along the axon length. **B:** Light microscopic reconstruction of collateral shown in A. The axons arise from the right forming very few branches. Laminae and their boundaries are indicated. **C:** Electron micrograph montage of a labeled bouton terminaux taken from the unbranched collateral shown in A. The bouton forms an asymmetric synapse (solid arrow head) with a spine (sp). **D:** Two labeled boutons en passant each forms an asymmetric synapse (solid arrowheads) with a spine (sp). Scale bars = 25 μm in A; 100 μm in B; 0.5 μm in C,D.

formed by labeled boutons were asymmetric (Gray's type 1).

The reaction endproduct was dark, although its intensity varied between boutons. Synaptic vesicles and mitochondria were clearly visible within the boutons and occasional boutons contained vacuoles (Fig. 4C,D). Most boutons were small (<0.5 μm), although the sample showed a considerable range of sizes. The boutons were filled with synaptic vesicles and usually contained at least one mitochondria. Within the target structure there was a

clear postsynaptic density. Puncta adherens (n = 9), when present, were closely associated with a synapse and its postsynaptic target. They could be identified by an absence of presynaptic vesicles within the bouton and a density (similar to the postsynaptic density) within the presynaptic terminal that was mirrored by a density within the target structure (Peters et al., 1991). Puncta were not included in our measurements of synapse size.

Synaptic targets were identified using standard ultrastructural criteria (Peters et al., 1991). Serially sectioning the bouton and its synaptic target assisted greatly in the identification of the target type. The majority of targets were spines (83%), the remainder were dendrites. We reconstructed the complete spine in order to discover if it received a second input, although following the spine neck back to its parent dendrite often proved impossible. Approximately 6% of the reconstructed spines received a second synapse from an unlabeled bouton. The second synapse was always identified as a symmetric (Gray's type 2) synapse. Dendrites often contain mitochondria or microtubules, making identification relatively simple.

Axons and their boutons

We reconstructed three single axons to illustrate the variety of axons seen in this projection (Figs. 2A,B, 3A–C, 4A,B). We sampled boutons from three regions: the densest area of innervation (Figs. 1C, 2A), ~500 μm posterior to this region (Fig. 3), and ~2 mm anterior of the region in which the axons appeared to arrive in layer 1 of V2 (Fig. 4). Axons tended to branch only when they reached layer 1 and not in the deeper layers. Figure 2A,B shows a photomicrograph and a partial reconstruction of an axon arborizing in layer 1. The majority of collaterals radiated away from the main axon trunk and traveled through layer 1. This axon also sent descending collaterals to the middle of layer 2/3 (Fig. 2A,B). The reconstruction is from a single 80-μm-thick section because the arbor was close to the densest region of innervation by labeled axons and so could not be traced unambiguously through adjacent sections. The axon is therefore not completely reconstructed, although it was striking because of the large caliber myelinated axon trunk (>2 μm, Fig. 2C) and the extensively branched collaterals.

Layer 1 boutons taken from this region for EM analysis could not be correlated with our LM observations because of the sheer density of labeled terminals. In sectioning through this dense region, we obtained a random sample of 46 labeled boutons forming 48 synapses. The boutons all came from the area in which we found the reconstructed axon illustrated in Figure 2C. The majority of synapses were formed with spines (75%) (Fig. 2D–F) and the remainder with dendritic shafts.

As well as examining the labeled boutons from this region of layer 1, we also measured the diameter of labeled, unmyelinated axons (n = 50) in the same region. There was remarkably little variation in size, the largest diameter reaching 0.25 μm, with a mean of 0.1 μm (standard error of the mean [SEM] = 0.007 μm).

The boutons in layer 2 (n = 27) could be correlated with our LM observations as there were very few labeled processes in this lamina. A labeled descending axon collateral pursued the same path as the parent ascending afferent axon trunk. In the LM it appeared to be in close apposition with the trunk and this was confirmed in the EM (Fig. 2C). The labeled boutons of layer 2/3 appeared to be somewhat larger (~1 μm, Fig. 2C) than the majority of those seen in layer 1, although this was not always the case (e.g., Fig. 2E). The 27 boutons formed 34 synapses. Boutons forming more than one synapse usually had a larger diameter. Only two of the target spines examined showed a second, symmetric synapse formed by an unlabeled bouton.

Axon 1

Another pattern of innervation by V4 axons in layer 1 can be seen in Figure 3. In this rare example, the bouton-rich axon collaterals formed grape-like clusters of boutons (Fig. 3A). The reconstructed axon shows the clusters separated by lengths of myelinated axon with no en passant boutons between arbors (Fig. 3B). The boutons within the clusters were closely spaced and covered all parts of the collateral (Fig. 3C). Most of the boutons on this axon were en passant: bouton terminaux represented only 18% of the boutons. Most of the boutons (89%) formed synapses with small to medium sized spines (Fig. 3D–F) and seldom with dendrites (Fig. 3F). Only one of the target spines formed a second, symmetric synapse.

Axon 2

The morphology of labeled axons most commonly found in layer 1 had more regular distribution of boutons over extensive lengths (>2 mm) of fine axon collateral (Fig. 4A). Varicose boutons were clearly visible, and because of the straight and largely unbranched trajectory of the collaterals, the bouton terminaux (26% of boutons) were particularly prominent. During the reconstruction of this axon (Fig. 4B) it became evident that the more proximal portions of the axon were myelinated and showed no bouton-like varicosities.

The ultrastructural quality of these axons was inferior to the other material used in this study (Fig. 4C,D). Nevertheless, we examined 22 boutons from these axons. Synapses formed mostly with spines (83%), the majority of which were rather small, and none formed a second synapse.

Layer 6

The animal that provided particularly good anterograde labeling in layer 1 also had occasional collaterals in layer 6. These fine collaterals frequently branched as they passed through layer 6, and passed back and forth between the laminar boundaries. Bouton terminaux accounted for 25% of all boutons on labeled collaterals in layer 6.

We examined 28 boutons from layer 6 and found that 94% of the synapses were formed with spines (Fig. 5). Three of the target spines also formed a second synapse of a symmetric morphology.

Dendrites

Dendritic shafts represented only a small proportion (17%) of the synaptic targets observed in this study (Fig. 6). Typically, excitatory cells have spiny dendrites that contain few mitochondria and few synapses on the dendritic shaft. In contrast, the dendrites of inhibitory cells are spine-free or smooth, contain numerous mitochondria, and form many synapses on the shaft. They may also have widely variable diameter over their length. Dendrites showing these characteristics have also been demonstrated to be GABAergic (Somogyi et al., 1983; Peters and Saint Marie, 1984; Kisvárday et al., 1985; Ahmed et al., 1997). Here the majority of dendritic shafts were small in

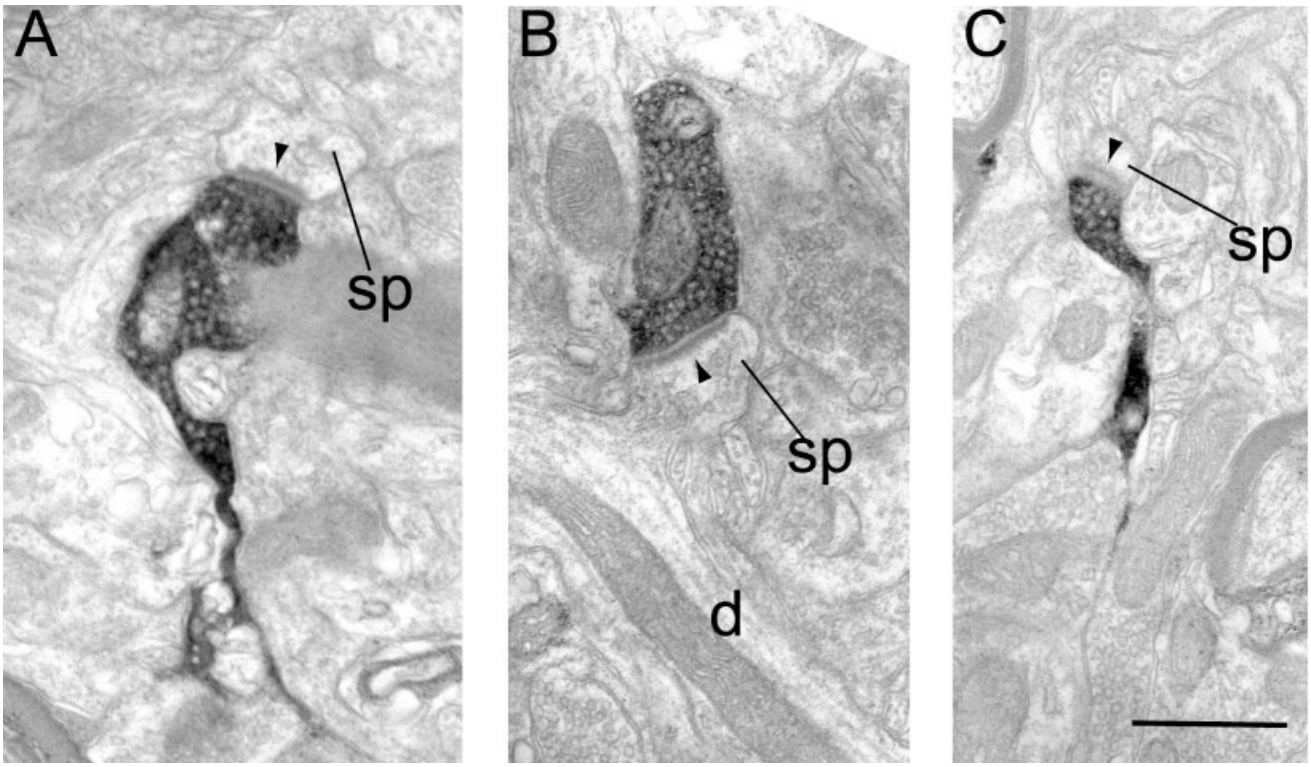

Fig. 5. Electron micrographs of BDA-labeled axons and boutons located in layer 6 of area V2. **A:** A labeled bouton forms an asymmetric synapse (solid arrowhead) with a spine (sp). **B:** A labeled bouton forms an asymmetric synapse with a spine that can be traced back to the parent dendrite (d). **C:** A small labeled bouton forms an asymmetric synapse (solid arrowhead) with a small spine (sp). Scale bar = 0.5 μm in C (applies to A–C).

diameter (~0.5 μm). In this study, serial section reconstruction was required to characterize neurons as smooth or spiny. On the basis of the established criteria, most of the target dendritic shafts (20/28 dendrites, 12.3% of all targets) originated from smooth, putative GABAergic neurons (e.g., Fig. 6A–D). The mean diameter of these dendrites at the position of the synapses was 0.58 μm.

Postsynaptic density

Reconstructing the boutons and their targets gave us the opportunity to view the complete postsynaptic density as a 2D or 3D structure. We have used this technique previously to obtain values for the surface area of synapses (Anderson et al., 1998; Anderson and Martin, 2002, 2005). By focusing on the postsynaptic specialization rather than the presynaptic membrane, we avoided detail being obscured by reaction endproduct in the bouton. We show a 2D projection of the postsynaptic densities in Figure 7. Comparisons between the distributions of the areas of synapses were confined to synapses made by spines due to the small numbers of dendritic synapses. There were few differences seen between those spinous synapses made by the different axons and the different laminae in which the samples were located (Fig. 8). The synapses of the clustered axon of layer 1 (axon 1; mean = 0.089 μm^2, SEM = 0.014) were not significantly different ($P = 0.196$, two-tailed t-test) from those of the random sample of layer 1 (mean, 0.117 μm^2, SEM = 0.015). Nor were the synapses of the unbranched axon (axon 2; mean, 0.126 μm^2; SEM = 0.022) significantly different from those of layer 1 ($P = 0.724$, two-tailed t-test). When comparing synapses from different laminae to those found in the random sample of layer 1, the layer 2/3 distributions overlapped considerably ($P = 0.36$, two-tailed t-test), while those of layer 6 (mean, 0.073 μm^2; SEM = 0.006) were significantly smaller ($P = 0.012$, two-tailed t-test).

There was no difference between the synapses of spines and dendrites when the data from all sources were pooled. The mean size of synapses with spines (mean, 0.1 μm^2; SEM = 0.006) was slightly larger than those of synapses with dendrites (mean, 0.08 μm^2; SEM = 0.009), although the difference was not significant ($P = 0.197$, two-tailed t-test).

The synapses of layer 1, layer 2/3, the clustered and the unbranched axons, all showed a longer tailed (skewed) distribution than the synapses of layer 6.

En face, the postsynaptic density could be a simple disc, or perforated, giving it a doughnut or horseshoe morphology. Figure 7 shows that the synapses with the more complex morphology are often formed with spines. A similar observation was made in the study of synapses made by V1 and V2 afferent boutons in area MT and V2 afferent boutons in area V3A (Anderson et al., 1998; Anderson and Martin, 2002, 2005).

Target types

The most frequently encountered targets of labeled boutons were spines. The major difference between the prin-

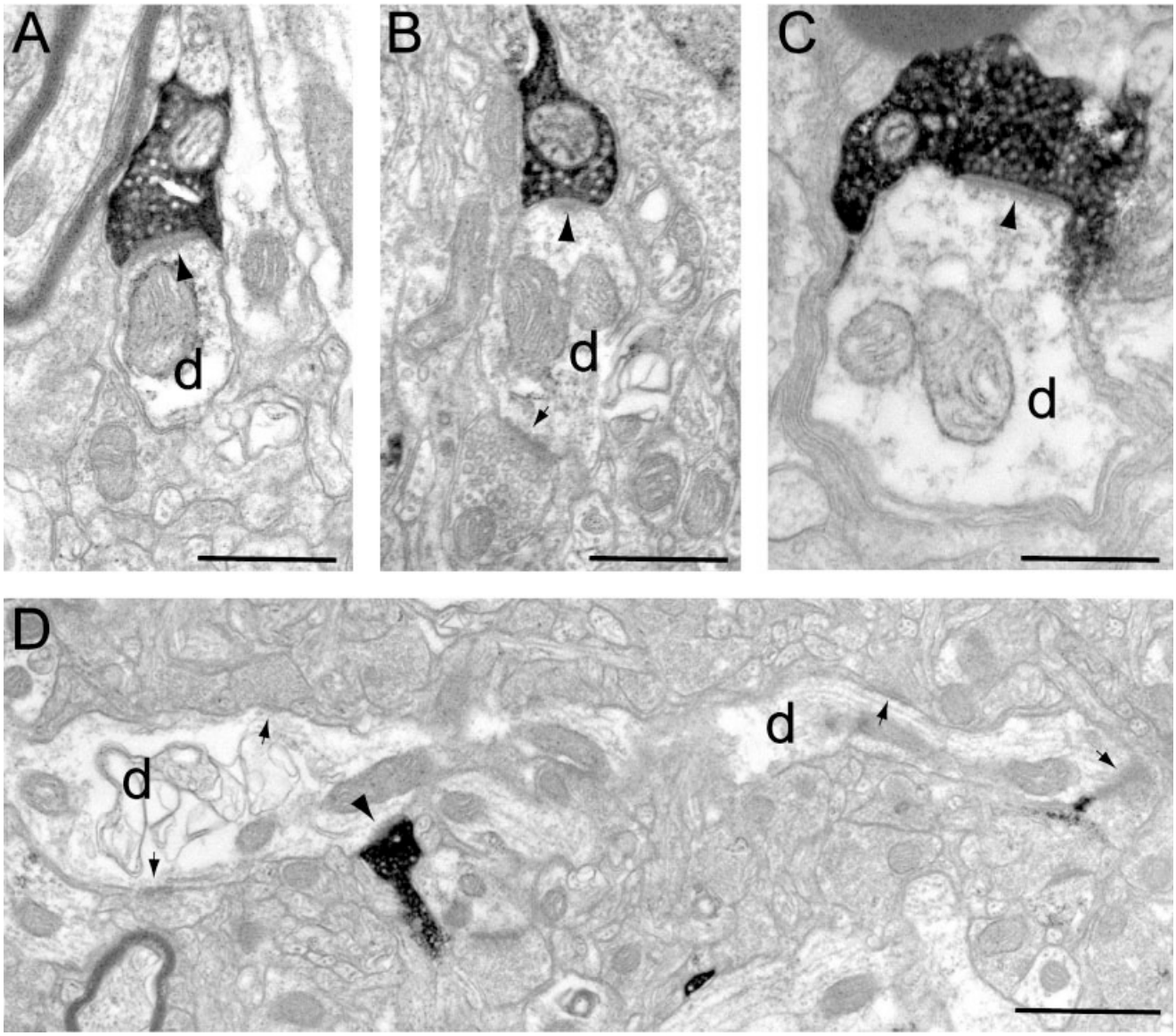

Fig. 6. Electron micrographs of labeled synaptic boutons forming synapses with dendrites containing numerous mitochondria and forming many synapses. These dendrites may also have a beaded morphology. These features are all characteristic of neurons that are GABAergic and have smooth dendrites. **A:** A labeled bouton forms an asymmetric synapse (solid arrowhead) with a small-caliber dendrite in layer 1. In subsequent sections the dendrite was seen to form asymmetric synapses with unidentified boutons. **B:** A small labeled bouton forms an asymmetric synapse (solid arrowhead) with a small-caliber dendrite (d) in layer 6. The dendrite forms an asymmetric synapse (small arrow) with an unidentified bouton. **C:** A large labeled bouton forms an asymmetric synapse (solid arrowhead) with a large-caliber dendrite (d) in layer 1. The dendrite contains many mitochondria and forms asymmetric synapses with other boutons when reconstructed from serial sections. **D:** A labeled bouton forms an asymmetric synapse (solid arrowhead) with a large-caliber dendrite in layer 1. The dendrite contains many mitochondria and forms numerous asymmetric synapses (small arrows) with unidentified boutons visible in the same section. Scale bars = 0.5 μm in A–C; 1 μm in D.

cipal laminae of innervation was in the proportion of spines to dendrites as targets, and for this reason we have shown all sources separately (random sampling and individual axons; Fig. 9). Taken together, the EM analysis shows that 80% of the labeled synapses in layer 1 were formed with spines and 20% were formed with dendritic shafts. In layer 6, 94% of the synapses were formed with spines and 6% with dendritic shafts (Fig. 9).

As indicated above (see Dendrites), smooth neurons provided the majority (69%) of the dendritic shaft targets in layer 1 and both of those in layer 6. The largest contributor to the putative non-GABAergic dendritic synapse was the random sample of layer 1, of which 42% (5/12) of dendrites were from spiny cells. The two axons in layer 1 both synapse only with the putative GABAergic type dendrite (4/4 and 3/3). In layer 2/3 almost all dendrites (6/7, 86%) were of the putative GABAergic type.

Serial reconstructions indicated that most boutons made only one synapse and only rarely more than two synapses (Fig. 10). On average, there were 1.1 synapses

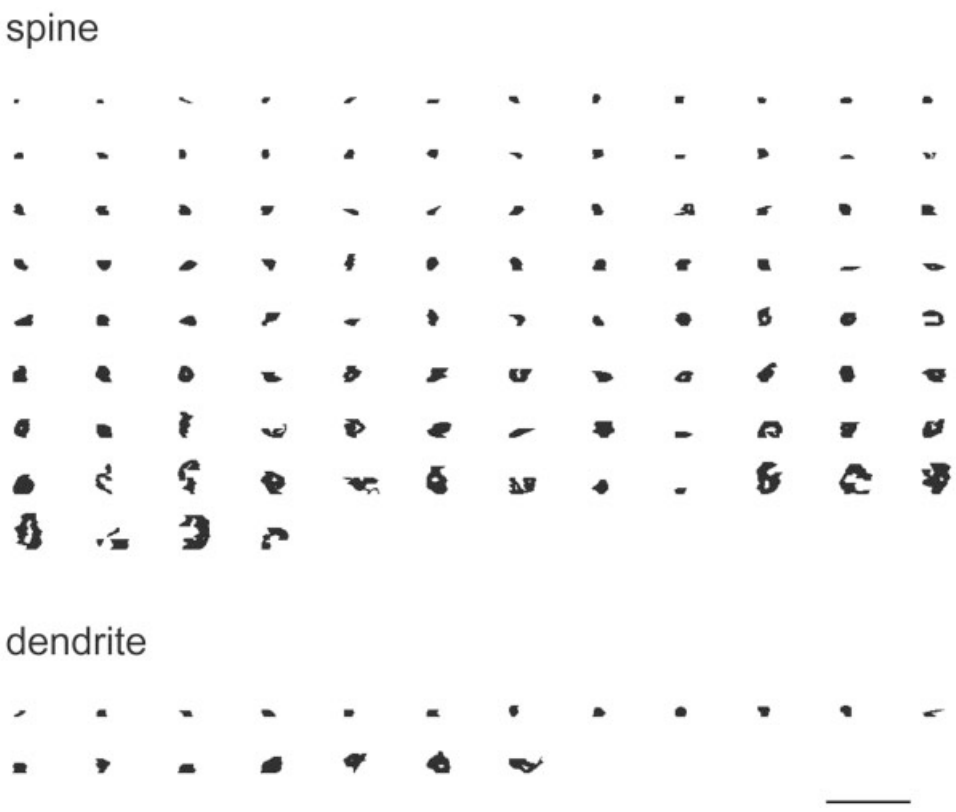

Fig. 7. Two-dimensional projection of the reconstructed postsynaptic densities found in layers 1, 2/3, and 6 on spines and dendrites postsynaptic to V4 labeled boutons in area V2. The densities are ordered by increasing surface area. Scale bar = 1 μm.

per labeled bouton. The sample with the highest synapse-to-bouton ratio was taken from layer 2/3, with 1.3 synapses per bouton, closely followed by the axon with the clustered terminals in layer 1, with 1.2 synapses per bouton. The random sample of 46 labeled boutons from layer 1 and 22 labeled boutons from the long, unbranched axon in layer 1 provided the lowest values in layer 1 of 1.05 and 1.04, respectively.

Synaptic density measurements

To estimate the relative proportion of synapses being contributed by V4 to V2, we made an unbiased stereological analysis of layer 1. We selected regions from within the densest areas of innervation for our analysis and applied the unbiased disector method (Sterio, 1984). We counted only those labeled synapses that disappeared in the "look-up" section when compared to a near adjacent "reference" section. Although the blocks of tissue used for reembedding were selected from the densest zones of innervation, the distribution of labeled synapses in any ultrathin section could vary greatly. From previous studies (Anderson and Martin, 2002) we know that if the disector region was selected using nonbiased features such as the edge of the tissue or a scratch on the block face, we counted no labeled synapses. If we selected the location of the disector by finding a labeled bouton and then sampling in the vicinity, we counted 2.2% (7 of 316) of disappearing labeled synapses. Larger patches of reconstructed tissue did not necessarily provide a higher proportion of disappearing labeled synapses. Some sample areas provided numerous boutons, but no disappearing synapses. We also noted more labeled axon profiles in this material than was seen in previous studies that looked at projections from lower to higher cortical areas terminating in layer 4.

DISCUSSION

The projection from V4 to V2 showed the classic features of a feedback projection (Kuypers et al., 1965; Pandya and Sanides, 1973; Tigges et al., 1974). We confirmed the observations of Rockland (1994, 1997; Rockland et al., 1994) that the major projection of individual axons was to layer 1, with additional sparse innervation of layers 2/3 and 6. In previous studies of feedforward projections we found patchy projections in layer 4 of the target area, despite large injections of tracers in the source area (Anderson et al., 1998; Anderson and Martin, 2002, 2005). By contrast, in the V4 projection to layer 1 of V2 the projections did not form patches. Although we found rare individual fibers that did form clustered terminals, most fibers traveled for millimeters through layer 1, presumably not aimlessly, but certainly being very discrete about what they were actually up to. This difference between the two modes of interareal connection, one punctate and patchy, the other diffuse, must reflect basic differences in their role in the circuit.

Our main interest here was in discovering whether there are qualitative or quantitative differences in the synaptic connections made by a feedback projection compared to other feedforward projections we have studied with the same methods. The projection neurons are typically glutamatergic pyramidal cells that connect mainly to other pyramidal cells. Our data were consistent with this pattern: 75% of the targets in layer 1 were spines and 94%

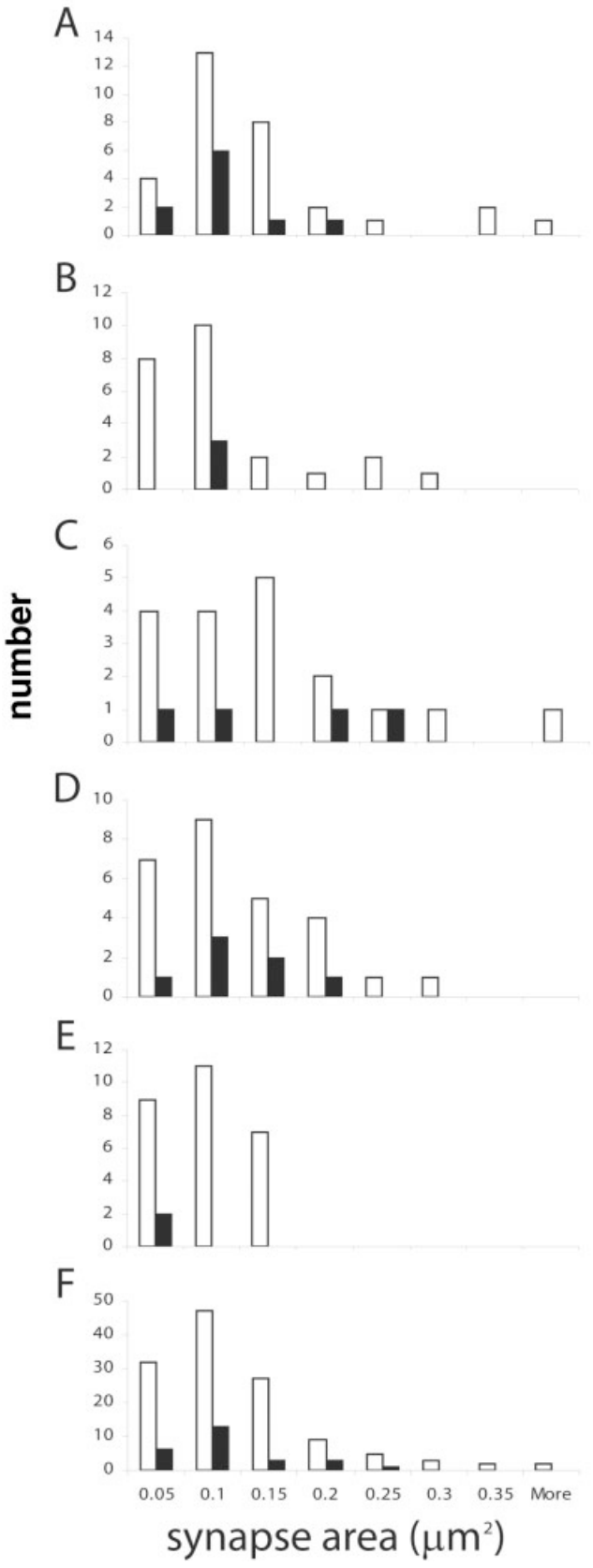

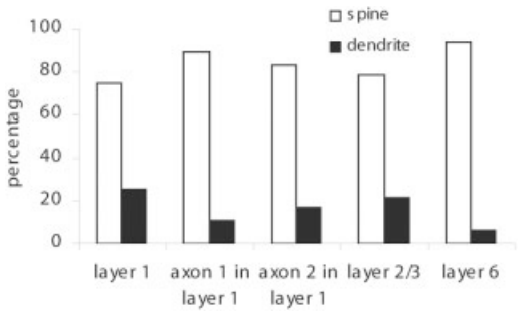

Fig. 9. Histogram of the synaptic targets of labeled V4 boutons in layers 1, 2/3, and 6 of area V2. For layer 1, n = 48; for clustered axon in layer 1, n = 27; for unbranched axon in layer 1, n = 23; for layer 2/3, n = 34; for layer 6, n = 31.

in layer 6 were spines. Rockland (1997) reported similar proportions for the feedback projection from V2 to V1 (82% spines, 18% dendritic shafts). These data indicate that pyramidal cells are the sole source and the major recipients of the intercortical connections.

As in the V2 to V1 projection studied by Rockland (1997), a minority of the targets of the V4 axons were dendritic shafts. We differentiated two types of dendrites, one of spiny, the other of smooth neurons, based on ultrastructural criteria examined over serial sections. Dendrites of smooth neurons formed 22/28 of the dendritic shafts that formed synapses with the V4 axons. This amounted to 12% of all targets. Taken together, these statistics lie well within the range of those we have compiled for feedforward projections using identical methods and criteria: the profile of synaptic targets for the V4 to V2 projection is broadly the same as that observed for the V1 to MT, the V2 to MT, and the V2 to V3A projections (Table 1; Anderson et al., 1998; Anderson and Martin, 2002, 2005).

The differences in the proportion of targets that were spines between the primary layer of innervation (layer 1; 73%) and the secondary layer of innervation (layer 6; 94%) was also a feature noted in two of the feedforward projections we studied, where layer 4 is the primary layer and layers 2/3 and 6 are the secondary layers. The synapses in layer 1 were formed mainly by en passant boutons, whereas 25% of the synapses in layer 6 were formed by bouton terminaux. In the projection from V2 to MT, 67% of the targets in layer 4 were spines, whereas in layer 2/3, 82% of the targets were spines. Similarly, in the feedforward projection from V2 to V3A, 76% of the layer 4 targets were spines, whereas in layer 2/3, 98% of the targets were spines. The major outlier was the projection from V1 to MT (Anderson et al., 1998), where spines formed only 54% of the targets in layers 4 and 6 and somata of smooth neurons formed a significant proportion (13%), with den-

Fig. 8. Histograms of the distribution of postsynaptic areas (μm^2) formed by labeled V4 boutons in layers 1, 2/3, and 6 of area V2. **A:** Unidentified labeled layer 1 synapses (n = 41). **B:** Synapses from axon with clustered terminals in layer 1 (Fig. 3) (n = 27). **C:** Synapses from unbranched axon in layer 1 (Fig. 4) (n = 22). **D:** Synapses from middle of layer 2/3 (Fig. 2) (n = 34). **E:** Synapses from layer 6 (Fig. 5) (n = 29). **F:** Pooled synapses of layers 1, 2/3, and 6 (n = 153).

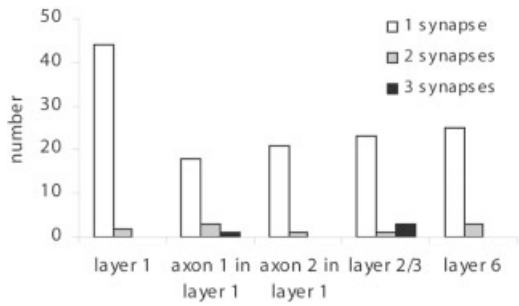

Fig. 10. Histogram of the number of synapses formed per labeled V4 bouton in layers 1, 2/3, and 6 of area V2.

dritic shafts of spiny neurons and smooth neurons making up the remainder. Also, no marked differences were seen between the principal layer (layer 4) and the secondary layer (layer 6) of termination in the proportion of innervated spines. However, in all other projections, V2 to MT, V2 to V3A, V4 to V2, there was a clear difference between the principal versus the secondary layer of innervation. A similar trend was observed by Johnson and Burkhalter (1996) for the feedforward projection from area 17 to the lateromedial area in the rat visual cortex. Here they noted that in layers 3 and 4, the primary layers of innervation, 87% of the targets were spines, whereas in the secondary layer, layer 1, 100% of the targets were spines. Since the dendritic shafts of smooth (presumed inhibitory) neurons form the majority of the targets that are not spines, it seems that a stronger inhibitory brake is required in the principal layer of termination than in the secondary layer or termination, where the density of synapses provided by the projection is in any event always extremely low. Similar trends have been noted in a combined ultrastructural and immunochemical study of the targets of the feedback and feedforward connections between area 17 and the lateromedial area in the rat cortex (Gonchar and Burkhalter, 2003).

The density, form, and size of the synaptic densities formed by the boutons were also studied. Here again, there were similarities with the feedforward pathways. If we chose EM sections with labeled synapses, we found that 2% of the asymmetric synapses in the densest part of the V4 to V2 projection were labeled. Using identical methods, the comparable percentages were 3% for the V1 to MT projection (Anderson et al., 1998), 4–6% for the V2 to MT projection (Anderson and Martin 2002), and 3.5–4.1% for the V2 to V3A projection (Anderson and Martin, 2005). In form, and in all interareal projections studied by us, the most complex shapes of the densities were always with spines. These synapses, which were also the largest, had perforated postsynaptic densities, which, when viewed en face, looked like horseshoes or doughnuts. The average size of the synapses on spines (~0.1 μm^2) was larger than those on dendritic shafts (0.08 μm^2) and the form of postsynaptic densities on dendritic shafts was always a simple disk. These same trends were seen in the feedforward projections cited above. For all projections we have studied, both feedforward and feedback, the average size of the spine synapses were within a close range of ~0.1–0.12 μm^2, while the synapses on dendritic shafts were ~0.07–0.09 μm^2.

TABLE 1. Putative GABAergic Targets of Interareal Connections[1]

		Projection			
		V1–V5	V2–V5	V2–V3A	V4–V2
%putative GABAergic targets	layer 1				**11**
	layer 2				18
	layer 3		8	0	
	layer 4	**18**	**15**	**10**	
	layer 6	14			6

[1]The proportion of putative GABAergic targets of three feedforward (V1 to V5, V2 to V5, V2 to V3A) (Anderson et al., 1998; Anderson and Martin, 2002, 2005) and one feedback projection (V4 to V2) in macaque cortex. The remainder of the targets were excitatory neurons. Principal layers of innervation are marked in bold. The V1 to V5 data included many somatic targets that formed multiple active zones with single boutons. These have been counted as single synapses for the purposes of this table.

From these comparisons, we conclude that the major differences between the feedback and feedforward projections are not to be found at the level of their synapses, possible differences in receptors notwithstanding. Both feedforward and feedback projections connect principally to spiny neurons, they both form synapses of similar size, and they both contribute only a few percent of the asymmetric synapses to the neuropil, even in their densest areas of innervation. Structurally, the major difference between the feedforward and feedback projections we have studied is thus the traditional one: the laminae they target. For the feedforward projections, the major targets are neurons in layer 4. For the feedback projection to layer 1, the distal tufts of the apical dendrites of pyramidal neurons form the major targets.

What differences in function are served by these differences in laminar termination of the feedforward and feedback projections, with their implicit differences in the position of their input on the dendritic trees of their target cells? At a biophysical level the differences between distal versus proximal synaptic inputs to pyramidal neurons have been the subject of intense debate. One recent view is that the location of the synapses does not matter (Magee and Cook, 2000), because in hippocampal pyramidal cells, at least, the excitatory synaptic conductance increases in proportion to the distance from the soma. The other view is that, as in real estate, location matters a great deal (Rall, 1967; Bernander et al., 1991; London and Segev, 2001). The principal argument for the importance of location is that if the neurons are embedded in an active network, the dendrites increase their electrotonic length due to the several-fold increase in membrane conductance produced by synaptic activity. More distal synapses are shunted by the increase in the conductance due to activation of synapses on more proximal dendrites. Since the apical tufts of the pyramidal cells are slender, inputs in layer 1 will be especially sensitive to the more proximal changes in conductance.

The receptive field size of feedforward and feedback pathways in V2 is different. In general, the receptive field sizes increase from V1, to V2, to V4 and MT (Van Essen and Zeki, 1978). Thus, for a given eccentricity the receptive fields of the neurons that feedback from V4 to V2 will be larger than the neurons to which they connect and much larger than the receptive fields of the V1 neurons that project to V2. Thus, an individual V2 neuron effectively "sees" a smaller piece of the visual field than its V4 neurons that provide the feedback inputs. This apparent paradox, that the V2 neurons have smaller receptive fields than their V4 inputs, suggests that the V4 inputs are not

driving the V2 neurons, but rather provide a modulation of the V2 activity.

What could be the role of this feedback from V4? One function that has been explored particularly in V2 and V4 of awake behaving monkeys is the role of attention. Attentional effects are seen throughout visual cortex and are manifest by an increased firing rate of neurons whose receptive fields lie in the attended part of the visual field. If two stimuli are placed within a single receptive field in V2, attention to one of the stimuli biases the responses of the neuron either up or down (Reynolds et al., 1999). The source of the biasing signal is unknown, but one candidate is, of course, the feedback from V4, where a similar interaction occurs (Reynolds et al., 1999). What seems clear from the anatomical data about the V4 to V2 feedback is that it does not seem well equipped to deliver fine-grained information to specific cells. At best, the feedback could provide a biasing signal that conveys simple information, delivered through a small excitatory input to many neurons.

LITERATURE CITED

Ahmed B, Anderson JC, Martin KAC, Nelson JC. 1997. Map of the synapses onto layer 4 basket cells of the primary visual cortex of the cat. J Comp Neurol 380:230–242.

Anderson JC, Martin KAC. 2002. Connection from cortical area V2 to MT in macaque monkey. J Comp Neurol 443:56–70.

Anderson JC, Martin KAC. 2005. Connection from cortical area V2 to V3A in macaque monkey. J Comp Neurol 488:320–330.

Anderson JC, Binzegger T, Martin KAC, Rockland KS. 1998. The connection from cortical area V1 to V5: a light and electron microscopic study. J Neurosci 18:10525–10540.

Bernander O, Douglas RJ, Martin KAC, Koch C. 1991. Synaptic background activity influences spatiotemporal integration in single pyramidal cells. Proc Natl Acad Sci U S A 88:11569–11573.

De Yoe EA, Van Essen DC. 1985. Segregation of efferent connections and receptive field properties in visual area V2 of the macaque. Nature 317:58–61.

Gonchar Y, Burkhalter A. 2003. Distinct GABAergic targets of feedforward and feedback connections between lower and higher areas of rat visual cortex. J Neurosci 23:10904–10912.

Kisvárday ZF, Martin KAC, Whitteridge D, Somogyi P. 1985. Synaptic connections of intracellularly filled clutch neurons, a type of small basket neuron in the visual cortex of the cat. J Comp Neurol 241:111–137.

Krubitzer LA, Kaas JH. 1989. Cortical integration of parallel pathways in the visual system of primates. Brain Res 478:161–165.

Kuypers HG, Szwarcbart MK, Mishkin M, Rosvold HE. 1965. Occipitotemporal corticocortical connections in the rhesus monkey. Exp Neurol 11:245–262.

Livingstone MS, Hubel DH. 1982. Thalamic inputs to cytochrome oxidase-rich regions in monkey visual cortex. Proc Natl Acad Sci U S A 79: 6098–6101.

Livingstone MS, Hubel DH. 1983. Specificity of cortico-cortical connections in monkey visual system. Nature 304:531–534.

London M, Segev I. 2001. Synaptic scaling in vitro and in vivo. Nat Neurosci 4:853–854.

Magee JC, Cook EP. 2000. Somatic EPSP amplitude is independent of synapse location in hippocampal pyramidal neurons. Nat Neurosci 3:895–903.

Munk M, Nowak L, Girard P, Chounlamountri N, Bullier J. 1995. Visual latencies in cytochrome oxidase bands of macaque area V2. Proc Natl Acad Sci U S A 92:988–992.

Pandya DN, Sanides F. 1973. Architectonic parcellation of the temporal operculum in rhesus monkey and its projection pattern. Z Anat Entwick 139:127–161.

Peters A, Saint Marie RL. 1984. Smooth and sparsely spinous nonpyramidal cells forming local axonal plexuses. In: Jones EG, Peters A, editors. Cerebral cortex, vol. 1. Cellular components of the cerebral cortex. New York: Plenum Press. p 419–445.

Peters A, Palay SL, Webster HDeF. 1991. The fine structure of the nervous system: neurons and their supporting cells, 3rd ed. Oxford: Oxford University Press.

Rall W. 1967. Distinguishing theoretical synaptic potentials computed for different soma-dendritic distributions of synaptic input. J Neurophysiol 30:1138–1168.

Reynolds JH, Chelazzi L, Desimone R. 1999. Competitive mechanisms subserve attention in macaque areas V2 and V4. J Neurosci 19:1736–1753.

Rockland KS. 1994. The organization of feedback connections from Area V2 (18) to V1 (17). In: Peters A, Rockland KS, editors. Cerebral cortex, vol. 10. Primary visual cortex in primates. New York: Plenum Press. p 261–299.

Rockland KS. 1997. Elements of cortical hierarchy revisited. In: Rockland KS, Kaas JH, Peters A, editors. Cerebral cortex, vol. 12. Extrastriate cortex in primates. New York: Plenum Press. p 243–293.

Rockland KS, Saleem KS, Tanaka K. 1994. Divergent feedback connections from areas V4 and TEO in the macaque. Vis Neurosci 11:579–600.

Shipp S, Zeki S. 1985. Segregation of pathways leading from area V2 to areas V4 and V5 of macaque monkey visual cortex. Nature 315:322–325.

Shipp S, Zeki S. 1989a. The organization of connections between area V5 and V1 in macaque monkey visual cortex. Eur J Neurosci 1:309–332.

Shipp S, Zeki S. 1989b. The organization of connections between areas V5 and V2 in macaque monkey visual cortex. Eur J Neurosci 1989 1:333–354.

Sincich LC, Horton JC. 2005. The circuitry of V1 and V2: integration of color, form and motion. Annu Rev Neurosci 28:303–326.

Somogyi P, Kisvárday Z F, Martin KAC, Whitteridge D. 1983. Synaptic connections of morphologically identified and physiologically characterised large basket cells in the striate cortex of cat. Neuroscience 10:261–294.

Sterio DC. 1984. The unbiased estimation of number and sizes of arbitrary particles using the disector. J Microsc 134:127–136.

Stettler DD, Das A, Bennett J, Gilbert CD. 2002. Lateral connectivity and contextual interactions in macaque primary visual cortex. Neuron 36: 739–750.

Suzuki W, Saleem KS, Tanaka K. 2000. Divergent backward projections from the anterior part of the inferotemporal cortex (area TE) in the macaque. J Comp Neurol 422:206–228.

Tigges J, Spatz WB, Tigges M. 1974. Efferent cortico-cortical fiber connections of area 18 in the squirrel monkey (Saimiri). J Comp Neurol 158:219–235.

Van Essen DC, Zeki SM. 1978. The topographic organization of rhesus monkey prestriate cortex. J Physiol 277:193–226.

Zeki S. 1969. Representation of central visual fields in prestriate cortex of monkey. Brain Res 14:271–291.

Zeki S. 1973. Colour coding in rhesus monkey prestriate cortex. Brain Res 53:422–427.

Zeki S, Shipp S. 1989. Modular connections between areas V2 and V4 of macaque monkey visual cortex. Eur J Neurosci 1:494–506.

3.5 V1 and V2 probably share the most studied interareal connections. These two areas enjoy a special relationship occupying a large area, sharing a large border and showing very asymmetric properties. We were able to separate two axons and their boutons from layer 1 which we present in the paper as they had strikingly different morphologies. The receptive field properties of cells from the early visual areas, V1, V2, V3, V3A and V4 show few differences making them largely indistinguishable from one another except for V4 showing a large number of colour sensitive cells. What they do show is a steady increase in RF size. The beginning of this chain of connections being V1 it was important to study its input.

Behavioral/Systems/Cognitive

The Synaptic Connections between Cortical Areas V1 and V2 in Macaque Monkey

John C. Anderson and Kevan A. C. Martin
Institute for Neuroinformatics, University of Zürich and ETH Zürich, 8057 Zürich, Switzerland

The primary visual cortex (V1) and V2 together form ~24% of the total neocortex of the macaque monkey and have each other as their major partners. The major target of the V1 projection to V2 is layer 4, where it forms clusters of boutons, which form asymmetric (excitatory) synapses mainly with dendritic spines (75%). The remainder form synapses with dendritic shafts. The synapses found on spines were often more complex, perforated postsynaptic densities than those found on dendritic shafts. The reciprocal projection from V2 to V1 targeted layers 1, 2/3, and 5 and was formed of axons of different morphologies. One axon type, originating from superficial layer pyramidal cells, had a morphology resembling those of local pyramidal cell collaterals. These axons arborized in layers 1, 2/3, and 5 of V1. Another type of axon, arborizing in layer 1, was slender (0.3 μm), unbranched, unmyelinated, and uniformly covered with boutons terminaux and formed asymmetric synapses mainly with slender spines. Yet a third type of axon also confined to layer 1, was thick (>1 μm), branched, heavily myelinated, and formed separate small clusters of large (~1 μm) en passant multisynaptic boutons that formed asymmetric synapses mainly with large flat spines. These data show the existence of a reciprocal excitatory loop between V1 and V2 that is formed by different axonal types, each with preferred layers of termination.

Introduction

The first two cortical visual areas in the macaque monkey are approximately equal in size and together form ~24% of the total surface area of the macaque cortex (Felleman and Van Essen, 1991). Quantitative studies by Kennedy and colleagues (Barone et al., 2000; Kennedy et al., 2000) show that 88% of the corticocortical projection neurons of V2 project to V1 and 81% of the corticocortical projection neurons in V1 project to V2 (Kennedy et al., 2000). The output from V1 to V2 divides into separate anatomical streams that map onto the patches of cytochrome oxidase staining in V1 and V2 (Livingstone and Hubel, 1983, 1984), although they now seem more mixed than originally supposed (Sincich and Horton, 2002a,b, 2005a,b).

There is a fundamental puzzle in the V1–V2 relationship. V1 is in a recurrent excitatory loop with V2, yet, when V1 is inactivated it virtually eliminates all activity in retinotopically related areas of V2 (Girard and Bullier, 1989), whereas the reverse is not true: inactivating V2 has little impact on most V1 neurons (Hupé et al., 2001). Why with such rich reciprocal connectivity is there such an asymmetrical effect? Although the inactivation experiments were performed under general anesthesia, it is clear that the depressing effects of anesthesia are not responsible, because the V2 neurons remain active and well driven by visual stimuli. Such asymmetrical effects, which are seen elsewhere (the geniculocortical loop, for example) are usually explained by the hypothesis that "feedforward" projections (e.g., V1 to V2) "drive" their target neurons, whereas "feedback" projections (e.g., V2 to V1) only "modulate" their target neurons (Hupé et al., 2001; Guillery and Sherman, 2002). This "explanation" begs the basic question of what possible biophysical differences could account for this profound difference in effect.

Perhaps driving inputs must enter at layer 4, which is the main thalamic recipient layer and, by definition, the main target of corticocortical feedforward projections? However, thalamocortical synapses form only ~10% of the excitatory synapses in layer 4 of V1 (Latawiec et al., 2000), which means that most projections to layer 4 do not drive cortex. Another possibility is that the feedback synapses are simply less effective than feedforward synapses. This is the preferred explanation of Guillery and Sherman (2002), for whom the geniculocortical loop is a cardinal example. In their view, axons of driving projections have large en passant boutons forming multiple complex contacts, while the small terminaux boutons of modulating projections form simple axodendritic contacts. Even under anesthesia, V1 neurons can be driven by electrical stimulation of V2 (Girard et al., 2001). In addition, Rockland and Virga (1989, 1990) found a complex picture of three different laminar patterns of termination for axons projecting from V1 to V2 and two major patterns for axons projecting from V2 to V1 and there may be yet additional complexities associated with the projections between the cytochrome oxidase compartments. Here we search for clues to differences in the effects of feedforward and feedback projections, by studying their ultrastructure.

Materials and Methods

The material presented here was taken from four adult male macaque monkeys and one adult female (*Macaca mulatta*), which were used in

Received Dec. 3, 2008; revised Aug. 4, 2009; accepted Aug. 7, 2009.

This work was funded by European Union (QULG3-1999-01064), Human Frontier Science Program (RG0123/2000-B), and Swiss National Science Foundation grants to K.A.C.M.

Correspondence should be addressed to either John C. Anderson or Kevan A. C. Martin, Institute for Neuroinformatics, University of Zürich and ETH Zürich, Winterthurerstrasse 190, 8057 Zürich, Switzerland, E-mail: jca@ini.phys.ethz.ch or kevan@ini.phys.ethz.ch.

DOI:10.1523/JNEUROSCI.5757-08.2009

 0270-6474/09/2911283-11$15.00/0

Table 1. Location and properties of tracer injections, axon distributions, and bouton numbers

Animal reference	Visual area injected	Tracer injected and method	Tracer injection size (μm)	Layers injected	Number of injections	Survival time (d)	Labeled material and target area	Boutons examined
M1	V1	Biocytin ionophoretic	320 diam.	2/3	1	1	Bouton clusters in V2	77
M2	V1	BDA ionophoretic	220 wide	2–6	3	10	Bouton clusters in V2	30
M3	V2	BDA ionophoretic	150 diam.	2/3	2	12	Bouton cluster in V1	59
M4	V2	PHA-L pressure	320 wide	3–6	3	1.5	"Thin" axon in V1	44
M5	V2	PHA-L pressure	150 wide	3–6	4	10	"Thick" axon in V1	34

acute electrophysiological experiments. Animal treatment and surgical protocols were performed in accordance with the guidelines of the Kantonal Veterinaeramt of Zurich. The following procedures are similar to those used by Anderson and Martin (2002). Animals were prepared for surgery after the administration of an intramuscular premedication of xylazine (Rompun, Beyelar, 0.5 mg/kg)/ketamine (Ketalar, Parke Davis, 10 mg/kg). This was followed by cannulation of a femoral vein for the delivery of alfaxalone/alphadolone (Saffan, Glaxo) to establish complete anesthesia.

Animals received from 1 to 4 injections of neuronal tracer (see Table 1). Biocytin (Sigma) was delivered as a 4% solution in Tris buffered KCl (0.2 M), biotinylated dextran amine (BDA) (Invitrogen) as a 10% solution in 0.01 M PBS, pH 7.4, and *Phaseolus vulgaris* leucoagglutinin (PHA-L) (Vector Laboratories) as a 2.5% solution in 0.01 M PBS, pH 7.4. The ionophoretic injections were made with a glass micropipette using a pulsed ionophoretic current of 2–4 mA over a 7–10 min period. After a 1–10 d survival period, the animals were very deeply anesthetized with intravenous pentobarbital (20 mg/kg) and then perfused transcardially with a normal saline solution, followed by a solution of 3.5% paraformaldehyde, 0.8% gluteraldehyde, and 15% picric acid in 0.1 M PB, pH 7.4. A block of cortex containing the injection site and areas V1/V2 was removed and sunk in sucrose solutions of 10, 20, and 30% in 0.1 M PB, then freeze-thawed in liquid nitrogen and washed in 0.1 M PB. Sections were cut from the block at 80 μm in the parasagittal plane and collected in 0.1 M PB. We used standard procedures to reveal the neuronal tracers. In brief outline; washes in PBS were followed by 10% normal swine serum (NSS) in PBS (1 h). When appropriate the antibody to PHA-L was diluted in the above at 1:200 and exposed for 48 h at 5°C. Further washes in NSS preceded overnight exposure (5°C) to an avidin–biotin complex (Vector ABC kit, Elite). The peroxidase activity was identified using 3,3-diaminobenzidine tetrahydrochloride (DAB). After assessment by light microscopy, selected regions of tissue were treated with 1% osmium tetroxide in 0.1 M PB. Dehydration through alcohols (1% uranyl acetate in the 70% alcohol) and propylene oxide allowed flat mounting in Durcupan (Fluka) on glass slides.

Light microscopic observations of labeled axons were performed to locate and select regions of interest for electron microscopy. We reconstructed individual collaterals in the less densely innervated areas for correlated light and electron microscopy. Serial ultrathin sections were collected at 60 or 70 nm thickness on Pioloform-coated single slot copper grids. Labeled boutons were photographed at a magnification of 21,000. Synapses and associated structures were classified using conventional criteria (Peters et al., 1991). Collections of serial sections were digitized and reconstructed using Trakem, an in-house EM-digitization package. To measure and display the postsynaptic densities of labeled boutons we used software developed by ourselves, which has been described in outline previously [see Anderson et al. (1998), their Materials and Methods]. We used a Philips CM100 electron microscope fitted with a Morada camera and ITM software. For figure preparation we used Adobe Illustrator CS3 and Photoshop CS3.

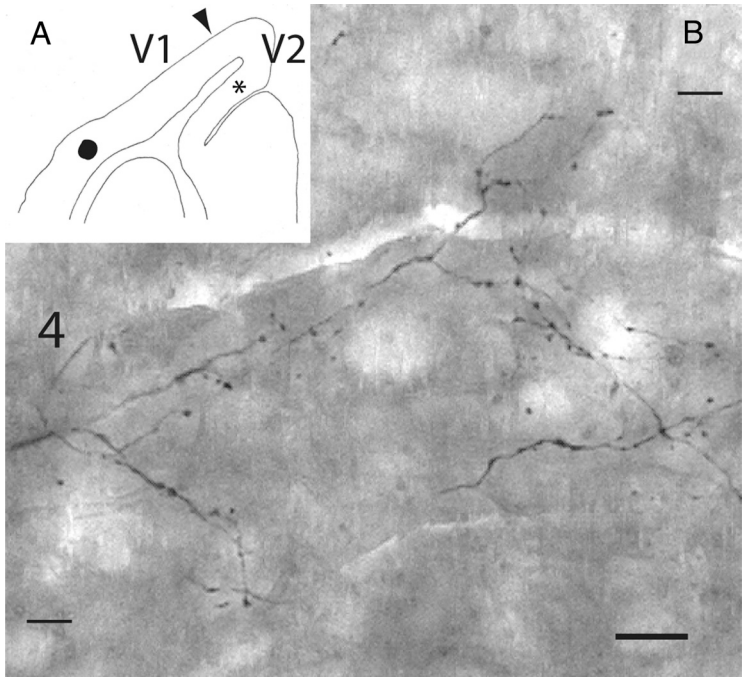

Figure 1. Location of injection site in V1 and labeled boutons in V2. ***A***, Low-power sketch of a parasagittal section through the lunate gyrus showing the approximate location of a BDA injection site (solid circle) in V1, the location of BDA-labeled boutons (asterisk), and the V1–V2 border (filled arrowhead). ***B***, Light photomontage of cortical area V2 showing BDA-labeled axons and their terminals in layer 4 that project from an injection of BDA made in area V1. Laminae and their boundaries are indicated to the bottom left and top right. Scale bar: ***B*** (bottom right), 15 μm.

Results

Light microscopy

Each of the five monkeys received ionophoretic injections of BDA, PHA-L, or biocytin that were confined to the gray matter of either area V1 (two cases) or area V2 (three cases).

V1 to V2

The injections into area V1 were placed at ~7–8 mm distance posterior to the lunate sulcus, well inside area V1 (see Fig. 1*A*). Two V1 injection sites were located in superficial layers and two injection sites involved all layers and labeled cells in layers 2–6. Dense labeling of cell bodies at most injection sites extended 0.2 mm to 0.3 mm from the penetration, although the appearance of label at the different injection sites varied. The termination zone of the BDA-labeled axons originating from the injection site illustrated in Figure 1*A* extended over ~2 mm of layer 4 on the posterior bank of the lunate sulcus in V2, with the denser innervation located closer to the tip of the gyrus. The axon termination zone in the other V1-injected monkey was located in three dis-

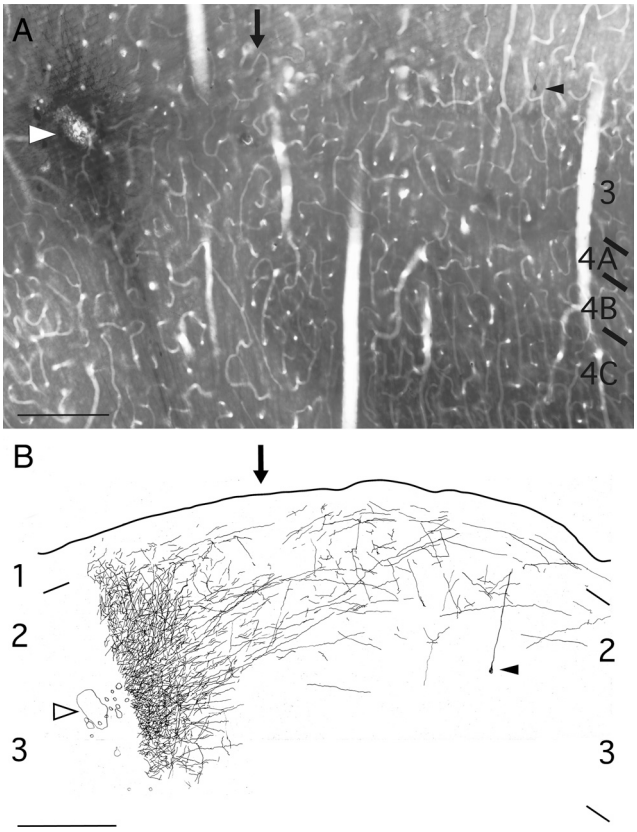

Figure 2. Location of injection site in V2. ***A***, Light photomontage of a parasagittal section through the cortex at the border between V1 and V2 (arrow) showing the injection site in V2 (white arrowhead) and the location of a weak retrogradely labeled pyramidal cell (arrowhead). V1 laminae are indicated to the right. ***B***, Light microscopic drawing of the section shown in ***A***. Anterogradely labeled axons projecting from the injection site (open arrowhead) cross the border into V2. Axons in the immediate vicinity of the injection site were not drawn because the density of label was too intense. The position of the weakly labeled pyramidal cell shown in ***A*** is indicated (arrowhead). Laminae and their borders are indicated to the left and right. Scale bars, 300 μm.

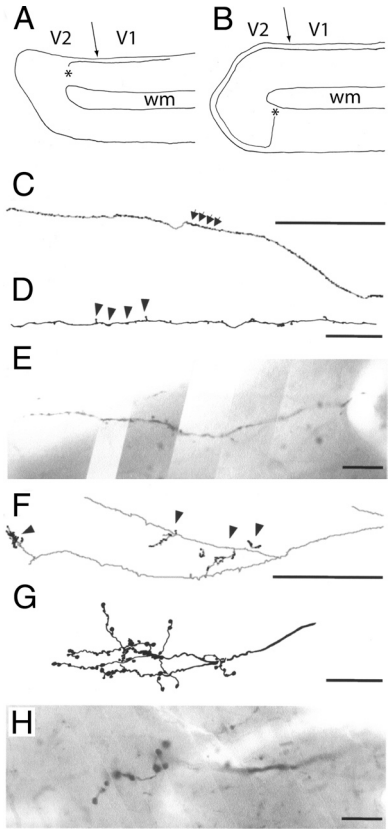

Figure 3. Two "feedback" axons labeled with PHA-L, confined to layer 1 and showing terminations in area V1. ***A***, ***B***, Low-power sketches of lunate gyrus showing approximate path of two axons through layer 1 and earliest appearance of axon (asterisk). The white matter (wm) and V1–V2 border are also indicated (arrow). Axon shown in ***A*** and ***C–E*** is referred to as the "thin" axon. ***C***, Light microscopic reconstruction of the thin axon showing a long, unbranched, bouton encrusted (small filled arrowheads) collateral. ***D***, High-magnification (100× oil objective) light microscopic drawing showing detail of thin axon and frequently located boutons (filled arrowheads). ***E***, Light microscopic photomontage of thin axon in layer 1. Axon shown in ***F–H*** is referred to as the "thick" axon. ***F***, Light microscopic reconstruction of thick, branched axon showing clusters of boutons (solid arrowheads). The computer assisted 3-D reconstruction of the axon is rotated to provide the view from the surface of the brain. ***G***, High-magnification light microscopic drawing showing detail from one bouton cluster. ***H***, Light microscopic photomontage of thick axon and bouton cluster. Scale bars: ***C***, ***F***, 0.5 mm; ***D***, ***G***, 25 μm; ***E***, ***H***, 10 μm.

crete clusters within the fundus of the lunate sulcus. Each cluster had a lateral spread within layer 4 ranging from 0.3 to 0.5 mm, separated by similarly sized zones that were relatively bouton free. Collaterals arising at the border of white matter and layer 6 were followed through the deep layers to their extensive arborizations layer 4. In one animal a few fibers entered lower layer 3. Both animals showed very little retrograde labeling of cell bodies. Axons traversing the deeper layers were myelinated, so often only the cut ends of these axons had strong reaction product. Upon reaching layer 4 the collaterals became unmyelinated, branched frequently, and became finer, and formed boutons, which were mainly en passant (~78%) in morphology (Fig. 1*B*). The sheer density of innervation in layer 4 made it impossible to reconstruct individual axons or accurately to correlate LM and EM.

V2 to V1

The injections in area V2 were made at the tip of the lunate gyrus and were confined to the gray matter. In the first animal only the superficial layers two and three were labeled with BDA (Fig. 2), while in the other two animals all layers of the cortex were labeled (Anderson and Martin, 2002, their Fig. 1*A*). In all three animals there was retrograde labeling of pyramidal cells in layers 2 and 3 of V1, although much less in the first animal where the injections were more localized (see Fig. 2). The axons of the retrogradely labeled cells arborized mainly in layers 2/3 and 5 but also provided a dense innervation of layer 1. This meant that the axons originating from pyramidal cells in V2 were mixed with axons originating from pyramidal cells in V1. Even axons traced from the white matter underlying V1 were found to originate from retrogradely labeled pyramidal cells in superficial layers of V1. Hence we examined only those axon collaterals that could be traced back to the injection site and, where possible, to a labeled cell body.

The first animal had a large number of axons originating from the labeled superficial layer pyramidal cells in V2 that did not enter the white matter, but projected laterally from layers 2/3 and 5 to arborize in layers 1, 2/3, and 5 of V1 (Fig. 2) and forming boutons over their entire length. The projection to layer 2/3 in V1 was the densest and showed the least retrograde contamination. Of the many labeled axons only a single axon in each of the second and third animals could be traced back to their origins in the injection sites in V2. These single axons also did not dive into the white matter beneath V2 to reemerge in V1, but instead were confined to layer 1 throughout their projection from V2 to V1. The morphologies of the two single axons were strikingly different from each other.

The single axon from the second animal, referred to here as the "thin" axon, emerged from a radially aligned myelinated fiber in layer 1 at a point directly above the infragranular layer injection site in V2, ~1.3 mm from the V1/V2 border. It then abruptly turned right angles to traverse the middle of layer 1 in a posterior direction toward V1 and remained tangential to the surface of the cortex until its termination in V1. In V1 this axon was very thin (0.3 μm), unmyelinated, and unbranched. It had many boutons terminaux distributed over its entire length (2 mm) in layer 1 (Fig. 3*A*, *C–E*). Axons showing this pattern of trajectory have been described by Rockland (1994).

The second single axon from the third animal we will refer to as the "thick" axon. It arose from an injection site in infragranular layers of V2 and traveled radially toward the cortical surface of the posterior bank of the lunate sulcus. Upon reaching layer 1 the axon abruptly turned right angles and traversed V2, remaining tangential to the surface of the cortex. Continuing just above the middle of layer 1 the axon passed around the tip of the lunate gyrus. The labeling of the axon was dark and continuous until it reached the opercular surface of V1, where it became myelinated and the label became intermittent. But in each section, the cut ends of the axon were clearly labeled and the thickness of the axon made it easy to follow despite the absence of continuous label. This axon was thick (>1 μm), branched, heavily myelinated, and formed separate, small clusters of large (~1 μm) en passant boutons (Fig. 3*B*,*F–H*) through the thickness of layer 1. Some of these V2 to V1 axon features were also described by Rockland and Virga (1989). The fact that the axons projecting from V2 to V1 passed through the gray matter and not the white matter is unusual. However, the injection sites were relatively close to the V1–V2 border and passage through gray matter may be more economical. The axons also formed boutons in the V2 portion of their trajectory.

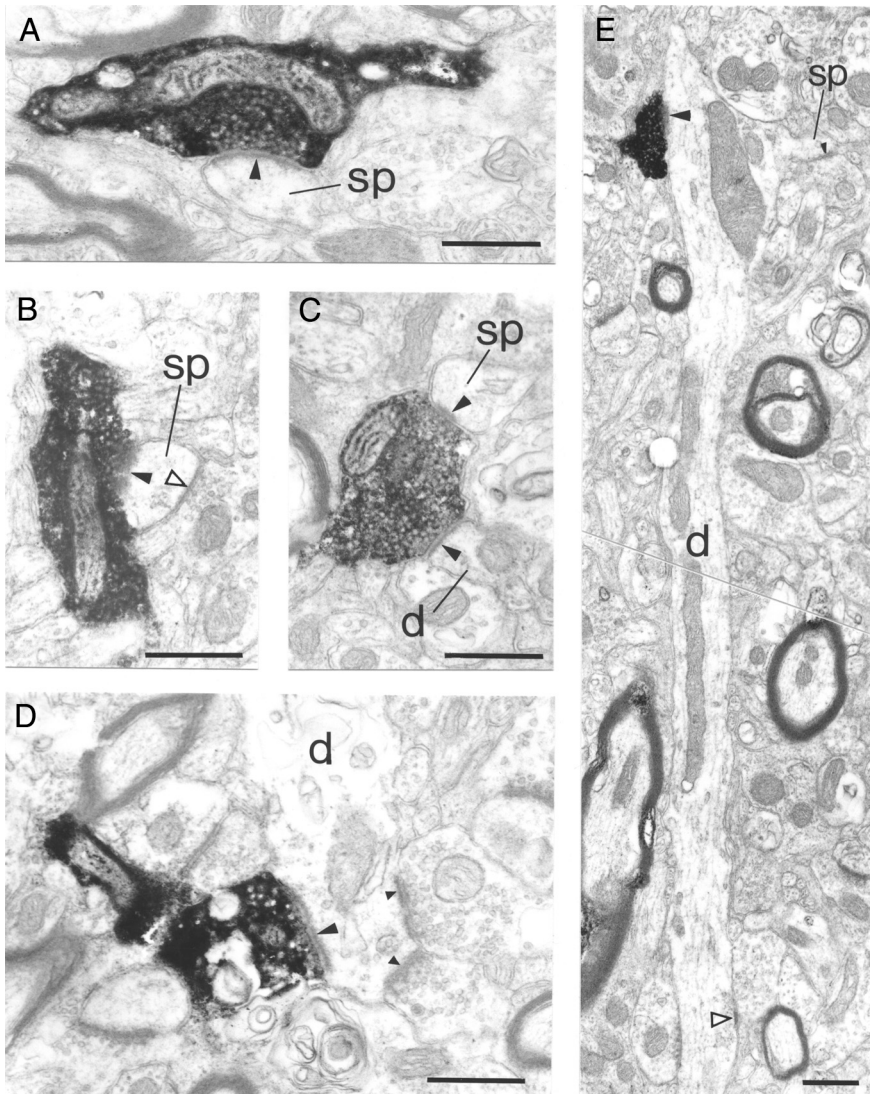

Figure 4. Electron photomicrographs taken from cortical area V2 showing BDA-labeled boutons in layer 4. ***A***, A labeled bouton en passant forms an asymmetric synapse (solid arrowhead) with a spine (sp). ***B***, A spine (sp) forms an asymmetric synapse (solid arrowhead) with a labeled bouton and a symmetric synapse (open arrowhead) with an unidentified bouton. The asymmetric synapse of the labeled bouton has been cut rather obliquely obscuring the synaptic cleft and smearing the postsynaptic density. ***C***, A labeled bouton forms two asymmetric synapses (solid arrowheads) with a spine (sp) and a small caliber dendritic shaft (d). ***D***, A large-caliber dendritic shaft (d) forms an asymmetric synapse (solid arrowhead) with a labeled bouton. The dendrite (d) forms a further two asymmetric synapses (small solid arrowheads) with two unidentified boutons. Serial section reconstruction of the dendrites shown in ***C*** and ***D*** revealed that both formed more synapses and contain numerous mitochondria. These features are characteristic of GABA-containing smooth cells. ***E***, A lower-power electron micrograph showing a labeled bouton forming an asymmetric synapse (solid arrowhead) with a medium-caliber dendritic shaft (d). The dendrite produces a spine (sp), opposite the labeled bouton, that forms an asymmetric synapse (small solid arrowhead). An unidentified bouton forms a symmetric synapse (open arrowhead) with the dendritic shaft. Dendrites showing few shaft synapses, few mitochondria, and forming spines are features of spiny cells, probably pyramidal cells. Scale bars: ***A–E***, 0.5 μm.

We have previously described the variations in bouton morphology and density for the axons of spiny neurons (Martin and Whitteridge, 1984; Anderson and Martin, 2001). Boutons are usually recognized as beads along an axon (bouton en passant) or swellings on short processes extending from the axon (bouton terminaux). Using correlated LM and EM we have repeatedly verified here, and in previous studies (Anderson et al., 1998; Anderson and Martin, 2002, 2005, 2006) that boutons identified at light microscope level form synaptic specializations and that synapses in the interbouton segments are rare.

Electron microscopy

We examined a total of 107 labeled V1 boutons in layer 4 of area V2. The labeled V1 terminals in V2 provided 126 synaptic specializations. For the projection from V2 to V1 we examined 137 boutons, which formed a total of 165 synapses. From the cluster of layer 3 cells labeled in V2 axons, we sampled 59 boutons in layers 1 and 2/3 of V1, together with 44 boutons in layer 1 of V1 from the V2 thin axon and 34 boutons in layer 1 of V1 from the thick axon. The thin axon provided 44 synapses and the thick axon, 61 synapses. All boutons from these individual axons were

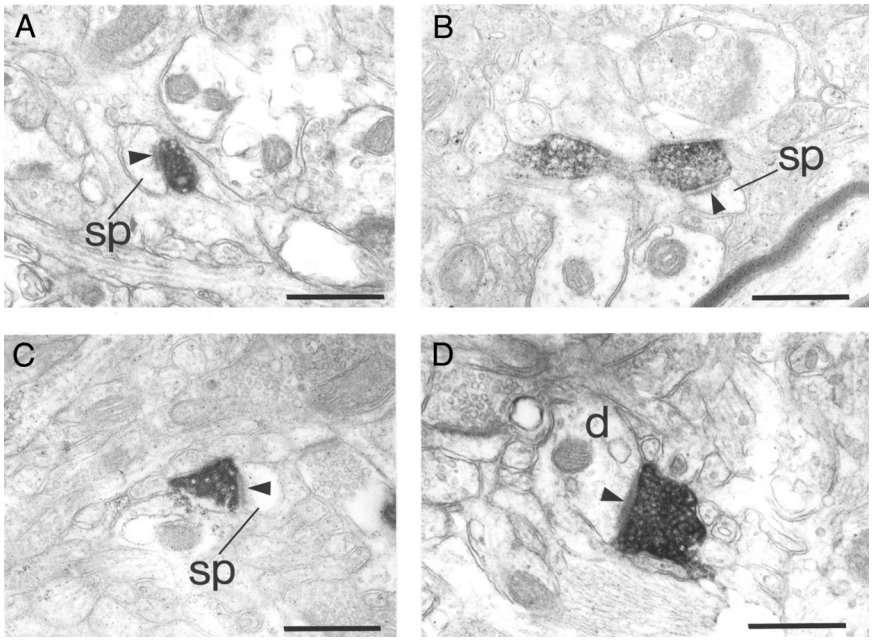

Figure 5. Electron photomicrographs taken from cortical area V1 showing PHA-L-labeled boutons in layer 1. All examples are taken from the "thin" axon (Fig 1; ***A–C***). ***A–C***, Examples of small boutons forming asymmetric synapses (solid arrowheads) with spines (sp). The majority of labeled boutons and their targets were of similar dimensions. ***D***, A labeled bouton forms a synapse (solid arrowhead) with a small caliber dendrite (d). The dendrite formed a second synapse with another labeled bouton from the same axon. The ultrastructural characteristics of the dendrite (variable diameter, numerous mitochondria, and forming many synapses) indicate that it is from a GABAergic neuron with smooth dendrites. Scale bars, 0.5 μm.

serially sectioned and reconstructed. Synapses from V2 boutons in layers 1 and 2/3 were serially sectioned and 27 of 60 were reconstructed. All labeled boutons formed asymmetric synapses (Gray's type 1). Those synapses that were incomplete were excluded from the measurements of the area of the postsynaptic densities.

The reaction end-product was dark, although of variable intensity in different boutons. Vesicles and mitochondria were clearly visible within the boutons and the synaptic clefts were not obscured by diffusion of the label. Myelinated axons were also labeled, indicating that the antibody sometimes had penetrated, despite the barrier to diffusion of the reagents presented by the myelin. Small vacuoles formed in some labeled structures (e.g., Figs. 4*A*, *D*, 6*A*). The V1 to V2 population showed relatively little variation in bouton size (~0.5 μm). Occasionally we found labeled myelinated axons (0.12–0.5 μm diameter) with a myelin wall thickness of ~0.1 μm. For the V2 to V1 projections, the boutons of the thin axon were uniformly small (~0.3 μm) and were mostly bouton terminaux (Figs. 5, 7*A*). In contrast, the thick axon (~1 μm diameter) formed large bouton en passant (~1 μm) (Figs. 6, 7*B*) with occasional smaller boutons, such as the small bouton terminaux in Figure 6*D*. The larger the bouton the greater the number of mitochondrial profiles in single sections. The myelin sheath covering the thick axon had a wall thickness of ~0.15 μm. The very small boutons of the thin axon rarely contained a mitochondrion. Boutons from the thick axon could contain several mitochondria. Single sections of the V1 to V2 boutons of intermediate size usually contained one or two mitochondrial profiles. All the remaining space within the labeled boutons was packed with vesicles, which sometimes extended into the axon (e.g., Fig. 6*E*). Synapses were indicated by the presence of vesicles, a synaptic cleft and a postsynaptic density. The postsynaptic density could be a simple disc shape or perforated.

Targets of synaptic boutons: spines

Serially sectioning the bouton, synapse, and target structures greatly assisted in determining the type of target that formed synapses with the labeled boutons. We also used standard ultrastructural criteria to classify targets (Peters et al., 1991). The most frequent targets of both projections were spines (Figs. 4–6). Occasionally we were able to trace spines back to a parent dendrite (Fig. 6*A*, *C*). The target spines of the V1 to V2 projection were all small (Fig. 4*A–C*). A second synapse from an unlabeled bouton was seen on 17 of 91 spines. The second synapse was always of a symmetric morphology (Gray's type 2) (Fig. 4*B*). This is an unusually high proportion of dual input spines (19%), but was strongly biased by the data from one animal in particular (14 of 62 spines, 23%). The second animal provided three dual input spines (3 of 29, 10%), which is closer to the range that is normally encountered in studies of spines and their synapses.

The boutons of the two individual feedback V2 to V1 axons formed synapses with spines of very different sizes. The thin axon boutons formed synapses with spines that were equally tiny (Fig. 7*A*). The large boutons of the thick axon formed synapses with spines that were clearly large and flattened when seen after serial section reconstruction (Fig. 7*B*). Figure 8 shows the reconstructed spines contacted by boutons of the thin (Fig. 8*A*) and thick (Fig. 8*B*) axons. Rockland has also noted that the majority of synaptic targets of the feedback projection in layer 1 were spines (Rockland, 1994).

The spine targets of the upper layer 2/3 projecting axons were usually small (<0.5 μm) in diameter. Only one bouton of the population of V2 to V1 axons shared its target spine with a second (symmetric) synapse. A light and diffuse labeling appeared in some of the smaller spines (Fig. 6*A*). The label helped us to trace back to the parent dendrite that also showed light labeling. We attributed this light labeling to retrograde uptake of PHA-L at the injection site, which would indicate that neurons that project to V2 also receive input from V2.

Targets of synaptic boutons: dendritic shafts

Dendritic shafts were also the targets of labeled boutons. They were usually identified by reconstruction from serial sections, or by the presence of mitochondria and microtubules. Overall, labeled boutons formed synapses with a range of dendrites of different diameters (~0.5–1.5 μm). Dendrites sometimes contained numerous vacuoles and ultrastructurally tended to suffer more than spines when they formed synapses with labeled boutons (e.g., Figs. 4*D*, 6*D*, *E*). We have no explanation for this, but it was clearly related to the presence of the label. From the serial section reconstructions we grouped the dendrites into two classes. Sixteen of the 34 synapses from the V1 to V2 synapses in layer 4 were formed with the shafts of dendrites that varied little in diameter and formed very few synapses along the shaft. These features are characteristic of the spiny dendrites of excitatory neurons, a characterization that was occasionally confirmed in this material by spines emerging from the shafts of dendrites with

these characteristics. Three of the six dendritic shafts that formed synapses with the thin axon and 5 of 14 synapses formed by the thick axon were with shafts of spiny neurons. In one case the thin axon formed two synapses with a target dendrite: one synapse with the shaft and one with a spine.

A second class of dendrite varied in its diameter, it contained numerous mitochondria and formed many shaft synapses with unidentified boutons. These features were usually clearer when the dendrite was serially reconstructed. Neurons with these features have smooth dendrites and have been shown to contain the inhibitory neurotransmitter GABA (Somogyi et al., 1983; Peters and Saint Marie, 1984; Kisvárday et al., 1985; Beaulieu et al., 1992; Ahmed et al., 1997; Meskenaite, 1997). Just over half (18 of 34, 53%) of the target dendrites of the projection from V1 to V2 were of the smooth type. The V2 to V1 boutons from the thin axon formed synapses with 3 smooth dendrites. One of these dendrites formed synapses with two labeled boutons. In the case of the thick axon 9 of 14 (64%) of the dendritic shaft synapses were formed with the dendrites of smooth neurons. Three of the dendrites formed two synapses with boutons of the thick axon (e.g., Fig. 7*B*). One smooth dendrite also formed numerous tiny processes (Fig. 6*E*) each of which formed one or two synapses with unidentified boutons. These "spinules" appeared to be headless and varied in length from 0.1 to 0.5 μm. The ultrastructural morphology was not that of any recognizable excitatory or spiny neuron (e.g., pyramidal cell) but clearly showed features of smooth neurons, perhaps an intrinsic GABAergic neuron of layer 1. All of the target dendrites (11) from the projection to layers 1 and 2/3 of V1 showed features of smooth dendrites.

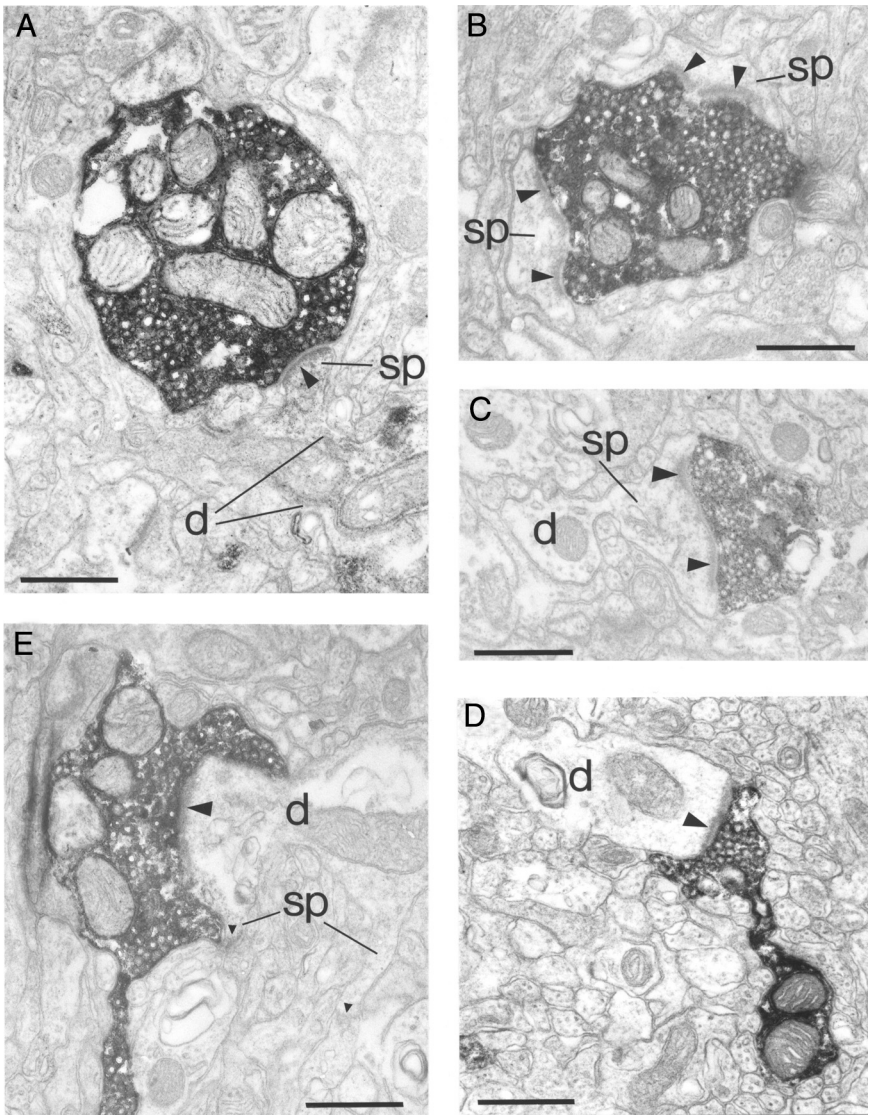

Figure 6. Electron micrographs of PHA-L-labeled boutons forming synapses in layer 1 of area V1. All examples are taken from the "thick" axon (Fig. 1; ***D–F***). ***A***, A large labeled bouton forms an asymmetric synapse (solid arrowhead) with a small spine (sp). The spine and parent dendrite (d) are weakly labeled with retrogradely transported PHA-L. ***B***, Two large spines (sp) each form a perforated asymmetric synapse (solid arrowheads) with a large labeled bouton. ***C***, A medium sized bouton forms a perforated asymmetric synapse (solid arrowheads) with a spine (sp) that can be followed back to the small caliber parent dendrite (d). ***D***, A small bouton terminaux forms an asymmetric synapse (solid arrowhead) with a medium-caliber dendrite (d). The dendrite contained few mitochondria, formed no other synapses and showed little variation in diameter. These features are characteristics of neurons with spiny dendrites, probably pyramidal cells. ***E***, A large bouton en passant forms an asymmetric synapse (solid arrowhead) with a large-caliber dendrite (d). The dendrite was unusual in that it formed synapses with the shaft and with small and slender spinous processes that each formed at least one asymmetric synapse (small solid arrowheads). The shaft also contained numerous mitochondria. Scale bars, 0.5 μm.

Targets of synaptic boutons: somata

Only one synapse was seen between a labeled bouton and a soma, which was located in layer 4 of V2. There were many organelles within the soma and it also received numerous synapses from unidentified boutons, which are features of smooth neurons.

Postsynaptic density

Reconstructing the bouton and its target gave us the opportunity to view the complete postsynaptic density (PSD) as a two-dimensional (2-D) or 3-D structure. We have used this technique previously to obtain values of the surface area of synapses (Anderson et el., 1998; Anderson and Martin, 2002, 2005, 2006). By focusing on the postsynaptic specialization rather than the presynaptic membrane, we avoided detail being obscured by reaction end-product in the bouton. We show a 2-D projection of the PSDs in Figures 9–11. There was no difference seen in the distributions of the areas of synapses made with the two main target types for the V1 to V2 axons, which were spines (0.081 μm^2, SEM, 0.004) and dendrites (0.077 μm^2, SEM, 0.006) ($p = 0.6$, two-tailed t test) (Fig. 12).

The data for the projection from V2 to V1 were derived from a random sample taken from superficial layers as well as an extensive series of EMs from two very different single axons, and so were not pooled (Fig. 13). The synapses formed by the thin axon were very small (0.032 μm^2, SEM, 0.004), while those of the thick axon were very large (0.17 μm^2, SEM, 0.016) (Fig. 13) and those

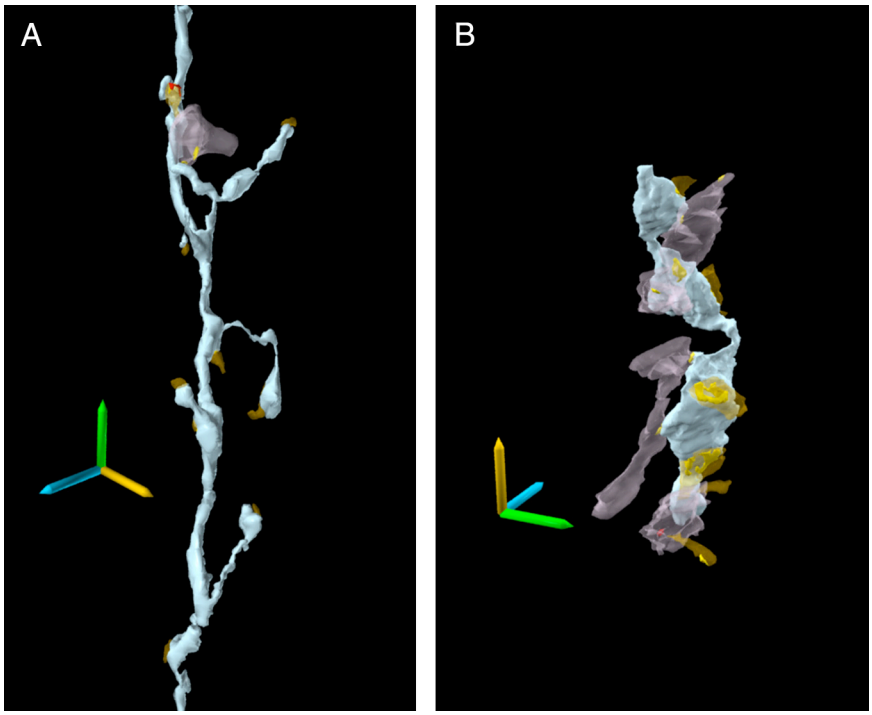

Figure 7. Three-dimensional reconstruction from serial ultrathin sections of PHA-L-labeled boutons in layer 1 of V1 showing synaptic targets. ***A***, Thin axon (blue) showing numerous projecting boutons terminaux each forming a single synapse (yellow) in most cases with a small spine (transparent brown). Near the top of the reconstruction a bouton terminaux branches to form two boutons, one of which forms a synapse with a dendritic shaft (transparent mauve). A spine projects from the uppermost surface of the dendrite and forms another synapse with the labeled axon. This same spine also forms a symmetric synapse (red) with an unidentified bouton. ***B***, Thick axon (blue) showing a string of three boutons en passant and their synaptic targets; spines (transparent brown) and dendritic shafts (transparent mauve). Postsynaptic densities, often complex, are shown in yellow. The two uppermost boutons each form two synapses, one each with a spine and the second with a dendritic shaft that passes between the two boutons. The dendrite also receives an asymmetric synapse from an unidentified bouton. The lower bouton forms four synapses; two with spines and two with a dendritic shaft. One of the spines can be traced back to the parent dendrite showing more spines and forms an asymmetric synapse (red) on the shaft. Scale bars, 2 μm.

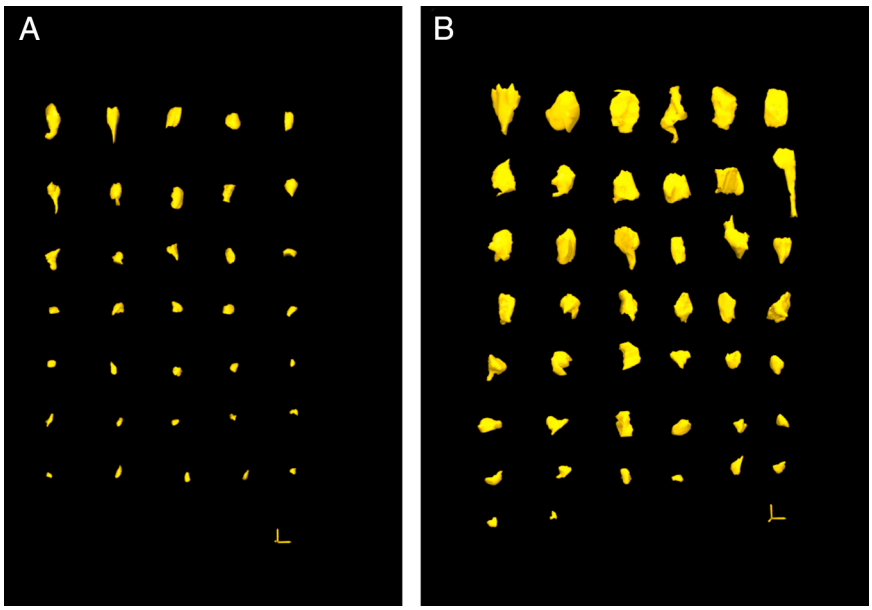

Figure 8. Reconstructed spines found postsynaptic to labeled boutons of thin axon (***A***) and thick axon (***B***). The spines have been ordered roughly by size. Each spine has been rotated to present its broadest face. Scale bars, 0.5 μm.

of the random sample from superficial layers fell between the two (0.08 μm^2, SEM 0.008). The spine synapses formed by the thick axon (0.19 μm^2, SEM, 0.02) were significantly larger than those formed with dendritic shafts (0.10 μm^2, SEM, 0.02) ($p = 0.018$, two-tailed t test). This was also true of the random superficial layer sample (spine 0.08 μm^2, SEM 0.01; dendrite 0.05 μm^2, SEM 0.009; $p = 0.029$ two-tailed t test). The PSDs of the thin axon were predominantly simple disc-shaped structures, while those of the thick axon showed greater complexity in shape with numerous perforations, particularly in spines. PSDs formed with the spines of the V1 to V2 projection also had a complex, perforated morphology, which we have reported in other projections in monkey cortex (Anderson et el., 1998; Anderson and Martin, 2002, 2005, 2006).

Target types

The most frequently encountered targets of V1-labeled boutons in V2 and for V2-labeled boutons in V1 were spines. One clear difference between the various axons was in the proportion of spines to dendrites as targets (Fig. 14). In layer 4 of V2, 72% of the labeled V1 synapses formed with spines, 27% with dendritic shafts, and 1% with somata. In layer 1 of V1, the thin axon from V2 formed 84% of its synapses with spines and 16% with dendritic shafts, whereas the thick axon formed 77% of its synapses with spines and 23% with dendritic shafts. In layers 1 and 2/3 of V1, the proportion of spines to dendritic shafts was similar to that seen for the thin axon in layer 1: 82% spines and 18% dendritic shafts. The majority of labeled boutons for all projections formed one synapse, although single boutons could form up to four synapses (Fig. 15). The thin axon from the V1 to V2 pathway only ever formed one synapse per bouton.

Discussion

Light microscope observations

We confirmed many of the morphological observations made by Rockland and Virga (1989, 1990). The V1 projection to V2 formed clusters of boutons concentrated in layer 4, but with additional collaterals in layers 3 and 6. Rockland and Virga (1989) described two types of axons projecting from V2 to layer 1 of V1, one of which formed clusters of boutons, and the other that was continuously studded with bouton terminaux, as in our "thin" axon. They, as did we, also observed a third type of axon, which formed en passant boutons principally in layers 5 and 3 of V1.

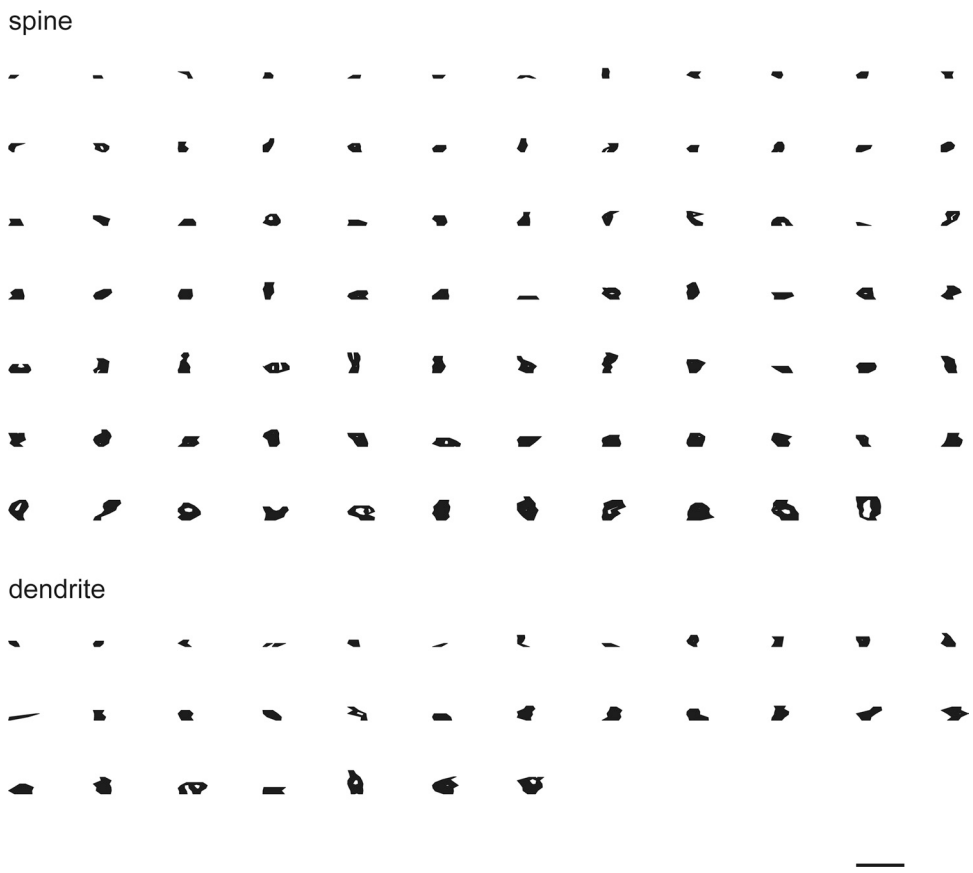

Figure 9. Two-dimensional projection of the reconstructed postsynaptic densities found on spines, soma, and dendrites postsynaptic to V1-labeled boutons in layer 4 of area V2. The densities are ordered by increasing surface area. Scale bar, 1 μm.

Figure 10. Two-dimensional projection of the reconstructed postsynaptic densities found on spines and dendrites postsynaptic to V2-labeled boutons in layers 1 and 2/3 of area V1. The densities are ordered by increasing surface area. Scale bar, 1 μm.

However, Rockland and Virga's axons emerged from the white matter, whereas the axons we traced streamed across the V1/V2 border in the gray matter, even when the injections were some millimeters from the border. Although the "thick" axon formed clusters of boutons in layer 1, its clusters were more reminiscent of the morphology of Meynert cell axons of macaque V1 (Rockland and Knutson, 2001) than of the type of axon with clustered boutons described by Rockland and Virga (1989). Since large solitary pyramidal neurons are also found in the deep layers of V2, it would be interesting to discover whether these are the source of the thick axons that project to layer 1 of V1.

We could find no morphological evidence to suggest that all the V1 to V2 axons were feedforward "drivers" and all the V2 to V1 axons were feedback "modulators." In the V2 to V1 projection we only recovered one axon (the "thin" axon) that resembled Guillery and Sherman's (2002) description of "modulating axon." The "thick" axon, which projected from V2 to V1, had the features of a "driving axon." Indeed, the most common type of axon we found projecting from the superficial pyramidal cells in V2 to the superficial layers of V1 was morphologically indistinguishable from the axons that projected from V1 to V2.

Ultrastructure of synapses. Postsynaptic density size and spine morphology

It is evident from the ultrastructure of the target spines that bigger spines have bigger PSDs. This relationship has been reported for pyramidal cells in the hippocampus (Harris and Stevens, 1989) and mouse barrel cortex (Knott et al., 2006). The PSDs of the thin axon were almost one-third the size of most interareal spine synapses (0.032 versus ~0.1–0.12 μm^2). Most remarkable were the size of the PSDs of the thick axon in layer 1, which were larger (0.19 μm^2) than anything yet reported for macaque cortex. The

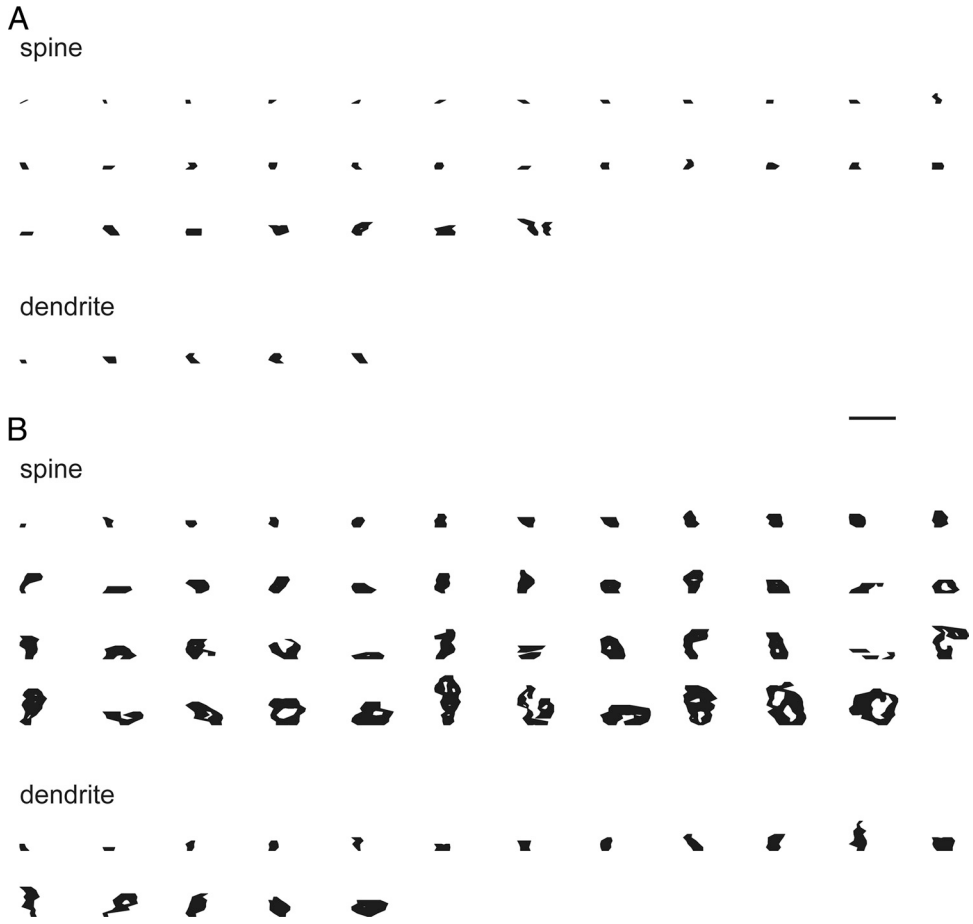

Figure 11. Two-dimensional projection of the reconstructed postsynaptic densities found on the spines and dendrites postsynaptic to labeled boutons in layer 1 of area V1 from thin axon (***A***) and thick axon (***B***). The densities are ordered by increasing surface area. Scale bar, 1 μm.

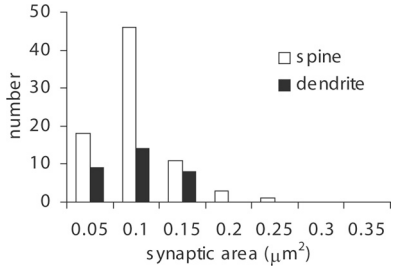

Figure 12. Histogram showing the distributions of postsynaptic areas (in square micrometers) formed with spines and dendrites by labeled V1 boutons in layer 4 of V2.

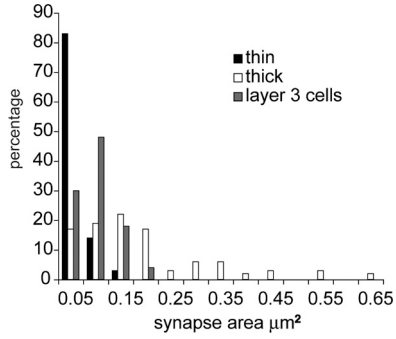

Figure 13. Histograms of the distributions of postsynaptic density areas (in square micrometers) formed by labeled V2 boutons in superficial layers of V1. Shown are thin axon (black, $n = 44$), thick axon (white, $n = 61$), and layer 3 pyramidal cells (gray, $n = 27$).

previous largest were the V1 to MT projection (Anderson et al., 1998), which were 0.127 μm^2. Cortical synapses of comparable size (~0.18 μm^2) have only been seen once before in the thalamic projection to layer 4 of the cat visual cortex (Dehay et al., 1991; Friedlander et al., 1991). The range of areas of the postsynaptic specialization within most single populations of reconstructed synapses is at least an order of magnitude [e.g., V1 to MT (Anderson et al., 1998) and V4 to V2 (Anderson and Martin, 2006)], although the average size between these populations is surprisingly similar. The functional consequences of this variance remains unexplained, as does the correlation we observed between spine size and synapse size. However, the data from Stevens and colleagues indicates that there is a positive correlation between size of synapse and the release probability and amplitude of glutamatergic synapses (Schikorski and Stevens, 1997; Murthy et al., 2001), so that our measures of PSD size may give a qualitative indication of synaptic strength.

Synaptic interrelationships

The V1 to V2 axons in layer 4 formed 72% of their synapses with pyramidal dendritic spines. This is comparable to the projections from V2 to V3A (76%) (Anderson and Martin, 2005) and V2 to MT (67%) (Anderson and Martin, 2002), but is different from the V1 to MT projection, which forms significantly fewer spine synapses (54%) (Anderson et al., 1998) due to some large boutons that form multiple somatic synapses. The projection from

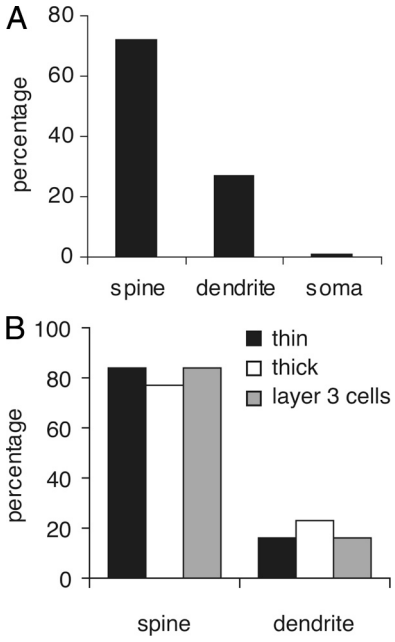

Figure 14. ***A***, Histogram of the synaptic targets of labeled V1 boutons in area V2. Spine $n = 91$, dendrite $n = 34$, soma $n = 1$. ***B***, Histogram of the synaptic targets of the boutons of two labeled V2 axons in layer 1 of area V1 and a group of labeled synapses in layers 1 and 2/3 of V1 from superficial layer 3 pyramidal cells in V2. For the thin axon, $n = 44$, and for the thick axon, $n = 61$. For the group of V2-labeled layer 3 cell boutons in V1, $n = 60$.

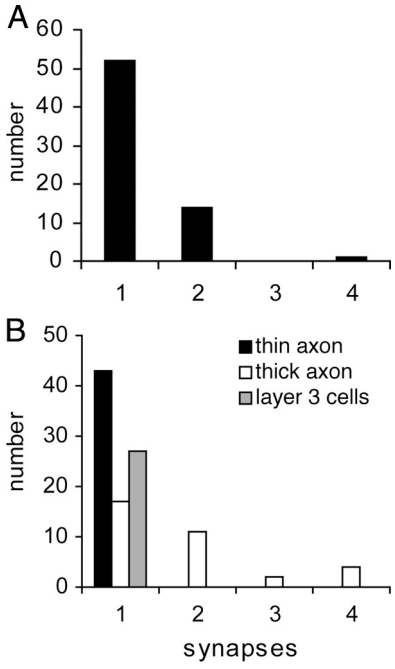

Figure 15. ***A***, Histogram of the number of synapses formed per labeled V1 bouton in layer 4 of area V2. ***B***, Histogram of the number of synapses formed per labeled V2 bouton in superficial layers of area V1.

V2 to V1 also targeted mainly spines (84% and 77% for the two axons) in layer 1, which is its primary layer of innervation. These targets are comparable to the projection to layer 1 in the V4 to V2 pathway (75%) (Anderson and Martin, 2006). This is different from the rat, where the ascending projection from primary visual cortex to extrastriate cortex formed 90% of its synapses with spines, while the descending projection formed 98% of its synapses with spines (Johnson and Burkhalter, 1996). Our results for putative GABAergic targets (V1 to V2 and V2 to V1; ~14%).

The pattern of projection of V2 to V1 resembles that of V4 to V2 (Anderson and Martin, 2006) in that two morphologically distinct axons stream through layer 1. The most common in the V4 to V2 projection were axons with boutons (many terminaux) covering the entire length of axon. A second, rarer morphology was that of thicker axons and boutons (mostly en passant) arranged in discrete grape-like clusters. Both these distinct axon morphologies appear in descending pathways [e.g., V4 to V2 (Anderson and Martin, 2006) and area TE to TEO (Suzuki et al., 2000)], and functionally they are likely to have different roles, since it seems likely that different cell types would be the source of such different axon morphologies, as is evident for the local axon collaterals in cat and monkey (Martin and Whitteridge, 1984; Anderson et al., 1993).

The asymmetric relationship between V1 and V2

V1 is at the root of the tree of visual cortical areas, and so we are not surprised that cooling V1 eliminates all activity in V2 (Girard and Bullier, 1989). However, on the basis of the comparable magnitudes of the projection between V1 and V2 (Barone et al., 2000; Kennedy et al., 2000), we would not predict that inactivating V2 would have a negligible effect on most V1 neurons, but it does (Hupé et al., 2001), even though electrical stimulation showed that V2 neurons can activate V1 neurons with similar latencies to the activation of V2 by V1 neurons (Girard et al., 2001).

Thus, although V1 and V2 are very tightly coupled, the asymmetry of their physiological influence on one another is profound. However, our structural data challenges the notion that the marked difference in their effects can be explained on the basis of fundamental differences in axonal morphology and synapse size or target. Thus, instead of tackling the general question posed by Bullier (2006), "What is fed back?" we can try to answer the simpler question of what factors other than numbers of synapses or their physiology might explain this asymmetry of effect between V1 and V2.

In our studies of the long-distance projections in cat and monkey, we have been struck by the small numbers of synapses they provide to their target areas (Anderson et al., 1998; Latawiec et al., 2000; Anderson and Martin, 2002, 2005, 2006). The largest projection we have seen numerically is from the lateral geniculate nucleus, which provides only 10% of the excitatory synapses in layer 4 (and <1% of all excitatory synapses in area 17). Of course, theoretically, if there is the strong constraint of minimizing wiring, whether in brains or silicon chips (Mead, 1989), long-distance connections should be reduced to the minimum.

However, there are perils in wire minimization: in simulations with a biophysically realistic model of spiny stellate cells in layer 4 (Banitt et al., 2007), we discovered that even with optimally oriented stimulation, additional "background" excitation is required to depolarize the cells sufficiently to enable the small modulated LGN inputs to drive the cells to spike. At nonoptimal orientations, the unmodulated excitation from the LGN did not reach threshold. This resembles stochastic resonance. Such observations have led us to propose that the brain does attempt to minimize wire and adds a second important constraint: time. To drive a neuron to threshold, sufficient excitation must arrive within a narrow temporal window. We summarized these two constraints as "just-enough, just-in-time" (Douglas and Martin, 2007).

We can now offer a different interpretation of the structural and functional relationship between V1 and V2. Our hypothesis

is that differential effects seen with inactivation are not because of synaptic numbers and/or synaptic location or physiology, but simply because V1 provides V2 with a much tighter temporal window of excitation than V2 does V1, at least most of the time. As with the analogy of the orientation model, the more temporally dispersed input from V2 to V1 can be effective in assisting a second modulated input to be effective, but itself is subthreshold and invisible to an extracellular electrode. However, some stimuli might evoke similarly short epochs of excitation in V2 and so enable it to evoke spikes in V1 neurons. Thus, the rigid feedforward and feedback pathway is substituted by a more dynamic interaction where the direction of effective action depends on the stimulus being processed. This hypothesis accounts for the observed functional asymmetry seen between areas, and may be a general principle of cortical wiring and operation. Importantly, it is experimentally testable.

References

Ahmed B, Anderson JC, Martin KAC, Nelson JC (1997) Map of the synapses onto layer 4 basket cells of the primary visual cortex of the cat. J Comp Neurol 380:230–242.

Anderson JC, Martin KAC (2001) Does bouton morphology optimize axon length? Nat Neurosci 4:1166–1167.

Anderson JC, Martin KAC (2002) Connection from cortical area V2 to MT in macaque monkey. J Comp Neurol 443:56–70.

Anderson JC, Martin KAC (2005) Connection from cortical area V2 to V3A in macaque monkey. J Comp Neurol 488:320–330.

Anderson JC, Martin KAC (2006) Synaptic connection from cortical area V4 to V2 in macaque monkey. J Comp Neurol 495:709–721.

Anderson JC, Martin KAC, Whitteridge D (1993) Form, function, and intracortical projections of neurons in the striate cortex of the monkey *Macacus nemestrinus.* Cereb Cortex 3:412–420.

Anderson JC, Binzegger T, Martin KAC, Rockland KS (1998) The connection from cortical area V1 to V5: a light and electron microscopic study. J Neurosci 18:10525–10540.

Banitt Y, Martin KAC, Segev I (2007) A biologically realistic model of contrast invariant orientation tuning by thalamocortical synaptic depression. J Neurosci 27:10230–10239.

Barone P, Batardiere A, Knoblauch K, Kennedy H (2000) Laminar distribution of neurons in extrastriate areas projecting to visual area V1 and V4 correlates with the hierarchical rank and indicates the operation of a distance rule. J Neurosci 20:3263–3281.

Beaulieu C, Kisvarday Z, Somogyi P, Cynader M, Cowey A (1992) Quantitative distribution of GABA-immunopositive and -immunonegative neurons and synapses in the monkey striate cortex (area 17). Cereb Cortex 2:295–309.

Bullier J (2006) What is fed back? In: 23 Problems in systems neuroscience (van Hemmen JL, Sejnowsky TJ, eds), pp 103–132. New York: Oxford UP.

Dehay C, Douglas RJ, Martin KAC, Nelson C (1991) Excitation by geniculocortical synapses is not "vetoed" at the level of dendritic spines in cat visual cortex. J Physiol 440:723–734.

Douglas RJ, Martin KAC (2007) Recurrent neuronal circuits in the neocortex. Curr Biol 17:R496–R500.

Felleman DJ, Van Essen DC (1991) Distributed hierarchical processing in the primate cerebral cortex. Cereb Cortex 1:1–47.

Friedlander MJ, Martin KAC, Wassenhove-McCarthy D (1991) Effects of monocular visual deprivation on geniculocortical innervation of area 18 in the cat. J Neurosci 11:3268–3288.

Girard P, Bullier J (1989) Visual activity in area V2 during reversible inactivation of area 17 in the macaque monkey. J Neurophysiol 62:1287–1302.

Girard P, Hupé JM, Bullier J (2001) Feedforward and feedback connections between areas V1 and V2 of the monkey have similar rapid conduction velocities. J Neurophysiol 85:1328–1331.

Guillery RW, Sherman SM (2002) Thalamic relay functions and their role in corticocortical communication: generalizations from the visual system. Neuron 33:163–175.

Harris KM, Stevens JK (1989) Dendritic spines of CA1 pyramidal cells in the rat hippocampus: serial electron microscopy with reference to their biophysical characteristics. J Neurosci 9:2982–2997.

Hupé J-M, James AC, Girard P, Bullier J (2001) Response modulations by static texture surround in area V1 of the macaque monkey do not depend on feedback connections from V2. J Neurophysiol 85:146–163.

Johnson RR, Burkhalter A (1996) microcircuitry of forward and feedback connections within rat visual cortex. J Comp Neurol 368:383–398.

Kennedy H, Barone P, Falchier A (2000) Relative contribution of feedforward and feedback inputs to individual areas. Eur J Neurosci 12 [Suppl 11]:489.

Kisvárday ZF, Martin KAC, Whitteridge D, Somogyi P (1985) Synaptic connections of intracellularly filled clutch neurons, a type of small basket neuron in the visual cortex of the cat. J Comp Neurol 241:111–137.

Knott GW, Holtmaat A, Wilbrecht L, Welker E, Svoboda K (2006) Spine growth precedes synapse formation in the adult neocortex in vivo. Nat Neurosci 9:1117–1124.

Latawiec D, Martin KAC, Meskenaite V (2000) Termination of the geniculocortical projection in the striate cortex of macaque monkey: a quantitative immunoelectron microscopy study. J Comp Neurol 419:309–319.

Livingstone MS, Hubel DH (1983) Specificity of cortico-cortical connections in monkey visual system. Nature 304:531–534.

Livingstone MS, Hubel DH (1984) Anatomy and physiology of a color system in the primate visual cortex. J Neurosci 4:309–356.

Martin KAC, Whitteridge D (1984) Form, function and intracortical projections of neurones in the striate cortex of the cat. J Physiol 353:463–504.

Mead C (1989) Analog VLSI and neural systems. Reading, MA: Addison-Wesley.

Meskenaite V (1997) Calretinin-immunoreactive local circuit neurons in area 17 of the cynomolgus monkey, *Macaca fascicularis.* J Comp Neurol 379:113–132.

Murthy VN, Schikorski T, Stevens CF, Zhu Y (2001) Inactivity produces increases in neurotransmitter release and synapse size. Neuron 32:673–682.

Peters A, Saint Marie R (1984) Smooth and sparsely spinous non-pyramidal cells forming local axonal plexuses. In: Cerebral cortex, Vol 1. Cellular components of the cerebral cortex (Jones EG, Peters A, eds), pp 419–445. New York: Plenum.

Peters A, Palay SL, Webster Hd (1991) The fine structure of the nervous system: neurons and their supporting cells, Ed 3. Oxford: Oxford UP.

Rockland KS (1994) The organization of feedback connections from area V2 (18) to V1 (17). In: Cerebral cortex (Peters A, Rockland KS, eds), Vol 10, pp 243–293. New York: Plenum.

Rockland KS, Knutson T (2001) Axon collaterals of Meynert cells diverge over large portions of area V1 in the macaque monkey. J Comp Neurol 441:134–147.

Rockland KS, Virga A (1989) Terminal arbors of individual "feedback" axons projecting from area V2 to V1 in the macaque monkey: a study using immunohistochemistry of anterogradely transported Phaseolus vulgaris-leucoagglutinin. J Comp Neurol 285:54–72.

Rockland KS, Virga A (1990) Organization of individual cortical axons projecting from area V1 (area 17) to V2 in the macaque monkey. Vis Neurosci 4:11–28.

Schikorski T, Stevens CF (1997) Quantitative ultrastructural analysis of hippocampal excitatory synapses. J Neurosci 17:5858–5867.

Sincich LC, Horton JC (2002a) Divided by cytochrome oxidase: a map of the projections from V1 to V2 in macaques. Science 295:1734–1737.

Sincich LC, Horton JC (2002b) Pale cytochrome oxidase stripes in V2 receive the richest projection from macaque striate cortex. J Comp Neurol 447:18–33.

Sincich LC, Horton JC (2005a) Input to V2 thin stripes arises from V1 cytochrome oxidase patches. J Neurosci 25:10087–10093.

Sincich LC, Horton JC (2005b) The circuitry of V1 and V2: integration of color, form, and motion. Annu Rev Neurosci 28:303–326.

Somogyi P, Kisvárday ZF, Martin KAC, Whitteridge D (1983) Synaptic connections of morphologically identified and physiologically characterized large basket cells in the striate cortex of cat. Neuroscience 10:261–294.

Suzuki W, Saleem KS, Tanaka K (2000) Divergent backward projection from the anterior part of the inferotemporal cortex (area TE) in the macaque. J Comp Neurol 422:206–228.

3.6 The final publication was an extensive study of projections of frontal eye fields or FEF. After a propitious start at the Royal Society in the hands of David Ferrier in the 19th century, FEF has grown in the minds of many to be of special importance in relation to consciousness. FEF involvement with eye movement is a short stop to attention. This has led to a plethora of models of attention some of which have included specific characteristics of cells, such as inhibition. For cortical areas as far forward as those considered here (area 46, LIP, FEF) we often have cells with properties unlike those of earlier sensory cortices such as attention, cognition and reward expectation. What is striking in physical terms is the anterior distance of FEF from early visual cortices, with which it still provides an input to areas such as V4. Some of the projection patterns of these attentional areas were predicted to be feedback-like, but proved not to be so straight forward to classify. These experiments were conducted in collaboration with Kennedy of Lyon, France.

Behavioral/Systems/Cognitive

Pathways of Attention: Synaptic Relationships of Frontal Eye Field to V4, Lateral Intraparietal Cortex, and Area 46 in Macaque Monkey

John C. Anderson,[1] Henry Kennedy,[2] and Kevan A. C. Martin[1]

[1]Institute for Neuroinformatics, University of Zürich and ETH Zürich, 8057 Zürich, Switzerland, and [2]Stem Cell and Brain Research Institute, Institute National de la Sante et de la Recherche Medicale U846, 69500 Bron, France and Université de Lyon, Université Lyon 1, 69003 Lyon, France

The frontal eye field (FEF) of the primate neocortex occupies a pivotal position in the matrix of inter-areal projections. In addition to its role in directing saccadic eye movements, it is the source of an attentional signal that modulates the activity of neurons in extrastriate and parietal cortex. Here, we tested the prediction that FEF preferentially excites inhibitory neurons in target areas during attentional modulation. Using the anterograde tracer biotinylated dextran amine, we found that the projections from FEF terminate in all cortical layers of area 46, lateral intraparietal area (LIP), and visual area V4. Axons in layer 1 spread extensively, those in layer 2/3 were most numerous, individual axons in layer 4 formed sprays of collaterals, and those of the deep layers were the finest caliber and irregular. All labeled synapses were the typical asymmetric morphology of excitatory synapses of pyramidal neurons. Dendritic spines were the most frequent synaptic target in all areas (95% in area 46, 89% in V4, 84% in LIP, 78% intrinsic local FEF). The remaining targets were one soma and dendritic shafts, most of which showed characteristics of inhibitory neurons with smooth dendrites (5% of all targets in area 46, 2% in V4, 9% in LIP, and 13% in FEF).

Introduction

The prefrontal cortical area of the frontal eye field (FEF) (area 8A) occupies a pivotal position in the primate visual system. Although best known for its key role in eye movements (Ferrier, 1874; Robinson and Fuchs, 1969; Schiller et al., 1979; Goldberg and Bushnell, 1981), FEF is also implicated in working memory (Balan and Ferrera, 2003), decision-making (Ferrera et al., 2009), and mechanisms of attention (Moore and Fallah, 2001). Attention has been shown to enhance oscillatory activity originating in FEF (Buschman and Miller, 2009) and the coupling between FEF and area V4 (Gregoriou et al., 2009). Electrical stimulation of FEF in monkeys drives attention-like changes in receptive fields in extrastriate cortex, modulates attentional performance, and modulates the blood oxygen level-derived (BOLD) signal across a wide swathe of visual areas (Moore and Fallah, 2004; Armstrong et al., 2006; Armstrong and Moore, 2007; Ekstrom et al., 2008). In humans, transcranial magnetic stimulation of FEF modulates the BOLD signal in the visual cortex (Ruff et al., 2006).

Received Feb. 4, 2011; revised May 20, 2011; accepted June 2, 2011.

Author contributions: J.C.A., H.K., and K.A.C.M. performed research; J.C.A., H.K., and K.A.C.M. wrote the paper.

We acknowledge the support of the European Union; Daisy Grant FP6-2005-015803 (to H.K. and K.A.C.M.) and Swiss National Science Foundation, National Centres of Competence in Research Grant "Neuroplasticity and Repair" (to K.A.C.M.). We thank Rita Bopp, German Köstinger, Pascale Giroud, and Nuno da Costa for expert technical assistance.

Correspondence should be addressed to either John C. Anderson or Kevan A.C. Martin, Institute for Neuroinformatics, University of Zürich and ETH Zürich, Winterthurerstrasse 190, 8057 Zürich, Switzerland, E-mail: jca@ini.phys.ethz.ch or kevan@ini.phys.ethz.ch.

DOI:10.1523/JNEUROSCI.0622-11.2011

 0270-6474/11/3110872-10$15.00/0

Neurons in V4 increase their firing when the monkey attends to a stimulus within their receptive fields (Luck et al., 1997; McAdams and Maunsell, 1999, 2000; Reynolds et al., 1999, 2000). Mitchell et al. (2007) found that presumed inhibitory neurons show larger attention-dependent increases in firing rates than do presumed excitatory neurons. Hussar and Pasternak (2009) reported similar biases for presumed inhibitory neurons in the effects of attention in area 46, which is monosynaptically connected to FEF (Barbas and Mesulam, 1981; Huerta et al., 1987; Barbas and Pandya, 1989; Stanton et al., 2005). Inhibitory neurons have also been implicated in the strong suppression effects of distractors on area 46 neurons (Lennert and Martinez-Trujillo, 2011).

There is, however, a gap in our knowledge about the anatomical pathways whereby FEF exerts its effects on visual areas (Kayser and Logothetis, 2006). The most direct and likely route is the monosynaptic connection from the FEF to the posterior parietal and the occipital lobe (Huerta et al., 1987; Stanton et al., 1995), including area V1 (Clavagnier et al., 2004), V2 (Markov et al., 2011), and V4 (Stanton et al., 1995; Barone et al., 2000). In the occipital lobe, the earliest and strongest effects of the attentional signal are seen in V4, with progressively later and lesser effects in V2 and V1 (Buffalo et al., 2010).

For the inhibitory neurons to be activated differentially from their neighboring excitatory cells under the conditions of an attentional signal, their excitatory input must shift from local sources (Binzegger et al., 2004) to external sources, such as the inter-areal connections or the thalamus. This requires that projections from the source of the attentional signal, in this case FEF, strongly target inhibitory neurons. We tested this prediction by defining quantitatively the synaptic targets of FEF projections to

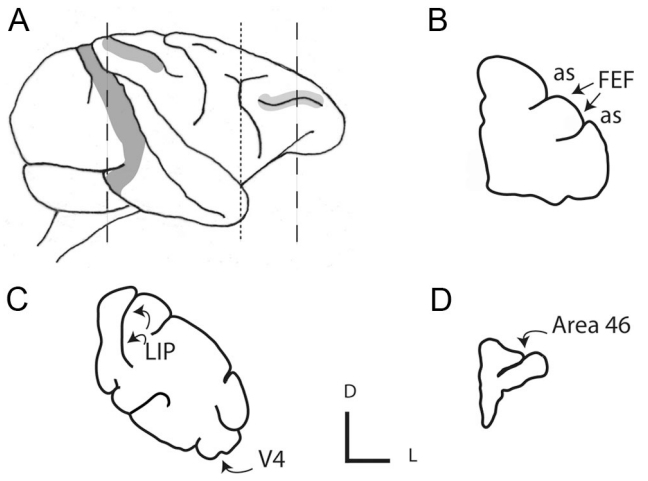

Figure 1. Location of injection sites and labeled boutons. ***A–D***, Schematic drawing of a macaque brain (***A***) showing cortical areas V4 (left, dark gray), LIP (middle, gray), and area 46 (right, light gray). Also shown are schematic sections made in the coronal plane through the following: tip of prearcuate gyrus (dotted line), shown in ***B*** (as, arcuate sulcus); dorsal prelunate area (dashed line, left), shown in ***C***; and prefrontal cortex (dashed line, right), shown in ***D***. The injection sites in FEF are indicated in ***B*** (arrows). Labeled boutons were taken (curved arrows, ***C***, ***D***) from areas LIP, V4, and 46, as well as the FEF injection site area. Small axes, L, lateral; D, dorsal.

V4, area 46, and lateral intraparietal area (LIP). Our data support the null hypothesis: in all areas we found that the overwhelming majority of targets were the spines of excitatory pyramidal cells, not putative inhibitory neurons.

Materials and Methods

The material presented here was taken from two adult female cynomolgus monkeys (*Macaca fascicularis*) and one adult female rhesus monkey (*Macaca mulatta*). Animal treatment and surgical protocols were performed in accordance with the guidelines of the Direction départementale de services vétérinaires du Rhône and the Kantonal Veterinaeramt of Zurich (the experimental protocols for the project "Microcircuits of Neocortex" were approved by the Kantonal Veterinaeramt of Zurich, which issued the license numbers 50/3002 and 50/2003 to K.A.C.M.). Animals were prepared for surgery after intramuscular premedication with Largactil (0.5 ml), atropine (1.25 mg), and dexamethasone (4 mg), followed by ketamine hydrochloride (20 mg/kg) or ketamine hydrochloride (10 mg/kg) and xylazine (0.5 mg/kg), followed by alphaxalone/alphadalone (Saffan). Anesthesia was continued with halothane in N_2O and O_2 (70:30). The following procedures are similar to those used by Anderson and Martin (2002).

Two animals received pressure injections of the neuronal tracer biotinylated dextran amine (BDA) (Invitrogen) as a 10% solution in 0.01 M PBS, pH 7.4, using a Hamilton syringe. One of these animals received two injections into ventrolateral FEF (lateral area 8) of each hemisphere. The second of these animals received four injections into dorsomedial FEF (medial area 8) of one hemisphere and three injections into ventrolateral FEF (lateral area 8) of the other hemisphere. The location of area 8/FEF was determined using recognizable landmarks (Fig. 1).

After a 14 d survival period, the animals were very deeply anesthetized with pentobarbital (20 mg/kg, i.v.) and then perfused transcardially with a normal saline solution, followed by a solution of 4% paraformaldehyde, 0.3% glutaraldehyde, and 15% picric acid in 0.1 M phosphate buffer (PB), pH 7.4. To explore the local projections within FEF, the third animal received small iontophoretically delivered injections of BDA into the superficial layers of FEF (area 8L) using ~1 μA for 10–30 s. The tip diameter of the delivery pipette was from 0.02 to 0.04 μm. The animal was maintained under general anesthesia for 30 h and then perfused as above. The brain was removed and blocks of cortex containing the injection site and areas 46, V4, and LIP were taken. The block was cryoprotected by sinking in sucrose solutions of 10, 20, and 30% in 0.1 M PB, then freeze-thawed in liquid nitrogen and washed in 0.1 M PB. Sections were cut from the block at 80 μm in the coronal plane and collected in 0.1 M PBS. We used standard procedures to reveal the neuronal tracers. In brief outline, washes in PBS were followed by 10% normal swine serum (NSS) in PBS (1 h). Further washes in NSS preceded overnight exposure (5°C) to an avidin-biotin complex (Vector Laboratories ABC kit Elite). The peroxidase activity was identified using 3,3′-diaminobenzidine tetrahydrochloride (DAB) with nickel intensification. After assessment by light microscopy, selected regions of tissue were treated with 1% osmium tetroxide in 0.1 M PBS. Dehydration through alcohols (1% uranyl acetate in the 70% alcohol) and propylene oxide allowed flat mounting in Durcupan (Fluka) on glass slides. Some non-osmicated sections were Nissl-stained with cresyl violet to identify cortical laminae.

Light microscopic observations of labeled axons were performed to locate and select regions of interest for electron microscopy. We reconstructed groups of collaterals over one or two sections to show the general pattern of innervation and to locate individual collaterals in specific laminae. This was followed by correlated light and electron microscopy. Serial ultrathin sections at 40 or 60 nm thickness were collected on Pioloform-coated single-slot copper grids. Labeled boutons were photographed at a magnification of 21,000×. Synapses and associated structures were classified using conventional criteria (Peters et al., 1991). Collections of serial sections were digitized, reconstructed, and measured using Reconstruct (Fiala, 2005). We used the "rare event systematically optimized random sampling" (RESORS) physical disector method (da Costa et al., 2009) for counting rare events, to estimate the proportion of labeled synapses. Adobe Photoshop CS and Adobe Illustrator CS were used to prepare digital photomicrographs and enhance image contrast.

Results

Light microscopy

Both female cynomolgus monkeys (*Macaca fascicularis*) received pressure injections of BDA into area 8A (FEF) in a crescent along the anterior edge of the arcuate sulcus, medial and lateral to a caudal projection of the principal sulcus (Fig. 1). The needle passed vertically through the lip of the arcuate sulcus, down its anterior bank, labeling cells to the fundus of the sulcus through all layers of cortex. In one animal, two 0.5 μl pressure injections were made into each hemisphere along the lip of the arcuate gyrus, lateral to the caudal projection of principal sulcus, described as area 8A/45 border (Saleem and Logothetis, 2007). This region is generally accepted as the lateral portion of the FEF. In the second animal, three 0.2 μl injections of BDA were made into the lateral area 8A of one hemisphere, and in the other hemisphere, four injections were made along the lip of the arcuate sulcus, medial to the caudal projection of the principal sulcus. Lateral injections had BDA label more confined to the lateral regions of the area 8, whereas the medial injections, because they descend vertically, resulted in more extensive labeling of area 8. The BDA label around the injection sites spread over >1 mm in the case of the larger injection volumes and ~0.5 mm for the smaller injections. The regions nearest to the penetration were diffusely labeled with a penumbra of scattered and dispersed pyramidal cells. Pressure injections were all confined to the gray matter, and the BDA label could be seen in all laminae, which made it impossible to identify the precise laminar location of the cells of origin of the projecting axons.

A third monkey (rhesus, *Macaca mulatta)* received small iontophoretic injections into layer 2/3 of lateral area 8A. Each iontophoretic injection labeled a small cluster of ~5–10 labeled neurons in layer 2/3. Most of the labeled cells were pyramidal. Occasionally, a cell with smooth dendrites and lacking an apical dendrite was found amid the tangle of spiny cells. Myelin is a

barrier to the penetration of the reagents, and thus axons were stained only at their cut ends, nodes, or branch points from where the collaterals emerged.

In the pressure-injected animals, anterogradely labeled axonal arbors were found in extrastriate visual areas and prefrontal cortex as well as the STS, intraparietal sulcus, and postcentral gyrus. Pale-stained somata of deep and superficial layer neurons were occasionally seen, due to weak retrograde transport of the BDA. They had a very lightly scattered, grainy reaction-product within the cell soma, but their dendrites and axon collaterals were not labeled. The small iontophoretic injections labeled local neurons, but not other cortical areas. Most of the labeled axons were seen in the immediate vicinity of the labeled cell bodies. More distal boutons were rarely seen and were not examined in the electron microscope.

V4, area 46, and LIP

Labeled axons and their terminals were found in all layers of areas V4 (Fig. 2), area 46, and LIP. Fibers entered from the white matter and projected upward to the pial surface. The path of the projection was radial and oblique and spread over large areas of cortex. Bouton-rich collaterals formed in all layers. Sometimes a thicker fiber traversed through a particular lamina, sending out fine collaterals that radiated or even descended when in layers 4, 5, and 6, and when in layer 2 and 3, climbed to layer 1. Layer 1 had long, horizontally projecting axons that occasionally dropped collaterals down into layers 2 and 3. The fine horizontal fibers of layer 1 and the fibers that descended to layers 2 and 3 showed bouton-like swellings that were later demonstrated by electron microscopy to be synaptic. However, the thicker horizontal axons in layer 1 had fewer swellings, many of which proved to be nonsynaptic in the electron microscope. These fibers were intermittently myelinated, and so they appeared and disappeared from view in the light microscope as the penetration of the reagents varied. This description of the overall LM appearance applies equally to areas 46, LIP, and V4.

In addition to the general features described above, we found some variations in the patterns of innervation. For example, in V4, layer 4 was innervated in only one of the two pressure-injected animals. Terminal boutons were found in all laminae of LIP in one hemisphere of one animal, while in the second animal, the densest boutons were predominantly in deep and superficial layers, although at the fringes of the densest innervation, layer 4 did contain boutons. The densest labeling of boutons in LIP was consistently in layers 1 and 2. We could not relate these variants to differences in the location of our pressure injection sites. For example, after injections in lateral FEF in one animal, there were labeled boutons in all layers including 4 of V4, but despite similar injection locations in the other hemisphere, labeled boutons appeared in all layers except layer 4.

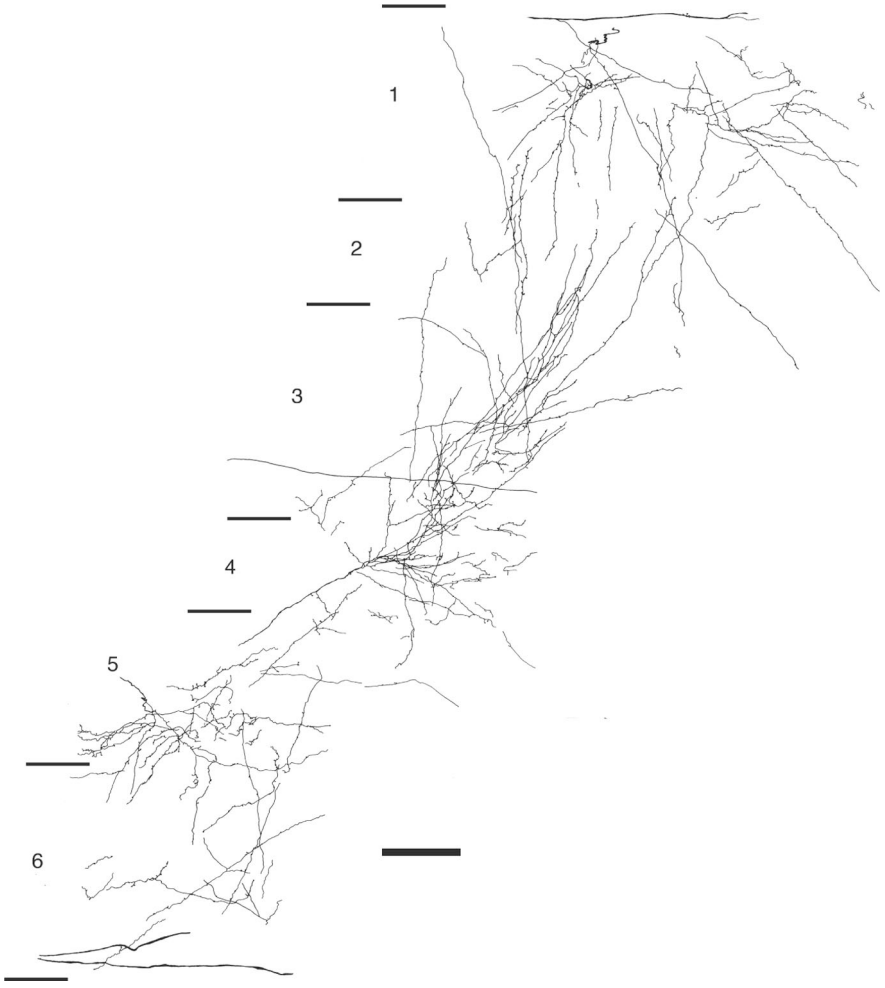

Figure 2. Light microscopic reconstruction of BDA-labeled terminals and their boutons in area V4. The reconstruction is composed from two adjacent 80-μm-thick sections. Laminae and their boundaries are indicated to the left. Scale bar, 100 μm.

Electron microscopy

To provide a convincing test of the hypothesis that smooth neurons were the principal target of the FEF projection, we examined a total of 555 boutons (158 in V4, 195 in LIP, 202 in area 46). Of this sample, 395 single boutons were serially sectioned and completely reconstructed so that the area of the postsynaptic density (PSD) could be measured. The remaining 53 boutons were not sufficiently complete for quantification of their synapses, but were used in the assessment of synaptic targets. Altogether, we examined 120 boutons from layer 1, 166 from layer 2/3, 125 from layer 4, and 144 from layer 5/6. All the synapses formed by labeled boutons were asymmetric (Gray's type 1), which is typical of pyramidal cell axons.

The reaction end-product was electron dense, though its intensity varied between boutons. Synaptic vesicles and mitochondria were clearly visible within the boutons, and occasional boutons contained vacuoles (Fig. 3; see Figs. 5, 7*B*). Most boutons were small (<0.5 μm), although the sample showed a considerable range of sizes. The labeled boutons were filled with synaptic vesicles and usually contained at least one mitochondria, and a clear density was seen postsynaptically.

Synaptic targets were identified using standard ultrastructural criteria (Peters et al., 1991). Serial sections through the bouton and its synaptic target assisted greatly in the identification of the target type. The majority of targets were spines (89%); the re-

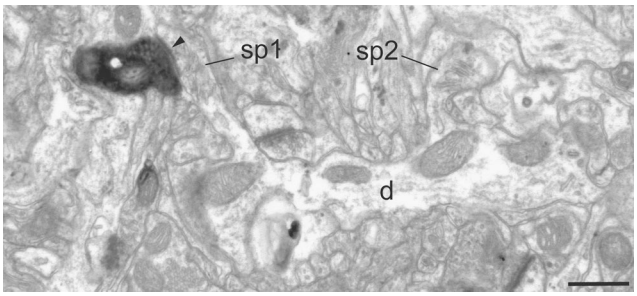

Figure 3. Electron micrograph of BDA-labeled bouton located in layer 1 of area V4. A labeled bouton forms an asymmetric synapse (solid arrowhead) with a spine (sp1) that can be traced back to the parent dendrite (d). A second spine (sp2) can be seen to connect with the same dendritic shaft (d). Scale bar, 0.5 μm.

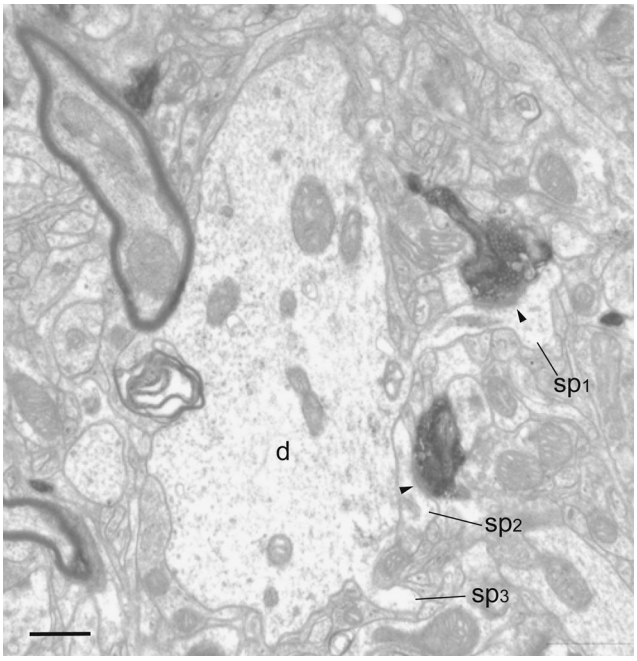

Figure 4. Electron micrograph of BDA-labeled axon and boutons located in layer 2/3 of area V4. The boutons form asymmetric synapses (solid arrowheads) with spines (sp1 and sp2). One of the synapse-bearing spines (sp1) can be traced back to the large dendrite (d). The second spine (sp2) was not connected to the dendrite, and a third spine (sp3) just begins to emerge from the large dendrite (d). Scale bar, 0.5 μm.

mainder were dendritic shafts, and only 1 soma. We reconstructed complete postsynaptic spines to discover whether they formed a second synapse, but following the thin spine neck back to its parent dendrite often proved impossible. Approximately 2% of the reconstructed spines received a second synapse from an unlabeled bouton. The second synapse was always identified as a symmetric (Gray's type 2) synapse. Dendrites often contained mitochondria or microtubules, making their identification relatively simple.

Layer 1 boutons were relatively easy to locate in V4, area 46, and LIP (Fig. 3; see Figs. 6*A*,*B*, 9*A*), as the axons often traversed the lamina horizontally. In layer 1 we examined 35 boutons in V4, 45 in area 46, and 40 in LIP. Spines were the most frequent target (V4, 86%; area 46, 96%; LIP, 93%). We pooled the boutons from layers 2 and 3 (Fig. 4). We selected 55 boutons from V4, 58 from area 46, and 53 from LIP. Samples from V4 and area 46 showed spines to be 92% of targets and in LIP, 89%. The remainder were dendritic shafts.

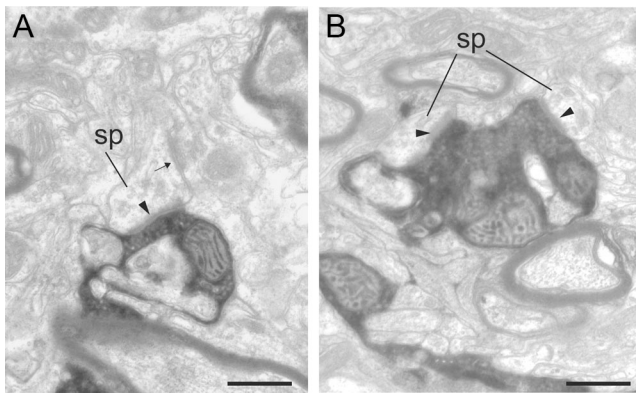

Figure 5. Electron micrographs of BDA-labeled boutons located in layers 4 and 5/6 of area V4. ***A***, A labeled bouton in layer 4 forms an asymmetric synapse (solid arrowhead) with a spine (sp). The spine also forms a symmetric synapse (small arrow). ***B***, A labeled bouton in layer 5/6 forms two asymmetric synapses with spines (sp). Scale bars, 0.5 μm.

Boutons in layer 4 proved more difficult to obtain than in other layers. The lamina was thin (~100 μm) and made the accurate verification of the boutons' location critical in order not to misidentify the lamina location of the boutons. Only one animal provided boutons from layer 4 of V4 (Fig. 5*A*); the second animal provided no equivalent material in osmicated tissue. In the non-osmicated sections, a few axon collaterals could be seen that lay on the layer 3–4 border and passing through layer 4, but most were not bouton bearing. For the layer 4 samples, we sectioned 21 boutons (86% spines) from V4, 46 boutons from area 46 (96% spines) (see Fig. 7*A*), and 58 boutons from LIP (78% spines) (see Fig. 9).

It was also difficult to harvest boutons from layers 5 and 6, because the axons were very fine and scattered, sometimes more densely in layer 5 and sometimes more in layer 6. We examined 47 boutons from V4, 53 from area 46, and 44 from LIP (Fig. 5*A*; see Figs. 7*B*, 9). Spines were the predominant target, 92% in V4, 95% in area 46, and 81% in LIP. The only somatic synapse to be formed with a labeled bouton came from this sample, taken from area 46 (see Fig. 7*B*). All other synapses were formed with dendritic shafts (see Fig. 8). In FEF itself, we sampled boutons taken near somata labeled by the small iontophoretic injections. All 82 boutons we examined were located in layers 2 and 3. Spines were the predominant target (78%) and the remainder were dendritic shafts.

Axons of all areas were sometimes myelinated (Fig. 6*D*), and the largest caliber axons were up to 0.7 μm in diameter. The majority of myelinated axons were ~0.5 μm in diameter, and regardless of diameter, most axons bore a 0.1-μm-thick sheath of myelin. The collaterals bearing boutons were very fine, and sometimes the label was intermittent in the finest axons (~50 nm).

Spines

Serial sectioning and reconstruction helped with the identification of synaptic targets (see Fig. 10). We also used standard ultrastructural characteristics to classify targets (Peters et al., 1991). Spines could be identified by their small size; their heads often contained spine apparatus, and they were filled with pale and fluffy cytoplasm. The spine neck was often too thin and tortuous to follow for any distance, although occasionally it could be traced back to a parent dendrite (Figs. 3, 4, 7*A*; see Fig. 9*A*). Rarely did a spine form a second synapse, and when it did occur, it was always a symmetric synapse (Fig. 5*A*). The dual input spines constituted 2.5% of spines in V4, 2% of spines in area 46, and 3.5% in

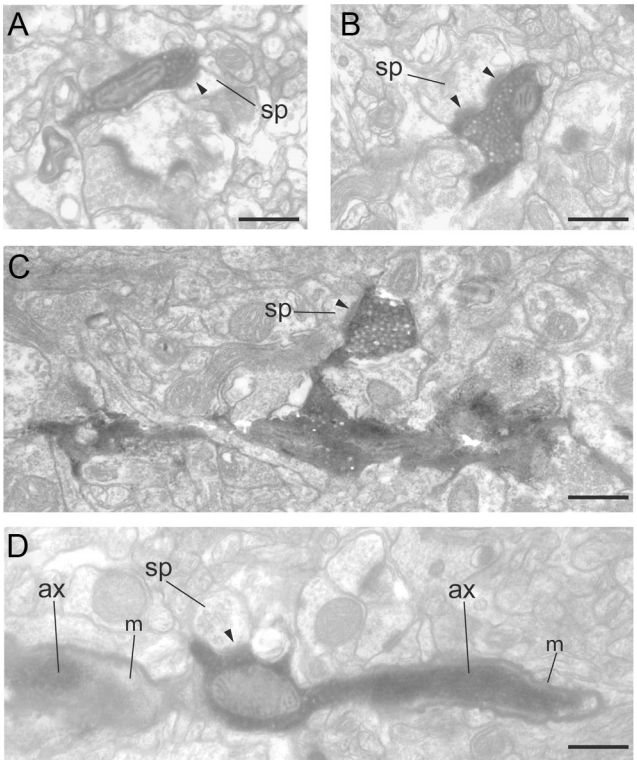

Figure 6. Electron micrographs of BDA-labeled axons and synaptic boutons in layers 1 and 2/3 of area 46. ***A***, A labeled bouton forms an asymmetric synapse (solid arrowhead) with a small spine (sp) in layer 1. ***B***, A labeled bouton forms a perforated asymmetric synapse (solid arrowheads) with a medium-sized spine (sp) in layer 1. ***C***, A labeled bouton terminal forms an asymmetric synapse (solid arrowhead) with a small spine (sp) in layer 2/3. The labeled bouton can be traced back to the main axon. ***D***, A labeled bouton *en passant* forms an asymmetric synapse (solid arrowhead) with a small spine (sp) in layer 2/3. The bouton forms part of the path of the labeled axon (ax) and emerges from an interruption in the myelin sheath (m). Scale bars, 0.5 μm.

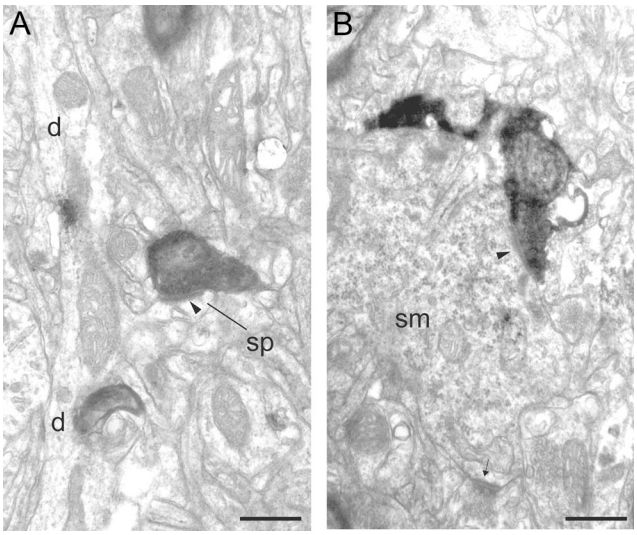

Figure 7. Electron micrographs of BDA-labeled boutons in layer 4 and 5/6 of area 46. ***A***, A labeled bouton forms an asymmetric synapse (solid arrowhead) with a small spine (sp) in layer 4. The spine (sp) can be traced back to the parent dendrite (d). ***B***, A labeled bouton forms an asymmetric synapse (solid arrowhead) with a neuronal soma (sm) in layer 5/6 that also forms a second asymmetric synapse (small arrow) with an unidentified bouton. The soma forms numerous asymmetric synapses and contains many perikaryal organelles and rough endoplasmic reticulum. These features are characteristic of neurons with smooth dendrites that are GABAergic. Scale bars, 0.5 μm.

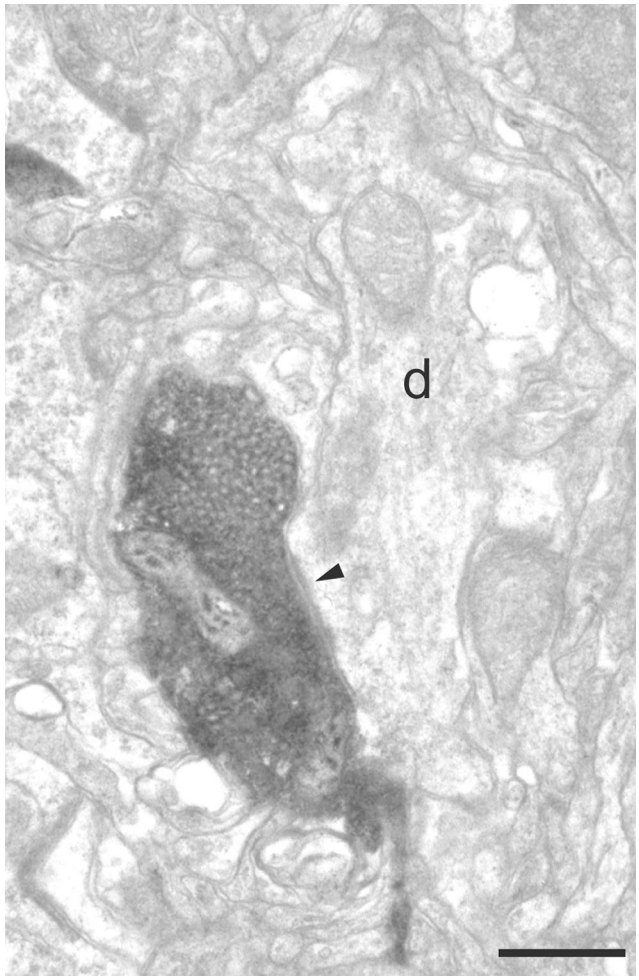

Figure 8. Electron micrographs of a BDA-labeled bouton in layer 2/3 of area 46. The labeled bouton forms an asymmetric synapse (solid arrowhead) with a dendritic shaft (d). The dendrite was seen to contain numerous mitochondria and forms asymmetric synapses with unidentified boutons in subsequent sections. These features are characteristic of neurons with smooth dendrites that are GABAergic. Scale bar, 0.5 μm.

LIP. In the small iontophoretic injection sites in layer 2/3, 6.25% of spines showed dual input.

Dendrites

Dendritic shafts represented only a small proportion of the synaptic targets: 13% in V4, 5% in area 46 (Fig. 8), 16% in LIP, and 22% in FEF. Typically, excitatory cells have spiny dendrites that contain few mitochondria and form few synapses on their dendritic shafts. In contrast, the dendrites of inhibitory cells are spine free or smooth, contain numerous mitochondria, and form relatively more synapses on the shaft. They may also have widely variable diameter over their length. Dendrites with these characteristics contain γ-aminobutyric acid (GABA) and are GABAergic (Somogyi et al., 1983; Peters and Saint Marie, 1984; Kisvárday et al., 1985; Ahmed et al., 1997). The majority of dendritic shafts were small in diameter ($\sim$0.5 μm or less), and serial sections were usually required to characterize neurons as smooth or spiny. On the basis of the established criteria, most of the target dendritic shafts originated from smooth, putative GABAergic neurons. The dendritic shaft targets of intrinsic FEF synapses formed 13.4% (11 of 82) of all targets. Of these, 61% (11 of 18) were smooth and GABAergic in appearance. In area 46, all of the dendritic shafts (100%) were of smooth GABAergic neurons (4.8%

of all targets), 22% in V4 (2.4% of all targets), and 55% in LIP (8.5% of all targets). One of the area 46 target dendrites of layer 1 forming multiple asymmetric shaft synapses also bore a synaptic spine. We have noted this unusual configuration previously among the profiles of layer 1, and this is probably a characteristic of GABAergic neurons of layer 1.

Somata

Only one synapse was formed with a soma, which was located in layer 5 of area 46 (Fig. 7*B*). Although the profile of the soma was very small in our series of sections (a section through the edge of the soma), there were enough features to classify the neuron as GABAergic. There were numerous asymmetric synapses formed with unidentified boutons, and the cytoplasm was filled with rough endoplasmic reticulum and perikaryal organelles, which are characteristic features of GABAergic neurons (Somogyi et al., 1983).

Postsynaptic density. Reconstructing the boutons and their targets gave us the opportunity to measure the area of the complete PSD (see Fig. 11). We have used this technique previously to obtain values for the surface area of synapses (Anderson et el., 1998; Anderson and Martin, 2002, 2005, 2006, 2009). By focusing on the PSD rather than the presynaptic membrane, we avoided the difficulties that details might be obscured by the reaction end-product in the presynaptic bouton. Due to the small numbers of dendritic synapses, we confined our comparisons between the distributions of synaptic areas to synapses made by spines. There were relatively few significant differences seen between those spinous synapses made in different areas or different laminae. The range of synaptic areas on spines (~0.07–0.13 μm^2) was similar to those of previous studies of inter-areal connections (Anderson et al., 1998; Anderson and Martin, 2002, 2005, 2006, 2009). The areas of layer 1 PSDs were consistently the largest and those from layers 4 and 5/6 consistently the smallest. Within V4, PSD areas showed no significant laminar differences with the exception of layer 1 synapses (mean = 0.103 μm^2, SEM = 0.012), which were larger ($p = 0.09$, two-tailed t test) than those of layer 4 (mean = 0.078 μm^2, SEM = 0.007). In area 46, both layer 1 synapses (mean = 0.098 μm^2, SEM = 0.008) and synapses located in layers 2 and 3 (mean = 0.082 μm^2, SEM = 0.005) had significantly larger PSDs ($p = 0.0005$ and 0.04, respectively, two-tailed t test) than did synapses of layer 4 (mean = 0.067 μm^2, SEM = 0.005). The PSDs of LIP synapses showed the most significant differences. Layer 1 PSDs were significantly larger (mean = 0.131 μm^2, SEM = 0.014) than those of synapses in layers 2 and 3 (mean = 0.095 μm^2, SEM = 0.007, $p = 0.020$), layer 4 (mean = 0.075 μm^2, SEM = 0.007, $p = 0.0006$), and layer 5/6 (mean = 0.075 μm^2, SEM = 0.005, $p = 0.0004$, two-tailed t test). PSDs from layer 2/3 were just significantly larger than those of layer 4 ($p = 0.050$, two-tailed t test) and layer 5/6 ($p = 0.030$, two-tailed t test). When comparing the PSD sizes of synapses between areas, the only significant difference came from the labeled synapses of layer 1 in LIP, which had slightly larger PSDs than those of area 46 (mean = 0.098 μm^2, SEM = 0.002, $p = 0.030$, two-tailed t test). Labeled spine synapses from the two superficial layer iontophoretic injection sites showed no differences in PSD sizes and so were pooled (mean = 0.139 μm^2, SEM = 0.012).

Synapses formed with dendritic shafts were few and had consistently smaller PSDs (V4: 0.073 μm^2, SEM = 0.015; area 46: 0.074 μm^2, SEM = 0.006; LIP: 0.076 μm^2, SEM = 0.010) than the spine synapses (V4: 0.089 μm^2, SEM = 0.004; area 46: 0.09 μm^2, 0.007; LIP: 0.095 μm^2, SEM = 0.005). When pooled, the PSDs of dendritic synapses of V4, area 46, and LIP were not significantly different from one another. However, on target dendritic shafts of putative GABAergic cells ($n = 11$), the mean size of the PSDs ($n = 36$; 0.068 μm^2, SEM = 0.006) formed by the FEF boutons was significantly larger than that of PSDs formed by unlabeled boutons on the same dendritic shafts ($n = 39$; 0.045 μm^2, SEM = 0.003; Wilcoxon rank $p = 0.003$).

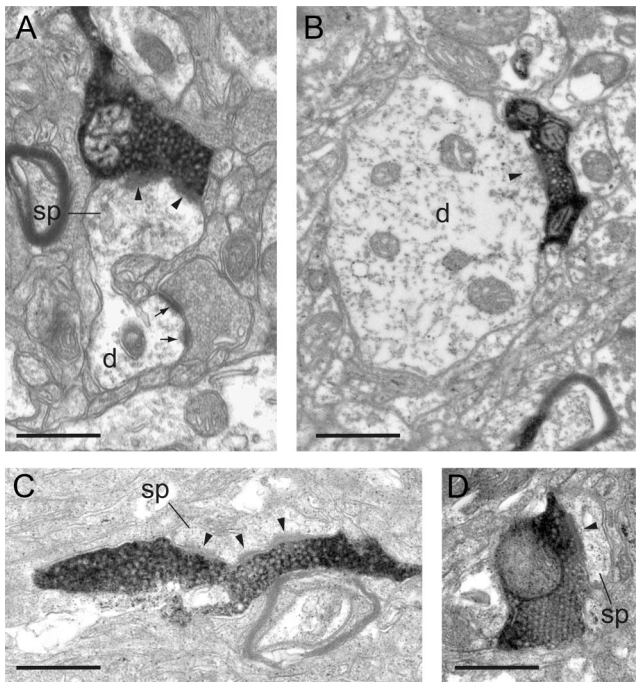

Figure 9. Electron micrographs of BDA-labeled boutons in layers 1, 2/3, 4, and 5/6 of area LIP. ***A***, A labeled bouton of layer 1 forms an asymmetric synapse (solid arrowhead) with a large spine (sp) that can be followed back to the parent dendrite (d). ***B***, A labeled bouton in layer 2/3 forms an asymmetric synapse (solid arrowhead) with a large-diameter dendritic shaft (d). The dendrite formed asymmetric synapses with unidentified boutons and contained numerous mitochondria. These features are characteristic of neurons with smooth dendrites and that are GABAergic. ***C***, A slender, labeled bouton in layer 4 forms a perforated synapse (solid arrowhead) with a spine (sp). ***D***, A vesicle-packed labeled bouton in layer 5/6 forms a synapse (solid arrowhead) with a spine (sp). Scale bars, 0.5 μm.

Viewed *en face*, the shape of the PSD was a simple disc, or doughnut, or horseshoe shaped. In single sections these latter synapses appear to be perforated. They were more frequently formed with spines than dendritic shafts (Fig. 6*B*). Similar observations were made in the study of synapses made by reciprocal V1 and V2 boutons, V1 and V2 afferent boutons in area MT, V2 afferent boutons in area V3A, and V4 afferent boutons in V2 (Anderson et al., 1998; Anderson and Martin, 2002, 2005, 2006, 2009).

Target types. Spines were the dominant target in all layers and all areas (Figs. 3–7*A*, 9; see Fig. 12). A slightly higher proportion of spine synapses was found in area 46 (95%) than in V4 (89%), LIP (84%), or FEF (78%). Within each cortical area there were also differences in the proportion of synapses formed with spines and dendrites in respective laminae. The range of numbers of spine synapses across different laminae was 92–96% for area 46, 84–92% for V4, and 78–93% for LIP. The remaining targets were dendritic shafts. Of these, smooth GABAergic neurons provided the majority of the dendritic shaft targets in LIP (55%) and FEF (61%), respectively, all of those in area 46 (Fig. 8), and 22% of those in V4.

Serial reconstructions indicated that most boutons made only one synapse and only rarely made two or more synapses (Fig. 5*B*;

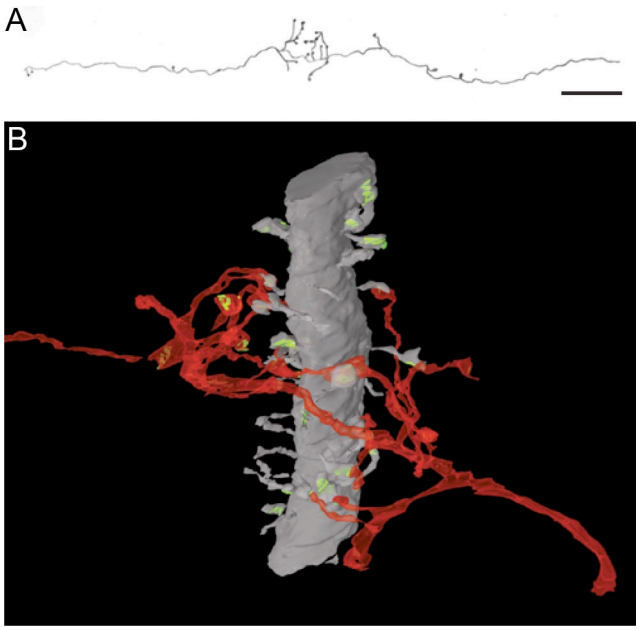

Figure 10. ***A***, LM reconstruction of axon shown in ***B***. ***B***, Three-dimensional reconstruction of BDA-labeled axon (red) in layer 2/3 of area V4 from serial ultrathin sections. The main trajectory of the axon is right to left and is roughly orthogonal to the radially aligned large-caliber dendrite (gray) (approximately 2 μm in diameter). The dendrite is spine bearing (also gray), and all reconstructed spines formed a synapse (green). At the point of intersection of the dendrite and the axon, the latter produces a flurry of mostly bouton terminals. Eleven of these labeled boutons form synapses with spines coming from the reconstructed dendrite. Ten more of the labeled boutons formed synapses with spines (data not shown) that could not be traced back to the large dendrite. One labeled bouton formed a synapse with a small dendrite and one formed no synapse. The large dendrite shows many features characteristic of the apical dendrite of a large pyramidal neuron. Scale bar (***A***): 12 μm.

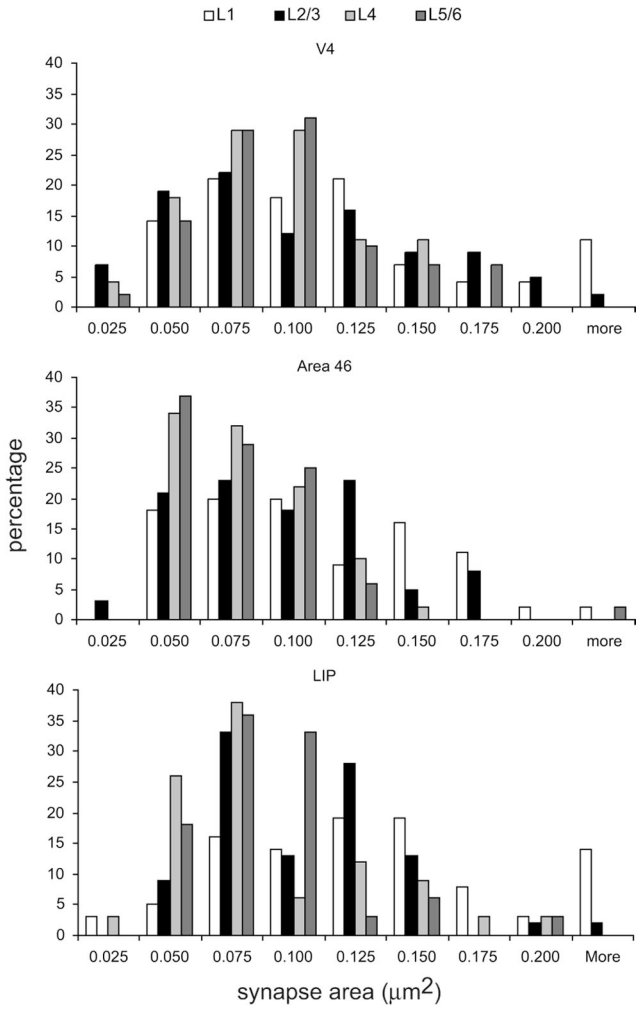

Figure 11. Histograms of the distribution of postsynaptic areas (μm^2) formed with spines and labeled FEF boutons in layers 1, 2/3, 4, and 5/6 of areas V4, 46, and LIP.

see Fig. 13). On average, there were 1.05 synapses per labeled bouton, both for V4 and area 46, and 1.03 in LIP. Exceptionally, a bouton might form three or even four synapses, each on a different target dendrite. A single bouton that formed four synapses was found in layer 5/6 of area 46. The multisynaptic boutons tended to have larger than average diameters, up to 1 μm.

We have rarely encountered multiple synapses formed on a target dendrite by the same axon. This may be simply due to the short lengths of dendrite that can be followed in serial electron microscopy. However, from detailed LM observations, we identified one possible multisynaptic configuration. In the light microscope we followed an unbranched axon, which passed through layer 2/3 of V4, covering a distance of ~400 μm within a single section and showing few features, other than the occasional bouton terminal. At one point, however, it produced a spray of fine bouton terminals over a very limited length of axon (11 μm). At the EM level, the cluster of labeled boutons was found to form synapses with 21 spines and one small-diameter dendrite. One bouton did not form a synapse (Fig. 10). Eleven target spines were followed back to a large-diameter (~2 μm), radially oriented dendrite. The dendrite contained many microtubules and few mitochondria, and formed numerous synaptic spines and very few dendritic shaft synapses, but it could not be traced back to a parent soma. These ultrastructural features are characteristic of the apical dendrite of a large layer 3 or layer 5 pyramidal cell (Fig. 10).

Synaptic density measurement

Using the RESORS method (da Costa et al., 2009), we estimated the relative proportion of labeled synapses in LIP that appeared to be the most densely innervated region we found after a tracer injection in FEF. We developed this method to estimate accurately synapse numbers when they were sparsely distributed. Previously, we sampled from an area that contained a labeled synapse, which we recognized biased our sampling procedure. Without this priming, however, we counted no labeled synapses with standard physical dissector sampling. Using RESORS, this bias is removed. We sampled at random from many (~1000) small sites in layers 1 and 2 of LIP in one animal. We estimated that only 0.16% of synapses in layer 1 were formed by labeled boutons, despite the fact that in the light microscope it appeared as the most densely labeled layer of LIP. In layer 2, the next most densely innervated layer, this value fell to 0.04%.

Discussion

We have investigated the hypothesis that the attentional signal from area 8A, or FEF, is transmitted by a monosynaptic connection from FEF neurons selectively to GABAergic neurons in areas 46, V4, and LIP. This hypothesis was originally proposed to account for the observation that during attention, fast-spiking neurons of areas V4 and 46 increase their firing relative to regular-spiking neurons. Since the fast-spiking neurons are thought to be putative GABAergic neurons of the parvalbumin subtype (Mitchell et al., 2007), this selective activation of inhibition is consistent with normalization models of attention,

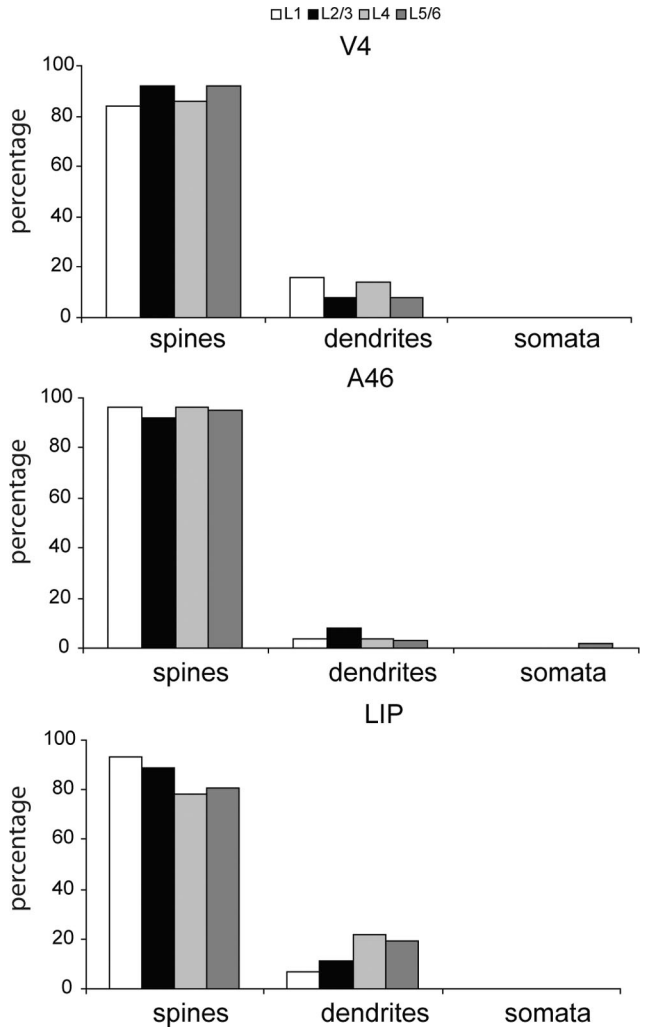

Figure 12. Histograms of the synaptic targets of labeled FEF boutons in layers 1, 2/3, 4, and 5/6 of areas V4 (147 spines, 19 dendrites), 46 (190 spines, 10 dendrites, 1 soma), and LIP (169 spines, 31 dendrites).

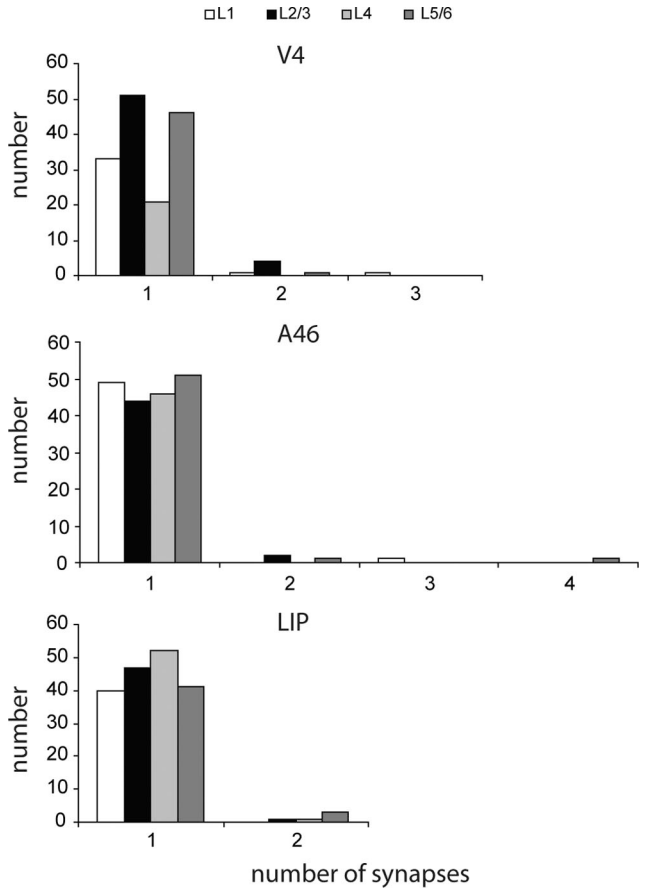

Figure 13. Histogram of the number of synapses formed per labeled FEF bouton in layers 1, 2/3, 4, and 5/6 of areas V4, 46, and LIP.

which rely on divisive inhibition (Reynolds and Heeger, 2009), and with attention-dependent response synchronization due to fast inhibition (Fries et al., 2001). However, our data do not support the hypothesis that FEF has private lines to the inhibitory circuits of its target areas. The data that led us to this conclusion are as follows.

FEF projections excite mainly pyramidal cells in areas 46, V4, and LIP

Our data indicate that FEF connects predominantly to pyramidal cells in areas 46, V4, and LIP. The neurons of FEF that project to V4, area 46, and LIP provide input to both superficial and deep layer pyramidal cells. If anything, more spines are targeted (89% in V4, 95% in area 46, 84% in LIP) than for most other pathways we have examined (V1 to MT, 54%; V2 to MT, 67%; V2 to V3a, 76%; V4 to V2, V1 to V2, 72%; V2 to V1 84%; Anderson et al., 1998; Anderson and Martin, 2002, 2005, 2006, 2009; see also Rockland, 1997). Apart from one soma, the dendritic shafts of smooth (putative GABAergic) and spiny neurons make up the remaining targets of the FEF projection in roughly equal proportion.

Significance of laminar specificity

Attentional signals are particularly prominent in V4, influencing 73% of recorded neurons according to the recent study by Buffalo et al. (2010). FEF afferents are unusual in forming synapses in all layers of V4. In addition, retrograde tracer studies show that the projection from FEF to V4 arises mainly from superficial layer cells, not the deep layer cells typically associated with "feedback" projections (Barone et al., 2000; Pouget et al., 2009; Markov et al., 2011). The FEF projection connections could excite neurons weakly to provide a stochastic resonance-like mechanism that biases the local circuits for top-down versus bottom-up saliency (Baluch and Itti, 2011).

One difficulty with any explanation is quantitative: our previous estimates of inter-areal bouton density indicated that they contribute only 2–6% of excitatory synapses in their densest patches of innervation (Anderson and Martin, 2002, 2005, 2006). This is already low, but because we were able to eliminate the sampling bias acknowledged in our previous studies (da Costa et al., 2009), we find here that the unbiased densities are even lower, $<$0.16% of excitatory synapses. This weak input to V4 is consistent with the "weight" measured in terms of the number of FEF neurons that contribute to the V4 projection. This weight value is several orders of magnitude lower than that seen for the heaviest cortical input and the thalamic input to V1 (Markov et al., 2011). Such low values imply that the number of synapses FEF contributes to any target neuron is probably in single digits. The question, then, is how the FEF projections come to be at all effective.

Amplification via recurrent circuits?

The minimal excitatory input from FEF might be amplified by local recurrent circuits in much the same way that the small thalamic input is amplified in visual cortex. We found evidence for such recurrent circuits within FEF itself, where pyramidal cells connect mainly with other pyramidal cells (87%), the remaining 13% of synapses being with GABAergic neurons. This ratio is typical of local cortical circuits: the sole exception is for area 9 of macaque prefrontal cortex, where Melchitzky et al. (2001) reported that pyramidal cells divide their local output equally between spines and GABAergic dendrites.

Recurrent circuits of excitatory and inhibitory neurons can readily be configured to express a rich palette of computational primitives, including amplification, signal restoration, and decision-making (Douglas and Martin, 2004, 2007). Our biologically based model of FEF microcircuits (Heinzle et al., 2007) exploits some of these computational primitives to compute a saliency map in the middle layers and an attentional signal in the superficial layers (whose pyramidal neurons provide the major output to areas 46, LIP, and V4; Markov et al., 2011). Recent recordings from FEF by Cohen et al. (2010) indicated that there is an increased interaction between pairs of cells that are involved in the attentional selection of a target embedded in distractors. Their data are consistent with a soft winner-take-all operation in which excitation between neurons with similar parameter preferences is amplified, and those with dissimilar or competing preferences are suppressed by inhibition (Douglas and Martin, 2004).

The role of these local circuits also goes some way to explain the mismatch in the latency to the attention-driven changes. We found that the FEF afferents were myelinated, even in the gray matter, and thus the conduction time from FEF to V4, the most caudal area we examined, is probably 10–20 ms, in agreement with indirect estimates of 8–13 ms (Gregoriou et al., 2009), whereas the latencies of attention are an order of magnitude longer (Buffalo et al., 2010). The explanation for this is probably the time for recurrent processing in local circuits (Baluch and Itti, 2011).

Amplification by synapse strength?

The postsynaptic densities formed between FEF afferents and the smooth dendrites of putative GABAergic neurons were larger than the unlabeled asymmetric synapses formed on the same smooth dendrites, albeit smaller than FEF synapses formed with spines. The unlabeled asymmetric synapses, which were much more numerous, presumably originated mainly from the recurrent collaterals of local pyramidal cells (Binzegger et al., 2004; Markov et al., 2011). We assume that larger postsynaptic densities correlate with physiological strength, so the larger synapses on GABAergic dendrites may partially compensate for the tiny number of synapses delivered to V4 by FEF.

We found that synapses in the superficial layers were consistently larger than those of layers 4, 5, and 6, although this difference was only significant in the case of LIP. The smallest synapses were those in layer 4, though not significantly so. The largest synapses were formed in layer 1, which might indicate that FEF input to the pyramidal cells' apical tufts in layer 1 evoke larger EPSPs than synapses in other layers.

Amplification by apical dendrites?

The FEF afferents form synapses with the apical dendrites of pyramidal cells, and it is possible that this input is amplified by an active calcium conductance in the apical dendrites of pyramidal cells (Larkum and Zhu, 2002; Larkum et al., 2007). Our data also indicated the existence, albeit rare, of a highly focused, multiple synaptic innervation, as revealed by the 11 excitatory inputs from a single labeled axon to one small region of a putative apical dendrite in layer 2/3 of V4. It may be that this focused input to the main shaft of the apical dendrite is also "just enough" (Douglas and Martin, 2007) to have a consequence on spike output. Certainly, the probability of activating downstream neurons (Moore and Fallah, 2004; Armstrong et al., 2006; Armstrong and Moore, 2007) or BOLD signal (Ruff et al., 2006) is increased by the highly synchronized FEF output evoked by electrical or magnetic stimulation, which effectively produces attention-like changes in neuronal activity. However, Ekstrom et al. (2008) claim that the top-down modulation only acts if there is also bottom-up activity.

Circuits of attention

To explain the effects of FEF on attention, there are two competing ideas. One is that attention increases the signal-to-noise ratio (Tolhurst et al., 1983; McAdams and Maunsell, 1999; for review, see Salinas and Sejnowski, 2001; Reynolds and Heeger, 2009; Baluch and Itti, 2011), which could be achieved if the FEF neurons synchronize their output and drive their target inhibitory neurons more strongly and with less variance (Mitchell et al., 2007). The other idea is that the attentional signal reduces the correlation in the firing of the target neurons (Cohen and Maunsell, 2009; Mitchell et al., 2009), thus allowing the independent noise contributed by individual neurons to be averaged out. In the first case, the prediction is that the inhibitory neurons are more active in reducing background noise. In the second case, where there is decreased noise correlation, the prediction is that the inhibitory influence is reduced (Cohen and Maunsell, 2009). Could we reconcile these functional data with our structural data by supposing that FEF drives selectively a disinhibitory circuit in V4? The answer is no, for the reason that our structural data indicate that most of the targets of the FEF projection are pyramidal cells, whereas the functional data indicate that the principal change in firing during attention occurs selectively in putative inhibitory neurons (Mitchell et al., 2007). These yet unresolved puzzles indicate how incomplete our understanding is of the wiring of the inter- and intra-areal circuits that form the "pathways of attention."

References

Ahmed B, Anderson JC, Martin KAC, Nelson JC (1997) Map of the synapses onto layer 4 basket cells of the primary visual cortex of the cat. J Comp Neurol 380:230–242.

Anderson JC, Martin KAC (2002) Connection from cortical area V2 to MT in macaque monkey. J Comp Neurol 443:56–70.

Anderson JC, Martin KAC (2005) Connection from cortical area V2 to V3A in macaque monkey. J Comp Neurol 488:320–330.

Anderson JC, Martin KAC (2006) Synaptic connection from cortical area V4 to V2 in macaque monkey. J Comp Neurol 495:709–721.

Anderson JC, Martin KAC (2009) The synaptic connections between cortical areas V1 and V2 in macaque monkey. J Neurosci 29:11283–11293.

Anderson JC, Binzegger T, Martin KAC, Rockland KS (1998) The connection from cortical area V1 to V5: A light and electron microscopic study. J Neurosci 18:10525–10540.

Armstrong KM, Moore T (2007) Rapid enhancement of visual cortical response discriminability by microstimulation of the frontal eye field. Proc Natl Acad Sci U S A 104:9499–94504.

Armstrong KM, Fitzgerald JK, Moore T (2006) Changes in visual receptive fields with microstimulation of frontal cortex. Neuron 50:791–798.

Balan PF, Ferrera VP (2003) Effects of gaze shifts on maintenance of spatial memory in macaque frontal eye field. J Neurosci 23:5446–5454.

Baluch F, Itti L (2011) Mechanisms of top-down attention. Trends Neurosci 34:210–224.

Barbas H, Mesulam MM (1981) Organization of afferent input to subdivisions of area 8 in the rhesus monkey. J Comp Neurol 200:407–431.

Barbas H, Pandya DN (1989) Architecture and intrinsic connections of the prefrontal cortex in the rhesus monkey. J Comp Neurol 286:353–375.

Barone P, Batardiere A, Knoblauch K, Kennedy H (2000) Laminar distribution of neurons in extrastriate areas projecting to visual areas V1 and V4 correlates with the hierarchical rank and indicates the operation of a distance rule. J Neurosci 20:3263–3281.

Binzegger T, Douglas RJ, Martin KAC (2004) A quantitative map of the circuit of cat primary visual cortex. J Neurosci 24:8441–8453.

Buffalo EA, Fries P, Landman R, Liang H, Desimone R (2010) A backward progression of attentional effects in the ventral stream. Proc Natl Acad Sci U S A 107:361–365.

Buschman TJ, Miller EK (2009) Serial, covert shifts of attention during visual search are reflected by the frontal eye fields and correlated with population oscillations. Neuron 63:386–396.

Clavagnier S, Falchier A, Kennedy H (2004) Long-distance feedback projections to area V1: implications for multimodal integration, spatial awareness and visual consciousness. Cogn Affect Behav Neurosci 4:117–126.

Cohen HR, Maunsell JH (2009) Attention improves performance primarily by reducing interneuronal correlations. Nat Neurosci 12:1594–1600.

Cohen JY, Crowder EA, Heitz RP, Subraveti CR, Thompson KG, Woodman GF, Schall JD (2010) Cooperation and competition among frontal eye field neurons during visual target selection. J Neurosci 30:3227–3238.

da Costa NM, Hepp K, Martin KAC (2009) A systematic random sampling scheme optimized to detect the proportion of rare synapses in the neuropil. J Neurosci Methods 180:77–81.

Douglas RJ, Martin KAC (2004) Neuronal circuits of the neocortex. Annu Rev Neurosci 27:419–451.

Douglas RJ, Martin KAC (2007) Mapping the matrix: The ways of neocortex. Neuron 56:226–238.

Ekstrom LB, Roelfsema PR, Arsenault JT, Bonmassar G, Vanduffel W (2008) Bottom-up dependent gating of frontal signals in early visual cortex. Science 321:414–417.

Ferrera VP, Yanike M, Cassanello C (2009) Frontal eye field neurons signal changes in decision criteria. Nat Neurosci 12:1458–1462.

Ferrier D (1874) The localization of function in the brain. Proc R Soc Lond Biol Ser B 22:229–232.

Fiala JC (2005) Reconstruct: a free editor for serial section microscopy. J Microsc 218:52–61.

Fries P, Reynolds JH, Rorie AE, Desimone R (2001) Modulation of oscillatory neuronal synchronization by selective visual attention. Science 291:1560–1563.

Goldberg ME, Bushnell MC (1981) Behavioral enhancement of visual responses in monkey cerebral cortex. II. Modulation in frontal eye fields specifically related to saccades. J Neurophysiol 46:773–787.

Gregoriou GG, Gotts SJ, Zhou H, Desimone R (2009) High-frequency, long-range coupling between prefrontal and visual cortex during attention. Science 324:1207–1210.

Heinzle J, Hepp K, Martin KAC (2007) A microcircuit model of the frontal eye fields. J Neurosci 27:9341–9353.

Huerta MF, Krubitzer LA, Kaas JH (1987) Frontal eye field as defined by intracortical microstimulation in squirrel monkeys, owl monkeys, and macaque monkeys. II. Cortical connections. J Comp Neurol 265:332–361.

Hussar CR, Pasternak T (2009) Flexibility of sensory representations in prefrontal cortex depends on cell type. Neuron 10:730–743.

Kayser C, Logothetis N (2006) Vision: stimulating your attention. Curr Biol 16:R581–R583.

Kisvárday ZF, Martin KAC, Whitteridge D, Somogyi P (1985) Synaptic connections of intracellularly filled clutch neurons, a type of small basket neuron in the visual cortex of the cat. J Comp Neurol 241:111–137.

Larkum ME, Zhu JJ (2002) Signaling of layer 1 and whisker evoked Ca^{2+} and Na + action potentials in distal and terminal dendrites of neocortical pyramidal neurons *in vitro* and *in vivo*. J Neurosci 22:6991–7005.

Larkum ME, Waters J, Sakmann B, Helmchen F (2007) Dendritic spikes in apical dendrites of neocortical layer 2/3 pyramidal neurons. J Neurosci 27:8999–9008.

Lennert T, Martinez-Trujillo J (2011) Strength of response suppression to distracter stimuli determines attentional-filtering performance in primate prefrontal neurons. Neuron 70:141–152.

Luck SJ, Chelazzi L, Hillyard SA, Desimone R (1997) Neural mechanisms of spatial selective attention in areas V1, V2, and V4 of macaque visual cortex. J Neurophysiol 77:24–42.

Markov NT, Misery P, Falchier A, Lamy C, Vezoli J,Quilodran R, Gariel MA, Giroud P, Ercsey-Ravasz M, Pilaz LJ, Huissoud C, Barone P, Dehay C, Toroczkai Z, Van Essen DC, Kennedy H, Knoblauch K (2011) Weight consistency specifies regularities of macaque cortical networks. Cereb Cortex 21:1254–1272.

McAdams CJ, Maunsell JH (1999) Effects of attention on the reliability of individual neurons in monkey visual cortex. Neuron 23:765–773.

McAdams CJ, Maunsell JH (2000) Attention to both space and feature modulates neuronal responses in macaque area V4. J Neurophysiol 83:1751–1755.

Melchitzky DS, González-Burgos G, Barrionuevo G, Lewis DA (2001) Synaptic targets of the intrinsic axon collaterals of supragranular pyramidal neurons in monkey prefrontal cortex. J Comp Neurol 430:209–221.

Mitchell JF, Sundberg KA, Reynolds JH (2007) Differential attention-dependent response modulation across cell classes in macaque visual area V4. Neuron 55:131–141.

Mitchell JF, Sundberg KA, Reynolds JH (2009) Spatial attention decorrelates intrinsic activity fluctuations in macaque area V4. Neuron 63:879–888.

Moore T, Fallah M (2001) Control of eye movements and spatial attention. Proc Natl Acad Sci U S A 98:1273–1276.

Moore T, Fallah M (2004) Microstimulation of the frontal eye field and its effects on covert spatial attention. J Neurophysiol 91:152–162.

Peters A, Saint Marie RL (1984) Smooth and sparsely spinous nonpyramidal cells forming local axonal plexuses. In: Cerebral cortex, Vol 1, Cellular components of the cerebral cortex (Jones EG, Peters A, eds), pp 419–445. New York: Plenum.

Peters A, Palay SL, Webster HDeF (1991) The fine structure of the nervous system: neurons and their supporting cells, Ed 3. New York: Oxford OUP.

Pouget P, Stepniewska I, Crowder EA, Leslie MW, Emeric EE, Nelson MJ, Schall JD (2009) Visual and motor connectivity and the distribution of calcium-binding proteins in macaque frontal eye field: implications for saccade target selection. Front Neuroanat 3:2.

Reynolds JH, Heeger DJ (2009) The normalization model of attention. Neuron 61:168–185.

Reynolds JH, Chelazzi L, Desimone R (1999) Competitive mechanisms subserve attention in macaque areas V2 and V4. J Neurosci 19:1736–1753.

Reynolds JH, Pasternak T, Desimone R (2000) Attention increases sensitivity of V4 neurons. Neuron 26:703–714.

Robinson DA, Fuchs AF (1969) Eye movement evoked by stimulation of frontal eye fields. J Neurophysiol 32:637–648.

Rockland KS (1997) Elements of cortical hierarchy revisited. In: Cerebral cortex, Vol 12, Extrastriate cortex in primates (Rockland KS, Kaas JH, Peters A, eds), pp 243–293. New York: Plenum.

Ruff CC, Blankenburg F, Bjoertomt O, Bestmann S, Freeman E, Haynes JD, Rees G, Josephs O, Deichmann R, Driver J (2006) Concurrent TMS-fMRI and psychophysics reveal frontal influences in human retinotopic visual cortex. Curr Biol 16:1479–1488.

Saleem KS, Logothetis NK (2007) The rhesus monkey brain in stereotaxic coordinates. New York: Elsevier Academic.

Salinas E, Sejnowski TJ (2001) Correlated neuronal activity and the flow of neural information. Nat Rev Neurosci 2:539–550.

Schiller PH, True SD, Conway JL (1979) Effects of frontal eye field and superior colliculus ablations on eye movements. Science 206:590–592.

Somogyi P, Kisvárday ZF, Martin KAC, Whitteridge D (1983) Synaptic connections of morphologically identified and physiologically characterized large basket cells in the striate cortex of cat. Neuroscience 10:261–294.

Stanton GB, Bruce CJ, Goldberg ME (1995) Topography of projections to posterior cortical areas from the macaque frontal eye fields. J Comp Neurol 353:291–305.

Stanton GB, Friedman HR, Dias EC, Bruce CJ (2005) Cortical afferents to the smooth-pursuit region of the macaque monkey's frontal eye field. Exp Brain Res 165:179–192.

Tolhurst DJ, Movshon JA, Dean AF (1983) The statistical reliability of signals in single neurons in cat and monkey visual cortex. Vision Res 23:775–785.

Chapter 4 General Discussion

4.1 The Labeled Hierarchy

The observations of Rockland have become part of the understanding we use today that helps guide us through the interareal connectivity of macaque cortex. We found a great deal of our own labeled interareal axon material formed patterns similar to those reported in earlier publications. Like Rockland and Pandya (1979) we found axons passing from caudal to rostral in early visual cortices mostly terminated in layer 4 and in the reverse direction terminated mostly in layer 1. This is the basis for the idea of feedforward and feedback connectivity (Maunsell and Van Essen, 1983; Felleman and Van Essen, 1991) often associated with bottom up and top down processing within cortex and in models of bottom up object recognition for example (Grossberg and Mingolla, 1985; Li, 1998; Mumford, 1992). The findings in this collection of publications (Anderson et al, 1998, Anderson and Martin 2002, 2005, 2006, 2009, Anderson et al, 2011), are in agreement with those of others at the light microscopic level but nonetheless offered up surprises that could alter our interpretation of a pathway. What is instantly striking is how different each projection appears. When a drawing of a strip of cortex and its labeled axon and boutons is compared with strips containing label from other areas this difference becomes most clear (Fig 1). Rockland and colleagues often reported on the spread of axons beyond the principle target zone (e g. Rockland and Virga, 1990; Rockland, 1992). This spreading factor associated probably with most pathways was most noticeable in our sample when the label was dense or when we reconstructed axon processes from over several serial sections and then superimposed sections together (Fig. 1). The appearance of labeled FEF axon in all layers of V4 for example does not comply with the Felleman and Van Essen picture of that path being a feedback

pathway. Instead, from our data, it looks more like a columnar or lateral connection and so resembles more closely the prediction of Markov and Kennedy (2013) using the SLN method of hierarchical determination. There were differences also in the distribution of label in LIP that were striking. The labeled profiles could innervate all laminae and specially layer 1 but clearly not upper layer 4 and lower layer 3 or it could innervate all laminae equally (Fig 1). The different innervation patterns no doubt relate to different groups of projection cells being labeled. One possible source of difference could be related to whether the injection of tracer was made in dorsal or ventral FEF which was the case in the injections made in one of our animals. Dorsal FEF has been shown to be involved in making small saccadic eye movements and ventral FEF being involved with larger and smooth pursuit eye movements (MacAvoy et al, 1991). The labeling of profiles in our sections was dense enough to prevent individual axons being reconstructed, which gives a slightly different perspective from the findings of Rockland (1997). She noted that at the level of individual axons innervation could pass from lower layer 4 to upper layer three, 'almost indiscriminately' (Rockland, 1997; Budd 1998). The principle object of the papers presented here however was to examine labeled axons and their boutons at the synaptic level using the EM (summary in Fig. 2).

Figure 1

Light microscopic reconstructions of BDA- labeled terminals and their boutons in visual and attentional cortex. The reconstruction is taken from 80 μm thick sections of cortex. In the case of FEF to V4 two adjacent sections were used. The drawing were all made at the same magnification. Lamina boundaries are indicated to the left or right of the strip of cortex, white matter at the bottom. FEF to LIP is composed of 3 strips of cortex from LIP. The two lower left strips are from the termination zone of a dorsal injection in FEF, the left most is from a more central region of the zone and the next right is taken from a more peripheral site of the same zone. The next right strip of LIP cortex is taken from a ventral FEF injection. Scale bar = 100 μm.

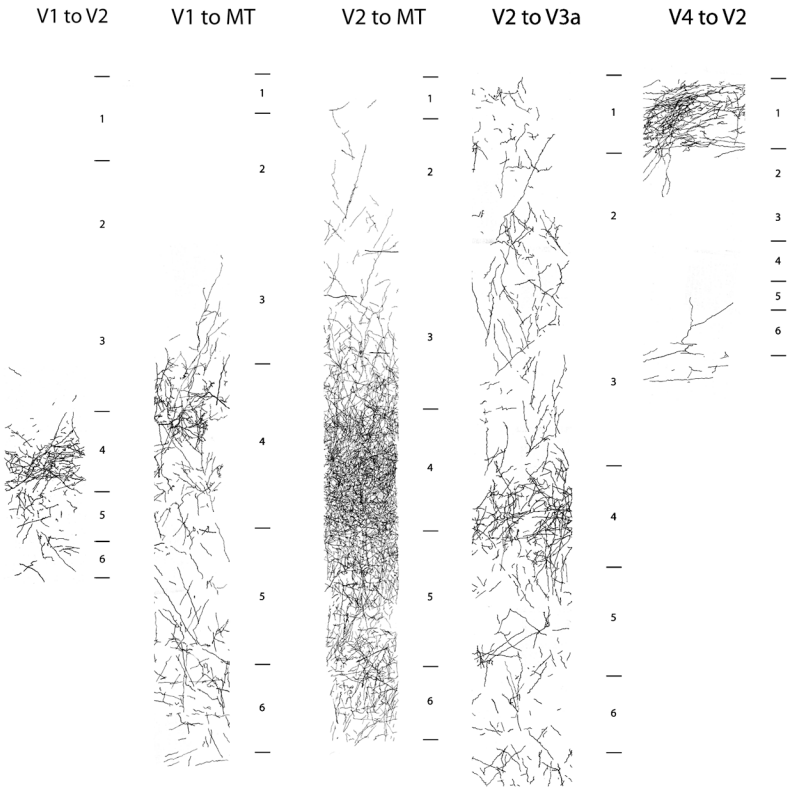
V1 to V2
V1 to MT
V2 to MT
V2 to V3a
V4 to V2
FEF to LIP
dorsal injections
ventral injections
FEF to A46
FEF to V4
WM

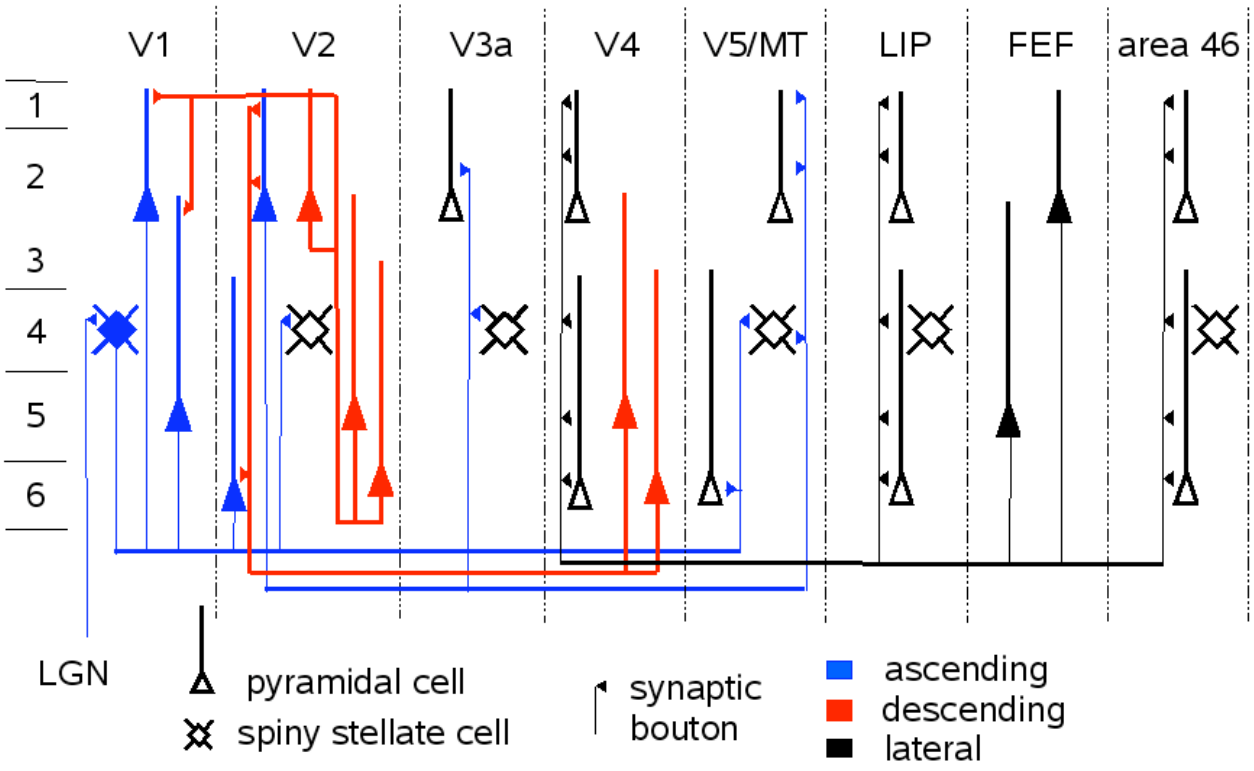

Figure 2

Schematic representation summarizing the excitatory targets of this study. The majority of synapses were formed with spines belonging to pyramidal and spiny stellate cells. The different paths are colour coded; feedforward or ascending in blue, feedback or descending in red and lateral or columnar in black. Lamina are indicated to the left. Vertical dashed lines represent cortical area boundaries.

4.2 Interareal Boutons

In the EM we could confirm that labeled bouton-like swellings of the axon were invariably synaptic. The majority of boutons formed only one synapse (V1/V2, 1 synapse per bouton; V1 to MT, 1.7; V2 to MT, 1.1; V2 to V3A, 1.1-1.2; V4 to V2, 1.03; FEF related 1.05) though occasionally there were two and sometimes up to four. The larger boutons (~ 1μm diameter), such as those described for V1 to MT

(Anderson et al, 1998) and the large layer 1 feedback axon connecting V2 to V1(Anderson and Martin, 2009) tended to form the most (3 or 4) multiple contacts. The majority of boutons were of the *en passant* type (~80%) with the exception being a slender feedback V2 to V1 axon in layer 1 that had the majority (70%) of its boutons as the *terminaux* type. We see this preponderance of bouton terminaux on the axons of layer 6 pyramidal cells in the cortex of cat and monkey (Martin and Whitteridge, 1984; Anderson et al, 1993). In some samples (e.g. V1 to MT, V2 to MT, V2 to V1) the boutons were often large enough to embed entirely the synaptic spine-head within its volume (Fig 6, 7, Anderson et al, 1998). The more complete the embedding the more removed from 'view' was the synapse. Up to 50% of the V1 to MT boutons had a spine thus embedded. Large boutons of the V1 to MT projection could cover up to three spines in this way. Some of the larger boutons formed synapses with the same target twice as when a bouton is lodged between a dendritc shaft and its spine (Fig 2E, Anderson et al, 1998). Another projection that showed targets being embedded by boutons was V2 to MT (Anderson and Martin, 2002). In this case some of the labeled axon projected to layer 1 and completely surrounded the spine head with a thin coating of labeled bouton (see Fig. 7, Anderson and Martin, 2002). These boutons all appeared to be filled with vesicles and contained mitochondria though less than half showed any synaptic specialization. By far the majority of labeled boutons from all these different projections were generally small (~ 0.5 μm diameter) and vesicle and mitochondria packed and contacted by a spine. In one case (V2 to V1, Anderson and Martin, 2009) we were able to reconstruct two lengths of labeled axon innervating layer 1 including their target spines and dendrites. The striking difference between the two axons was their diameter and the size of their boutons. One axon, unbranched and unmyelinated, very fine (0.3 μm diameter) with tiny boutons, formed contacts with equally small spines. The other, myelinated and very thick (> 1 μm) and bearing massive boutons also contacted spines and yet they were massive spines, almost pressed into the largest surface of the bouton

(see Fig . 7 and 8, Anderson and Martin, 2009).

4.3 Intereal synapses

All of the labeled synapses in this collection of studies were asymmetric. The asymmetry, identified by Grey (1959a, b) as a characteristic of a certain class of synapse later to be interpreted as excitatory (Uchizono, 1965), appears as a thickening of the postsynaptic density (PSD). When we refer to a measured synapse it is to the PSD that we usually refer. The thickening is generally at its most extensive in spines, less so in dendrites and least prominent in somata. This was the pattern we observed in our sample. An advantage of serial reconstruction however is that we can reconstruct the postsynaptic density and examine both morphology and size. There was an extensive range of size and complexity in our sample. Spines tended to form the largest and most complex synapses. The synapses formed with dendritic shafts were smaller and usually less perforated and somata formed the smallest and simplest synapses. The smallest synapse areas belonged to a fine axon of the feedback connection found in layer 1 from V2 to V1 (0.032 μm^2) and the largest from the thick axon of the same pathway, also in layer 1 (0.19 μm^2). The complexity of the synapse can increase with size to include complete perforations, even double perforations. Fifty percent of the V1 to MT spine synapses were perforated. In the FEF related pathways the labeled synapses of layer 1 were consistently the largest and those of layer 4 were the smallest (layer 1: LIP = 0.131 μm^2, area 46 = 0.131 μm^2, V4 = 0.103 μm^2; layer 4: LIP = 0.075 μm^2, area 46 = 0.067 μm^2, V4 = 0.078 μm^2) though rarely were differences between adjacent lamina (supragranular and infragranular) significantly different. In the feedforward projection of the visual pathway labeled layer 4 synapses were the largest and those of secondary laminae smaller. Similarly in the V4 to V2 feedback projection the labeled synapses of the primary lamina were larger (mean = 0.117 μm^2) than those of the secondary lamina (mean =0.073 μm^2). A similar trend has been

noticed in the synapse size of the thalamic W pathway in the cat primary visual cortex (Anderson et al, 2009). The largest synapses were seen on spines in layer 1 (0.16 μm^2), the next largest in layer 2/3 (0.1 μm^2) and the smallest in layer 5 (0.09 μm^2). The size of spine synapses in a sample of thalamic X and Y cell axons in cat primary visual cortex (0.163 μm^2, Anderson et al, 2009) was found to be not significantly larger than the W synapses found in layer 1.

4.4 Targets:

4.4.1 Spiny cells as targets.

Using the electron microscope we have been able to take a step which brings us closer to the functionality of some of the different interareal pathways of monkey cortex. There have been very few attempts to coordinate light and electron microscopy in the context of monkey interareal connections. The exception being a study by Rockland and Douglas (1993) looking at feedback to layer 1 of V1 from V2. The dependence in the past has been upon degeneration or bulk filling to retrogradely label and identify cell somata that project and anterogradely label and locate the laminae of axon collaterals. Obviously what this is not telling us about is the target or the projecting axons relationship with its targets.

The labeled boutons all came from pyramidal cells and less frequently spiny stellate cells (Lund et al, 1975; Shipp and Zeki, 1989). The pathways we examined and their excitatory targets are summarized in Fig 2. Cells with spiny dendrites such as those we analyze here have been demonstrated to form asymmetric synapses (Grey, 1959b) and to be excitatory (Uchizono, 1965; Saint Marie and Peters, 1985; Kisvárday et al, 1986; McGuire et al, 1991). The speculation of Ramon y Cajal (1888) that dendrites formed spines, that were not an artifact of histology as many believed, including Golgi, in order to provide potential sites of connection was vindicated when it became clear that most synapses

were formed with spines while the dendritic shaft was relatively synapse free (Gray, 1959b). All labeled synapses were asymmetric but not all labeled synapses were formed with spines. A number of the targets were dendritic shafts and very occasionally cell bodies. By serial section reconstruction we were able to identify and characterize these subgroups of targets. Some of the dendritic shaft targets bore spines, contained few mitochondria, showed few variations in diameter and few synapses on the shaft. These features have been shown to be characteristic of the dendrites of excitatory cells. Another group of features that identify dendrites include those that contain numerous mitochondria, frequently form unidentified synapses, do not form spines and vary in shaft diameter to form swellings or varicosities. Dendrites with these characteristics have been shown to contain GABA and therefor to belong to putative inhibitory cells (Somogyi et al, 1983; Peter and St Marie, 1984; Kisvarday et al, 1985; Ahmed et al, 1997). The proportion of synapses formed with the dendrites of smooth cells in this sample ranged from 5 to 26%. This range falls within more or less expected values for neocortex, i.e. less than 25% (Beaulieu and Colonnier, 1985; Hendry et al, 1987; Beaulieu et al, 1992; Gabbott and Bacon, 1996).

4.4.2 Smooth cells as targets

The V1 to MT sample showed the largest proportion of GABAergic targets (26%). The large boutons associated with the V1 to MT axons formed synapses with a number of somata that were characterized as GABAergic, due to large numbers of mitochondria and other cellular organelles, rough endoplasmic reticulum, deep nuclear invaginations and forming numerous unidentified asymmetric synapses (Peters and Saint Marie, 1984). The size of the synapses formed between these boutons and their target somata were small though there could be up to five individual synapses formed between a single bouton and a single soma. Whether it was better to consider these multiple synapses as one complex synapse or to treat each small synapse as separate was not obvious. In the publication, Anderson et al, 1998, we show

these small synapses separately and in this current overview it was decided to group these multiple synapses for the histogram (Fig 3), reducing the proportion of GABAergic targets to 13% (from 27%). As well as this projection having the smallest proportion of spines as targets (54%) and the largest proportion of dendritic shaft synapses (33%) it had among the largest and most vesicle and mitochondria packed boutons. We reconstructed some of the mitochondria from the V1 to MT boutons to discover that sometimes there were relatively few mitochondria but that they were looped and branched and could occupy up to 22% of the volume of the bouton. There appears to be a significant role for mitochondria in synaptic transmission (Nicholls and Åkerman, 1982; Herrington et al, 1996; Tang and Zucker, 1997; Xu et al, 1997; Peng, 1998) and so it seems noteworthy that we invariably found a mitochondria in even the smallest bouton.

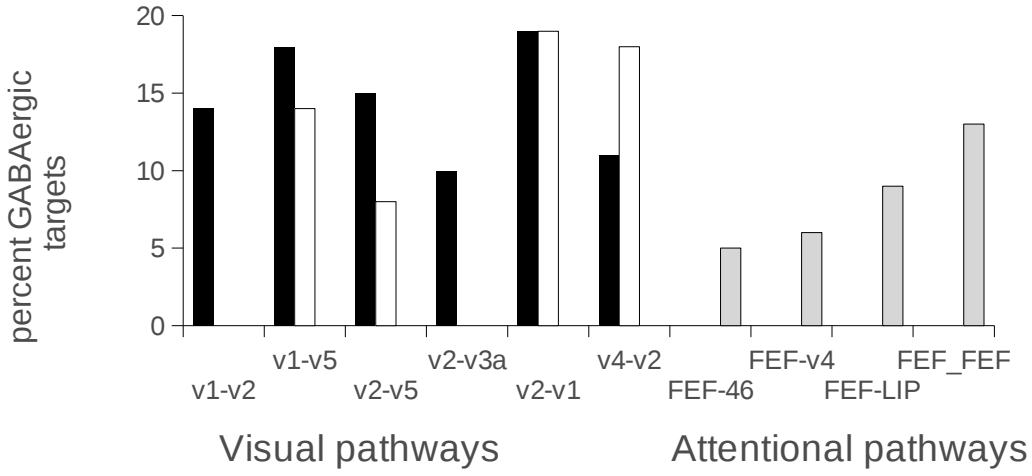

Figure 3

Histogram of the distribution of percent of targets showing features that are characteristic of cells containing GABA, taken from visual (left) and visual-attentional (right) related cortical areas. Targets of the visual cortex (left) are divided into primary laminae of termination (black) and secondary laminae (white). This is possible because the Visual-attention related cortex showed no such organization as the labeled termination pattern appeared lateral or

columnar, innervating all lamina equally. This is unlike the visual cortex targets as they arise from what appear to be lamina specific feedforward or feedback pathways, each with preferred laminae of innervation and other laminae showing significantly less innervation by labeled terminals.

In cases were a projection terminates in two non-adjacent laminae such as is found in V1 to MT and V4 to V2 we find more GABAergic targets associated with the primary lamina (18% in layer 4 versus 14% in layer 6 of V1 to MT; 11% in layer 1 versus 6% in layer 6 of V4 to V2). The secondary lamina in both these cases is layer 6 and so it resembles the thalamic innervation of V1 by X and Y cell axons which also have a small, secondary innervation of layer 6 in both cat and monkey (Hendrickson et al, 1978; Blasdel and Lund 1983; Freund et al, 1985).

In the rat visual cortex a similar situation has been found with the primary lamina of innervation having mostly spines as targets (87%) and secondary laminae having all spines (100%) (Gonchar and Burkhalter, 2003). Furthermore, pyramidal cells are the most frequent target of the feedback projection in rat (98%) and less so in the feedforward projection (90%) (Johnson and Burkhalter, 1996). The implication in these two studies being that if it is not a spine (a pyramidal cell) the target must be the dendrite of a smooth cell and therefor inhibitory. Hence it would seem that in both the feedforward pathway and in the primary lamina of innervation inhibition has a more important role. This is not entirely consistent with the monkey however as feedback pathways in the visual cortex have consistently high numbers of GABAergic targets with 19% for V2 to V1 and 11% and 18% for V4 to V2 in layers 1 (primary) and 2 (secondary) (respectively).

The same does not apply to the FEF related pathways as most laminae are innervated in a columnar or lateral connection pattern. The exception to this is the FEF to LIP projection in one animal that clearly targeted layer 1, the densest layer of innervation and so clearly looking like a feedback pathway, and yet no GABAergic targets where found in our sample from layer 1. On the other hand in layer 4 of the

clearly columnar innervation of LIP by FEF in the second animal we found 19% of targets to be GABAergic.

4.5 Drivers and Modulators

The sample of projections connecting V1 and V2 did not wholly represent the Guillery-Sherman picture of drivers and modulators. There is something of a mixed bag of driver and modulator characteristics in the feedback pathway. One thin, unmyelinated axon traversing layer 1 had a very fine structure arguably resembling the classic modulator, bearing tiny synapses (the smallest we have seen, mean = 0.032 μm^2) formed with small boutons of the terminaux type morphology and small spines. Another, thick, myelinated axon also feeding back from V2 and passing through layer 1 was bearing large boutons forming large, complex synaptic densities with large spines and effectively looking like a driver, but in fact was feeding back. In fact these synapses were the largest recovered from macaque cortex (0.19 μm^2) and were larger than anything seen in any other projection of macaque. The next largest synapse being V1 spine synapses in V5; 0.13 μm^2 (Anderson et al, 1998). So there is quite an array of synapse sizes ranging from the smallest on the thin axon to the largest on the thick axon. Equally surprising perhaps is the range of synapse dimensions, and synapse complexity, seen for any one group. What these different dimensions mean is as yet unknown. We see something similar in cat thalamocortical connections, considered to be the classic driver pathway (Sherman and Guillery, 1998), in that the largest cortical synapse is found between thalamic boutons and cortical layer 4 cells (~ 0.18 μm^2,Dehay et al, 1991; Friedlander et al, 1991). But the V1-V2 relationship is not equal as was outlined in the Introduction. De-activate V1 and V2 is no longer responsive, de-activate V2 and V1 remains responsive despite their close relationship in terms of reciprocally connecting cell numbers (Barone et al, 2000). It may be that the signal from V1 to V2 is simply not always tight enough to activate an

EPSP and the feedback simply provides some signal to apical dendrites of pyramidal cells that results in increased background, in the same way that there may be thalamocortical synapse enhancement by intrinsic cells of layer 4 (London and Segev, 2001). V1 may be maintained during reversible blocking due to the thalamic input provided to layers 4 and 6.

As we have seen earlier in "**Interareal synapses**" there are 'tendencies' amongst interareal synapse sizes, such as the principle laminae of innervation having larger synapse areas in the feedforward direction in layer 4 and in the feedback direction in layer 1and becoming smaller as we pass on to deeper laminae . Layer 1 also has the larger synapses in the lateral or columnar projection of the mostly modulatory projections of the attention pathways. The driver and modulator roles appear each to be composed of a principle component lamina in which synapses are larger perhaps indicating a source of larger or more reliable EPSP's. Synapse size is not stated explicitly to be a criteria defining driver or modulator but is implicit in the assumption that the terminal size of a driver should be large and that of a modulator to be small (Guillery and Sherman, 2002). Corticothalamic X and Y cells are perhaps the archetypal drivers and are associated with an appropriately large synapse. However, as we have seen (Anderson et al, 2009) the synapses of the W pathway in cat have similarly large synapses and is otherwise inferred to be a modulator (Usrey, 1992). And of course one must keep in mind that there is a large degree of overlap between the size of synapse from different laminae and different paths. So the indication is that both modulators and drivers can have similar synapse sizes.

4.6 Influence of Synapse Location.

Most of the axon projection patterns stemming from FEF appeared to have the lateral or columnar appearance of areas in close association (Mausell and Van Essen, 1983). This was the case even when one or more levels of the hierarchy had been traversed such as FEF to LIP or V4 (Felleman and Van

Essen, 1991). Both areas V4 and LIP (ventral) when targets of FEF innervated all laminae, indicating all cells as possible sites for synapse formation. The feedforward and feedback pathways however terminate in distinct laminae and therefore only have access to specific populations of cells or different portions of the dendritic tree of these cells. There is a difference of opinion regarding the importance of positioning of synapses in the dendritic tree (Magee and Cook, 2000; London and Segev, 2001). The issue revolves around work on the in vitro hippocampus that showed changes in synaptic conductance, which gets larger, as one moves along the dendrite from proximal to distal. This effectively renders all points equally viable in initiating action potentials (Magee and Cook, 2000). Instead it was demonstrated that when *in vivo* the conditions are so different when compared to *in vitro* that location becomes very important and that distal synapses become weaker at the soma (London and Segev, 2001). The reason being that in *in vivo* circumstances there is more synaptic activity around (Borg-Graham et al, 1998; Rapp et al, 1992) which increases dendritic membrane conductance which increases their electrotonic length. If it is important where a synapse is located on the dendritic tree then it seems less a model of wiring economy or development that determines where the site is located. Instead we can say that the fact of massive innervation of layer 1 by cells providing feedback gives special significance, a functional role, to the tops of apical dendrites, which are the most likely spine bearing structures in layer 1 and are of course the apical dendrites of pyramidal cells in layer2/3 and 5. Modulatory input arriving from cells in higher or equally placed positions within the hierarchy may require enhancement by use of background noise rather like the dLGN and spiny stellate model of Banitt et al, (2007). Not only may the distal location diminish its efficacy at the soma but the alarmingly small number of synapses or inputs provided by FEF to LIP in layer 1 (0.16%, Anderson et al, 2011) for example may also be the reason for needing amplification. This may be similar to the numerically small dLGN input to primary visual cortex in cat and monkey (Ahmed et al,1994; Latawiec et al, 2000) that requires some background activity before an EPSP can be generated (Banitt

et al, 2007) as the modulated dLGN alone could not evoke spikes once driven into a steady state. But unlike the thalamocortical pathway it has yet to be ascertained what the fine grain physiology of the cell in FEF or, the 'attention' pathway, is like. At a first pass it may be reasonable to assume that recipient cells of FEF are not radically different from the findings of Banitt et al (2007) in the thalamorecipient cells of cat area 17.

This use of background noise, from intrinsic layer 2/3 pyramidal cells, could be the means of changing the gain of the local circuit which results in the changes we see being brought about by attention. The apical dendrites of layer 2/3 and 5 pyramidal cells are being subject to feedback from other cortical areas that is not enough to constantly drive them (due to low numbers and/or distal location or some biophysical feature that renders them unlikely to drive), when attending, and showing a constant state of change in gain, presumably necessary if the local circuit is to reach a steady state until the next input requires re-convergence of the network. From this flux of shifting gain parts of the local circuit are made more significant either by timing (Seidemann et al, 1998; Salinas and Sejnowski, 2001) or by a 'soft winner take all'-type network which would be the net result of feedforward competition.

It is probable that we are at an advantage when identifying targets, particularly shafts, because we can use our serial section reconstructions of labeled profiles and their targets. It is noticeable in our data that the proportion of shafts as targets is greatest when layer 4 is the target lamina. This may reflect the nature of the neuropil (few spines) or a selectivity for shafts both GABA positive and negative. By targeting layer 4 one of the more likely sources of excitatory profiles will be the spiny stellate (Straford et al, 1996). In the cat primary visual cortex spiny stellates have been shown to have fairly low spine counts and have been found to form ~50% of their asymmetric synapses with the dendritic shaft (Anderson et al, 1994b). Saint Marie and Peters (1985) however found only 5-25% of asymmetric synapses were formed with the dendritic shafts of spiny stellates in macaque.

Layer 4 of monkey has been shown to have 45% of neurons in V1 but only 35% of synapses (O'Kusky

and Colonnier, 1982). This could indicate that the high density of neurons in layer 4 precludes excessive wiring 'accessories' such as spines and /or this increases shaft synapses resulting in increased summation between shaft synapses, thus becoming an alternative means of using synapses to compute without relying on spines.

We reconstructed many synaptic contacts between labeled boutons and their unidentified targets. In one case we noted in the LM an axon in V4 traversing layer 3 producing a spray of fine axon terminals over a limited range (~ 11 μm) of the path of the axon (Anderson and Martin, 2009). In the EM we were able to identify 11 asymmetric synapses formed with the labeled axon and spines of a 2μm diameter dendrite. The size and orientation of the dendrite indicates that it came from a large layer 3 or 5 pyramidal cell and is the most numerous excitatory to excitatory connection thus far described for cortex. There were other synapses formed with spines (and one dendritic shaft) but not all spines could be traced back to the large dendrite.

4.7 Receptive Fields

Climbing the hierarchy has been an intuitive approach to many of the influential models in neuroscience since the advent of the neuron doctrine (Waldeyer, 1891) and Cajal's law of dynamic polarization (1897). The more recent uses of this approach include the model for developing increasingly complex receptive fields (RF's) by compounding the field of one cell with that of another through synapses (Hubel and Wiesel, 1962). Advancing through the hierarchy this 'simple' additive process can be used to account for findings such as the circle-surround RF of the dLGN cell becoming the simple RF of cortical cells in thalamorecipient layer 4. Following from this comes the

transformation from 'simple' to 'complex' RF's beyond cortical layer 4. When the RF's become larger, which they do when we advance rostrally through the visual cortex (Van Essen and Zeki, 1978), and more complex, it seems we are simply building increasingly complex feature detectors. If we now consider what happens when we go in the opposite direction and descend the hierarchy, we are trying to map the larger fields of V4 for instance onto smaller fields in V2 in order to provide feedback. In this case the RF's are not being rewritten or driven by this feedback. Instead they may be added to by creating the active subfields of surround suppression of a cells oriented RF center (Levitt and Lund, 2002).

The differences between cortical areas in terms of RF properties make them an attractive proposition for modeling cortex. For many modelers the feedforward or bottom up approach of a rigid hierarchy revealed too many limitations for anything other than object recognition. Instead, by iterating between recurrent feedforward and feedback networks in the ventral stream of cortex, in which task independent inferences about structure occur, the feedforward sensory information of scene composition can be compared to top down hypotheses requiring verification of expectation (Lee and Mumford, 2003). Recognition in this scheme occurs with the ascent to higher cortical areas and matching of the prediction with the sensory input. This kind of model, a Bayesian approach, and the alternative model that exploits high resolution information being manipulated by top down effects driven by attention that can influence earlier visual areas are seen as the two main contenders after rigid hierarchical models (Poggio and Serre, 2013). How these models relate to synapses is unclear particularly in the light of the feedback pathways being less distinguished as feedback and more columnar or lateral and hence see them more as providers of parallel input to all laminae. Equally interestingly is the fact that we now know these inputs are numerically very small (~0.16% in LIP layer 1, Anderson et al, 2011) and the distribution of synapses formed with GABAergic targets amongst these FEF connected areas is vanishingly small. It seems clear that a single iteration of feedback or feedforward processing would

never be sufficient to drive or even modulate any RF. So we come back to the most likely candidate of cortical recurrence.

There are claims that axons of the feedforward pathway terminate in relatively tight clusters (200-250 μm diameter) with an increase in patch size as one progresses rostrally from V1 (Yoshioka et al, 1992; Lund et al, 1993; Rockland, 1997). However feedback terminal patches are described as being more spread, over millimeters, although as Rockland (1997) points out these views are not derived from single axon fillings. We noted a similar spreading of labeled axons in the V4 to V2 feedback pathway where they traversed several millimeters through layer 1 (Anderson and Martin, 2006). Layer 1 of the FEF to V4 pathway was also populated by thick and thin axons traversing horizontally (Anderson et al, 2011). In higher cortical areas of course we find varying degrees of dependence upon lower cortical areas (Rodman et al, 1989; Girard et al, 1991; 1992). This could be a reflection of their degree of connectivity to subcortical structures for example (Rodman et al, 1989).

4.8 Models of attention

For models of attention that required FEF boutons to target selectively the inhibitory, GABAergic, parvalbumin expressing interneurons (Hendry, 1987; Connors and Gutnick, 1990; Condé et al, 1994; Mitchell et al, 2007) this may seem unsatisfactory. The model requires that the FEF signal synchronize their targets and acts to increase the signal to noise ratio (Tolhurst et al, 1983; McAdams and Maunsell, 1999; Reynolds and Heeger, 2009; Baluch and Itti, 2011). Using the criteria adopted by Mitchell et al, (2007; Connors and Gutnick, 1990) the main target of the FEF feedback to V4 should be inhibitory cells because they are associated with fast spiking physiology and showed the greatest attention dependent and spontaneous increases in spike rate (in fact doubling). Instead we found most targets to be putative pyramidal cells which should show wide or slow spiking behaviour and respond less

reliably when attending to a stimulus in the RF.

Using alert monkey's, attention has been used to show how extrastriate and striate cortex interact. Attention was generally thought of as enhancing one feature in the field due to behavioural relevance and was found by a scanning process. Accumulating evidence redirected thinking away from this 'spotlight' concept to one of biased competition (Desimone, 1998). For example when two objects enter the RF of a V2 cell attending to one object biases the response to the other cell (Reynolds et al, 1999). This bias could be argued to be modulation since the V2 cell is clearly not being driven or it would presumably develop a larger RF. However we know that being driven by a particular pathway does not mean that the RF properties of the driven cell are determined by that pathway. For instance the Hubel and Wiesel model (1962) of thalamic afferents driving cells of cortical layers 4 and 6 and thereby forming simple RF's from the spatial arrangement of the RF's of thalamic afferents is an incomplete picture because also there are monosynaptically driven cells with complex RF's in both layers 4 and 6 (Ferster and Lindstrom, 1983). Presumably these cells are not having their RF's determined solely by thalamic afferents.

Another scenario is that attention decreases intrinsic low frequency noise correlation which affects populations of sensory neurons (Cohen and Maunsell, 2009; Mitchell et al, 2009) by increasing firing rates. Rate increases enhance the signal to noise ratio. This fits with the view that there is an overall decrease in the input strength of the inhibitory cell population (Mitchell et al, 2007). Again the inhibitory cell population show no signs of conforming to the model as broad spiking, putative pyramidal cells predominate as targets. Another interpretation of attention is the idea that there is a decrease in the activity that causes divisive normalization, due to fast inhibition (Fries et al, 2001), and which is necessary when several objects fall within the scope of a receptive field (Lee and Maunsell, 2010; Reynolds et al, 1999; Reynolds and Heeger, 2009). This is secure as long as there is no prerequisite for the selective innervation of inhibitory cells. In the model of Reynolds and Heeger

(2009) they make no proposal for a biologically plausible circuit or cellular mechanism.

We have already seen how specific cell classes can be used in models of attention (Mitchell et al, 2007). By examination and digitization of series of sections we were able to reconstruct the targets of the different pathways and identify different classes of cells. Using established criteria (Ahmed et al, 1997, Somogyi et al, 1983; Peters and Saint-Marie, 1984) we recognized that a proportion of targets (5-18%) were the dendrites and somata of smooth cells or putative inhibitory interneurons (see Fig 3). The dendrites were characteristically smooth (spine-free) and beaded or varicose containing numerous mitochondria and the somata contained many mitochondria and cellular organelles and frequently formed numerous asymmetric and symmetric synapses. They usually contain the inhibitory neurotransmitter GABA and have become a fundamental component of circuit modeling.

A model of cortical circuitry in macaque dorsolateral prefrontal cortex (DLPFC) or area 9 has been proposed using two distinct streams of inhibition (Medalla and Barbas, 2009). Both anterior cingulate cortex (ACC) and area 46 project to area 9 where they innervate mostly pyramidal cells and a small proportion of inhibitory cells (18% and 13%, respectively) most of which were GABA positive. The inhibitory cells forming synapses with ACC boutons tended also to be calbinidin positive and to provide inhibition to pyramidal cells whereas the inhibitory cells forming synapses with area 46 boutons were both GABA positive and calretinin positive and provided disinhibition by mostly targeting inhibitory cells. This provides a potential mechanism for noise suppression in DLPFC during cognitive tasks. In the projections presented in this thesis the feedforward pathways are primarily innervating layers 4 and forming synapses with GABAergic targets in this laminae. Calbindin and calretinin positive cells are found in the superficial layers 2 and 3 of macaque (Meskenaite, 1997; Hof et al, 1998) making them unlikely targets for feedforward pathways. In the case for both feedback and FEF related (lateral) pathways the two classes of calcium binding cells are possible candidates for

synapse formation because of the more extensive interareal axon cover of the superficial laminae. Areas 46 and 9 are involved in working memory (Goldman-Rakic, 1995; Tanji and Hoshi, 2008) and area 46 may have an inhibitory role to play in area 9 extracting signal from noise. We also know that FEF targets inhibitory cells in area 46 (Anderson et al. 2011) however most of the targets are excitatory pyramidal cells. This local pyramidal cell recurrence could be the amplifier necessary to drive the subtleties of the models' inhibition with FEF providing the attentional signal via a highly recurrently connected excitatory circuit necessary for identifying the signal that needs enhancing by noise reduction.

It is interesting to note the distribution of targets amongst the FEF projecting axons with the type of connection being changed to one of lateral or columnar and not feedback. The largest GABAergic population of targets is in the deep layers, 4, 5 and 6, of LIP. The other FEF projecting terminals in area 46 and V4 show smaller numbers and in the superficial layers more in the case of FEF to V4 and less in LIP. We found no GABAergic targets in layer 1 of the FEF to LIP pathway and yet this was the densest labeled synapse projection we have measured (0.16 %). What these differences indicate is not clear. One view is that more inhibitory targets equals the need for a stronger inhibitory brake. If this is so then more braking is required in LIP layers 4-6 and V4 layers 1,2 and 6. Area 46 seems not to show this shift in GABAergic targets but instead has a more regular distribution. Whether these differences in the proportion of GABAergic targets are the source of a target cells particular RF properties is open to speculation.

The proportion of targets that are GABAergic in this collection of studies falls within the expected range of up to 25% (Beaulieu and Colonnier, 1985; Hendry et al, 1987; Beaulieu et al, 1992; McGurie et al, 1991; Gabbott and Bacon, 1996; Melchitzky et al, 1998). The greater part of the circuit diagram is composed of spines as targets, belonging to the excitatory pyramidal cell, which provides the means for the local excitatory recurrence. When we examined the targets of local recurrence in FEF we found

only 13% were GABAergic , the rest are spines of excitatory pyramidal cells (Anderson et al, 2011). So we would expect this pool of inhibition to be just enough to maintain a poised system. There is a contender to this view however in the PFC, area 9, of macaque (Melchitzky et al, 2001) where it has been shown that only 50% of the targets of local recurrent axon from intrinsic cells are excitatory and the remainder GABAergic. Thus far it appears this finding is an exception.

4.9 Conclusion

We now have a rich understanding of some of the interareal pathways found in cortex. The strong evidence for the importance of recurrent excitation in networks continues whilst the subtleties of inhibition continue to arouse speculation. There are still unanswered issues about how effective these two types of pathway are, or perhaps wherein lies their effectiveness? In what ways is synapse size and morphology important and what makes a 'strong' connection between areas? We have some insight into connection strengths from large injections filling cells retrogradely though we know little of the contribution of a single axon to an area. How many synapses they form with a target and with what specificity they select their target is as yet unknown. In this study we see highly focused convergence of a single axon forming many (11) synapses with a single dendrite on the one hand (Anderson and Martin, 2009) and on the other what appears to be the expected wide divergence of excitatory connections by forming few synapses with any one cell. Many cellular mechanisms remain to be understood providing an almost limitless horizon for modelers and speculation which anatomy can accommodate and furnish with direction, as we have done here. Just how does one get a small amount of inhibition to be effective without being too late? The relatedness to the canonical microcircuit makes this study almost an extension to earlier circuit building in the cat cortex for example, in which strong local recurrence dominates over interlaminar connections.

Our attempts to define the circuitry of cortex have come from such early work that required even the

concept of 'the cell' to be accepted and not just considered a radical notion. Now we make advances with scarcely a thought for our predecessors trials and so it goes throughout our inquiries. Now we have reached a point of having resolved many details of the neocortex and have the need to re-establish them into something more manageable. Having released the detail of the neuron from the tangle of a cellular jungle, from the reticulum and syncitium and the anastomosing processes of the 19th century, we attempt to return it to a place where it has computational consequence and remains part of the whole. With the introduction of the law of dynamic polarization by Cajal and chains of cells, connecting and communicating, our perception of neural events was changed. The law gave us a stepwise procession of effect as well as many attempts by others to imagine the most salient of circuits required to exploit this process. Each attempt has exploited this law but leaves us with a discrete series of events passed from cell to cell. In fact what is a more likely scenario is the passing of a signal from one cell to many in both space and time, requiring both anatomy and physiology. It is this latter perspective that has shaken the traditional models of circuitry by bringing both excitation and inhibition closer together until they become concomitant.

Chapter 5 References

Ahmed B, Anderson JC, Martin KAC, Nelson JC (1994) Polyneuronal Innervation of spiny stellate neurons in cat visual cortex. J Comp Neurol 341:39-49.

Ahmed B, Anderson JC, Martin KAC, Nelson JC (1997) Map of the synapses onto layer 4 basket cells of the primary visual cortex of the cat. J Comp Neurol 380:230-242.

Allman JM, Kaas JH (1971) A representation of the visual field in the caudal third of the middle temporal gyrus of the owl monkey (*Aotus trivirgatus*). Brain Res 31:85-105.

Allman JM, Kaas JH (1974) The organization of the second visual area (V-II) in the owl monkey: a second order transformation of the visual hemifield. Brain Res 76: 247-265.

Allman JM, Kaas JH (1975) The dorsomedial cortical visual area: a third tier area in the occipital lobe of the owl monkey (*Aotus trivirgatus*). Brain Res 100: 473-487.

Allman JM, Kaas JH (1976) Representation of the visual field on the medial wall of the occipital-parietal cortex in the owl monkey. Science 191: 572-575.

Anderson JC, Martin KAC, Picanco-Diniz CW (1992) The neurons in layer 1 of cat cortex. Proc Roy Soc 248: 27-33.

Anderson JC, Martin KAC, Whitteridge D (1993) Form, function, and intracortical projections of neurons in the striate cortex of the monkey *Macacus nemestrinus*. Cereb Cortex 3:412-420.

Anderson JC, Douglas RJ, Martin KAC, Nelson JC (1994a) Synaptic output of physiologically identified spiny stellate neurons in cat visual cortex. J Comp Neurol 341:16-24.

Anderson JC, Douglas RJ, Martin KAC, Nelson JC (1994b) Map of the synapses formed with the dendrites of spiny stellate neurons of cat visual cortex. J Comp Neurol 341:25-38.

Anderson JC, Binzegger T, Martin KAC, Rockland KS (1998) The connection from cortical area V1 to

V5: A light and electron microscopic study. J Neurosci 18:10525-10540.

Anderson JC, Martin KAC (2002) Connection from cortical area V2 to MT in macaque monkey. J Comp Neurol 443: 56-70.

Anderson JC, Martin KAC (2005) Connection from cortical area V2 to V3A in macaque monkey. J Comp Neurol 488:320-330.

Anderson JC, Martin KAC (2006) Synaptic connection from cortical area V4 to V2 in macaque monkey. J Comp Neurol 495: 709-721.

Anderson JC, Da Costa NM, Martin KAC (2009) The W cell pathway to cat primary visual cortex. J Comp Neurol 516: 20-35.

Anderson JC, Martin KAC (2009) The synaptic connections between cortical areas V1 and V2 in macaque monkey. J Neurosci 29:11283-11293.

Anderson JC, Martin KAC, Kennedy H (2011) Pathways of attention: synaptic relationships of frontal eye field to V4, lateral intraparietal cortex, and area 46 in macaque monkey. J Neurosci 31:10872-10881.

Andersen RA, Asanuma C, Essick G, Siegel RM (1990) Corticocortical connections of anatomically and physiologically defined subdivisions within the inferior parietal lobule. J Comp Neurol 296: 65-113.

Anzai A, Chowdhury SA, DeAngelis GC (2011) Coding of stereoscopic depth information in visual areas V3 and V3A. J Neurosci 28: 10270-10282.

Armstrong KM, Fitzgerald JK, Moore T (2006) Changes in visual receptive fields with microstimulation of frontal cortex. Neuron 50:791-798.

Armstrong KM, Moore T (2007) Rapid enhancement of visual cortical response discriminability by microstimulation of the frontal eye field. Proc Natl Acad Sci USA 104: 9499-94504.

Baizer JS, Ungerleider LG, Desimone R (1991) Organization of visual inputs to the inferior temporal

and posterior parietal cortex in macaques. J Neurosci 11:168-190.

Balan PF, Ferrera VP (2003) Effects of gaze shifts on maintenance of spatial memory in macaque frontal eye field. J Neurosci 23:5446-5454.

Baluch F, Itti L (2011) Mechanisms of top-down attention. TINS 34:210-224.

Banitt Y, Martin KAC, Segev I (2007) A biologically realistic model of contrast invariant orientation tuning by thalamocortical synaptic depression. J Neurosci 27: 10230-10239.

Barash S, Bracewell RM, Fogassi L,Gnadt JW, Anderen RA (1991) Saccade-related activity in the lateral intraparietal area. II. Spatial properties. J Neurophysiol 66: 1109-1124.

Barbas H, Mesulam MM (1981) Organization of afferent input to subdivisions of area 8 in the rhesus monkey. J Comp Neurol 200:407-431.

Barbas H, Pandya DN (1989) Architecture and intrinsic connections of the prefrontal cortex in the rhesus monkey. J Comp Neurol. 286:353-375.

Barone P, Batardiere A, Knoblauch K, Kennedy H (2000) Laminar distribution of neurons in extrastriate areas projecting to visual areas V1 and V4 correlates with the hierarchical rank and indicates the operation of a distance rule. J Neurosci 20: 3263-3281.

Beaulieu C, Colonnier M (1985) A laminar analysis of the number of round-asymmetrical and flat-symmetrical synapses on spines, dendritic trunks, and cell bodies in area 17 of the cat. J Comp Neurol 231: 180-189.

Beaulieu C, Kisvárday Z, Somogyi P, Cynader M, Cowey A (1992) Quantitative distribution of GABA-immunopositive and -immunonegative neurons and synapses in the monkey striate cortex (area 17). Cereb Cortex 1992 2:295-309.

Bendiksby MS, Platt ML (2006) Neural correlates of reward and attention in macaque area LIP. Neuropsychologia 44: 2411-2420.

Benevento LA, Rezak M (1976) The cortical projections of the inferior pulvinar and adjacent lateral

pulvinar in the rhesus monkey (*Macaca mulatta*): an auto radiographic study.

Binzegger T, Douglas RJ, Martin KAC (2004) A quantitative map of the circuit of cat primary visual cortex. J Neurosci 24: 8441-8453.

Binzegger T, Douglas RJ, *Martin* KAC (*2007*) Stereotypical bouton clustering of individual neurons in cat primary visual *cortex*. J Neurosci 27: 12242–12254.

Blackstad TW (1965) Mapping of experimental axon degeneration by electron microscopy of Golgi preparations. Z Zellforsch Mikrosk Anat, 67: 819–834.

Blasdel GG, Lund JS (1983) Termination of afferent axons in macaque striate cortex. J Neurosci 7:1389-413.

Blatt GJ, Andersen RA, Stoner GR (1990) Visual receptive field organization and cortico-cortical connection of the lateral intraparietal area (area LIP) in the macaque. J Comp Neurol 299: 421-445.

Borg-Graham LJ, Monier C, Fregnac Y (1998) Visual input evokes transient and strong shunting inhibition in visual cortical neurons. Nature 393: 369-373.

Boussaoud D, Ungerleider LG, Desimone R (1990) Pathways for motion analysis: cortical connections of the medial superior temporal and fundus of the superior temporal visual areas in the macaque. J Comp Neurol 296:462-495.

Brodmann K (1905) Beitraege zur histologischen Lokalisation der Grosshirnrinde: dritte Mitteilung: Die Rindenfelder der niederen Affen. Journal fur Psychologie und Neurologie 6: 177-226.

Brodmann K (1909) Vegleichende Lokalisationslehre der Grosshirnde. Barth, Leipzig.

Budd JML (1998) Extrastriate feedback to primary visual cortex in primates: a quantitative analysis of connectivity. Proc Roy Soc B 265: 1037-1044.

Buffalo EA, Fries P, Landman R, Liang H, Desimone R (2010) A backward progression of attentional effects in the ventral stream. Proc Natl Acad Sci USA 107:361-365.

Buschman TJ, Miller EK (2009) Serial, covert shifts of attention during visual search are reflected by

the frontal eye fields and correlated with population oscillations. Neuron 63: 386-396.

Campbell AW (1905) Histological studies on the localisation of cerebral function. Cambridge University Press; Cambridge.

Colby CL, Gattass R, Olson CR, Gross CG (1988) Topographical organization of cortical afferents to extrastriate visual area PO in the macaque: a dual tracer study. J Comp Neurol 269:392-413.

Constantinidis C, Goldman-Rakic PS (2002) Correlated discharges among putative pyramidal neurons and interneurons in the primate prefrontal cortex. J Neurophysiol 88: 3487-3497.

Clavagnier S, Falchier A, Kennedy H (2004) Long-distance feedback projections to area V1: implications for multimodal integration, spatial awareness and visual consciousness. Cogn Affect Behav Neurosci 4: 117-126.

Cohen HR, Maunsell JHR (2009) Attention improves performance primarily by reducing interneuronal correlations. Nature Neurosci. 12: 1594-1601.

Cohen JY, Crowder EA, Heitz RP, Subraveti CR, Thompson KG, Woodman GF, Schall JD (2010) Cooperation and competition among frontal eye field neurons during visual target selection. J Neurosci 30:3227–3238.

Condé F, Lund JS, Jacobowitz DM, Baimbridge KG, Lewis DA (1994) Local circuit neurons immunoreactive for calretinin, calbindin D-28k or parvalbumin in monkey prefrontal cortex: Distribution and morphology. J Comp Neurol 341: 95-116.

Colonnier M (1968) Synaptic patterns on different cell types in the different laminae of the cat visual cortex. An electron microscope study. Brain Res 9: 268-287.

Connors BW, Gutnick BW (1990) Intrinsic firing patterns of diverse neocortical neurons. Trends Neurosci 13: 99-104.

Creutzfeld OD (1977) Generality of the functional structure of the neocortex. Naturwissenschaften 64: 507-517.

Crick F, Koch C (1998) Constraints on cortical and thalamic projections: the no-strong-loops hypothesis. Nature 391: 245-250.

Da Costa NM, Hepp K, Martin KAC (2009) A systematic random sampling scheme optimized to detect the proportion of rare synapses in the neuropil. J Neurosci Methods 30: 77-81.

Da Costa NM, Martin KAC (2009) The proportion of synapses formed by the axons of the lateral geniculate nucleus in layer 4 of area 17 of the cat. J Comp Neurol 516: 264–276.

Da Costa, NM, Martin KAC (2011) How thalamus connects to spiny stellate cells in the cat's visual cortex. J Neurosci 31: 2925–2937.

Da Costa, NM (2012) The diversity of thalamorecipient spine morphology in cat visual cortex and its implication for synaptic plasticity. J Comp Neurol doi:10.1002/cne.23272

Daniel PM, Whitteridge D (1959) The representation of the visual field on the cerebral cortex of monkeys. J Physiol Lond 159:203-221.

Dehay C, Douglas RJ, Martin KAC, Nelson JC (1991) Excitation by geniculocortical synapses is not ‘vetoed’ at the level of dendritic spines in cat visual cortex. J Physiol 440:723-734.

Desimone, 1998 Visual attention mediated by biased competition in extrastriate visual cortex. Phil Trans Roy Soc Lond 353: 1245-1255.

De Yoe EA, Van Essen DC (1985) Segregation of efferent connections and receptive field properties in visual area V2 of the macaque. Nature 6032: 58-61.

Distler C, Boussaoud D, Desimone R, Ungerleider LG (1993) Cortical connections of inferior temporal area TEO in macaque monkeys. J Comp Neurol 334: 125-150.

Douglas RJ, Martin KAC (2004) The circuits of neocortex. Ann Rev Neurosci

Douglas RJ, Martin KAC Whitteridge D (1989a) A canonical microcircuit for neocortex. Neural Comput 1:480-488.

Douglas RJ, Martin KAC, Whitteridge D (1989b) A functional microcircuit for cat visual cortex. J

Physiol 440:735-769.

Douglas RJ, Martin KAC (1991) A functional microcircuit for cat visual cortex. J Physiol 440:735-769.

Dubner R, Zeki S (1971) Response properties and receptive fields in an anatomically defined region of the superior temporal sulcus in the monkey. Brain Res 35:528-532.

Duhamel JR ,Colby CL, Goldberg ME (1992) The updating of the representation of visual space in parietal cortex by intended eye movements. Science 255: 90-92.

Eccles JC (1964) The physiology of synapses. Berlin-Goettingen-Heidelberg Springer Verlag.

Economo C von, Koskinos GN (1925) Die cytoarchitektonik der hirnrinde des erwachsenen menschen. Wien: Springer Verlag.

Ekstrom LB, Roelfsema PR, Arsenault JT, Bonmassar G, Vanduffel W (2008) Bottom-up dependent gating of frontal signals in early visual cortex. Science 321:414-417.

Faber DS, Korn H (1988) Synergism at central synapses due to lateral diffusion of transmitter. Proc Natl Acad Sci USA 85: 8708-8712.

Fanini A, Assad JA (2009) Direction selectivity of neurons in the macaque lateral intraparietal area. J Neurophysiol 101: 289-305.

Felleman DJ, Van Essen DC (1991) Distributed hierarchical processing in the primate cerebral cortex.Cereb Cortex. 1:1-47

Felleman DJ, Burkhalter A, Van Essen DC (1997) Cortical connections of areas V3 and VP of macaque extrastriate visual cortex. J Comp Neurol 379:21-47.

Ferrera VP, Yanike M, Cassanello C (2009) Frontal eye field neurons signal changes in decision criteria. Nature Neurosci 12:1454-1458.

Ferrier, D (1874) The localization of function in the brain. Proc Roy Soc London Ser B 22:229 – 232.

Ferster D, Lindstrom S (1983) An intracellular analysis of geniculocortical connectivity in the cat. J Physiol Lon 342: 181-216.

Fiala JC (2005) Reconstruct: a free editor for serial section microscopy. J Microsc 218: 52-61.

Fitzpatrick D, Lund JS, Schmetchel DE, Towles AC (1987) Distribution of GABAergic neurons and axon terminals in the macaque striate cortex. J Comp Neurol 264: 73-91.

Foster M (1897) A text-book of physiology. Part III Lond Macmilllan.

Freund TF, Somogyi P (1983) The section-Golgi impregnation procedure 1. Description of the method and its combination with histochemistry after intracellular iontophoresis or retrograde transport of horseradish peroxidase. Neuroscience 9:463-474.

Freund TF, Martin KAC, Whitteridge D (1985) Innervation of cat visual areas 17 and 18 by physiologically identified X- and Y-type thalamic afferents. I. Arborization patterns and quantitative and quantitative distribution of postsynaptic elements. J Comp Neurol 242: 263-274.

Freund TF, Martin KAC, Soltesz I, Somogyi P, Whitteridge D (1989) Arborisation pattern and postsynaptic targets of physiologically identified thalamocortical afferents in striate cortex of the macaque monkey. J Comp Neurol 289:315-336.

Friedlander MJ, Martin KAC, Wassenhove-McCarthy D (1991) Effects of monocular visual deprivation on the innervation of cortical area 18 in the cat by individual thalamocortical axons. J Neurosci 11:3268-3288.

Friedman DP (1983) Laminar patterns of termination of corticocortical afferents in the somatosensory system. Brain Res 273: 147-151.

Fries W, Keizer K, Kuypers HG (1985) Large layer VI cells in macaque striate cortex (Meynert cells) project to both superior colliculus and prestriate visual area V5.

Fries P, Reynolds JH, Rorie AE, Desimone R (2001). Modulation of oscillatory neuronal synchronization by selective visual attention. Science 291:1560–1563.

Friston KJ, Buchel C (2000) Attentional modulation of effective connectivity from V2 to V5/MT in humans. Proc Natl Acad Sci USA 97: 7591-7596.

Fuchs AF (1967) Saccadic and smooth pursuit eye movement s in the monkey. J Physiol Lond 191: 609-631.

Gabbott PLA and Somogyi P (1986) Quantitative distribution of GABA-immunoreactive neurons in the visual cortex (area 17) of the cat. Exp Brain Res 61: 323-331.

Gabbott PLA, Martin KAC, Whitteridge D (1987) Connections between pyramidal neurons in layer 5 of the cat visual cortex (area 17). J Comp Neurol 259: 364-381.

Gabbott PLA, Bacon SJ (1996) Local circuit neurons in the medial prefrontal cortex (areas 24a,b,c, 25 and 32) in the monkey: II. Quantitative areal and laminar distributions. J Comp Neurol 364: 609-636.

Gaska JP, Jacobson LD, Pollen DA (1988) Spatial and temporal frequency selectivity of neurons in visual cortical area V3a of the macaque monkey. Vision Res 28:1179-91.

Gattass R, Sousa APB, Mishkin M, Ungerleider LG (1997) Cortical projections of area V2 in the macaque. Cereb Cortex 7:1047-3211.

Gilbert CD (1977) Laminar differences in receptive field properties of cells in cat primary visual cortex. J Physiol 268:391-421.

Gilbert CD, Kelly JP (1975) The projections of cells in different layers of the cats visual cortex. J Comp Neurol 163: 81-105.

Gilbert CD, Wiesel TN (1979) Morphology and intracortical projections of functionally characterized neurons in cat visual cortex. Nature 5718: 120-125.

Gilbert CD (1983) Microcircuitry of the visual cortex. Annual review of Neuroscience 6: 217-247.

Girard P, Bullier J (1989) Visual activity in area V2 during reversible inactivation of area 17 in the macaque monkey. J Neurophysiol 62: 1287-1302

Girard P, Salin PA, Bullier J (1991) Visual activity in areas V3a and V3 during reversible inactivation of area V1 in the monkey. J Neurophysiol 66:1493-1503.

Girard P, Salin PA, Bullier J (1992) Response selectivity of neurons in area MT of the macaque monkey during reversible inactivation of area V1. J Neurophysiol 67:1437-1446.

Goldberg ME, Bushnell MC (1981) Behavioral enhancement of visual responses in monkey cerebral cortex. II. Modulation in frontal eye fields specifically related to saccades. J Neurophysiol 46: 773-787.

Goldman-Rakic PS (1987) Motor control function of the prefrontal cortex. Ciba Found Symp 132:187-200.

Goldman-Rakic PS (1995) Cellular basis of working memory. Neuron 14: 477-485.

Gonchar Y, Burkhalter A, (2003) Distinct GABAergic targets of feedforward and feedback connections between lower and higher areas of rat visual cortex. J Neurosci 23: 10904-10912.

Grafstein B (1971) Transneuronal transfer of radioactivity in the central nervous system. Science 172:177–179.

Gray EG (1959a) Axosomatic and axodendritic synapses in the cerebral cortex: An electron microscopic study. J Anat 93:420-433.

Gray EG (1959b) Electron microscopy of synaptic contacts on dendrite spines of the cerebral cortex. Nature 183:1592-3

Gregoriou GG, Gotts SJ, Zhou H, Desimone R (2009) High-frequency, long-range coupling between prefrontal and visual cortex during attention. Science 324: 1207-1210.

Grossberg S, Mingolla E (1985) Neural dynamics of perceptual grouping: textures boundaries and emergent segmentations. Perception and Psychophysics 38: 141-171.

Guillery RW, Sherman SM (2002) Thalamic relay functions and their role in corticocortical communication: generalizations from the visual system. Neuron 33: 163-175.

Hanks TD, Ditteritch J, Shadlen MN (2006) Microstimulation of macaque area LIP affects decision-making in a motion discrimination task. Nat Neurosci 9: 682-689.

Harris KM, Stevens JK (1989) Dendritic spines of CA1 pyramidal cells in the rat hippocampus: Serial

electron microscopy with reference to their biophysical characteristics. J Neurosci 9:2982-2997.

Heinzle J, Hepp K, Martin KAC (2007) A microcircuit model of the frontal eye fields. J Neurosci 27:9341-9353.

Hendrickson AE, Wilson JR, Ogren MP (1978) The neuroanatomical organization of pathways between the dorsal lateral geniculate nucleus and visual cortex in old world and new world primates. J Comp Neurol 182: 123-136.

Hendry SH, Schwark HD, Jones EG, Yan J (1987) Numbers and proportions immunoreactive neurons in different areas of monkey cerebral cortex. J Neurosci.7:1503-19.

Herrington J, Park YB, Babcock DF, Hille B (1996) Dominant role of mitochondria in clearance of large Ca^{2+} loads from rat adrenal chromaffin cells. Neuron 16: 219-228.

Hilgetag CC, O'Neill MA, Young MP (1996) Indeterminate organization of the visual system. Science 271: 776-777.

Hitzig E, Fritsch GT (1870) Uber die elektrische Erregbarkeit des Grosshirns Arch Anat Physiol pp. 300-322

Hof PR, Glezer II, Condé F, Flagg RA, Rubin MB, Nimchinsky EA, Vogt Weisenhorn DM (1998) Cellular distribution of the calcium-binding proteins parvalbumin, calbindin and calretinin in the neocortex of mammals: phylogenetic and developmental patterns. J Chem Neuroanat 16: 77-116.

Hubel DH, Wiesel TN (1962) Receptive fields, binocular interaction and functional architecture in the cats visual cortex. J Physiol 160: 106–154.

Hubel DH, Wiesel TN (1974) Uniformity of monkey striate cortex: A parallel relationship between field size, scatter and magnification factor. J Comp Neurol 158: 295-305.

Huerta MF, Krubitzer LA, Kaas JH (1987) Frontal eye field as defined by intracortical microstimulation in squirrel monkeys, owl monkeys, and macaque monkeys. II. Cortical connections. J Comp Neurol 265: 332-361.

Hupé JM, James AC, Payne BR, Lomber SG, Girard P, Bullier J (1998) Cortical feedback improves discrimination between figure and background by V1, V2 and V3 neurons. Nature 394: 784-787.

Hupé JM, James AC, Girard P, Bullier L (2001) Response modulations by static texture surround in area V1 of the macaque monkey do not depend on feedback connections from V2. J Neurophysiol 85: 146-163.

Hussar CR, Pasternak T (2009) Flexibility of sensory representations in prefrontal cortex depends on cell type. Neuron 10: 730-743.

Hussar CR, Pasternak T (2012) Memory-guided sensory comparisons in the prefrontal cortex: contribution of putative pyramidal cells and interneurons, J Neurosci 32: 2747-2761.

Janssen P, Srivastava S, Ombelet S, Orban GA (2008) Coding of shape and position in macaque lateral intraparietal area. J Neurosci 28: 6679-6690.

Johnson RR, Burkhalter A (1996) Microcircuitry of of forward and feedback connections within rat visual cortex. J Comp Neurol 368:383-398.

Jouvé B, Rosenthiehl P, Imbert M (1998) A mathematical approach to the connectivity between the cortical visual areas of the macaque monkey. Cereb Cortex 8: 28-39.

Kawaguchi Y (1993) Groupings of nonpyramidal and pyramidal cells with specific physiological and morphological characteristics in rat frontal cortex. J Neurophysiol 69: 416-431.

Kennedy H, Bullier J (1985) Double-labeling investigation of the afferent connectivity to cortical areas V1 and V2 of the macaque monkey. J. Neurosci. 10: 2815-2830.

Kisvárday ZF, Martin KA, Whitteridge D, Somogyi P (1985) Synaptic connections of intracellularly filled clutch cells, a type of small basket neuron in the visual cortex of the cat. J Comp Neurol 241:111-137.

Kisvárday ZF, Martin KA, Freund TF, Maglóczky Z, Whitteridge D, Somogyi P (1986) Synaptic targets

of HRP-filled layer III pyramidal cells in the cat striate cortex. Exp Brain Res 64: 541-52.

Knott GW, Holtmaat A, Wilbrecht L, Welker E, Svoboda K (2006) Spine growth precedes synapse formation in the adult neocortex in vivo. Nat Neurosci 9:1117-24.

Kőlliker A (1896) Handbuch der Gewebelehre des Menschen, 6th Ed Vol 2: Nervensystems des Menschen und Thiere. Leipzig: Engelmann.

Krubitzer LA, Kaas JH (1989) Cortical integration of parallel pathways in the visual system of primates. Brain Res. 478:161-5.

Kuypers HGJM, Szwarcbart MK, Mishkin M, Rosvold HE (1965) Occipitotemporal corticocortical connections in the rhesus monkey. Exp Neurol 11:245-262.

Lasek R Joseph BS Whitlock DG (1968) Evaluation of a radioautographic neuroanatomical tracing method. Brain Res 8: 319-336

Lashley KS, Clark G (1946) The cytoarchitecture of the cerebral cortex of *Ateles*: a critical examination of the architectonic studies. J Comp Neurol 85: 223–305.

Latawiec D, Martin KAC, Meskenaite V (2000) Termination of the geniculocortical projection in the striate cortex of macaque monkey: A quantitative immunoelectron microscopic study. J Comp Neurol 419:306-319.

Lee J, Maunsell JH (2010) Attentional modulation of MT neurons with single or multiple stimuli in their receptive fields. J Neurosci 30: 3058-3066.

Lee TS, Mumford D (2003) Hierarchical Bayesian inference in the visual cortex. J Opt Am A Opt Image Sci Vis 20:1434-1448.

Levitt JB, Lund (2002) The spatial extent over which neurons in macaque striate cortex pool visual signals. Vis neurosci 19:439- 452.

London M, Segev I (2001) Synaptic scaling in vitro and in vivo. Nature Neurosci 4:853-854.

Lorente de No R (1949) Cerebral cortex: Architecture, intracortical connections, motor projections. In: 'Physiology of the nervous system' by Fulton, Oxford Medical Publications.

Leon MI, Shadlen MN (1999) Effect of expected reward magnitude on the response of neurons in the dorsolateral prefrontal cortex of the macaque. Neuron 24: 415-425.

Livingstone MS, Hubel DH (1982) Thalamic inputs to cytochrome oxidase-rich regions in monkey visual cortex. Proc Natl Acad Sci USA. 79:6098-101.

Livingstone MS, Hubel (1983) Specificity of cortico-cortical connections in monkey visual system. Nature 304:531-534.

Li Z (1998) A neural model of contour integration in the primary visual cortex. Neural Comput 10: 903-940.

Luck SJ, Chelazzi L, Hillyard SA, Desimone R (1997) Neural mechanisms of spatial selective attention in areas V1, V2, and V4 of macaque visual cortex. J Neurophysiol 77:24-42.

Lund JS, Lund RD, Hendrickson AE, Bunt AH, Fuchs AF (1975) The origin of efferent pathways from the primary visual cortex, area 17, of the macaque monkey as shown by retrograde transport of horseradish peroxidase. J Comp Neurol 164:287-303.

Lund JS, Henry GH, MacQueen CL, Harvey AR (1979) Anatomical organization of the primary visual cortex (area 17) of the cat. A comparison with area 17 of the macaque monkey. J Comp Neurol 184: 599-618.

Lund JS,Yoshioka T, Levitt JB (1993) Comparison of intrinsic connectivity in different areas of macaque monkey cerebral cortex. Cereb Cortex 3: 148-162.

MacAvoy MG, Gottlieb JP, Bruce C J (1991) Smooth-pursuit eye movement representation in the primate frontal eye field. Cereb Cortex 1: 95-102.

Magee JC, Cook EP (2000) Somatic EPSP amplitude is independent of synapse location in hippocampal pyramidal neurons. Nat Neurosci 3: 895-903.

Maimon G, Assad JA (2006) A cognitive signal for the proactive timing of action in macaque LIP. Nat Neurosci 9: 948-955.

Malonek D, Tootell RB, Grinvald A (1994) Optical imaging reveals the functional architecture of neurons processing shape and motion in owl monkey area MT. Proc Biol Sci 258:109-119.

Markram H, Toledo-Rodriguez M, Wang Y, Gupta A, Silberberg G, Wu C (2004) Interneurons of the neocortical inhibitory system. Nat Rev Neurosci 5: 793-807.

Markov NT, Misery P, Falchier A, Lamy C, Vezoli J,Quilodran R, Gariel MA, Giroud P, Ercsey-Ravasz M, Pilaz LJ, Huissoud C, Barone P, Dehay C, Toroczkai Z, Van Essen DC, Kennedy H, Knoblauch K (2011) Weight consistency specifies regularities of macaque cortical networks. Cereb Cortex 21: 1254-1272.

Markov NT, Kennedy H (2013) The Importance of being hierarchical. Current opinion in neurobiology, 23:1-8.

Martin KAC, Whitteridge D (1984) Form, function and intracortical projections of spiny neurons in the striate cortex of the cat. J Physiol Lond 353: 463-504.

Maunsell JHR, Van Essen DC (1983) The connections of the middle temporal visual area (MT) and their relationship to a cortical hierarchy in the macaque monkey. J Neurosci 3:2563-2586.

McAdams CJ, Maunsell JH (1999) Effects of attention on the reliability of individual neurons in monkey visual cortex. Neuron 23: 765–773.

McAdams CJ, Maunsell JH (2000) Attention to both space and feature modulates neuronal responses in macaque area V4. J Neurophysiol 83:1751-1755.

McEwen BS, Graphstein B (1968) Fast and slow components in axonal transport of protein. J Cell Biol 38: 494-508.

McGuire BA, Hornung JP, Gilbert CD, Wiesel TN (1984) Patterns of synaptic input to layer 4 of cat striate cortex. J Neurosci 4: 3021-3033.

McGuire BA, Gilbert CD, Rivlin PK,Wiesel TN (1991) Targets of horizontal connections in macaque primary visual cortex. J Comp Neurol 305: 370-392.

Medalla M, Barbas H (2009) Synapses with inhibitory neurons differentiate anterior cingulate from dorsolateral prefrontal pathways associated with cognitive control. Neuron 61:609-620.

Meskenaite V (1997) Calretinin-immunoreactive local circuit neurons in area 17 of the cynomolgus monkey, *Macaca fascicularis*. J Comp Neurol 379: 113-132.

Melchitzky DS, Sesack SR, Pucak ML, Lewis DA (1998) Synaptic targets of pyramidal neurons providing intrinsic horizontal connections in monkey prefrontal cortex. J Comp Neurol 390: 211-224.

Melchitzky DS, Gonzalez-Burgos G, Barrionuevo G, Lewis DA (2001) Synaptic targets of the intrinsic axon collaterals of supragranular pyramidal neurons in monkey prefrontal cortex. J Comp Neurol 430:209-221.

Meller K (1992) Axoplasmic transport of horseradish peroxidase in single neurons of the dorsal root ganglion studied in vitro by microinjection. Cell Tissue Res 270:139-148.

Miller EK, Cohen JD (2001) An integrative theory of prefrontal cortex function. Annu Rev Neurosci 24: 167-202.

Mitchell JF, Sundberg KA, Reynolds JH (2007) Differential attention-dependent response modulation across cell classes in macaque visual area V4. Neuron 55:131-141.

Mitchell JF, Sundberg KA, Reynolds JH (2009) Spatial attention decorrelates intrinsic activity fluctuations in macaque area V4. Neuron 63:879-888.

Moore T, Fallah M (2001) Control of eye movements and spatial attention. Proc Natl Acad Sci USA 98: 1273-1276.

Moore T, Fallah M (2004) Microstimulation of the frontal eye field and its effects on covert spatial attention. J Neurophsiol 91:152-162.

Morel A, Bullier J (1990) Anatomical segregation of two cortical visual pathways in the macaque

monkey. Vis Neurosci 4:555-578.

Mountcastle VB (1978) “An organizing principle for cerebral function: The unit model and the distributed system.” in Edelman GM and Mountcastle VB, The Mindful Brain, 7-50 MIT Press.

Movshon JA, Newsome WT (1984) Functional characteristics of functional cortical neurons projecting to MT in the macaque. Soc Neurosci Abstr 10:933.

Movshon JA, Newsome WT (1996) Visual response properties of striate cortical neurons projecting to area MT in macaque monkeys. J Neurosci 16:7733-7741.

Mumford D (1992) On the computational architecture of the neocortex. II. The role of cortico-cortical loops. Biol Cybern 66: 241-251.

Munk M, Nowak L, Girard P, Chounlamountri N, Bullier J (1995) Visual latencies in cytochrome oxidase bands of macaque area V2. Proc Natl Acad Sci USA 92: 988-992.

Nakamura K, Colby CL (2000) Visual, saccade-related, and cognitive activation of single neurons in monkey extrastriate area V3a. J Neurophysiol 84:677-692.

Nakamura H, Kuroda T, Wakita M, Kato A, Mikami A, Sakata H, Itoh K (2001) From three-dimensional space vision to prehensile hand movements: The lateral intraparietal area links the area V3a and the anterior intraparietal area in macaques. J Neurosci 21:8174-8187.

Nakamura K, Colby CL (2002) Updating of the visual representation in monkey striate and extrastriate cortex during saccades. Proc Natl Acad Sci USA 99: 4026-4031.

Nauta W,Gygax PA (1951) Silver impregnation of degenerating axon terminals in the central nervous system (1) Technic (2) Chemical notes 26: 5-11.

Nicholls DG, Åkerman KEO (1982) Mitochondrial calcium transport. Biochim Biophys Acta 683: 57-88.

Nowak LG, Azouz R, Sanchez-Vives MV, Gray CM, McCormick DA (2003) Electrophysiological classes of cat primary visual cortical neurons in vivo as revealed by quantitative analyses. J Neurophys-

iol 89: 1541-1566.

O'Kusky J, Colonnier M (1982) A laminar analysis of the number of neurons, glia, and synapses in the adult cortex (area 17) of adult macaque monkeys. J Comp Neurol 210:278-290.

O'Leary JL (1941) The structure of the area striata of the cat. J Comp Neurol 75: 131-164.

Orban GA, Fize D, Hendrik P, Denys K, Nelissen K, Sunaert S, Todd J, Vanduffel W (2003) Similarities and differences in motion processing between the human and macaque brain: evidence from fMRI. Neuropsychologia 41:1757-1768.

Otsuka R, Hassler R (1962) On the structure and segmentation of the cortical center of vision in the cat. Arch Psychiatr nervenkr Z Gesamte Neurol Psychiatr 203:212-234.

Palade GE, Palay SL (1954) Electron microscope observation of interneuronal and neuromuscular synapses. Anat Rec 118: 335-336.

Palade GE (1954) Electron microscope observations of interneural and neuromuscular synapses. Anat Rec 118:335-336.

Palay SL (1956) Synapses in the central nervous system. J Biophys Biochem Cytol Suppl 2: 193-206.

Patel GH, Shulman GL, Baker JT, Akbudak E, Snyder AZ, Snyder LH, Corbetta M (2010) Topographic organization of macaque area LIP. Proc Natl Acad Sci USA 107: 4728-4733.

Peng Y-Y (1998) Effects of mitochondrion on calcium transients at intact presynaptic terminals depend on frequency of nerve firing. J Neurophysiol 80:186-195.

Peterhans E, von der Heydt R (1993) Functional organization of area V2 in the alert macaque. Eur J Neurosci 5:509-524.

Peters A, Saint Marie RL (1984) Smooth and sparsely spinous non-pyramidal cells forming local axonal plexuses. In: Jones EG and Peters A, editors. Cerebral cortex Vol 1. Cellular components of the cerebral cortex. New York: Plenum Press. p 419-445.

Peters A, White EL, Fairen A (1977) Synapses between identified neuronal elements. An electron mi-

croscopic demonstration of degenerating axons terminals synapsing with Golgi impregnated neurons. Neuroscience Letters 2-3: 6.

Peters A, Palay SL, Webster HDeF (1991) The fine structure of the nervous system: neurons and their supporting cells. 3rd Edition Oxford OUP.

Petrides M, Pandya DN (1999) Dorsolateral prefrontal cortex: comparative cytoarchitectonic analysis in the human and the macaque brain and corticocortical connection patterns. Eur J Neurosci 11: 1011-1036.

Petrides M (2005) Lateral prefrontal cortex: architectonic and functional organization. Phil Trans R Soc Lond B 360: 781- 795.

Petrides M, Pandya DN (2007) Efferent association pathways from the rostral prefrontal cortex in the macaque monkey. J Neurosci 27: 11573-11586.

Phillips CG (1959) Actions of antidromic pyramidal volleys on single Betz cells in the cat. Q J Exp Physiol Cogn Med Sci. 44:1–25.

Platt ML, Glimcher PW (1999) Neural correlates of decision variables in parietal cortex. Nature 400: 233-238.

Poggio T, Serre T (2013) Models of visual cortex. Scholarpedia 8_3516 doi: 10.4249/scholarpedia. 3516.

Ponce CR, Lomber SG, Born RT (2008)Integrating motion and depth via parallel pathways. Nat Neurosci 11: 216-223.

Ponce CR, Hunter JN, Pack CC, Lomber SG, Born RT (2011) Contributions of indirect pathways to visual response properties in macaque middle temporal area MT. J Neurosci 31:3894-3903.

Pouget P, Stepniewska I, Crowder EA, Leslie MW, Emeric EE, Nelson MJ, Schall JD (2009) Visual and motor connectivity and the distribution of calcium-binding proteins in macaque frontal eye field:

implications for saccade target selection. Front Neuroanat 3: 1-14.

Powell TPS, Cowan WM (1964) A note on retrograde fiber degeneration. J Anat Lond 98: 579-585.

Raiguel SE, Lagae L, Gulyàs B, Orban GA (1989) Response latencies of visual cells in macaque area V1, V2 and V5. Brain Res 493: 155-159.

Ramon y Cajal (1888/9) see Shepherd GM 1991 pp 197-198 Foundations of the neuron doctrine. New York Oxford: OUP.

Ramon y Cajal (1888) in Garcia-Lopez P, Garcia-Marin V, Freire M (2007) The discovery of dendritic spines by Cajal in 1888 and its relevance in the present neuroscience. Progress in neurobiology 83: 110-130.

Rao SG, Williams GV, Goldman-Rakic PS (1999) Isodirectional tuning of adjacent interneurons and pyramidal cells during working memory: evidence for microcolumnar organization in PFC. J Neurophysiol 81: 1903- 1916.

Rapp M, Yarom Y, Segev I (1992) The impact of parallel fiber background activity on the cable properties of cerebellar Purkinje cells. Neural Computation 4:518-533.

Reynolds JH, Chelazzi L, Desimone R (1999) Competitive mechanisms subserve attention in macaque areas V2 and V4. J Neurosci 19: 1736-1753.

Reynolds JH, Pasternack T, Desimone R (2000) Attention increases sensitivity of V4 neurons. Neuron 26: 703-714.

Reynolds JH, Heeger DJ (2009) The normalization model of attention. Neuron 61:168-185.

Ribak CE (1978) Aspinous and sparsely-spinous stellate neurons in the visual cortex of rats contain glutamic acid decarboxylase. J Neurocytol 7: 461-478.

Rockland KS, Pandya DN (1979) Lamina origins and terminations of cortical connections of the occipital lobe of the rhesus monkey. Brain Res 179: 3-20.

Rockland KS (1989) Bistratified distribution of terminal arbors of individual axons projecting from

area V1 to middle temporal area (MT) in the macaque monkey. Vis Neurosci 3:155-170.

Rockland KS, Virga A (1989) Terminal arbors of individual "feedback" axons projecting from area V2 to V1 in the macaque monkey: a study using immunohistochemistry of anterogradely transported Phaseolus vulgaris-leucoagglutinin. J Comp Neurol 285: 54-72.

Rockland KS, Virga A (1990) Organization of individual cortical axons projecting from area V1 (area 17) to V2 (area 18) in the macaque monkey. Vis Neurosci 4:11-28.

Rockland KS (1992) Configuration in serial reconstruction of individual axons projecting from area V2 to V4 in the macaque monkey. Cereb Cortex 5:353-374.

Rockland KS, Douglas KL (1993) Excitatory contacts of feedback connections in layer 1 of area V1: An EM biocytin study in the macaque. Neurosci Abst 19: 424.

Rockland KS, Saleem KS, Tanaka K (1994) Divergent feedback connections from areas V4 and TEO in the macaque. Vis Neurosci 11: 579-600.

Rockland KS (1994) The organization of feedback connections from Area V2 (18) to V1 (17). In Peters A and Rockland KS, editors. Cerebral Cortex Vol 10. Primary visual cortex in primates. New York: Plenum Press. P 261-299.

Rockland KS (1995) Morphology of individual axons projecting from area V2 to MT in the macaque. J Comp Neurol 355:15-26.

Rockland KS (1997) Elements of cortical hierarchy revisited. In Rockland KS, Kaas JH and Peters A, editors. Cerebral Cortex Vol 12. Exstrastriate cortex in primates. New York: Plenum Press. p243-293.

Robinson DA, Fuchs AF (1969) Eye movement evoked by stimulation of frontal eye fields. J Neuro-physiol 32: 637-648.

Rockel AJ, Hiorns RW, Powell TPS (1980) The basic uniformity of the neocortex. Brain 103: 221-244.

Rodman HR, Gross CG, Albright TD (1989) Afferent basis of visual response properties in area MT of

the macaque. II. Effects of striate cortex removal. J Neurosci 10:2033—2050.

Rodman HR, Gross CG, Albright TD (1990) Afferent basis of visual response properties in area MT of the macaque. II. Effects of superior colliculus removal. J Neurosci 10:1154-1164.

Saint-Marie RL, Peters A (1985) The morphology and synaptic connections of spiny stellate neurons in monkey visual cortex (area 17): A Golgi-electron microscopic study. J Comp Neurol 233: 213-235.

Saleem KS, Logothetis NK (2007) Atlas of the rhesus monkey brain in stereotaxic coordinates. Elsevier Academic Press.

Salin PA, Bullier J (1995) Corticocortical connections in the visual system: structure and function. Physiol Rev 75: 107-154.

Salinas E, Sejnowski TJ (2001) Correlated neuronal activity and the flow of neural information. Nature Rev Neurosci 2:539- 550.

Salzman CD, Murasugi CM, Britten KH, Newsome WT (1992) Microstimulation in visual area MT: Effects on direction discrimination performance. J Neurosci 12: 2331-2355.

Schall JD, Morel A, King DJ, Bullier J (1995) Topography of visual cortex connections with frontal eye field in macaque: convergence and segregation of processing streams. J Neurosci 15:4464-4487.

Schiller PH, Malpeli JG (1977) The effect of striate cortex cooling on area 18 cells in the monkey. Brain Res 126: 366-369.

Schiller PH, True SD, Conway JL (1979) Effects of frontal eye field and superior colliculus ablations on eye movements. Science 206: 590-592.

Schultz RL, Maynard EA, Pease DC (1957) Electron microscopy of neurons and neuroglia of cerebral cortex and corpus collosum. Amer J Anat 100: 369-388.

Schwann T (1839) Mikroskopische Untersuchungen uber die Uebereinstimmung in der Struktur und dem Wachsthum der Thiere und Pflanzen. Berlin GE Reimer.

Seidemann E, Zohary U, Newsome WT (1998) Temporal gating of neural signals during performance

of a visual discrimination task. Nature. 394:72- 75.

Sereno AB, Amador SC (2006) Attention and memory-related responses of neurons in the lateral intraparietal area during spatial and shape-delayed match-to-sample tasks. J Neurophysiol 95: 1078-1098.

Sereno AB, Maunsell JH (1998) Shape selectivity in primate lateral intraparietal cortex. Nature 395: 500-503.

Shepherd G (1991) Foundations of the neuron doctrine. New York, Oxford: Oxford University Press.

Sherman SM, Guillery RW (1998) On the actions that one nerve cell can have on another: distinguishing 'drivers' from 'modulators'. Proc Natl Acad Sci USA 95:7121-7126.

Shipp (2001) Corticopulvinar connections of area V5, V4, and V3 in the macaque monkey: a dual model of retinal and cortical topographies. J Comp Neurol 439: 469-490.

Shipp S, Blanton M, Zeki S (1998) A visuo-somatomotor pathway through superior parietal cortex in the macaque monkey: cortical connections of areas V6 and V6a. Eu J Neurosci 10:3171-3193.

Shipp S, Zeki S (1985) Segregation of pathways leading from area V2 to areas V4 and V5 of macaque monkey visual cortex. Nature 315:322-5.

Shipp S, Zeki S (1989) The organization of connections between area V5 and V1 in macaque monkey visual cortex. Eur J Neurosci 1:309-332.

Sincich LC, Horton JC (2002a) Divided by cytochrome oxidase: a map of the projections fromV1 to V2 in macaques. Science 295:1734-1737.

Sincich LC, Horton JC (2002b) Pale cytochrome oxidase stripes in V2 receive the richest projection from Macaque striate cortex. J Comp Neurol 447: 18-33.

Sincich LC, Horton JC (2003) Independent projection streams from macaque striate cortex to the second visual area and middle temporal area. J Neurosci 23: 5684-5692.

Sincich LC, Horton JC (2005a) The circuitry of V1 and V2: integration of color, form and motion.

Annu Rev Neurosci 28:303-26.

Sincich LC, Horton JC (2005b) Input to V2 thin stripes arises from V1 cytochrome oxidase patches. J Neurosci 25: 10087-10093.

Sincich LC, Jocson CM, Horton JC (2010) V1 interpatch projections to V2 thick stripes and pale stripes.

Small JV (1968) Measurement of section thickness: In proceedings 41h European Congress of Electron Microscopy (Bocciarelli EDS ed), Tipografia poliglotta Vaticana: Rome.

Somogyi P (1978) The study of Golgi stained cells and of experimental degeneration under the electron microscope: a direct method for the identification in the visual cortex of three successive links in a neuron chain. Neuroscience 3: 167-180.

Somogyi P, Hodgson AJ,Smith AD (1979) An approach to tracing neuron networks in the cerebral cortex and basal ganglia. Combination of golgi staining, retrograde transport of horseradish peroxidase and anterograde degeneration of synaptic boutons in the same material. Neuroscience 4: 1805-1852.

Somogyi P, Kisvárday Z F, Martin KAC, Whitteridge D (1983) Synaptic connections of morphologically identified and physiologically characterized large basket cells in the striate cortex of cat. Neuroscience 10:261- 294.

Sporns O, Tononi G, Edelman GM (2000) Theoretical neuroanatomy: relating anatomical and functional connectivity in graphs and cortical connection matrices. Cereb Cortex 10: 127-141.

Stanton GB, Deng S-Y, Goldberg EM, McMullen NT (1989) Cytoarchitectural characteristic of the frontal eye fields in macaque monkeys. J Comp Neurol 282: 415-427.

Stanton GB, Bruce CJ, Goldberg ME (1993) Topography of projections to the frontal lobe from the macaque frontal eye fields. J Comp Neurol 330: 286-301.

Stanton GB, Bruce CJ, Goldberg ME (1995) Topography of projections to posterior cortical areas from the macaque frontal eye fields. J Comp Neurol 353: 291-305.

Stanton GB, Friedman HR, Dias EC, Bruce CJ (2005) Cortical afferents to the smooth-pursuit region of the macaque monkey's frontal eye field. Exp Brain Res 165:179-192.

10:261-294.

Stell WK (1965) Correlation of retinal cytoarchitecture and ultrastructure in Golgi preparations. Anat Rec 153: 389–397.

Sterio DC (1984) The unbiased estimation of number and sizes of arbitrary particles using the disector. J Microsc 134:127-136.

Stettler DD, Das A, Bennett J, Gilbert CD (2002) Lateral connectivity and contextual interactions in macaque primary visual cortex. Neuron 36:739-50.

Stratford KJ, Tarczy-Hornoch K, Martin KAC, Bannister NJ, Jack JJB (1996) Excitatory synaptic inputs to spiny stellate cells in cat visual cortex. Nature 382:258-261.

Stretton AO, Kravitz EA (1969) Neuronal geometry: determination with a technique of intracellular dye injection. Science. 162:132–134.

Suzuki W, Saleem KS, Tanaka K (2000) Divergent backward projections from the anterior part of the inferotemporal cortex (area TE) in the macaque. J Comp Neurol 422: 206-28.

Szentágothai J (1978) The neuron network of the cerebral cortex: A functional interpretation. proceedings of the Royal Society B 201, 219-248.

Talbot SA and Marshall WH (1941) Physiological studies on neural mechanisms of visual localization and discrimination. Am J Ophthalmol 24: 1255-1263.

Tang Y-G, ZuckerRS (1997) Mitochondrial involvement in post-tetanic potentiation of synaptic transmission. Neuron 18: 483-491.

Tanji J, Hoshi E (2008) Role of the lateralprefrontal cortex in executive behavioral control. Physiol Rev 88:37-57.

Thiele A, Distler C, Hoffmann KP (1999) Decision-related activity in the macaque dorsal visual

pathway. Eu J Neurosci 11-2044-2058.

Thompson JM, Woolsey CN, Talbot SA (1950) Visual areas 1 and 2 of cerebral cortex of rabbit. J Neurophysiol 13: 277-288.

Tigges J, Spatz WB, Tigges M (1973) Reciprocal point-to-point connections between parastriate and striate cortex in the squirrel monkey (*Saimiri*). J Comp Neurol 148: 481-489.

Tolhurst, DJ, Movshon, JA, Dean, AF (1983) The statistical reliability of signals in single neurons in cat and monkey visual cortex. Vision Res 23:775–785.

Tootell RBH, Mendola JD, Hadjikhani NK, Leddon PJ, Liu AK, Reppas JB, Sereno MI, Dale AM. (1997) Functional analysis of V3a and related areas in human visual cortex. J Neurosci 17:7060-7078.

Ts'o DY, Wang Roe A, Gilbert CD (2001) A hierarchy of the functional organization for color, form and disparity in primate visual area V2. Vis Res 41:1333-1349.

Uchizono K (1965) Characteristics of Excitatory and Inhibitory Synapses in the Central Nervous System of the Cat. Nature 207: 642-643.

Ungerleider LG, Mishkin M (1982) Two cortical visual systems. In Ingle, Goodale, Mansfield. Analysis of visual Behavior. Boston MIT Press.

Ungerleider LG, Galkin TW, Mishkin M (1983) Visuotopic organization of projections from striate cortex to inferior and lateral pulvinar in rhesus monkey. J Comp Neurol 217: 137-157.

Ungerleider LG, Desimone R (1986) Cortical connections of visual area MT in the macaque. J Comp Neurol 248:190-222.

Usrey WM, Muly EC, Fitzpatrick D (1992) Lateral geniculate projections to the superficial layers of visual cortex in the tree shrew. J Com Neurol 319:159-171.

Van Essen DC Zeki SM (1978) The topographic organization of rhesus monkey prestraite cortex J Physiol 277:193-226.

Van Essen DC, Newsome WT, Maunsell JH, Bixby JL (1986) The projections from striate cortex (V1)

to areas V2 and V3 in the macaque monkey: asymmetries, areal boundaries, and patchy connections. J Comp Neurol 244:451-480.

Walker E (1940) A cytoachitectural study of the prefrontal area of the macaque monkey. J Comp Neurol 73: 59-86.

Waldeyer-Hartz, HWG von (1891) Uber einige neuere Forschungen im Gebiete der Anatomie des Centralnervensystems. Deutsch Med Wschr 17.

Watts DJ, Strogatz SH (1998) Collective dynamics of 'small-world' networks. Nature 393: 409–10

White EL (1989) Cortical circuits. Boston: Birkhauser.

Webster MJ, Bachevalier J, Ungerleider LG (1994) Connections of inferior temporal areas TEO and TE with parietal and frontal cortex in macaque monkeys. Cereb Cortex 4:470-483.

Wilson FA, O'Scalaidhe SP, Goldman-Rakic PS (1994) Functional synergism between putative gamma-aminobutyrate-containing neurons and pyramidal neurons in prefrontal cortex. Proc Natl Acad Sci USA 91:4009-4013.

Xu T, Naraghi M, Kang H, Neher E (1997) Kinetic studies of Ca 2+ binding and Ca2+ clearance in the cytosol of adrenal chromaffin cells. Biophys J 19:532-545.

Yoshioka T, Levitt JB, Lund JS (1992) Intrinsic lattice connections in macaque monkey visual cortical area V4. J Neurosci 12: 2785-2802.

Yoshioka T, Dow BM (1996) Color, orientation and cytochrome oxidase reactivity in areas V1, V2 and V4 of macaque monkey visual cortex. Behav Brain Res 76: 71-88.

Young MP (1992) Objective analysis of the topological organization of the primate cortical visual system. Nature 358: 152-155.

Zeki S (1969) Representation of central fields in prestriate cortex of monkey. Brain Res 19:63-75.

Zeki S (1974) Functional organisation of a visual area in the posterior bank of the superior temporal sulcus of the rhesus monkey. J Physiol 236:549-573.

Zeki S (1978) Uniformity and diversity of structure and function in rhesus monkey prestriate visual cortex. J Physiol 277: 273-290.

Curriculum Vitae

ANDERSON, John Carl

Present position Wissenschaftlicher Mitarbeiter
Address Institute for Neuroinformatics
University/ETH Zurich
Winterthurerstr. 190
8057 Zurich
Phone 0041 1 6353044
Email jca@ini.phys.ethz.ch

Date of birth 26/4/55

1974-1977 BSc (Honours) 2:1, psychology and anthropology, Oxford Polytechnic.
1987-1980 research chemist in paint and adhesives industry, Humbrol, Hull, UK.
1981 forestry in Wytham Woods, Oxford, Oxford University, UK.
1981-1985 research technician to KAC Martin/Prof. D Whitteridge, MRC research project, Dept. of Experimental Psychology, Oxford University.

1985-1995 research assistant to KAC Martin/Prof. D Whitteridge, MRC Anatomical Neuropharmacology Unit, Oxford.
1995- present wissenschaftlicher Mitarbeiter, Institute for Neuroinformatics Univ/ETH, Zurich.

Research (keywords)
visual pathways, neuronal and synaptic morphology, intracortical and intercortical connectivity.

Collaborations
Inserm U371, Cerveau et Vision, Bron Cedex, France (H. Kennedy)
Dept. of Psychology, University of Newcastle upon Tyne, GB (M. Young)
Dept. of Anatomy and Neurobiology, University of Washington, St Louis, USA (A. Burkhalter)
Dept. of Physiology and Biophysics, University of Alabama, Birmingham, USA (MJ. Friedlander)

Publications.

Anderson, JC Kennedy, H and Martin, KAC (2011). Pathways of attention: synaptic relationships of frontal eye field to V4, lateral intraparietal cortex, and area 46 in macaque monkey. J Neurosci., 31:(30) 10872-81.

Anderson, JC Costa, NM and Martin, KAC (2009). The W cell pathway to cat primary visual cortex. J Comp Neurol, 516:(1) 20-35.

Anderson, JC and Martin, KAC (2009).The synaptic connections between cortical areas V1 and V2 in macaque monkey. J Neuroscience, 29:(36) 11283-11293.

Anderson, JC and Martin, KAC. (2006). Synaptic connection from cortical area V4 to V2 in macaque monkey, J Comp Neurol, 495:(6) 709-721.

Anderson, JC and Martin, KAC (2005). Connection from cortical area V2 to V3A in macaque monkey, J Comp Neurol, 488:(3) 320-330.

Anderson, JC and Binzegger, T and Douglas, RJ and Martin, KAC (2003).Chance or design: Some specific considerations concerning synaptic boutons in cat visual cortex, J Neurocytology, 31: 211-229.

Anderson, JC, and KAC Martin (2002) Connection from cortical area V2 to MT in macaque monkey. J Comp Neurol *44*:56-70.

Anderson, JC, and KAC Martin (2001) Does bouton morphology optimize axon length? Nature Neuroscience. *4*:1166-1167.

Anderson, JC ,T Binzegger, O Kahana, , KAC Martin and I Segev (1999) Dendritic asymmetry cannot account for directional responses of neurons in visual cortex. Nature Neuroscience *2*: 820-824.

Ahmed B, Anderson JC, Douglas RJ, Martin KAC, Whitteridge D (1998) Estimates of the net excitatory currents evoked by visual stimulation of identified neurons in cat visual cortex. Cereb cortex 8: 462-476.

Anderson, JC, T Binzegger, KAC Martin and KS Rockland (1998) The connection from cortical area V1 to V5: a light and electron microscopic study. J Neuroscience *18*: 10525-10540.

Ahmed B, JC Anderson, KAC Martin, JC Nelson (1997) Map of the synapses onto layer 4 basket cells of the primary visual cortex of the cat. J Comp Neurol 380:230-242.

Anderson, JC, RJ Douglas, KAC Martin, and JC Nelson (1994) Synaptic output of physiologically-identified spiny stellate neurons in cat visual cortex. J Comp Neurol *341*:16-24.

Ahmed, B, JC Anderson, RJ Douglas, KAC Martin, and JC Nelson (1994) The polyneuronal innervation of spiny stellate neurons in cat visual cortex. J Comp Neurol *341*:39-49.

Anderson, JC, RJ Douglas, KAC Martin, JC Nelson, and D Whitteridge (1994) Synaptic output of physiologically - identified spiny stellate neurons in cat visual cortex. J Comp Neurol 341:16-24.

Anderson, JC, RJ Douglas, KAC Martin, and JC Nelson (1994) Map of the synapses formed with the dendrites of spiny stellate neurons of cat visual cortex. J Comp Neurol 341:25-38.

Anderson, JC, KAC Martin and D Whitteridge (1993) Form, function and intracortical projections in the striate cortex of the monkey *Macacus nemestrinus*. Cerebral Cortex 3:412-420

Anderson, JC, KAC Martin and CWP Diniz (1992) The neurons in layer 1 of cat visual cortex. Proc R Soc Lond. B. 248, 27-33.

Anderson, JC, C Dehay, M Friedlander, KAC Martin and JC Nelson (1992) Synaptic connections of physiologically identified geniculocortical axons in kitten cortical area 17. Proc R Soc Lond B.250, 187-194.

Abstracts and conferences

Evidence for a significant excitatory input to the dendritic shafts of spiny stellate cells in cat visual cortex. Anderson, Douglas, Martin, Nelson, Whitteridge. Physiological Society Meeting Oxford 1993.

Polyneuronal innervation and specificity of innervation of dendrites in layer 4 of cat visual cortex. Ahmed, Anderson, Douglas, Martin, Nelson. Swiss Society for Neuroscience Bern 1996.

Current-discharge relationships of pyramidal neurons from the cat visual cortex: in vivo and in vitro. Ahmed, Anderson, Douglas, Martin, Nelson. Swiss Society for Neuroscience Bern 1996.

Innervation of monkey cortical area MT by neurons of area V1: bouton morphology and synaptic targets. Anderson, Binzegger, Martin, Rockland. Swiss Society for Neuroscience. Lausanne, 1998.

Innervation of monkey cortical area V5 by neurons of area V1: bouton morphology and synaptic targets. Anderson, Binzegger, Martin, Rockland. Swiss Society for Neuroscience. Zurich, 1999.

Parallel pathways from V2 to layer 1 of V1 in the macaque monkey. Anderson, Martin. ZNZ Symposium, Zurich 2002.

Map of synapses on dendrites of neurons in cat area 17. Binzegger, Anderson, Douglas, Martin. ZNZ Symposium, Zurich 2002.

Quantitative characterization of cortical circuits in cat area 17. Binzegger, Anderson, Douglas, Martin. Swiss Society for Neuroscience Geneva 2002

The connection from cortical area V2 to V5 in macaque monkey. Anderson, Martin. Swiss Society for Neuroscience, Geneva January 2002.

Parallel pathways from V2 to layer 1 of V1 in the macaque monkey, Anderson, Martin. FENS European Neuroscience, Paris July 2002.

Synaptic relations between visual areas in macaque monkey. Anderson, Martin. ZNZ Symposium, Zurich October 2003.

The W cell innervation of cat area 17. Anderson, da Costa, Martin. ZNZ Symposium Zurich 2006.

The W cell innervation of cat area 17. Anderson, da Costa, Martin. Swiss Society for Neuroscience Basel 2006.

The projection of frontal eye fields to visual cortical area V4. Anderson, Martin. ZNZ Symposium

Zurich September 2007.

A synaptic analysis of projections from FEF in macaque monkey, Anderson, Kennedy, Martin. FENS European Neuroscience, Geneva July 2008.

Strong loops and the small world architecture of the primate cerebral cortex. Markov N, Vezoli J, Dehay C, Knoblauch K, Anderson JC, Martin KAC, Kennedy H. FENS European Neuroscience, Geneva July 2008.

Principles of organization of the circuits of primate neocortex, Anderson, Kennedy, Martin. International Primatological Society Meeting XXII, Edinburgh UK, August 2008.

Principles of organization of the circuits of primate neocortex. Anderson, Kennedy, Martin. ZNZ Symposium Zurich September 2009.

Principles of organization of the circuits of primate neocortex. Anderson, Kennedy, Martin. Primate Neurobiology Meeting, Göttingen March, 2009.

Pathways of attention in the neocortex of macaque monkey. Anderson, Kennedy, Martin. Swiss Society for Neuroscience, Lausanne March 2010.

Pathways of attention in the neocortex of macaque monkey. Anderson, Kennedy, Martin. FENS

European Neuroscience, Amsterdam July 2010.

Local excitatory circuits of macaque area 8A. Anderson, da Costa, Martin, Primate Neurobiology Meeting, Tűbingen March 2010.

Excitatory cell axon morphology in superficial layers of macaque Frontal Eye Fields (FEF), Anderson, da Costa, Martin, Primate Neurobiology Meeting Gőttingen March 2011.

Excitatory cell axon morphology in superficial layers of macaque Frontal Eye Fields (FEF), Anderson, da Costa, Martin, Swiss Society for Neuroscience March 2011.

Local excitatory circuits of macaque area 8A (FEF). Anderson, da Costa, Martin, Swiss Society for Neuroscience, Basel 2011.

Local excitatory circuits of macaque area 8A. Anderson, da Costa, Kennedy, Martin. ZNZ Symposium Zurich September 2011.

Who's who in cortical neuropil? An immuno-ultrastructural study of macaquearea 17. Anderson, Bopp, Martin, Swiss Society for Neuroscience, Zurich February 2012.

Who's who in cortical neuropil? An immuno-ultrastructural study of macaquearea 17. Anderson, Bopp, Martin, ZNZ Symposium June 2012

Quantifying the local circuit of macaque cortex, Anderson, Martin, Spüler. Swiss Society for Neuroscience, Geneva February 2013.

Acknowledgements

It is naturally a pleasure to thank those involved in the work that made this possible. Colleagues and friends both within and without the Institute for which I am deeply grateful to have 'been there' to hear their support. Working with Kevan, Rodney and the team over so many years has been formative. How could it be anything else?

I offer thanks to Kevan and Rodney, for all the business of life and science that we have pursued along the way. To Henry Kennedy and Kathy Rockland for collaboration. To Klaus Hepp for pushing. Immense thanks to Rita Bopp and German Koestinger for bringing expert hands to bear on the vast numbers of images generated in the analogue days now past and the digital world it became. Thanks go to Kevan's team, past and present and institute members. Equally special and less obscured by the mists of time must thanks go to Nuno da Costa for toleration of my ignorance of the world of Photoshop and Illustrator and for showing such enthusiasm for so many things. Thanks to Tom Binzegger and Sylvia Schroeder for help with statistics.

The support I received from those outside the institute was so welcome, specially from Bruce and Gaby, from whom many a fine Burgundy was applied when necessary. Monumental thanks to Ruth, for clear and deliberate support that I found invaluable, often nutritious and always enough to keep me moving. Thanks again.